# Physical phenomena controlling quiescent flame spread in porous wildland fuel beds

Zakary Campbell-Lochrie


A thesis submitted in fulfilment of the requirements

for the degree of

Doctor of Philosophy

to

The University of Edinburgh

2021

# Physical phenomena controlling quiescent flame spread in porous wildland fuel beds

by

Zakary Campbell-Lochrie

This thesis has been supervised by

Dr R.M. Hadden

Dr S. Welch

# Declaration

This thesis and the work reported within has been conducted by Zakary Campbell-Lochrie at the University of Edinburgh under the supervision of Dr Rory M. Hadden and Dr Stephen Welch. This thesis has not been submitted in any previous application for a degree of any kind. Where other sources are used, this is highlighted and appropriate references are provided. The contributions of others have also been highlighted.

Zakary Campbell-Lochrie

August 2021

# Abstract

Despite well-developed solid surface flame spread theories, we still lack a coherent theory to describe flame spread through porous wildland fuel beds. This porosity results in additional complexity, reducing the thermal conductivity of the fuel bed, but allowing in-bed radiative and convective heat transfer to occur. While previous studies have explored the effect of fuel bed structure on the overall fire behaviour, there remains a need for further investigation of the effect of fuel structure on the underlying physical phenomena controlling flame spread. Through an extensive series of laboratory-based experiments, this thesis provides detailed, physics-based insights for quiescent flame spread through natural porous beds, across a range of structural conditions.

Measurements are presented for fuel beds representative of natural field conditions within an area of the fire-prone New Jersey Pinelands National Reserve, which compliment a related series of field experiments conducted as part of a wider research project. Additional systematic investigation across a wider range of fuel conditions identified independent effects of fuel loading and bulk density on the spread rate, flame height and heat release rate. However, neither fuel loading nor bulk density alone provided adequate prediction of the resulting fire behaviour. Drawing on existing structural descriptors (for both natural and engineered fuel beds) an alternative parameter $\alpha\sigma\delta$ was proposed. This parameter (incorporating the fuel bed porosity ($\alpha$), fuel element surface-to-volume ratio ($\sigma$), and the fuel bed height ($\delta$)) was strongly correlated with the spread rate.

One effect of the fuel bed structure is to influence the heat transfer mechanisms both above and within the porous fuel bed. Existing descriptions of radiation transport through porous fuel beds are often predicated on the assumption of an isotropic fuel bed. However, given their preferential angle of inclination, the pine needle beds in this study may not exhibit isotropic behaviour.

Regardless, for the structural conditions investigated, horizontal heat transfer through the fuel bed was identified as the dominant heating mechanism within this quiescent flame spread scenario. However, the significance of heat transfer contributions from the above-bed flame generally increased with increasing $\alpha\sigma\delta$ value of the fuel bed. Using direct measurements of the heat flux magnitude and effective heating distance, close agreement was observed between experimentally observed spread rates and a simple thermal model considering only radiative heat transfer through the fuel bed, particularly at lower values of $\alpha\sigma\delta$. Over-predictions occurred at higher $\alpha\sigma\delta$ values, or where other heat transfer terms were incorporated, which may highlight the need to include additional heat loss terms.

A significant effect of fuel structure on the primary flow regimes, both within and above these porous fuel beds, was also observed, with important implications for the heat transfer and oxygen supply within the fuel bed. Independent effects of fuel loading and bulk density on both the buoyant and buoyancy-driven entrainment flow were observed, with a complex feedback cycle occurring between Heat Release Rate (HRR) and combustion behaviour. Generally, increases in fuel loading resulted in increased HRR, and therefore increased buoyant flow velocity, along with an increase in the velocity of flow entrained towards the combustion region.

The complex effects of fuel structure in both the flaming and smouldering combustion phases may necessitate modifications to other common modelling approaches. The widely used Rothermel model under-predicted spread rate for higher bulk density and lower αsδ fuel beds. As previously suggested, an over-sensitivity to fuel bed height was observed, with experimental comparison indicating an under-prediction of reaction intensity at lower fuel heights. These findings have important implications particularly given the continuing widespread use of the Rothermel model, which continues to underpin elements of the BehavePlus fire modelling system and the US National Fire Danger Rating System.

The physical insights, and modelling approaches, developed for this low-intensity, quiescent flame spread scenario, are applicable to common prescribed fire activities. It is hoped that this work (alongside complimentary laboratory and field experiments conducted by various authors as part of a wider multi-agency project (SERDP-RC2641)) will contribute to the emerging field of prescribed fire science, and help to address the pressing need for further development of fire prediction and modelling tools.

# Lay Summary

At the time of writing, wildfires are receiving significant media and public attention. Amidst extreme heating events, and greater global attention upon climate effects, images of devastating fires across the globe have become a regular feature within news reports and columns. This has raised awareness in regions of the world without a significant cultural history of wildland fire and amongst people not previously directly affected by wildfire.

The interested reader may therefore reasonably approach this thesis with a simple question: how will this research help prevent or stop wildfires? The answer to this simple question is markedly complex, even putting aside the usual qualifications and limitations associated with much fundamental scientific research. For a start, in many parts of the world we are actually extremely effective at prevention and suppression of fires. In fact, in many cases, many scientists now argue that we have become too effective at excluding fire from many ecosystems, which historically would have been far more fire-prone.

Consideration of these fire histories (or fire regimes) is important if we want to understand the natural role that fire has played on earth. As a prehistoric force, fire far pre-dates human existence and has played a natural and important ecological role in many ecosystems. Fire can play an important role in the nutrient cycle, while some plant and animal species appear well-adapted to fire-prone environments. For example, seed dispersal in some serotinous pine species can be triggered by fire exposure. Therefore, it is important to understand the resulting ecological effects that will accompany any alteration to existing fire regimes.

Excluding fire from a previously fire-prone region may allow the accumulation of wildland vegetation, which previously may have been consumed by fire at more regular intervals. Since natural vegetation represents the fuel source for a wildland fire, an accumulation of vegetation increases the fuel load available for any fire that does eventually occur. This is important when we consider the major contribution (to total fire damages and loss of life) of the small minority of fires that do escape initial suppression efforts and develop into major large-scale fires, since an increased fuel load will (all else being equal) result in fires of greater intensity.

To address this accumulation of fuel, there are growing calls for increased use of prescribed fire within land management. These deliberately applied fires are typically of low-intensity, and often conducted in calm weather conditions in which greater control (and reduced likelihood of fire escape) can be achieved. These fires are ideally performed with a specific ‘prescription’ in mind, which will specify the desired fire behaviour and burn objectives. This must seek to balance competing objectives such as the consumption and reduction of fuel, alongside protection of important species/habitat and limitation of fire severity to prevent death of selected tree species.

Even where a consensus around greater proactive fire use emerges, barriers to greater prescribed fire activity remain. As in many other fields, the ethical burden (not to mention the legal liability) is often considered far greater in situations involving proactive intervention. Though we may aspire to ‘first do no harm’, how do we respond when the costs of both action and inaction are potentially vast?

The approach inspiring the work in this thesis is that if we wish to task fire agencies and land managers with the difficult task of planning and implementing proactive fire

management strategies, than we must provide them with accurate decision-making tools to inform, support and provide evidence for these plans. Our aspiration within the field of wildland fire science, is the development of accurate wildland fire spread modelling systems. However, as important is the determination and detailing of the limits of both the currently available predictive tools, and of our fundamental knowledge which underpins these. This is the only way in which reasonable expectations may be placed upon those tasked with the stewardship of fire within our natural environments.

This is not a novel proposal, and the development of fire modelling tools has a decades-long history. It is important however to reassess existing modelling tools, and the physical assumptions underpinning these tools, when applied to the novel challenges associated with greater prescribed fire use. The focus of a model intending to predict the growth rate (and required suppression response time) of a wildfire, may differ significantly from a modelling tool which aims to compare the smoke production from a low-intensity prescribed fire with that of a 'worst case' wildfire occurring under extreme weather conditions.

By exploring a low-intensity fire scenario, typical of many prescribed burns, the work in this thesis aims to provide greater insight into the key physical processes controlling the fire behaviour. By exploring a range of vegetation conditions (for litter layers typical of those accumulating because of the shedding of needles and leaves), the effect of fuel structure is investigated. These natural litter layers represent a complex, porous (solid:gas matrix) layer of fuel, and therefore important physical processes must be considered both above and within these fuel layers. By measuring these physical processes during several experimental series, an important dataset has been collected which will allow further testing and development of detailed flame spread models in the future.

In the meantime, the physical insights gained from this thesis were used to evaluate existing modelling tools (of varying complexity). This has highlighted limitations associated with the way in which existing models describe the release and transfer of heat energy, which is driven by the consumption of the vegetation fuel source. Similarly, the way in which existing models describe the subsequent transfer of this heat energy, and the flow of air and combustion gases, has been shown to require further development for the small-scale, litter layer fuels explored in this study.

Fire is a process that can vary greatly across scales, given the different physical phenomena that may occur at different scales. This limitation must be considered when evaluating the applicability of this work, however there is great scientific value in testing our ability even to model the small-scale flame scenarios described in this thesis. However, it is hoped that this thesis will allow greater exploration of these scaling and environmental effects, since the flame spread scenario and fuel types studied deliberately compliment those studied in a related series of field experiments. Indeed the work in this thesis sits within a wider series of multi-scale experiments conducted by authors from multiple institutions, and future comparison across these scales will provide further insight into existing modelling capabilities.

**Previous Publication**

Aspects of the work described in this thesis previously appeared in the following publications:

- Z. Campbell-Lochrie, C. Walker-Ravena, M. Gallagher, N. Skowronski, E.V. Mueller, & R.M. Hadden. Investigation of the role of bulk properties and in-bed structure in the flow regime of buoyancy-dominated flame spread in porous fuel beds. Fire Safety Journal, (2021). 120, 103035

- Z. Campbell-Lochrie, C Walker-Ravena, E.V. Mueller, R.M. Hadden, The effect of interstitial flow on the burning dynamics of porous fuel beds. Advances in Forest Fire Research 2018. Coimbra, Portugal, Nov 2018. doi.org/10.14195/978-989-26-16-506_72

- E.V. Mueller, Z. Campbell-Lochrie, W. Mell, R.M. Hadden, Numerical simulation of low-intensity fire spread in pine litter. Advances in Forest Fire Research 2018. Coimbra, Portugal, 9-16 Nov 2018. doi.org/10.14195/978-989-26-16-506_162

# Acknowledgements

This work would not have been possible without the help, support and guidance of so many people. Joining the Edinburgh Fire Research Centre has been like joining an additional family and I will always be grateful for the many amazing experiences throughout my time in the group and especially for the friendships with my kind and talented colleagues.

A huge thanks to Rory for introducing me to this second family and to the world of fire more generally. I could not have asked for a more supportive and enthusiastic supervisor and I really appreciate all the opportunities you've provided me with and the guidance and support you continue to offer.

Thanks to Eric, Chris and Simon for welcoming me to the group and helping me to navigate my way into the world of wildfires, I will always look up to you all. Thanks to Simone and Bhisham for joining us on the journey and adding insight and laughs in equal measure. My very first steps in the PhD were made alongside Carlos and I'm so pleased we've both made it to the finish line.

The opportunity to be involved in large-scale experiments and fires has been an enormous privilege and a great learning experience, while the many great times in New Jersey will live long in the memory. Thanks to Mike, Nick, Ken, Lexi, Matt and Jason for passing on your expertise and always offering a warm welcome to the Pine Barrens, and to the New Jersey Forest Fire Service for facilitating these larger experiments. I hope the work in this thesis can compliment these large-scale experiments and contribute in some small way to the important work you do.

A massive thanks to the entire fire group family, along with the 'non-fire' members of the John Muir family. Every one of you makes this such a special place to be and are the reason that I walked into work every single day with a giant smile on my face. Thanks also to Felix and Delia for a welcoming home away from my official residence in John Muir 1.4.

Finally, to my family for their love, support and kindness across all these years, I am and always will be more grateful than you can ever know.

# Contents

# List of Figures

# List of Tables

# Chapter 1

## Introduction

# 1. Introduction

*Is that not the Promethean fable, that the fire stolen from the gods will light men their way even while it burns their hands?*

***Zia Haider Rahman, In Light of What We Know [1]***

A growing consensus has emerged around the need for greater prescribed fire use within many ecosystems [2]. This focus on proactive fire use challenges many historical land management approaches in the U.S.A., which often prioritised fire prevention and suppression. Drawing heavily on existing European forestry approaches [3], these suppression efforts often prioritised the protection of valuable natural resources such as timber plantations.

The birth of key U.S. land management agencies (such as the U.S. Forest Service) coincided with a series of destructive fires in the early 20$^{th}$ Century (e.g. The Big Blowup of 1910) [4]. These 'mega-fires' arguably contributed greatly to the culture of fire exclusion that would come to dominate policy approaches within these organisations. This culminated in aggressive suppression efforts such as the 10 a.m. policy (requiring all reported fires to be under control by 10 a.m. the next morning) [5].

Two major issues emerged during this era of ambitious fire suppression. Firstly, it was impossible to prevent or rapidly contain all fires, with the small number of uncontrolled fires dominating overall damage costs [6]. Secondly, the natural fire regimes in many previously fire-prone regions were altered, allowing greater accumulation of wildland fuels.

Greater prescribed fire use has been widely heralded as a possible solution to these issues, but a strong scientific knowledge base will be required to allow the transition towards this greater proactive fire use [2,7]. As in other areas, the evidential burden and the responsibility to avoid harm, is particularly acute when such proactive action is taken. To ease the burden on fire agencies and land managers, the development of predictive tools is required to support planning and implementation of fire prescriptions. However, despite decades of wildland fire research, some long identified gaps remain in our fundamental understanding of wildland flame spread that continue to hinder these development efforts.

## 1.1. Wildland Flame Spread: Progress & Understanding

*The problems of fire are only in part the technical problems of prevention, detection, and extinguishment. They also cut deeply into the social and political fabric of the nation and raise important questions of management, organization, and economics.*

***The Committee on Fire Research, 1961 [8]***

The current need for continued, physics-based investigation of fire behaviour has long been recognised, and in 1961 led the Committee on Fire Research to propose a new research agenda to tackle the 'fire problem' [8]. The committee was convened by the National Academy of Sciences in 1955, at the behest of the Federal Civil Defense Administration [9], who were increasingly concerned by the fire risks presented by nuclear weapons [10]. The committee

brought together practitioners and academics from various fields in a desire to gain a holistic overview of the 'fire problem', and to provide advice on the establishment of a 'mass fires' research agenda [11].

This agenda [11] called for greater emphasis on fundamental research across four main categories: Laboratory-Based, Field-Based, Operations Research and Ad-Hoc Developments. The drive for greater fundamental research was informed by a belief that the vast post-war progress made in several key scientific disciplines (Physical Chemistry, Fluid Mechanics, Mathematics, Computational Methods) had not been translated into significant progress within fire science.

The committee highlighted the widespread adoption of relative forest fire danger indices, which had proven to be useful 'guides' in a routine fire management context. These indices allowed the ignition potential and the likely fire spread potential to be considered in parallel, while including consideration of the fuel, topography and weather conditions in the area of interest. The accuracy of these methods was limited by the precision of the sampling and weather prediction methods, therefore the performance of these metrics was often poor [8]. To allow proper evaluation of relative fire danger, physically informed models for fire ignition and growth were required, however, efforts to model the physical phenomena of fire were in their infancy.

A fire model, fit for operational use, was also required to inform initial attack resources, and appropriation of re-enforcement resources. If such a model was also able to predict the fire response to different suppression techniques, then this would also allow more effective planning of control efforts for more severe, 'non-routine' fires. The design of such models could be informed by the controlled burning of forested areas, in an effort to investigate the effect of suppression techniques and pre-fire planning efforts. Along with statistical data and fundamental insight into combustion phenomena, this would allow the construction of simple models for aspects of fire suppression.

A greater quantitative understanding of the governing variables of fire spread were required, especially in describing and understanding the effects of fuel structure. To aid these efforts, better measurement approaches for fire spread properties were necessary, including increased understanding of Fuel Moisture Content (FMC) effects, along with a better understanding of smouldering combustion. Overall, improved methods for characterising fuel properties were required, along with a greater understanding of the effect of fuel properties on fire behaviour. Many of these research needs continue to represent outstanding research questions, and are frequently identified as current research priorities, despite several decades of research after the publication of the committee's reports.

Following the committee's recommendations, the Office of Civil and Defense Mobilization provided funding to the US Forest Service to supplement existing fire modelling research [9]. This funding supported Project Fire Model [12–14], a detailed series of experiments involving flame spread through wood cribs. These cribs provided a 'diagnostic model' allowing the effects of various properties on the fire behaviour to be systematically investigated; alongside efforts to define simple formulations to predict fire behaviour e.g. rate of spread. This study represented a significant early contribution to the detailed, systematic study of model fuel beds, and a direct lineage can easily be drawn from this pioneering work to many of the modelling systems in operation presently (e.g. Rothermel's model).

In the 60 years since the committee's reports, and the launch of Project Fire Model, a large number of laboratory and field experiments have been conducted, resulting in significant advances in our physical understanding and modelling efforts. Yet in 2019, the need for further research on the 'Fundamentals of wildland fire ignition and spread' was again identified as a research priority in the 2030 Agenda of the International Association of Fire Safety Science (IAFSS) [15]. Similarly, the SFPE Research Roadmap [16] (first published in 2017) also identified a need for further data on wildland fire behaviour and fire spread, and for continued development of wildland fire modelling and fire behaviour prediction tools. This need for greater development of 'decision-support' tools for land managers (and the development of underpinning fire science knowledge) was also identified as a research priority within the U.S. Geological Surveys Wildland Fire Science 2021-2026 Strategic Plan [17].

Over recent decades, fire spread models of varying complexity have been proposed for a variety of wildland flame spread scenarios. Various authors have however, suggested that current tools continue to be hindered by knowledge gaps around fire behaviour, and the underlying physical phenomena that control wildland flame spread [18,19]. Older models, developed during research efforts focused towards suppression and fire control, may not adequately support present-day fire management priorities, given the increased prominence (particularly post-introduction of the 1995 Wildland Fire Management Policy [20]) of prescribed burning.

In existing physically informed models, in which the controlling heat transfer mechanisms are explicitly considered, the underlying assumptions vary widely. Finney *et al.* [19] discussed these discrepancies and suggested that these highlight the lack of a logical, coherent theory for wildland fire spread. This is in contrast to some other areas of fire science, with well-developed theories existing for flame spread across the surface of a solid [21,22].

It has also been suggested that existing models, developed for wildland fires, may lack applicability to prescribed fire scenarios, despite the increasing prominence of active fire management [2,23]. Hiers *et al*. [2] called for an increased and distinct focus on 'prescribed fire science', identifying fuels characterization (and the effect of fuel on fire behaviour across various spatial scales) as a key research priority within this new field. Whether or not it is accepted that this merits the designation of a distinct research field, it is clear that this shift in focus will challenge existing frameworks and operational models. Where, as in this thesis, a fundamental physical approach is taken, then insights gained may benefit all areas of wildland fire science by improving our ability to describe and predict key physical processes such as flame spread. A growing emphasis on prescribed fire (along with actively managed wildfires) underlies the importance of sufficiently accurate fire behaviour prediction in order to provide the basis for studies of fire effects and emissions.

Alongside these management challenges, the current research requirements exist amidst a backdrop of increasing Wildland Urban Interface (WUI) development, and the pressing effects of climate change (as detailed in the 6$^{th}$ Assessment Report of the Intergovernmental Panel on Climate Change [24]) which may result in increased drought pressure and fire weather severity in many regions [25–31]. These key drivers are reflected in the two Societal Grand Challenges for fire research identified in the 2030 Agenda of the International Association of Fire Safety Science (IAFSS) [15]. The first of which concerns 'Climate change, resiliency and sustainability' and the latter 'Population growth, urbanization and globalization', with wildland fire research identified as a critical research area for both challenges. A number of other drivers

of fire behaviour research are discussed in several excellent recent reviews [18,32,33], but the nascent field of 'prescribed fire science' also faces unique research drivers.

## 1.1. Emergence of (Prescribed) Fire Science

The Fire Research Committee drew a distinction between 'urban' fires, and 'forest' fires occurring in a natural environment [8]. These 'forest' fires can then be further sub-divided by forest type and regional climatic conditions. As we may have an interest in other (non-forested) natural environments, we can also use the alternative term 'wildland fire'. A term so broad, that it is impossible to succinctly discuss the physical behaviour of wildfires in general terms. This breadth is reflected in the extensive and wide-ranging existing literature in wildland fire science [18,32–34]. The focus and intent of past studies varies greatly, with past authors from a range of disciplines investigating topics as diverse as fire behaviour; ecological effects of fire; fire-weather interactions; smoke production and emissions; economic impacts; and evacuation.

The Committee on Fire Research were particularly interested in mass fires, situated as they were within the emerging nuclear era. Research at that time was primarily motivated by fire control efforts, alongside occasional exploration of the weaponisation of mass fires. Reviewing the committee records from this era through a modern lens reveals a noticeable lack of consideration of proactive prescribed fire use, even if limited proactive firefighting methods such as backfiring[1] were active research areas.

People play an important role in the wildland fire problem, whether through arson, accidental ignition, or through deliberate application of prescribed burns. In 1959, when the Committee on Fire Research was examining forest fires in the USA, 90 % were attributed to human causes, with around half occurring as a result of 'carelessness' e.g. trash fires, camping fires, discarded cigarettes [8]. In terms of more controlled applications of fire, The Committee on Fire Research makes no mention of the use of prescribed fire, as part of a proactive vegetation management or ecological plan.

The committee's major response to potential 'blow-up' fires was to expend greater initial-attack resources to more effectively suppress these fires (and the necessary research to enable identification of their likely occurrence), which otherwise, when fully developed, may be uncontrollable by available suppression resources. While the benefit of long-range planning (including inventorying of fuels, topography and resources) and land management activities (fuel clean-up, logging slash disposal, firebreak construction) were highlighted, the potential for prescribed fire use was not discussed. In the present day, the failure of heavily suppression focused fire strategies has been exposed, with 1 % of the largest, 'uncontrollable' fires accounting for between 80 to 96 % of the area burned annually in the U.S. [6].

Recently, there have been increasing calls for a more dedicated focus on prescribed fire science [2], involving fundamental research to support the growing application of prescribed fire. While forest fire science has, from an early stage, often had a focus on the rate of fire spread, the earliest studies often had fire control as their chief motivation [35,36], and drew largely from the observation of major natural fires. Necessarily, these observation studies were

[1] A backfire is a deliberately ignited fireline, set ahead of the main fire front, and designed to remove fuel ahead of the approaching flame front.

typically ad-hoc in nature, and therefore measurements of fuel properties, environmental conditions and fire behaviour were limited.

Other early studies, such as those by Curry and Fons [37], observed the growth of smaller fires from point ignition sources. In many respects, this heralded the emergence of the formal field of wildfire science, allowing the effect of fuel manipulation, along with variations in weather and terrain to be explored [37,38]. However, the lack of control in this field environment often precluded the isolation and systematic study of individual variables. Inventorying and suitably describing the fuel properties in these environments represented an additional impediment to scientific progress.

Within the U.S., these pioneering studies were followed by the development of fire danger rating systems [35], which would later incorporate semi-empirical models (such as the now ubiquitous Rothermel model). These early mathematical models demonstrated the significant practical benefits that can be gained from systematic laboratory-based investigation, supported by field observations for phenomena that could not be realistically recreated at the laboratory scale. However, while the use of these models remains widespread, few adaptations or improvements have typically been incorporated into these fire behaviour models despite the changing motivations and objectives within the wildland fire community.

A number of complimentary models have been added to many fire modelling systems, building on from the fire behaviour models. For example, estimates of fire intensity and flame height can be used to predict scorch heights, a potentially important consideration for those interested in fire effects or economic analysis of fire. The need for additional models will only grow as prescribed fire use intensifies. While where fires are deliberately applied, there will be a greater need for *a priori* evaluation of fire effects, smoke / emissions production and economic impacts. It is important that the development of underlying fire behaviour models keep pace with these demands, and that the applicability of these behaviour models within specific fire scenarios is subject to continual evaluation.

Even within a single fire scenario, the fire behaviour in a crown fire may differ greatly from that observed in a shrub fire, which itself may look entirely different to the fire behaviour observed in a surface fire through the litter layer. So any effort to develop quantitative analyses of wildland flame must necessarily be preceded by a qualitative description of the scenario of interest [8]. The Committee on Fire Research expressed a need to develop the scientific basis to allow us to move from these qualitative ‘essay[s] about the type of fuel found in a forest’ to ‘a set of numbers’ which quantitatively describes the fuel in a physically meaningful manner. The significance of fuel effects may be greater in the low-intensity flame spread scenarios typically encountered in prescribed burns, which are often conducted in less extreme weather conditions. Therefore, incorporating the effects of fuel structure will represent an important challenge within model development for low-intensity flame spread scenarios.

## 1.2. Fundamental Research Challenges in Flame Spread Modelling

A particular feature of fire problems, that separates them from combustion problems, in which the fuel rate is constant or altered deliberately, is the heating feedback effect on fuel supply [39]. The characteristic convective mechanisms within fire problems differs from the more well-understood cases involving non-reacting systems, [8] with the additional considerations of eddy transport of both flame and fuel mixtures, as well as the occurrence of fire-induced flows. Therefore, for several decades, a need for further study in areas which had previously

been of limited relevance to combustion research efforts has been noted including: Heat Release Rate (HRR) at normal atmospheric conditions and the resulting buoyant and induced flow profiles, ignition and pyrolysis behaviour, and the identification of dominant heat transfer mechanisms [39].

Developing a coherent theory of wildland flame spread, and developing representative models, is far from trivial. Many of the important mechanisms involved present distinct challenges compared to other areas of fire research. The complex, porous nature of wildland fuels makes them difficult to quantitatively describe (particularly at the field-scale) and requires the consideration of in-depth flow regimes and additional in-depth heat transfer mechanisms, that do not occur in solid surface flame spread. Efforts to understand the feedback effect between fuel structure, HRR and the resulting flow profiles occurring in porous wildland flame spread must also consider convection, radiation, and fire-induced flows within the porous fuel structure e.g. within a pine needle litter layer. All of which complicates efforts to develop physics-based models of wildland flame spread.

Even as the most recent generation of Computational Fluid Dynamics (CFD) based, multi-phase models are being developed, there remains a need for greater experimental development and validation of the sub-models being incorporated into these models [18,34]. Mueller [18] highlighted a historical lack of measurements of key physical properties of flame spread phenomena, required for 'measurement-driven model development', despite our current lack of understanding of the key physical phenomena controlling wildland flame spread [19].

In the early stages of the experimental work described in this thesis, clear discrepancies were apparent between experimental observations of flame spread behaviour and the predictions of current physics-based models. Mueller *et al*. [40] presented numerical simulations (using the Wildland Fire Dynamics Simulator (WFDS)) of a small number of the early flame spread experiments conducted in this study, as illustrated in Figure 1.1. Model predictions of extinction did not represent the sustained flame spread observed experimentally at the fuel bed conditions of interest.

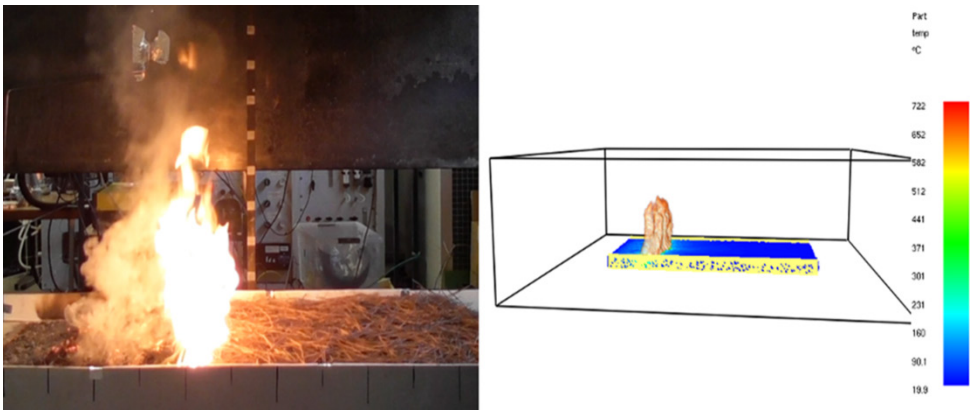


**Figure 1.1 - Illustration of the comparison between laboratory flame spread experiments and the Wildland Fire Dynamics Simulator (WFDS) numerical simulations conducted by Mueller *et al.*** [40] **simulating preliminary experiments conducted in this study. Extracted from Mueller *et al.* (2018)** [40]

This poor model performance provided clear motivation for continued experimental investigation of the physical mechanisms controlling flame spread at this scale. In particular,

it emphasised the need for further physical measurements as a function of fuel bed structure, in order to aid the development of sub-models and improve model accuracy.

A particular focus is required on experimental data supporting the development and assessment of sub-models describing the drag profile and convective heating within a porous fuel matrix [18,41]. Research needs within this area were already identified as a priority back in the era of the Committee on Fire Research. They highlighted a lack of either qualitative or quantitative knowledge of the key fluid flow profiles associated with a fire (buoyant plume and resulting fire induced flow), and the additional factors which affect the buoyant flow (e.g. ambient wind, topography, turbulence) and entrained flow profiles (e.g. gas expansion as a result of combustion) [11,39].

Additionally, improved modelling approaches are required for the smouldering combustion region behind the main flame front. Current models often neglect char oxidation and smouldering in this region despite the potentially significant influence of this combustion phase, particularly in opposed flow or downslope flame spread, or at higher FMC values [18,41]. Even where energy released in this smouldering region does not contribute significantly to the propagation energy, it is important that fuel decomposition, and associated physical changes, are adequately described if the drag effects of the remaining fuel structure are to be modelled. Where only smouldering combustion occurs there remains the potential for transition to flaming combustion to occur, and regardless the role of smouldering combustion on the resulting fire effects requires consideration [42].

Similarly, the smouldering combustion region is not considered in many semi-physical models (e.g. the widely-used Rothermel model [43]). While in some scenarios the heat transfer from this region may not significantly affect flame propagation, characterising combustion in this region is important in aiding the prediction of fuel consumption and emissions, or the heat output (and resulting ecological effects). In other flame spread scenarios (e.g. quiescent or opposed flow flame spread), the contribution from this region may be more significant given a reduction in flame heating.

For simplified physics-based models of porous flame spread, there remains disagreement over the dominant heat transfer mechanisms. For example, some authors, have proposed flame spread models in which pre-heating occurred only via radiative heating, with convection ignored or considered only as a cooling term [44,45], while a limited number of models allow for a scenario in which convective heating can dominate [46,47]. Physically meaningful descriptors of fuel complexes are also required if the convective and radiative heat transfer is to be understood. It is not always clear, in advance, what form these descriptors should take, while different problems may require structural descriptions at different scales.

The Committee on Fire Research identified several key fuel parameters in wildland flame spread: fuel distribution (fine fuel loading), available surface area for radiative absorption [8], bulk density. However, the link between many of these existing terms and the controlling flame spread mechanisms is often unclear. Therefore, efforts have been made to derive other dimensionless terms, informed by our understanding of the important physical phenomena. However, there remains a need to compare and consolidate findings from various types of model fuel beds, and to undertake greater measurement of the effect of fuel structure on key physical properties.

Future modelling efforts require both additional laboratory and field measurements of temperatures, flow profiles and heat fluxes both above and within porous fuel beds. In the laboratory, specific physical phenomena can be isolated and investigated in detail, such as the effect of fuel bed structure on the heat transfer to the fuel bed [18]. While a number of existing laboratory-based flame spread experiments have previously been undertaken, new studies can provide, in addition to greater measurement of physical properties, a substantial focus on pressing (but previously neglected) research areas such as smouldering combustion, fuel consumption and emissions, as required by modern practitioners.

## 1.3. The Challenge Ahead

While technology will continue to provide new methods of ignition prevention and detection, the extraordinarily successful fire suppression efforts over recent decades in the USA have presented new challenges. The accumulation of fuels, in areas previously host to fire at regular intervals, is one of the factors highlighted as a major contributor to recent 'megafires' of record size and intensity [48]. This has resulted in increased calls for fuel reduction treatments [30,49,50] which can reduce the build-up of surface fuels [51]. Future model developments are required to improve our ability to plan fuel treatments in order to achieve the desired fire behaviour and management objectives (e.g. fuel reduction).

If the challenge is not to hide ignition but where possible, to wield it proactively in our favour, then we must continue to step up to this challenge amidst uncertain times. Prescribed fire operations will neither be guaranteed, nor deserving, of unquestioning public, financial and political support. Climate and ecological impact assessment will rightly be demanded, as fire strategies are implemented within a global ecosystem geared towards meeting ambitious sustainable development goals and climate targets within the next ten to thirty years. Businesses and homeowners will seek guarantees that fire programs are in the public good and meet the interests of their communities. Past environmental aggressions live long in the memory, particularly among marginalised or vulnerable communities.

Yet amidst all these challenges, with a little imagination, there exists a better future. With the continuing hard work and diligence of workers in this and related fields, and in co-operation with wider society, we may yet realise this dream. It is my hope that the work described in this thesis may contribute in some small way to its realisation.

## 1.4. Thesis Objectives

**Overall Aim**

To evaluate and describe the effect of fuel bed structure on the flame spread processes in natural porous fuel beds.

**Supporting Objectives**

The key objectives of this work are based on the previously discussed gaps in existing work, and the pressing research needs identified by various authors and organisations. While the overarching focus is on expanding our understanding of the physical phenomena, controlling porous flame spread in the previously described flame spread scenario. This overall aim encompasses a number of specific objectives covered by this thesis:

- Provide a detailed review of the effects of porous fuel bed structure on the fire behaviour and the underlying physical phenomena, along with a review of relevant flame spread models for both porous and solid fuels.

- Systematically investigate the effect of fuel bed structure (fuel loading, bulk density, fuel bed height) on fire behaviour (flame spread rate, flame height, burning rate).

- Assess the applicability of common structural descriptors of natural porous fuel beds (fuel loading, bulk density, porosity) as predictors of fire behaviour, and consider alternative dimensionless parameters with greater physical relevance.

- Investigate the feedback loop between fuel structure, heat release rate, and the resulting buoyant fire-induced flow profiles, at a range of fuel bed conditions.

- Determine the dominant heat transfer mechanisms in opposed flow flame spread through porous fuel beds, and the effect of fuel bed structure on the relative importance of the heat transfer mechanisms.

- Assess the applicability of existing thermal models (developed for solid surface flame spread) to porous flame spread scenarios.

- Investigate the possible over-sensitivity of the Rothermel flame spread model to fuel bed height, for cases involving matt-type (pine needle) fuel beds.

- Assess the existing approaches to heat transfer sub-modelling within existing simplified physics-based models.

## 1.5. Thesis Outline

In addressing these aims and objectives, the thesis has been structured as follows:

- **Chapter 2 – Literature Review**

  Relevant literature is discussed covering two areas of focus. Initially, this covers broad aspects of flame spread theory and the limits of applicability of existing solid surface flame spread theories. Various areas of porous flame spread theory for which further comparison with detailed, experimental datasets is required are identified. Secondly, existing uses of model fuel beds (natural and 'artificial') in wildland flame spread studies are discussed. This highlights previously observed effects of fuel structure on the overall fire behaviour, and, where available, the effects on underlying physical mechanisms. Along with a discussion of existing structural fuel descriptors, this review highlights the need for continued development of physically meaningful fuel bed parameters.

- **Chapter 3 – Methods**

  A collected summary of the key experimental methods and apparatus used in this thesis. Covers the methodology associated with fuel collection and characterisation; fire behaviour measurements; and the measurement of physical properties (flow, heat

transfer, gas and solid phase temperatures, energy release rates). While the flame spread table, upon which the majority of the experimental work in this thesis was conducted, is described in detail.

- **Chapter 4 – Low-Intensity Flame Spread – Role of Fuel Properties**

An overview of fire behaviour measurements is presented for a series of laboratory-based flame spread studies in pine needle and/or oak leaf fuel beds. To provide a benchmark, these fuel beds were constructed to match the structural conditions of natural fuel beds sampled in an area of the New Jersey Pinelands National Reserve. The effect of various fuel manipulations (compaction, additional fuel accumulation, fuel mixes) on the overall fire behaviour is assessed. Observations are compared with the existing literature and can be compared with findings from complimentary research from the wider project (SERDP RC-2641). The limits of existing fuel bed structural descriptors are identified, along with a discussion of limitations associated with the model fuel beds and experimental design.

- **Chapter 5 – Flow in Porous Fuel Beds**

The effect on fire behaviour of isolated fuel bed structural parameters was analysed further via an additional systematic series of laboratory-based flame spread experiments. Given the limitations of existing structural parameters, an alternative dimensionless parameter $\alpha\sigma\delta$ is proposed, and the strong correlation with spread rate is discussed. The development of this dimensionless term (incorporating fuel bed porosity ($\alpha$), surface-to-volume ratio ($\sigma$), and fuel bed height ($\delta$)), and its relationship with similar previously proposed parameters is discussed in detail. Given the importance of the fuel bed porosity, detailed measurements of the flow regimes both within and above the fuel bed are analysed. The effects of fuel structure on both the buoyant flow and buoyancy-induced entrainment flow are discussed, along with the implications for oxygen supply and convective heating within the combustion region.

- **Chapter 6 – Heat Transfer in Porous Fuel Beds**

An important first step in the development of any flame spread theory is the identification of the dominant heat transfer mechanisms. Therefore, in this chapter, detailed measurements of the (radiant and total) heat flux both within and above the fuel bed are analysed for an additional series of laboratory-based flame spread studies. The dominance of the horizontal, in-bed heat transfer, particularly for fuel beds with lower $\alpha\sigma\delta$ values, is discussed, along with the increasing heating contribution of the above-bed flame at higher $\alpha\sigma\delta$ values. These measurements of heat flux and effective heating distance are used to assess the suitability of a simple thermal model (adapted from solid surface flame spread theory) via comparison with experimentally observed spread rates.

- **Chapter 7 – Applicability of the Rothermel Model**

Previous suggestions that the Rothermel flame spread model may be over-sensitive to fuel bed height are discussed and evaluated. A comparison of predicted and experimentally observed spread rates is presented for various fuel bed structural conditions, allowing the independent effects on fuel height of both the fuel loading and bulk density to be investigated. Possible mathematical and physical explanations for under-predictions of spread rates at higher bulk density and lower $\alpha\sigma\delta$ values are discussed, with previously presented measurements of physical properties allowing greater examination of the effects of fuel structure on intermediate model values (e.g. reaction intensity, reaction velocity).

- **Chapter 8 – Implications for Simplified Physics-Based Models**

Key assumptions and theoretical frameworks underpinning existing simplified physics-based porous flame spread models are discussed. The applicability of these formulations and assumptions for key physical mechanisms (ember radiation, fuel bed radiative attenuation, above-bed flame radiation) are examined via comparison with the measurements of physical properties presented in previous chapters. The selection of appropriate sub-models for future simplified physics-based models, and areas requiring further experimental research, are discussed.

- **Chapter 9 - Conclusions**

In this final chapter, the key findings of this work are discussed in greater detail. The implications for existing research and operational flame spread models are discussed, along with consideration of the implications for broader wildland fire science applications. Suggested areas of future research in order to support the continuing development of empirical, semi-empirical and physical models are presented. The value of model fuel bed experiments generally, and more specifically the measurements of physical properties presented in this thesis, in aiding the ongoing development of modelling tools is outlined.

# Chapter 2

## Literature Review

# 2. Literature Review

*'The ignition of one leaf by its neighbor, the fluctuation of a flame in the forest, wind turbulence, the hot gases rising from the brush to dry and ignite the crowns, the falling of burning embers into unignited fuel, ignition by radiation from flames and embers, the flashover of combustible vapors pyrolized from irradiated fuel all play their separate and interrelated parts. If the location of every leaf in the forest must be specified in order to calculate quantitatively the effect of every one of the above mechanisms of ignition, the fire-spread problem is indeed a hopeless one.'*

***Howard Emmons – Fire in the Forest, 1963*** [52]

## 2.1. Introduction

A key characteristic of wildland flame spread is the involvement of porous fuel matrices such as forest litter layers. In many ecosystems, the litter layer is a significant contributor to surface flame spread. Depending on the dominant vegetation, this fuel layer can be formed by an accumulation of fallen, dead needles, leaves, and woody debris from the above ground shrub, mid-level and canopy fuels. For many prescribed burns, a key objective is the reduction of this surface fuel accumulation in order to reduce the intensity of any future fire and/or to achieve specific ecological objectives [7].

Accurately predicting flame spread and fire behaviour through these natural porous fuel beds is therefore an important priority within prescribed fire science. Yet a coherent theoretical understanding of wildland flame spread, through porous natural fuels, still eludes us [19]. This is despite major advances in other areas of fire science, which have resulted in well-developed theories for flame spread over solid fuels [21,53]. An important focus of this thesis is the assessment of the limitations of these existing solid surface flame spread theories, and the identification of the key physical phenomena associated with porous flame spread that require further investigation, particularly in low-intensity scenarios relevant to prescribed burning.

Detailed reviews of existing opposed flow flame spread theories are available [54], however many of these existing models were developed for a scenario involving flame spread across the surface of a continuous solid. Wildland flame spread represents a specific theoretical and modelling challenge given the discontinuous, porous nature of most wildland fuels. This difference in structural properties is illustrated in Figure 2.1, and requires the consideration of a number of additional physical phenomena as summarised in Figure 2.2, and discussed in detail within this chapter.

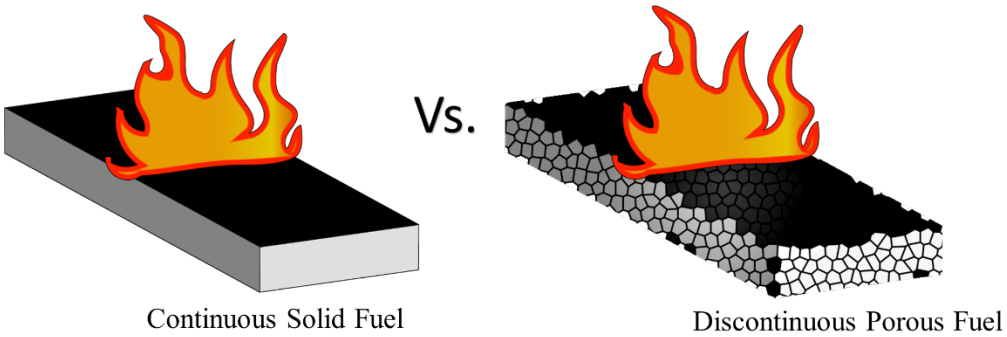


**Figure 2.1 - Illustration of the difference between continuous and discontinuous (porous) fuels typical of wildland fuel beds**

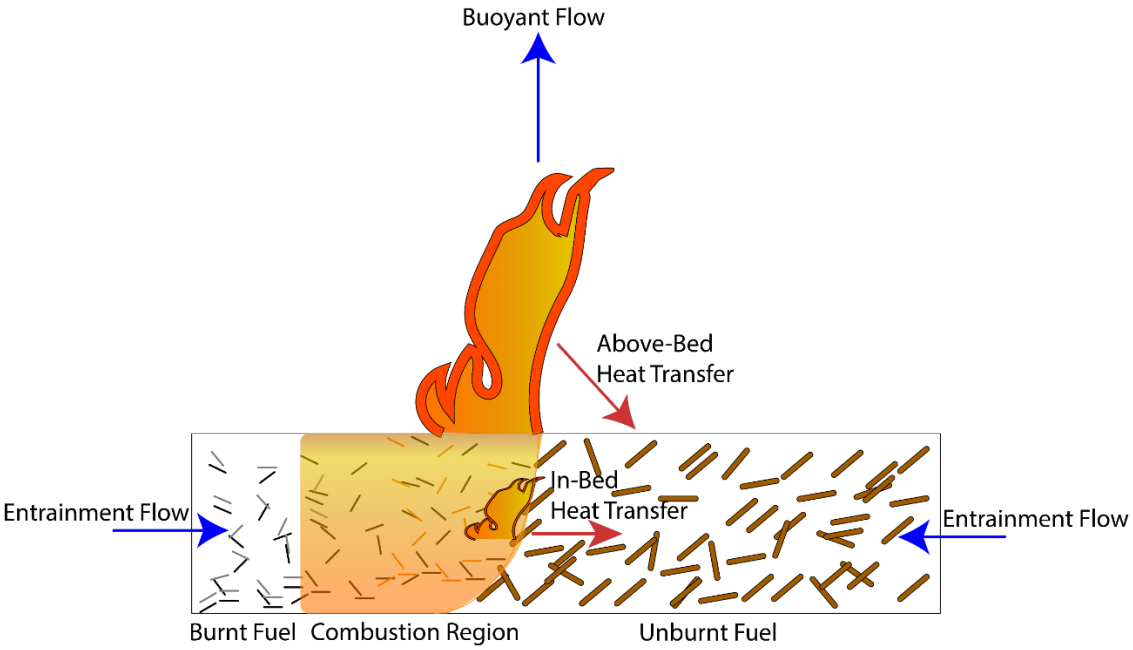


**Figure 2.2 - Illustration of the key physical mechanisms involved in porous flame spread**

As illustrated in Figure 2.2, porous flame spread involves a complex mix of interacting physical mechanisms. While the buoyant flow above the combustion region is present in both solid and porous flame spread, for porous fuels the resulting fire-induced flow also travels through the fuel bed. The drag forces exerted by the porous fuel matrix therefore affect the flow profile, while the convective heating or cooling of fuel elements by this in-bed flow must also be considered. For continuous solids, in-depth heat transfer is primarily via conduction [22], whereas in a porous fuel, the conductivity is typically significantly lower, and both convective and radiative heating (between fuel elements) can be significant. Both flaming and smouldering combustion may occur within the porous fuel bed (in addition to the above-bed flame) which complicates efforts to understand the heat transfer and combustion processes [55].

The condition and construction of the fuel bed will also affect the flame spread behaviour [56,57]. These effects can occur at various scales from the properties of individual fuel elements to the effect of fuel bed structure (fuel loading, bulk density). Given the wide variety of vegetation that can contribute to wildland flame spread, the potential fuel types are extensive.

Typically, at the laboratory-scale, the role of fuel bed properties has been investigated using model fuel beds constructed from either natural wildland fuels, or 'artificial' engineered materials. A number of artificial fuel beds have been used by past authors (including vertical stick arrays [58–60], excelsior [43,58,60–71], newspaper [61], laser-cut cardboard [72], and wood cribs [14,73–75]). Generally, these artificial fuel beds can allow even greater control and manipulation of fuel structure but represent an abstraction from natural fuels. However, it is not guaranteed that natural fuel beds will accurately represent natural wildland environments either, with significant variations in fuel structure, and resulting fire behaviour, often emerging unless the sampling and/or reconstruction methods are carefully controlled [56,57].

The limitations of natural fuel beds, and the desirable characteristics of an artificial fuel bed, were discussed in the 1963 thesis of P.J. Murphy [68], which reviewed existing artificial fuel

bed studies. A detailed review of later artificial fuel bed studies (post-1963) does not appear to exist (although McAllister and colleagues have discussed the relevance of existing wood crib studies to wildland flame spread [74,76,77]). Therefore, a review of artificial fuel beds is provided in this chapter, including discussion of the limitations of each fuel type, and the potential applicability of physical theories between various artificial and natural fuel beds.

Within different ecosystems and regions, dominant species will exist, and major contributors to wildland flame spread can be identified. This can be used to inform the selection of fuel species in a study involving natural fuels. Even for a single fuel species, the combustion behaviour can vary significantly with fuel condition, sampling location, and depending on the fuel component tested [32]. The majority of experiments in this study are conducted using fuel beds constructed from pine needles, and representing a forest litter layer. By limiting the focus to a single flame spread scenario, the effect of fuel bed structure (on the flame spread and fire behaviour) can be explored in detail for the model (pine needle) fuel beds studied in this thesis.

The flame spread scenario studied in this thesis will now be outlined. This allows an understanding of the important physical phenomena to be gained, while also highlighting which potential variables have been controlled during this study. Relevant aspects of existing flame spread theory are subsequently reviewed, with particular areas highlighted in which solid surface flame spread theory cannot be simply applied to porous fuels. This discussion, along with a detailed review of the model fuel beds used in past studies, then informs the selection of a number of existing fuel bed properties that may be particularly relevant within porous flame spread.

The development of wildland fire science has been a global effort, however much of the literature discussed in this section was conducted in the United States. There are both pragmatic and conceptual reasons for this US-centric focus but this does not seek to discount the contributions of authors from other regions. The work described in this thesis sits within a wider project, funded by the U.S. Department of Defense (DoD), which ultimately aims to support the continuing use of prescribed fire on DoD facilities across the eastern United States. This region has seen significant fire research over recent decades, while other areas of the United States also provide studies within similar ecosystems and fuel types, which allow close comparison with the work described in this thesis. Additionally, unlike some other fire research intensive countries, the United States has incorporated physically-inspired modelling systems into existing operational frameworks rather than following a primarily empirically-led approach, and this more closely aligns with the conceptual approach used to inform the work in this thesis.

## 2.2. Flame Spread Scenario

The safe and effective use of prescribed burning requires accurate prediction of fire behaviour and fuel consumption. If predictive tools are to be further developed then this must include an understanding of how key physical mechanisms controlling flame spread (such as heat transfer and flow dynamics) are affected by fuel structure. These physical phenomena can be studied in a variety of environments, but there remains a role for the continuing use of laboratory-based, flame spread experiments, involving model fuel beds in which the structure can be more straightforwardly described and systematically manipulated.

Simeoni [34] provided a thorough introduction to fire behaviour experimentation, defining five different experimental scales, ranging in scale from microscopic testing to observations of

uncontrolled wildfires. A similar categorisation of experiments will be used in this study, as shown in Figure 2.3.

Laboratory experiments can include both static fires (as shown in Figure 2.4) and dynamic spreading fires (as shown in Figure 2.5). While this study focuses on an extensive series of spreading fires, there is still much that can be learned from comparison with existing static fire studies. Therefore relevant static fire studies are reviewed in this chapter, especially those involving crib fires. These stationary crib fire studies are particularly relevant since they commonly involve a porosity factor (to describe the burning rate) which is similar to the approach taken in Chapter 5, where a dimensionless structural parameter is introduced to describe the natural fuel beds in this study.

**Material Scale Experiments**
**[TGA Experiments.]**
**Photo by C. Walker-Ravena**

**Static Bench-Scale Experiments**
**[Cone Calorimeter Testing]**

**Dynamic Laboratory Experiments**
**[Described in this study]**

**Small-Scale Field Experiments**
**[10 m x 10 m burn conducted as part of wider SERDP RC-2641 project]**

**Large-Scale Experimental or Observational Studies**
**[Large controlled fire experiment conducted during JFSP Project #15-01-04-55]**

**Figure 2.3 – Categorisation of fire behaviour experiments**

**Figure 2.4 – Exemplar static fire involving forest fuel debris**

Additional complexity is however introduced where spreading fires are considered. Flame spread behaviour can be greatly influenced by the ignition method and environmental properties. The ignition pattern will influence the initial spread and flame front shape, with typically a circular spread from a point ignition source, or a linear spread from a line ignition source occurring, as shown in Figure 2.5. In this study, line ignition sources are used in all experiments, and therefore comparisons to previous point ignition studies are conducted with caution.

**Point Ignition**

Ignition (t = 0 s) t = 40 s t = 100 s

**Line Ignition**

Ignition (t = 0 s) t = 40 s t = 100 s

**Figure 2.5 - Influence of ignition type (Point vs. Line Ignition)**

Following ignition, both the fuel and environmental conditions will also affect the resulting flame spread behaviour. The greater control of fuel and environmental conditions within the laboratory allows systematic investigation of these effects. In this study, the focus is on flame spread experiments conducted in quiescent conditions, in the absence of wind or slope. FMC is also controlled throughout this study, allowing a focus on the effect of fuel bed structure.

Quiescent flame spread is characterised by an upright flame front, positioned perpendicularly to the fuel bed (as shown in Figure 2.6). As there is no forced flow, the horizontal flow profile is dominated by the fire-induced, entrainment flow. This entrainment is driven by the buoyant flow profile in the heated plume above the fire. However, since this entrained flow travels towards the flame front, quiescent flame spread is also commonly viewed as conceptually similar to opposed flow cases. In the resulting low-intensity flame spread scenario that occurs, the importance of fuel bed structure and fuel properties may be more significant and demanding of greater attention than for example in strongly wind-aided scenarios.

**Figure 2.6 – Characteristic linear flame front in quiescent conditions, with largely upright flame**

In concurrent flow cases (forced flow applied in same direction as flame spread), the flame front can be tilted forwards towards the unburnt fuel ahead, particularly at higher flow velocities. In opposed flow cases (forced flow applied in opposite direction to flame spread), the flame can be tilted backwards away from the unburnt fuel ahead, again particularly at higher flow velocities.

This flame tilting can alter the view factor between the flame and the fuel bed, affecting the radiative energy transfer from the flame. Additionally, convective heat transfer ahead of the flame front may be increased by concurrent flow, whereas convective cooling (due to the in-draft of ambient air) may occur in opposed flow cases. As a result, flame spread rates are typically greater in concurrent flow cases than opposed flow cases, assuming the flow rates remain below the limits for blow-off extinction. Gollner *et al.* [78] provided an overview of concurrent flame spread dynamics, including a review of existing work in various scenarios and fuel types.

A number of studies have investigated the effect of wind speed, typically using wind tunnels to expose the fuel bed to a range of forced flow velocities [58,60,68,69,79,80]. Greater ambient wind speeds can affect flame spread in various ways including an increased oxygen supply rate (and hence combustion rate), increased flow of hot gases ahead of the flame front, and increased flame radiation (to unburnt fuels) if the flame is tilted forwards [8]. While more indirectly, greater ambient airflows may result in increased drying (curing) of wildland fuels.

Numerous previous laboratory studies have also explored the role of fuel bed angle of inclination on the flame spread behaviour [58,67,68,79,81]. The flame orientation (relative to the fuel bed) is also affected by the fuel bed orientation, and hence the heat transfer to the fuel bed can be affected. Where the fuel bed is inclined such that the flame spreads upslope, the flame is effectively tilted further towards the unburnt fuel, which can increase pre-heating (and as a result the spread rate). Conversely, if the flame spreads downslope, the flame tilts away from the unburnt fuel. In this study, the effects of fuel bed inclination are not studied, and this is controlled by conducting all experiments on a horizontal (0° angle of inclination) fuel bed.

Dynamic laboratory experiments form the core of this thesis; however, the images in Figure 2.3 are indicative of the multi-scale nature of the wider research project (SERDP RC-2641). This wider project involved material-scale and static-bench scale experiments [82,83], as well as dynamic laboratory and field experiments at multiple scales [84–87], alongside numerical model development efforts [40]. At various times in this thesis, data obtained from material-scale experiments (bomb calorimetry and thermogravimetric analysis) are used to provide the thermophysical properties of the studied fuels, and in subsequent modelling. The results and findings obtained from the laboratory flame spread experiments are often compared to those from previous bench-scale and field experiments. This includes both comparison to experiments conducted as part of this wider project, and to the work of author previous authors.

The level of experimental control decreases as the experimental scale increases. Moving from the field into the laboratory gives much greater control of the environmental conditions (e.g. weather, topography and Fuel Moisture Content). However, certain additional phenomena and aspects of ‘extreme fire behaviour’, such as fire whirls (as shown in Figure 2.7) or various forms of ‘eruption’ or ‘blow-up’, may not occur at the scale of laboratory studies. The loss of some physical phenomena is an inevitable part of many model studies, and a major step in the study conceptualisation is the determination of which variables can be safely neglected without significantly affecting the physical phenomena of interest [8]. For example, firebrand spot ignitions may also be absent in laboratory experiments despite representing an important propagation mechanism in many wildland fire scenarios. From an early stage, laboratory-based flame spread studies have often employed model fuel beds (e.g. pine needles, wood cribs) in which the effects of firebrand spotting are absent [8,14] however, this can be beneficial if the aim is to focus study on other physical mechanisms.

**Fire Whirls**

**Figure 2.7 – Development of a 'fire whirl' during a 10 m x 10 m field experiment [Conducted as part of wider SERDP RC-2641 project]**

In addition to fuel structure, flame spread in these porous litter beds is also strongly affected by the Fuel Moisture Content (FMC) [88]. There are several possible mechanisms by which the FMC may affect the heat transfer to the fuel and the overall fire spread rate [8], all of which require further theoretical and experimental analysis. Moisture evaporation during the pre-heating phase will increase the overall magnitude of the energy required for fuel ignition and hence increase the heat sink magnitude. The subsequent water vapour may be transported along the fuel bed, towards the flame (by the fire-induced flow), absorbing radiation directed towards the unburnt fuel (particularly for larger flames), and transporting sensible heat from the fuel surface. The in-flowing water vapour may limit oxygen entrainment, potentially causing flame detachment and hence reduced radiative heat transfer to the unburnt fuel.

Several previous laboratory-based studies have explored the effect of FMC on flame spread [13,43,80]. However, no coherent theory has been developed to explain fully the role of FMC. In this study, fuel beds are constructed solely using dead fuels of relatively consistent fuel moisture content.

## 2.3. Flame Spread Theory

Flame spread consists of multiple, distinct phases (pre-heating, flaming, and smouldering/glowing oxidation phases) which can also occur simultaneously and overlap [55]. The duration of each of these phases may be altered by the fuel properties [55]. For flame spread through solids or liquids it is the gaseous decomposition products, produced in the pyrolysis phase, which produce the flame (via a combustion reaction). This chemical decomposition process (pyrolysis) is endothermic and is reliant upon the heat energy supplied to the unburnt fuel during the pre-heating phase.

This pre-heating can occur via various mechanisms including radiative and convective heating from the flame, and conductive heating through the fuel. This pre-heating may be offset by heat losses such as convective cooling or radiative emissions from the fuel. During the pre-

heating period, other processes such as moisture evaporation and melting may occur, prior to reaching a temperature suitable for pyrolysis onset.

Gas phase ignition will occur once the pyrolysis rate is such that the fuel:air vapour above the fuel is within the flammability limits [89]. In normal atmospheric conditions, sustained combustion will result in a buoyant diffusion flame, which can promote lateral entrainment and alter the ambient flow fields. The flame front will then spread laterally as the cycle of pre-heating and subsequent ignition repeats. For some fuels, this flame front progression will be accompanied by a trailing smouldering region, in which a solid-phase combustion reaction occurs. In some fuels/conditions, only smouldering propagation will occur [90].

The relative importance of the pre-heating phase, the significance of each heat transfer mechanism, and the importance of fire-induced flows, will all vary with the fuel properties and environmental conditions. For up-slope flame spread, or with a concurrent wind flow, increased flame tilting towards the fuel will typically increase the flame pre-heating, resulting in increased spread rates. The reverse can occur when a flame spreads down-slope or into an opposed wind flow.

Quiescent (no wind, no flow) cases represent somewhat of a midway case, typically resulting in largely upright flames. However, given the fire-induced entrainment of ambient air towards the approaching flame front, these quiescent cases are often considered analogous to an opposed-flow scenario [91]. Similarly, various fuel properties (geometrical, thermophysical and thermochemical) can affect the spread rate and behaviour [14]. A key distinction can however be drawn between solid (solid-only) and porous (solid and gas matrix) fuels, with the physical phenomena controlling flame spread differing greatly for each of these fuel types [19].

The ultimate aim of flame spread modelling is to describe the relationship between the heat energy supplied to the fuel and the energy requirements for fuel ignition. Williams [92] described a ‘universal’ flame spread equation, in which the conservation laws were applied to the concept of a ‘surface of fire inception’,

$$V = \frac{\dot{q}}{\rho \Delta h} \tag{2.1}$$

Where $V$ is the flame spread rate, $\dot{q}$ is the rate of energy transfer across the surface of fire inception, and $\Delta h$ is the thermal enthalpy change required for ignition of the fuel.

Equation 2.1 implies that the spread rate is inversely proportional to the fuel density ($\rho$). Fuel Moisture Content (FMC) can also be incorporated (by including the heat of vaporisation of water), as can energy losses (although radiative losses are often considered negligible). This therefore relates the energy provided to the fuel (by several possible heat transfer mechanisms depending on the flame spread scenario) to the energy required for ignition of the fuel (which is dependent upon the fuel properties).

### 2.3.1. Heat Transfer Mechanisms

Equation 2.1 requires specification of an energy transfer rate ($\dot{q}$) across the surface of fire inception. Specifying the dominant heat transfer mechanisms across this boundary represents an important step in the development of any flame spread theory [92]. In solid surface flame

spread, the flame heats the solid fuel (via radiation and/or convection), and this energy can then be conducted through the solid, but the conductivity of porous fuels is much lower [22,93].

Several decades of research has allowed the identification of distinct flame spread regimes (and associated dominant heat transfer mechanisms) for solid surface flame spread [21,53]. The 1967 study of Tarifa and Torralbo [94] represented one of the earliest mathematical treatments describing surface flame spread along a liquid or solid, and allowing for flame radiation and convection, as well as conduction through the fuel bed. However, this model was limited to quiescent scenarios, since the gas phase was considered stationary prior to flame front arrival. Around the same time, Friedman [95] published one of the earliest reviews of flame spread studies, highlighting the need for greater understanding of propagation mechanisms, and improved methods for incorporating the complex physical and chemical processes controlling flame spread.

One of the earliest complete physical models for solid surface flame spread was proposed by De Ris in 1969 [21] and involved solutions for both thermally thin and thick cases. By assuming infinite kinetics, De Ris was able to develop a purely thermal model; however, this limited application to cases in which the Damköhler number is high, and therefore the kinetic effects negligible. This was later confirmed experimentally by Fernandez-Pello *et al.* [91,96] who studied the effect of wind speed and oxygen concentration on flame spread, identifying the distinct low and high Damköhler regimes. Further numerical and experimental investigations determined that gas phase conduction was dominant for thermally thin fuels, while for thermally thick fuels solid phase conduction dominates [22,53].

These dominant heat transfer mechanisms are not well defined for porous fuels. While the conductivity of porous fuels is lower, additional complexity emerges given the additional heat transfer pathways that can occur within the porous fuel (e.g. radiation between discrete fuel elements, convective heat transfer). Disagreement remains regarding the relative importance of the different sources of energy, and the current state of knowledge trails that which exists for solid surface flame spread scenarios [19].

### 2.3.2. Fuel Properties

Equation 2.1 also requires the specification of the 'heat sink' magnitude of the fuel, expressed as the product of the volumetric energy requirements for ignition and the fuel density. For porous fuels, the selection of an appropriate density ($\rho$) is complicated by the presence of gas pores within the discontinuous fuel structure. This pore structure will be affected by both the fuel bed packing and by the interaction and connectivity of individual fuel elements.

Not all of the fuel bed will necessarily be heated by the time of flame arrival. Williams [92] defined this heated fraction as the product of the fuel element surface-to-volume ratio ($\sigma$) and the heated layer thickness (estimated by $\sqrt{\alpha}/V$ multiplied by the square root of the heated fuel bed depth ahead of the fire inception surface). The heated depth of the fuel bed depends on the heat transfer mechanisms considered, and for radiative transfer a value similar to the optical depth ($1/\beta\sigma$) has often been proposed [97,98].

Applying this heating assumption to the universal flame spread equation (and assuming that radiation from the fuel region is the dominant energy transfer mechanism) results in a simple flame spread equation for thermally thick fuels. Although this case does not incorporate radiation from the overhead flames, or convective cooling or heating effects.

$$V = \frac{\epsilon^2 \sigma_{SB}^2 (T_s^4 - T_i^4)^2}{\beta \sigma \alpha_{diff} \rho_s^2 (\Delta h)^2} \quad (2.2)$$

Where $\epsilon$ is the emissivity of embers in the in-bed combustion region, $\sigma_{SB}$ is the Stefan-Boltzmann constant, $\beta$ is the packing ration and $\alpha_{diff}$ is the thermal diffusivity. $T_s$ and $T_i$ represent the solid and initial temperature respectively.

Determining an effective bulk density also complicates efforts to apply a simple conservation of energy approach to porous fuels. While a control volume within the porous fuel layer can be defined, appropriate methods for describing the bulk fuel properties within this control volume are required.

One of the earliest attempts to apply a conservation of energy approach to porous fuels was the work of Frandsen [99]. This model considered only the pre-heating phase (and therefore neglected kinetic effects) and included both vertical and horizontal heat flux components. The control volume was defined as the minimum volume for which the bulk fuel properties (bulk density) were represented. However, the effective bulk density, rather than the physical bulk density, was incorporated within the eventual conservation of energy calculation. This represents the non-uniform heating of fuel elements, with this non-uniformity greatest for thicker fuels (lower surface-to-volume ratio).

Frandsen's analysis would later form the theoretical basis of the Rothermel model [43], which remains one of the most-widely used operational models for flame spread prediction. This model, while based on a physical framework, requires several empirical closure terms that were calculated from an extended series of experiments in model fuel beds conducted over the course of a decade. Despite efforts in subsequent decades to further develop the Rothermel model, few improvements and modifications have been incorporated, while efforts to produce second-generation models also failed to see widespread adoption.

Similarly, despite several decades of development, simplified physics-based models, which consider the individual heat transfer mechanisms, have also failed to see operational use [100]. Many of the physical sub-models remain untested given the lack of appropriate experimental data for key physical processes (internal convective heating, radiative heating profiles, internal flow/drag effects). Therefore, there remains a need for further systematic investigation of model fuel beds, with a particular focus on further measurement of key physical properties. Additionally, given the importance of porous fuel structure, there is a need for further consolidation of existing findings, from a variety of model fuel beds, regarding the effect of fuel structure parameters on the physical phenomena controlling flame spread.

## 2.4. Model Fuel Beds for Investigation of Porous Flame Spread

Many of the earliest investigations of wildland flame spread involved observations of real fires or in-situ burning of natural vegetation in a field environment [37,101–103]. It was quickly realised however, that to advance our fundamental understanding of the flame spread process, basic research involving reduced scale models [8,12,104] was required. As in other fields of engineering and combustion research, the use of diagnostic models allows observation of important phenomena and systematic assessment of the importance of specific variables.

In the context of wildland flame spread, perhaps the earliest example of a deliberate diagnostic model, allowing the generation of systematic and repeatable fires, was Project Fire Model, conducted by researchers at the U.S. Forest Service [14]. This study involved the use of cribs, of deliberately ordered and arranged wood sticks, stacked vertically in layers, with gaps between fuel elements. These wood cribs were then used as model fuel beds in flame spread experiments, with systematic alteration and investigation of isolated variables e.g. wood density, crib height, Fuel Moisture Content (FMC).

Project Fire Model both prompted and coincided with a number of other flame spread studies in which wood cribs were used as model fuel beds [105,106]. Subsequently a variety of model fuel beds have been used to investigate porous flame spread [34,68,72,107–110]. These model beds have included both natural fuels (pine needles, leaves, grass) and engineered materials (excelsior, cardboard, wooden dowels).

An overarching aim of these studies has been to improve our understanding of 'real' or 'full-scale' wildland flame spread. However, this is very much a long-term aim and a more pressing challenge is to develop our fundamental understanding of just these model systems. Indeed our ability to describe theoretically the flame spread process, and predict the fire behaviour, of these porous fuel beds remains lacking compared to many other fuel types and flame spread scenarios [19].

Pine needle beds, typically of a few $m^2$ or less in size, have been used in the study of porous flame spread since the earliest laboratory-based studies [111]. In seeking to understand flame spread through these pine needle beds, it may be beneficial to explore which theories and phenomenological observations from other model fuel beds are applicable to pine needle fuel beds. Particularly, since a wealth of knowledge has been generated on the understanding of the burning behaviour of other fuel bed models such as wood cribs [14,112–116] and efforts to understand the link between crib models and wildland flame spread are ongoing [74,76].

There is less control of the structure of a natural fuel bed (such as a pine needle bed) than is achievable in wood crib studies. However, the individual fuel elements (e.g. individual pine needles) are fairly similar and repeatable and can be defined on an average basis (within a given sampling based standard deviation). An advantage of pine needle beds is that they incorporate actual fuel types present in wildland environments and participating in surface flame spread. Therefore, they may eventually allow a simpler path towards being able to focus efforts on addressing issues of scaling in wildland flame spread.

The focus of this review is therefore not to attempt to explain 'field-scale' wildland flame spread but to explore the similarity of these different fuel models. In particular, addressing the question of whether complimentary insights into porous flame spread can be generated by considering existing studies conducted in both wood cribs and natural fuel beds. Despite the greater heterogeneity and geometrical complexity of fuel beds of natural fuels (e.g. pine needle bed), this will require consideration of how the fuel bed structure affects the applicability of existing crib fire theory which includes the definition of two distinct regimes: loosely packed (in which the crib burning rate is similar to that of an individual fuel element) and densely packed (in which burning is ventilation limited, with burning rate varying with crib porosity).

### 2.4.1. Natural Fuel Beds

Many early experiments involving natural wildland fuels were field studies conducted in-situ, without prior modification or detailed characterisation of fuels [101]. Given the wide range of factors affecting spread rate, and the inter-related nature of many of these variables, the potential value of laboratory experiments, in which individual variables can be isolated and systematically altered, was soon noted. This led to an increase in the use of natural (albeit re-constructed) fuel beds within well-controlled laboratory conditions [101].

Curry and Fons [101] conducted one of the earliest studies to move away from the in-situ field approach. Initial in-situ experiments were followed by one of the earliest examples of experiments involving reconstructed pine needle beds. As a result, further work, involving pine needle beds of various compactions, was conducted by Fons [111], including several experiments conducted in a wind tunnel. Subsequently, many further flame spread studies have been conducted using reconstructed pine needle beds [69,79,81,111,117].

Clearly when reconstructing natural fuel beds it is important to be able to characterise and reproduce the desired fuel bed structure. This desired structure may be chosen to replicate the natural fuel conditions in an ecosystem of interest, or may be chosen arbitrarily during the study design. Recent studies [56,57,118] have highlighted the variations in fire behaviour that can occur if structural properties, such as permeability of the in-situ and reconstructed fuel beds, are not carefully aligned.

Schuette [119] provided an early guide to the construction of uniform and reproducible pine needle beds, including proposed methodologies for the collection and conditioning of fuel. By carefully controlling the fuel loading, fuel moisture content, and compactness, Schuette demonstrated that reproducible fuel beds exhibiting consistent fire behaviour (based on comparison of spread rates) could be produced. The importance of removing other litter layer components (e.g. twigs, leaves, branches) to produce homogeneous fuel beds of consistent pine needle mass, was also emphasised.

Since the pioneering work of Curry and Fons [101], pine needle beds have remained a well-used model fuel bed in laboratory-based flame spread studies. For example, pine needle beds were used extensively by researchers at the U.S. Forest Service's Northern Forest Fire Laboratory [120–125]. These studies made particular use of Ponderosa Pine and Western White Pine needles.

Using Ponderosa Pine needle beds, and through comparison with the earlier wind-aided and quiescent flame spread experiments of Rothermel and Anderson [125], Beaufait [120] studied the difference in fire behaviour of heading and backing fires. Understanding the resulting fire behaviour in each scenario was of great importance to prescribed burn practitioners, with Beaufait observing backing fires to burn 'slower, longer and deeper'. Headfires were sensitive to the applied wind speed, however backing fire spread rate (along with the residence time and flame depth) were not significantly affected, despite increased backwards tilting of the flame at higher wind speeds. This supports suggestions that the opposed and quiescent flame spread regimes can be considered in parallel, and questions the significance of the flame heating.

As with other fuel types, the relative contribution of flame heating will also depend upon the fuel bed angle, and the resulting angle between the flame and fuel bed. Van Wagner [126] explored the effect of fuel bed angle in a series of quiescent, laboratory-based flame spread

experiments involving Red Pine needle beds. As with Curry and Fons [101], these experiments were designed to complement a series of field experiments, in this case conducted in a Red Pine plantation. The spread rate and flame length both increased with increasing positive slope angle.

More recent studies have also investigated the combined effect of fuel bed angle and wind speed [117,127], and have addressed a historical lack of experimental investigation of downslope flame spread behaviour [127,128]. Liu *et al*. [129] investigated the role of convection during upslope flame spread, determining that both natural and fire-induced convection contribute significantly to cooling. In beds of *Pinus halepensis* fuel beds, burned under no-wind conditions, Dupuy and Marechal [130] also observed an important convective cooling effect and determined that radiant heating was dominant for slope angles from 0° to 20° however, convective heating was of greater importance at higher slope angles. In addition to the effect on the heat transfer mechanisms, the effect of the imposed wind speed on the mass and species transport must also be considered. Rossa *et al*. [127] observed an upper limit on the opposed wind speed in *Pinus pinaster* needle beds above which extinction occurred.

In his earlier study of backing fires, Beaufait [120] highlighted the need for improved understanding of the effects of fuel bed width and depth on the fire behaviour of pine needle beds. The effect of both fuel bed depth and width were however already under investigation by several of Beaufait's colleagues [121,131]. They observed an initial positive trend in various pine needle beds, between spread rate and either fuel width or fuel height. However, for both parameters, a maximum value was observed for some pine needle species, beyond which spread rate was unaffected by additional increases in fuel height or width. Both characteristics have since been studied further by subsequent authors [69,132].

Dupuy [132] observed a positive trend between fire width and spread rate, particularly at greater upslope angles. This effect was attributed to variations in the flow regime, with reduced edge effects, allowing greater fire-induced flow into the rear of the flame front. The effect of fuel depth is more complex, as the fuel depth can vary as a result of variations in fuel loading, bulk density, or a mixture of the two. If the bulk density is varied but the fuel loading held constant, then the porosity of the fuel bed will be altered. Anderson [133] observed a significant effect of porosity on the combustion behaviour (burning rate and flame length) of a pine needle bed, and suggested the existence of an optimum porosity value. However, these observations were made during a preliminary series of stationary burns, and detailed systematic study of porosity effects during flame spread were not conducted.

Understanding the relative importance of different heat transfer mechanisms and energy sources has been an important focus in several previous studies. Earlier studies typically focused only on measurements of radiation, with the positioning and view (e.g. of the flame and/or of embers in the combustion region) of radiometers varying widely (as shown in Chapter 6). Particle Image Velocimetry has also been used to visualise the flow above pine needle beds, providing insight into the convective cooling and heating patterns [67,134].

The vertical, buoyant flow above pine needle beds (driven by the temperature gradient occurring because of the energy release) has also been investigated experimentally. Marcelli *et al*. [135] and Santoni *et al*. [136] used a cross-correlation velocimetry method to measure the buoyant flow velocity (from in-plume temperature measurements) above *Pinus pinaster* beds of a single fuel loading and fuel bed structure. While vertical and horizontal flow profiles (and

gas temperatures) above pine needle beds have been investigated [136], there appears to have been little measurement of the flow profile within pine needle beds during flame spread. A notable exception is the recent work of Fehrmann *et al*. [57] and Figueroa *et al.* [56], which studied the effect of permeability on the wind-aided spread rate in small-scale pine needle beds, noting a strong influence at high wind speeds.

The pressure drop through natural fuel beds has also been investigated, in the absence of combustion, in order to characterise the drag profile of natural litter layers [83,137,138]. Wang *et al*. [137] investigated the permeability of broadleaf litter layers (along with examination of artificial fuel layers) with existing formulations (Kozeny-Carman equation) poorly predicting the observed pressure gradients. Similarly, Bebieva *et al*. [138] recently studied the airflow through pine needle (and artificial) fuel beds in the absence of flame spread. They observed a dependence of the in-bed flow velocity on the fuel bed porosity, with a significant vertical gradient in the lateral in-bed flow observed for the pine needle beds. Measurements presented within this thesis will seek to address this gap, alongside complimentary studies conducted by other authors [83], which have provided new insight into the drag profiles associated with pine needle beds of similar structure to those investigated in this thesis.

In addition to understanding the flow and convective heating/cooling within pine needle fuel beds, the radiation transfer through these fuel beds must also be characterised. Formulations describing the radiation attenuation properties of pine needle beds have been available for several decades [8]. Many existing simplified physical models assume that pine needle beds are isotropic and therefore adopt the attenuation term described by Hottel in the 1961 report of the Committee on Fire Research [8].

However, Vaz *et al*. [139] have questioned the applicability of this standard attenuation formula when applied to non-isotropic fuel beds formed when pine needles have a preferential angle of inclination. This is potentially highly relevant given the tendency of pine needles (particularly in more compacted fuel beds) to settle at an angle largely parallel to the substrate (e.g. soil layer). Therefore, further work is required to understand the implications of possible non-isotropic radiation properties in fuel beds at fuel conditions similar to natural field conditions.

Another important consideration for natural fuels is the fuel moisture content, hence the emphasis placed on appropriate fuel conditioning by Schuette [119]. However, even with proper fuel conditioning, the variation in moisture response of different fuel species, and the effect of fuel bed structure on moisture diffusivity, must also be considered [123,140]. Over recent decades, numerous authors [79,121,125,133,141] have investigated the effect of the fuel moisture content of pine needles on the resulting ignitability and fire behaviour. An important example is the 1969 study of Anderson [133], which informed the development of an empirical moisture correction factor in the widely-used Rothermel model [43], to account for the damping effect of moisture on flame spread.

The energy required for vaporisation of water is just one contributor to the overall energy required for the ignition of a pine needle (or other fuel element). Many existing flame spread models assume an ignition temperature, and the fuel temperature history is often calculated within physical models. Some past authors have attempted to measure the fuel temperature experimentally, despite the challenging nature of this measurement. De Mestre *et al.* [142] used a thin (0.025 mm dia.) thermocouple to measure the temperature of a surface pine needle, for comparison with their simplified physics-based model.

The chemical composition of natural fuels such as pine needles can also be difficult to characterise but may also affect ignitability and flammability [143]. For example, past authors have explored the relationship between terpene and volatiles contents and flammability [143,144], while the damping effect of the silica-free mineral content is well established [43,145]. This has led to speculation around the contribution of chemical differences to the observed variations in flammability and combustion behaviour of different natural fuel species. However further investigation of the roles of both fuel element and fuel bed structure are required if these chemical and structural contributions are to be assessed.

Significant insight can also be gained from the multitude of bench-scale studies involving pine needles [32,124,146–156] or broadleaves [157]. These studies can be used to investigate the effect of flow conditions, oxygen concentration, or fuel properties (e.g. fuel species, moisture content, live vs. dead fuels), on the ignition properties and subsequent combustion dynamics [124,146,147,149–151,153,158–160]. Much recent work has focused on the role of fuel structure at this bench-scale [82,148,152,154,159,160], however a number of these studies involved simultaneous variation of the fuel loading and bulk density. This limits efforts to understand the independent effects of fuel loading and bulk density (or porosity) on the combustion behaviour, however significant insight for numerical modelling has resulted from past bench-scale studies.

Numerical simulation of fire behaviour in pine needle beds has represented a common scenario for the testing and development of detailed physics-based models [40]. As discussed in Chapter 2, Mueller *et al.* [40] attempted to simulate preliminary flame spread experiments in this study using the Wildland Fire Dynamics Simulator (WFDS). Specific limitations have been highlighted within WFDS and other detailed physics-based modelling approaches, with a specific need identified for further investigation of the in-bed flow (and resulting convective heating) through these porous fuel beds. This must include investigation of the drag force associated with the vegetation structure both pre- and post-flaming combustion [18,40].

### 2.4.2. Artificial Fuel Beds

Replacing natural fuels with engineered fuels, may allow greater control, replication and description of the fuel bed structure. The materials may be chosen to closely mimic the properties of a given natural fuel strata or may be deliberate abstractions aiming to isolate particular physical processes. This abstraction may be at the expense of other phenomena, just as many reconstructed 'natural' fuel beds rarely incorporate all flame spread mechanisms.

Perhaps the earliest use of an artificial fuel bed was by Rowland (1939) and involved wood flour and `saltpeter' (potassium nitrate). While a wide variety of artificial fuels have been employed in past studies, a smaller number of fuel types have gained prominence or provided particular physical insight into the flame spread process in porous fuels.

#### 2.4.2.1. Wood Cribs

Wood cribs have been used extensively in the combustibility testing of wood-based products [161,162], and as ignition and fire sources across a vast array of fire research areas [163–167]. The ability to easily define and construct porous fuel arrays provide a relatively repeatable fire source [168], with alteration of the crib structure allowing manipulation of the fire growth and burning rate. The utility of wood cribs has benefited greatly from several decades of research and they continue to be used in multiple standards and testing procedures [169–173].

The earliest uses of wood cribs in fire science primarily occurred in studies dedicated to the development of fire extinguishment agents and application techniques [112,174–177]. For these experiments, the porous cribs incorporated the `natural draught' typical of real fire scenarios. Despite a focus on extinguishment, valuable combustion behaviour data was also presented for the wood cribs in some of these early studies.

From the earliest stationary crib fire experiments, it has been clear that overall crib structure can affect the burning rate and combustion behaviour. Folk(e)[2] [112] investigated the upward progression of the flaming and glowing phases through various woodpiles in which combustion was abruptly halted by placing a metal box over the entire woodpile. This allowed the remaining mass of each wood stick layer to be measured independently, and the progression of the fire front to be tracked. The speed of progression of the fire front appeared to vary amongst different woodpile arrangements. In certain cases, there was a clearly apparent progression of the fire front between layers, but in others, the woodpile appeared to burn effectively in unison. This variation was attributed to the effect of air supply into the woodpile on the spread rate.

Using various wood cribs, across a range of stick sizes, and by incorporating the earlier crib fire data of Folk, Gross [113] determined a correlation between a newly defined porosity factor and the scaled maximum burning rate of each crib. This porosity factor ($\phi$) incorporated both the `vent area' of the crib and the exposed surface area of the sticks,

$$\phi = N^{0.5} b^{1.1} A_v / A_s \tag{2.3}$$

Where $A_v$ is the vent area and $A_s$ is the total exposed area of the sticks, and these are defined respectively as,

$$A_v = b^2(10 - n)^2 \tag{2.4}$$

$$A_s = 2nb^2[n(21 - n) + n] \tag{2.5}$$

Where $N$ is the number of layers, $b$ is the width of individual stick and $n$ is the number of sticks in each layer of the crib. Gross identified three distinct regimes amongst the cribs studies:

1. Diffusion-Limited Combustion
2. Free Combustion
3. Non-Sustained Combustion

In the first regime, a scaled burning rate almost proportional to the porosity factor was observed, while during free combustion the burning rate was independent of the porosity factor. In the final regime, combustion was not sustained due to the `openness' of the crib. The presence of these two crib regimes capable of sustaining combustion have since been observed

[2] The only published research believed to be available by this author states that the authors surname is Folk. However this author is widely referred to as both Folk and Folke throughout the wider literature. The actual spelling, and the source of any erroneous translation or spelling is unclear.

by numerous subsequent authors [116,168], as has the relationship between burning rate and porosity factor [116,168,178–181].

Through theoretical and experimental demonstration, Block [116] similarly identified two regimes relative to the crib structure, as either densely packed or loosely packed configurations. In the densely packed region, the maximum specific burning rate was a strong function of the height and packing density of the crib. Whereas in the loosely packed regime, the burning rate was a function of the physical properties of the fuel elements (thickness) and was independent of the fuel bed geometry.

There are several intuitive explanations for the observed variations in burning rate as a function of porosity in closely packed cribs. The increased porosity may allow increased airflow into the crib, altering both the convective heat transfer (potentially providing heating or cooling) and the oxidiser supply rate. Similarly, the mixing rate of fuel and oxidiser may also be affected in addition to variations in the available oxygen, while the radiation transfer within the crib may also vary.

Many of the studies that have investigated the role of ventilation have involved the burning of cribs in enclosed environments such as tunnels and compartments [180,182–189]. In these studies, the interaction of ventilation and crib structure is further obscured by the additional influence of external ventilation restrictions (e.g. tunnel openings, compartment doors) and heat feedback (e.g. from the accumulation of smoke layers, or re-radiation from compartment surfaces.

The effect of forced flow may depend on whether the flow is directed into the crib itself or into the overhead flame/plume. In fuel beds composed of wood cubes, Grumer and Strasser [190] observed an influence on burning rate only when forced flow was directed into the fuel bed itself. Historical studies involving forced flow into wood cribs are limited, however Byram *et al.* [14,191] observed linearly increasing energy release rates with increased concurrent flow speeds. The observations of Byram *et al*. differed from later observations of pine needle beds by Beaufait [120], in which the energy release rate per unit area decreased at increased concurrent flow speeds. Although, as highlighted by McAllister and Finney [76], the methodology of both studies differed, as unlike Beaufait, Byram *et al.* did not normalise the energy release rate by the burning area.

For a detailed understanding of flame spread through wood cribs, it is also desirable to understand the accompanying variations in the physical processes that determine the burning rate as the crib geometry is varied. This understanding is particularly necessary if there is a desire to extrapolate findings to other fuel bed types e.g. pine needle beds.

##### 2.4.2.1.1. Relevance to Wildland Fire Science

From an early point, there have been efforts to explore possible links between these insights into the combustion behaviour of wood cribs and the fire behaviour of wildland fuels. Post-WWII, the U.S. military began investigating large-scale, free-burning fires, amidst growing fears of nuclear warfare [192]. During these projects, the fire expertise of USFS researchers appeared to be in regular demand, with these researchers recommending the use of wood cribs in a number of projects in which large, repeatable fire sources were required.

An unclassified study by the U.S. Naval Radiological Defense Laboratory [192] investigated the radiation characteristics of the flame above a wood crib (composed of large logs, as shown

in Figure 2.8). This followed a suggestion from U.S Forest Service (USFS) engineer Wallace Fons, that wood cribs could provide a highly-repeatable fire source, with flame emissions extending into the infrared region, for the U.S Navy's ongoing research into the effects of thermal radiation. Characterization of the flame, using radiometers originally designed for use at nuclear weapon test sites, suggested an equivalent blackbody radiation temperature of around 1200 K and an emissivity of 0.3.

Another study, conducted by the U.S Corps of Engineers [174], again with the assistance of USFS personnel, involved meteorological measurements of local atmospheric conditions in the vicinity of a crib fire (again composed of logs). This included observations of entrainment flow into the smouldering crib, after the main flaming combustion period had ended. These studies offer an indication of the potential for data collection, of phenomena relevant to the physical understanding of the combustion dynamics of porous fuels, within the course of these larger studies with entirely different focuses. A fact that was surely not lost on the USFS scientists involved.

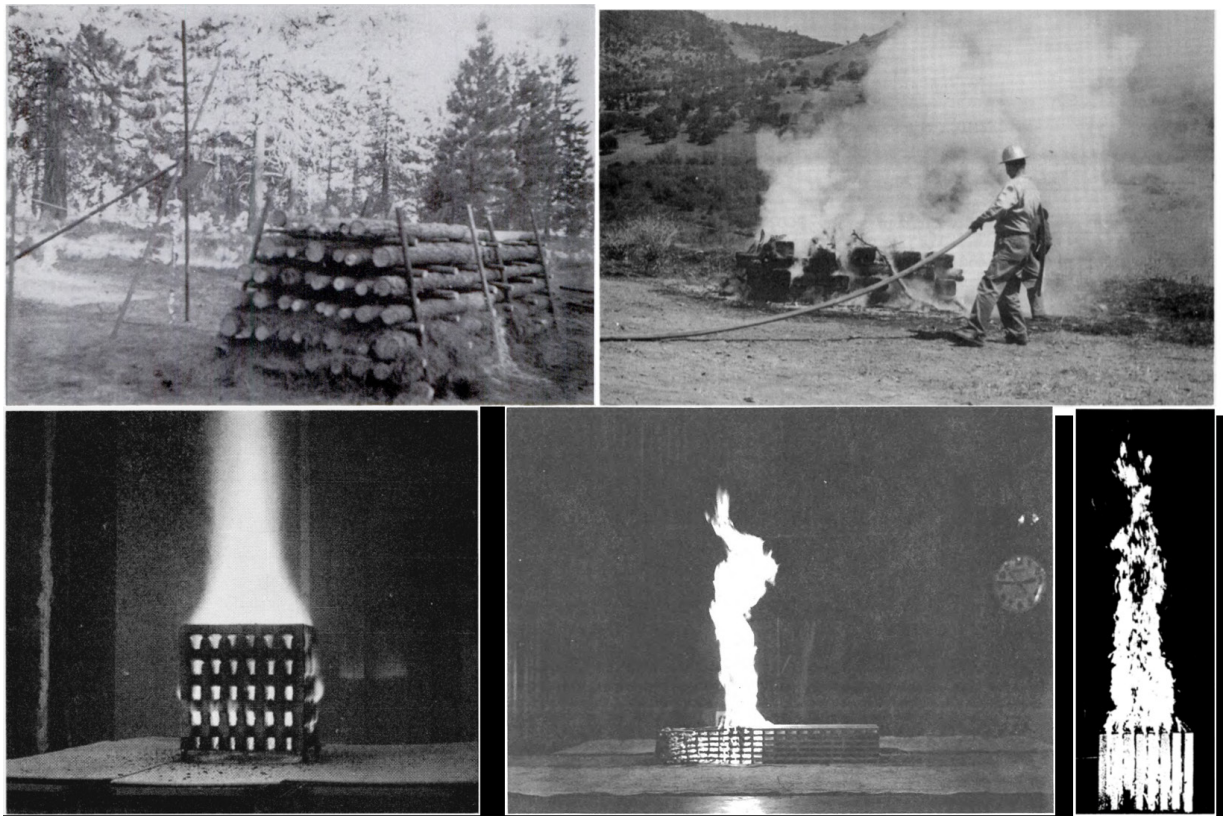

**Figure 2.8 - Composite of various wood cribs (Clockwise from top left: Wood log crib used in US Navy Study** [174]**; Railroad ties in crib formation used in an extinguishment study** [175]**; Ordered vertical sticks used in fire-induced air flow study of Grumer and Strasser** [190]**; Wood crib used in Project Fire Model** [12]**; Crib used by Gross in stationary burning study** [113]**)**

The late 1950s saw the launch of the first study specifically devoted to the use of crib fires to systematically investigate flame spread within the overall context of improving our understanding of wildland flame spread. Project Fire Model [12–14], was a USFS project (Pacific Southwest Forest and Range Experiment Station, in collaboration with the Office of Civil and Defense Mobilization) conducted over almost a decade. Highly repeatable wood cribs

were used as a diagnostic tool, allowing the effect of various fuel and environmental parameters on the flame spread process to be investigated.

Project Fire Model[3] marked a significant shift in approach from the USFS, who prior to this point had largely focused on conducting experiments under natural, or close to natural, conditions and with natural fuels [37,111,193]. This represented a new emphasis on fundamental research aimed at linking free burning wildland fires to the kind of basic research into combustion dynamics and fire behaviour undertaken in other fields. Therefore bridging the gap between controlled combustion studies and the phenomena involved in `uncontrolled aerothermodynamic systems' where the fuel consumption rate is dependent on both the HRR and the oxygen supply to the combustion region [12].

This followed the recommendations of the Committee on Fire Research [8] who concluded that further fundamental understanding of fire behaviour was required, if a resilience to forest fires and urban conflagrations was to be achieved. Seven priority areas for research were identified, and one of these (determination of model laws for fire spread) was addressed by Project Fire Model. The heavily instrumented flame spread experiments of Project Fire Model explored the effect of the size and density of wood sticks (of square cross-section) and the fuel bed width and height. Along with detailed characterisation of the flame and convection column; the energy released; mass consumption; and emissions products.

At the same time as work for Project Fire Model was proceeding, Thomas [194] published a theoretical model for flame spread in continuous fuel beds such as long wood cribs, and including the effect of wind. This study included some initial wood crib experiments to investigate the applicability of the developed model. This appears to be one of the earliest, physically based flame spread theories with explicit applicability to crib fires. Thomas however noted the similarity of this model with that previously developed by Fons [111] for forest fuels. Thomas' model however, provided more detailed analysis of the burning region within the fuel bed, with Fons having neglected the effect of the burning region size on heat transfer to the unburnt fuel ahead.

Thomas, along with other colleagues [195], would later also derive a simple relationship for the spread rate of crib fires in quiescent conditions, which was found to be proportional to the fuel bed bulk density. Some agreement with this relationship was also observed with a subset of past experimental observations of rate of spread in natural fuels (separately pine needles and sticks) [101]. However, an additional effect was observed in these natural fuel experiments, with the spread rate dependent not just on bulk density but also the volume of voids per unit surface area.

The Thomas model followed on from previously published work by Thomas and colleagues [196], in which stationary crib fire experiments were included in efforts to derive a dimensionless relationship for buoyant diffusion flames. This development cycle, in which initially stationary burning was explored prior to expanding the theory to spreading fires, highlights an important benefit of using wood crib models. At the time of Thomas' work, there were already several important studies on the stationary burning of wood cribs and the number

[3] Project Fire Model was initially led by Wallace Fons, who sadly passed away before the project was completed, with George Byram taking over responsibility for the project [415].

of available studies, and our theoretical understanding of the combustion behaviour, has expanded significantly since then.

However, gaps in our understanding of the stationary burning of wood cribs remain, while the popularity of wood cribs as model fuel beds in flame spread experiments has waned. This risks missing the potential to incorporate more recent stationary crib fire knowledge into flame spread processes, not just in wood cribs but also in other model fuel bed types. Where research has continued, important crossovers continue to be identified between crib fire flame spread phenomena and wildfire (porous) flame spread more generally.

##### 2.4.2.1.2. Continuing Research

Given the importance of the flow conditions in wildland fire, there has been ongoing work to understand the effect in wood cribs. Studying multiple crib configurations, of different porosity and fuel element thickness (0.64 cm and 1.27 cm), McAllister and Finney [74,76] investigated the influence of forced flow on the crib burning rate using a large wind tunnel. McAllister and Finney noted that the effect of wind was dependent on both the fuel thickness and the porosity. The burning rates of the thicker fuel elements were positively correlated with the wind speed, however for the thinner fuel elements a decreased burning rate was observed at non-zero wind speeds. The changing influence of the wind was attributed to the competition between increased oxidiser supply and heat losses by the fuel elements.

While the stick thickness was varied in the above study, even the thinnest sticks (6.4 mm) were still significantly thicker than typical pine needles (circa. 1 mm). A subsequent study has extended the range of crib configurations investigated, incorporating fuel elements as thin as 3.2 mm [77]. There remains a need to explore whether the same trends and underlying physical processes apply to typical wildland fuel beds with thinner fuel elements and where the aspect ratio of fuel elements may differ. For example, some of the existing correlations have been shown to poorly predict the burning rate when cribs are constructed of thin fuel elements.

Similarly, the applicability of other key observations about the controlling mechanisms of crib fire burning to wildland fuel beds requires further clarification. The dominant heat transfer process for crib burning (in quiescent conditions) has been identified as the heat transfer through the crib rather than the overhead flame [115,197]. Similar, often qualitative, observations have been made for pine needles fuel beds, but there has been little detailed investigation of the effect of fuel bed structure on these heat transfer mechanisms.

Additionally, it is important to understand the source terms for the in-bed energy transfer. For wood cribs it appears that the char oxidation of fuel elements provides much of this energy. Such an understanding is important in understanding the effect of other factors such as ventilation effect. Harmathy [189] compared the burning rates of cribs constructed from charring and non-charring materials respectively, finding that an increased burning rate with forced ventilation was only observed for charring materials (however, an optimum ventilation rate was observed). While sub-models have been proposed to describe the char oxidation of pine needle beds, there appears to have been limited research into the significance of its contribution. This is despite recent WFDS-based modelling efforts suggesting that contribution to overall HRR may be significant in laboratory flame spread studies [198].

There remains significant potential for greater comparison of the burning behaviour of crib fires and natural wildland fuel beds. Given the ubiquitous use of crib fires throughout the field

of fire safety engineering, there remains a clear need to better predict and describe the burning behaviour of cribs, with efforts to improve the physical models used to predict this fire behaviour ongoing [199]. It is likely that further complimentary insights between crib fires and other model porous fuels will remain fruitful and allow further examination of wildland fire phenomena. In particular, the greater understanding of crib structure effects on burning rate may complement existing operational fire models in which burning rate is not currently included explicitly (e.g.BEHAVEPlus, FARSITE, FOFEM) [200–202].

#### 2.4.2.2. Other Artificial Fuels

##### 2.4.2.2.1. Excelsior

A particularly popular fuel bed type involves thin strands of wood, known in North America as excelsior (referred to as wood wool in many other regions)[4] which has been used in several previous studies [35,43,60,61,63,69,203–209]. As a widely manufactured product, large volumes, with highly consistent properties, can be easily obtained. In his detailed assessment of possible artificial fuel types, Murphy [68] noted that, while easily ignitable and sustainable, excelsior fuel beds exhibited rapid flame spread in wind-driven scenarios which was unsuited to small-scale studies.

Rothermel [43] used experimental observations from excelsior fuel beds (in addition to experiments involving wood cribs and stick tripods) to determine many of the empirical closure terms in his mathematical flame spread model. Some important variations in fire behaviour were observed in the excelsior fuel beds, in which, unlike with the wood cribs, an optimum packing ratio (at which a maximum spread rate would occur) was not observed. Given the lower thickness (higher surface-to-volume ratio) of excelsior, these variations may be of importance when considering thinner natural fuels such as pine needles.

##### 2.4.2.2.2. Discrete Wooden Sticks

In addition to the well-ordered wood cribs discussed earlier, a number of other experiments have been conducted involving other deliberate and random configurations of discrete wooden sticks [46,59,69,111,210]. A few previous authors have constructed fuel beds from very thin, vertically aligned wood sticks such as ‘toothpicks’ [59,210] and matchsticks [46,211–213], or in a similar manner with paper strips [205,214]. While other studies [58,60,86,87,215] have explored fuel beds composed of thicker sticks (e.g. rods or dowels), sometimes in combination with other fuels such as excelsior in order to create a mixed fuel bed.

Often, a key focus of these studies is understanding the effect of stick thickness and/or stick spacing on the spread rate and fire behaviour. This flame spread can vary qualitatively from that observed in natural porous fuel beds, given the highly discrete fuel structure at larger spacing. The effects of fuel bed slope/orientation [211,213] and forced-flow speed [59,210,212] have also been investigated.

Simplified physics-based models have been proposed to describe this flame spread process. Vogel and Williams [46] derived one of the few simplified physical models to allow for a scenario in which convective heating is dominant, with spread rate predictions closely matching experimental observations. The dominance of convective heating was also observed

[4] In many other regions this product is described as wood wool, however in North America this term is typically reserved for a particular grade of excelsior (0.012 to 0.020 inch thick in the USA).

in an analytical analysis of a horizontal flame spread through a matchstick array by Carrier *et al*. [210], in which radiative heating was only significant at higher fuel loadings.

#### 2.4.2.3. Laser-Cut Cardboard

A small but influential number of recent studies have investigated flame spread using laser-cut cardboard [72,216]. In a series of forced-flow flame spread experiments, Finney *et al*. [72,216] observed intermittent flame heating, as a result of buoyant instabilities, to be the dominant pre-heating mechanism. High temperature fluctuations were observed as advection of small flame parcels occurred, originating from instabilities at the rear of the flame front and resulting in flame impingement of fuel elements in the near range of the flame front leading edge.

These studies are in contrast to the greater focus on radiative heating mechanisms in many earlier studies. The dominant role of buoyancy has important implications for the scaling of laboratory and field experiments, given the relatively consistent temperature within diffusion flames [72]. Further work is required to understand and describe appropriate scaling relationships, while the applicability to other fuel types (e.g. more tightly packed pine needle beds) requires further investigation.

#### 2.4.2.4. Wooden Pallets

A similar but distinct area of research to crib fires has emerged regarding the burning behaviour of wooden pallets. The motivation for understanding the combustion behaviour of pallets is clear given their abundant use in large warehouses and industrial sites. However, there has been little use of pallets as model fuel beds and therefore comparisons with the burning behaviour of other models are limited.

While these pallets are somewhat similar to wood cribs, they involve rectangular elements where wood cribs can also be formed of fuel elements with circular, square or more complex cross-sections [217]. These wooden elements are also arranged in standardised configurations to form a pallet, although individual pallets may then be stacked together to various heights. An example of a pallet burn, conducted along with various colleagues at the University of Edinburgh Fire Research Centre, is shown in Figure 2.9.

**Figure 2.9. Exemplar wooden pallet fire conducted underneath a large calorimetry hood**

Interestingly, equations to describe the HRR ($\dot{q}$), and HRR per unit pallet on floor area basis ($\dot{q}''$), can be derived as a function of the pallet stack height ($h_p$) and moisture content ($M$) only [217],

$$\dot{q} = 1368\left(1 + 2.14h_p\right)(1 - 0.03M) \tag{2.6}$$

$$\dot{q}'' = 919\left(1 + 2.14h_p\right)(1 - 0.03M) \tag{2.7}$$

Although comparison with experimental results [217,218] indicates that these equations may overestimate the burning rate at low stack heights (< 0.5 m). Above this height, a largely linear positive relationship between stack height and peak HRR has been observed. The simplicity of this formulation will partly reflect the highly standardised geometry of wooden pallets.

## 2.5. Porous Fuel Bed Structure

### 2.5.1. Fuel Loading

The role and significance of fuel loading in flame spread remains a matter of debate [219]. Contradictory findings exist regarding the effect of fuel loading on important fire behaviour parameters such as rate of spread. The difficulty in interpreting these existing studies is exacerbated by the fact that in many past field experiments [220,221], a number of other factors (such as wind speed, relative humidity and fuel moisture content, fuel heterogeneity) also affect fire behaviour, complicating efforts to isolate the effect of fuel structure.

In past laboratory and field experiments, even where greater isolation of the fuel loading is possible, manipulations of fuel loading have often simultaneously altered the bulk density (or packing ratio) of the fuel bed. If the effect of fuel loading is to be understood, it is vital to note the two methods by which the fuel loading can be altered; by varying the fuel height (for a fixed bulk density) or varying the bulk density (for a fixed fuel height).[5] Therefore, the effect of fuel loading may depend upon the manner in which it is altered, with Rothermel [43] suggesting that the spread rate will vary positively with fuel height increases (at constant bulk density) but negatively with bulk density increases (at constant fuel height). As such, the two fuel loading manipulation methods have contradictory effects on the spread rate, and the role of both fuel height and bulk density must be understood (these are discussed further in Sections 2.5.2 and 2.5.3).

The existence of contradictory findings on fuel loading effects has also been noted for smaller, bench-scale experiments [32]. Thomas [32] noted discrepancies amongst previous studies conducted using the Fire Propagation Apparatus (FPA); a standardised testing apparatus allowing the examination of the burning properties of small fuel samples. Again, this was complicated by the fact that several previous studies had simultaneously varied both the fuel loading and the bulk density [222][147][223].

The FPA is well-suited to the examination of ignition and the effect of fuel structure, with both Bartoli and Jervis observing no effect of fuel loading on the time to ignition, except at very low fuel loadings [147,224]. This may relate to the marginal burning conditions that can occur at especially low fuel loadings, leading to extinction (or no ignition) at a lower fuel loading limit.

[5] The different manipulation methods are visually demonstrated in the video available at: https://tinyurl.com/2vyk9f82

Jervis [224] observed a negative trend between fuel loading and the normalised mass loss occurring prior to ignition. This was attributed to the lower fuel vaporisation rate at lower fuel loadings, which necessitates greater overall pyrolysis before a flammable fuel:air vapour is produced, which, in extreme cases, may also contribute to non-ignition/extinction in marginal burning conditions.

In larger flame spread experiments, the separation distance of fuel particles at lower fuel loadings may also contribute to extinction in marginal burning conditions. While even at higher fuel loadings, this fuel element separation distance may affect the ventilation conditions and resulting flame spread behaviour and fuel consumption. For laboratory flame spread experiments involving pine needle fuel beds composed either of *Pinus halepenis* or *Pinus Ponderosa* needles, Dupuy [81] noted variations in fuel consumption (and hence combustion efficiency) which were attributed to the difference in inter-needle separation distances for each fuel type.

In addition to inter-species differences in fuel consumption, Dupuy [81] observed a slight positive trend between fuel loading and fuel consumption for *Pinus halepensis* fuel beds. However, for fuel beds composed of *Pinus pinaster* needles, no fuel loading effect was observed, with fuel consumption remaining consistent, and relatively complete (circa. 95 %) across all fuel loadings. This is in contrast to previous field-scale observations in pine:oak dominated ecosystems. For a series of experimental burns in the New Jersey Pinelands National Reserve (PNR), Mueller [18] observed a highly linear trend ($r^2 = 0.87$) between the pre-fire surface fuel loading and the overall fuel consumption. A similar trend was previously observed by Clark *et al*. [225] for prescribed burns conducted within the PNR.

As a key objective of prescribed burning, fuel consumption is of great importance, and therefore improved capability for prediction of fuel consumption from the initial fuel conditions is of great value. It is important however to understand not only the total consumption but also the consumption ratio and consumption efficiency (percentage of fuel consumed in the flaming phase). This is particularly relevant given the additional prescribed burning objectives of reducing unnecessary smoke production, particularly given the significant contributions of the surface fuel loading to the total PM 2.5 production [225]. Similarly, while fuel loading is linked to fire intensity, for example within Byram's formulation for fireline intensity [102], it is the actual mass of fuel consumed in flaming (rather than initial fuel loading) which determines the resulting intensity.

Laboratory investigations of fuel loading effects on fuel consumption and efficiency offer a valuable opportunity to explore this relationship in a systematic manner. While the high consumption ratios observed by Dupuy [81] are notable, it is important to investigate further the relative contribution of the smouldering and flaming combustion phases within such laboratory flame spread experiments. In a series of laboratory flame spread experiments, Morandini *et al*. [226] observed no effect of fuel loading (for a constant bulk density) on the combustion efficiency and effective heat of combustion of pine needle beds of various fuel loadings (0.6, 0.9 and 1.2 kg/m$^2$). To provide useful insight for the development of operational tools, further investigation of the effects of the experimental set-up (e.g. substrate material, fuel bed scale, edge effects) in these classic laboratory flame spread experiments is required, in order to understand the relationship to field observations.

In addition to the work of Dupuy [81] and Morandini *et al.* [226], a number of other laboratory-based studies [227,228] have investigated the role of fuel loading in the flame spread behaviour of pine needle beds (and are therefore highly relevant to this present study). In these studies [226–228], generally a positive trend has been observed between fuel loading and rate of spread, and where measured, between fuel loading and heat release rate, total heat release, mass loss rate and flame height.

In some cases [81,228], these laboratory studies have also considered the combined effect of other factors such as fuel bed slope, on the effect of fuel loading. For a sloped fuel bed, flame tilting typically occurs, however a decrease in the flame tilt angle has been observed for pine needle beds of higher fuel loading [228]. This was attributed to the greater buoyancy effect at higher fuel loadings, however this buoyant flow profile was not measured [228]. Changes in the flame tilt angle can vary the view factor and average distance between the fuel bed and flame, which may have important implications for pre-heating of unburnt fuel.

Morandini *et al.* [226] measured both the radiant and total heat flux within the pre-heating phase for pine needle beds of varying fuel loading (0.6, 0.9 and 1.2 kg/m$^2$) and relatively consistent bulk density (17 – 20 kg/m$^3$). A positive trend between fuel loading and the total heat flux was observed within this pre-heating region. Separate radiant heat flux measurements of the flame and ember region were conducted, with the radiant heating fraction of the embers increasing at greater fuel loadings (attributed to the increased volume of the ember region) while a slight decrease in the radiant heating fraction of the flame occurred.

In a related series of up-slope flame spread experiments, Tihay *et al.* [228] observed a similar positive trend between fuel loading and heat flux, as well as with the ember radiative fraction. However, unlike in the no-slope case [226], the flame radiative fraction also increased with increasing fuel loading. This was attributed to greater backwards-tilting of the flames in the no-slope experiments conducted by Morandini *et al* [226]. A positive trend between fuel loading and radiative flux was also observed by Frankman [229] during the stationary burning of excelsior and pine needles respectively, however the bulk density was also allowed to vary in these experiments. Morandini and Silvani [230] also observed fuel loading effects on the dominant heat transfer mechanisms during a series of field experiments in Mediterranean shrublands.

Past field experiments in other fuel types have often led to contradictory findings regarding the effect of fuel loading. For example, Cheney and Gould conducted over 100 experimental wind-aided grassfires, observing no significant effect of fuel loading, in contrast to previous grassfire observations [231]. The continuing uncertainty around the role of fuel loading, has led to disagreement regarding the importance of including this parameter within fire spread models [219].

While often assumed to have an important role in flame spread, several past studies have observed at most a slight effect of fuel loading on the overall spread rate [60,220,232]. Therefore, while included as a vital component within semi-physical and physical models [233], fuel loading has frequently been discounted during the development of many empirical models [219]. However, it is often difficult to determine to what extent these field observations are affected by the difficulty of measuring and controlling field conditions (e.g. fuel structure and homogeneity, and weather conditions) [219]. Therefore, to support continuing model development, there remains a need for systematic laboratory-scale investigation of the effect

of fuel structure, given the greater isolation and control of fuel loading available in this environment.

The lack of existing experimental data to support these model development efforts is highlighted by the recent modelling study of Overholt *et al*. [234]. Using the Wildland Fire Dynamics Simulator (WFDS), Overholt *et al*. examined the model sensitivity to fuel loading (amongst other factors) for a simulation of flame spread through Little Bluestem grass. No significant effect of fuel loading on spread rate was predicted across the simulated range 0.73 to 1.4 kg/m$^2$), however no direct comparison to experimental data was provided.

Greater experimental comparison was possible in the numerical study of marginal burning in chaparral, conducted by Zhou *et al*. [235], however only two fuel loadings were studied. Using FIRELES (a 2-D, Reynolds Averaged Navier-Stokes model) for a no-wind, no-slope scenario, accurate predictions of non-propagation in the lower fuel loading case, and slightly over-predicted (18 %) the spread rate at the higher fuel loading were obtained. The availability of detailed, measurements of physical properties for flame spread experiments across a wider range of fuel loadings would allow wider analysis in future model evaluation/development studies.

### 2.5.2. Bulk Density

Within a field environment, the role of bulk density has been studied in past experiments and observation studies in various fuel types [236]. However, disentangling the respective effects of fuel loading, fuel height and bulk density presents an even greater challenge in these studies given the spatial variability that can occur, and the difficulty in accurately measuring these fuel properties. This is in addition to the challenges presented by the variability in weather and topography, whose effect must be separated from that of the fuel conditions.

Despite these difficulties, insight into the role of fuel structure has been gained from such studies. Thomas [236] compared the observed spread rates in previous field experiments (in heather and gorse) with observations from wood crib flame spread experiments. A relationship describing the spread rate $R$ in both fuel types, as a function of the wind speed and the consumed fuel bulk density ($\rho_b'$) was proposed,

$$R\rho_b' \propto 1 + U \tag{2.8}$$

With a different constant of proportionality suggested for each fuel type. In this equation, the consumed fuel bulk density represents the mass of fuel consumed per unit volume. This differs from the bulk density (which relates to the initial fuel loading), and in this manner Thomas accounted for incomplete combustion.

The importance of suitably incorporating the influence of bulk density during numerical model simulation of low-intensity fires, was illustrated in a recent study by Mueller *et al.* [40]. Using the Wildland Fire Dynamic Simulator (WFDS), this study attempted to model two conditions from the early flame-spread experiments conducted at the outset of the work presented in this thesis. The two conditions involved pine needle fuel beds of identical fuel loading but different bulk densities (11 kg/m$^3$ and 20 kg/m$^3$ respectively).

Current model limitations were apparent given the prediction of flame spread extinction at the lower bulk density (11 kg/m$^3$) condition (as seen in the predicted mass loss rate curve shown

in Figure 2.10) despite the fact that sustained flame spread was experimentally observed at this fuel condition. While prior to predicted extinguishment, the predicted flame spread rate (0.43 cm/s) was almost double that observed experimentally (0.22 cm/s)

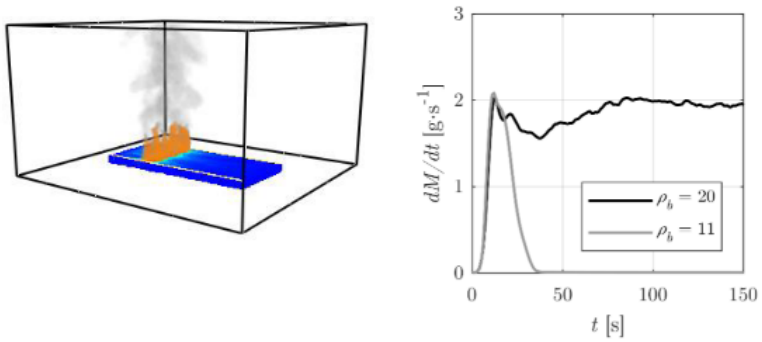


**Figure 2.10. Illustration of Wildland Fire Dynamics Simulator (WFDS) flame spread simulation by Mueller *et al.*, and simulation predictions of mass loss rate for two fuel beds of identical fuel loading but different bulk density ($\rho_b$) – From Mueller *et al.* 2018 [40]**

A possible explanation for the divergence from experimental observations was suggested: increased entrainment flow at lower bulk densities and hence greater convective cooling. It was suggested that this in-bed flow magnitude may be under-predicted, particularly behind the flame front due to inadequate modelling of fuel consumption and removal, and hence under-prediction of flow magnitude behind the flame front [40]. However, the remaining fuel structure may exert an important influence on the drag profile of the fuel bed.

A major aim of this thesis is to investigate these physical phenomena over a wider range of fuel conditions (including across a wider range of bulk densities) and to better characterise which physical phenomena require improved representation within current models. Current understanding is limited by a lack of available measurement data for the entrained flow profile within porous fuel beds (and the effect of fuel structure), and this is something which this thesis (and ongoing complimentary work by other authors [83]) seeks to address.

The importance of providing additional physical insight and data is not limited to this single experimental scenario or to the development of the WFDS. Other authors [154,237] have previously identified the need for improved representation of bulk density effects within detailed physics-based models. Marino *et al*. [237] previously observed an oversensitivity of the FIRETEC model to bulk density, during a numerical analysis of wind tunnel experiments involving shrub fuels. Similarly, while using a multi-phase model developed in OpenFOAM to simulate bench scale experiments (combustion of pine needles in the FPA), El Houssami *et al.* [154] observed weaker agreement with experimental observations at lower bulk densities.[6]

### 2.5.3. Fuel Bed Height

A substantial area of research into fuel height has involved the study of grass fuels, yet there remains a lack of agreement as to whether or not the effects of fuel height (in particular on spread rate) are well-understood [238,239]. Fuel height can be easily manipulated in grass fuels

[6] Interpretation of this greater divergence between model predictions and experimental observations was complicated by aspects of the experimental set-up. The experimental approach may have introduced a variation in the radiative heating of thinner samples, and it is difficult to identify the contribution of this effect to model performance.

by applying a range of treatments such as mowing or rolling (which are also common fire mitigation treatments [240]). This clearly however has the potential to vary the fuel loading depending on whether or not any cuttings are collected or allowed to accumulate on the ground.

By applying different cutting treatments, past studies have observed larger flame heights and spread rates in uncut grasses, although the variation in spread rate could not be fully explained by either changes in bulk density or fuel height [220,239]. Similarly, understanding the independent effect of fuel loading has proven difficult, and while it has been explicitly included in some operational grass fire models, it has not been considered in others. In Australia, for example, the Grassland Fire Danger Meter Mk IV, while warning that over-predictions may occur did not incorporate a fuel loading metric, however in the Mk V Danger Meter, spread rates were directly proportional to fuel loading [220].

There would appear to be some clear and important differences between these grass fuels and packed beds of pine needles / oak leaves. For one thing, the fuel heights commonly observed in some grasslands can reach heights in excess of 2 m [93], which greatly exceeds both the vertical length scale of the fuel beds studied in this chapter, but is also much greater than litter layer fuel bed heights observed naturally. Similarly, while the fuel element structure and inter-element arrangement may vary across different grass types and areas, the overall structure is likely to be less tightly packed than the litter layer fuel beds, and more regularly arranged/oriented (e.g. vertical grass stems).

These grass fuel types however, usefully illustrate an essential challenge in understanding the role of fuel height on fire behaviour. In manipulating the fuel height, other commonly studied variables are also necessarily altered, making it difficult to disentangle changes in physical process attributable to fuel height changes, from the effects of variations in bulk density, fuel loading and fuel element structure. It is sometimes possible to control some but not all of these additional variables. For example, in a fuel bed of fixed area, the fuel height can be altered while controlling either the fuel loading or the bulk density respectively; however, in many previous studies all three of these parameters have been simultaneously varied. This greatly complicates any effort to understand the individual importance of these variables, even though statistical methods can be employed.

Even amongst studies considering pine needle beds (or similar lab-scale fuel bed models), the observed effects of fuel bed height have varied considerably. Several laboratory based studies [59,69] have suggested a weak or insignificant effect of bed height on spread rate. Rothermel's original spread model [69] for example, exhibits a strongly linear dependence on bed height for both reaction intensity and spread rate (although the experiments upon which the model was formulated considered only a single bed height for each fuel type, with reaction time therefore considered independent of bed height). Across a wider experimental range, Wilson observed a positive relationship between spread rate and the square root of the bed depth [62]. In understanding the reasons for these discrepancies, it has been suggested that it is vital to discern between cases in which height is altered by varying fuel loading and cases in which the bulk density is altered.

Ultimately an understanding of the different physical processes associated with these fuel bed variations is required encompassing the relative importance of competing heat transfer mechanisms and other potential factors such as oxidiser supply rates [69]. Even when considering studies where fuel height is varied by altering only either fuel loading or bulk density, the chosen variable remains an important consideration when comparing between

studies and when attempting to draw wider conclusions from trends in the existing literature. It is reasonable to question therefore whether the underlying physical mechanisms driving these variations in fire behaviour are similarly altered depending on how fuel height is manipulated.

### 2.5.4. Dimensionless Fuel Bed Descriptors

Rothermel and Anderson highlighted the discrepancy in observations of spread rate trends at elevated wind speeds for different porous fuel beds [125]. A dimensionless parameter $\sigma\lambda$ was suggested by Rothermel and Anderson, to rectify these fire behaviour differences amongst various fuel types. This incorporates the surface-to-volume ratio of the fuel elements ($\sigma$), which was known to be important in the radiative pre-heating of fuels (and will also affect convective heat transfer) [93]. The term $\lambda$ represents porosity, defined by Rothermel and Anderson as the void volume divided by the surface area of fuel in the bed. The void volume is equal to the total fuel bed volume minus that which is occupied by fuel. This dimensionless parameter was correlated with the rate of spread (for a fixed fuel loading) as shown in Figure 2.11.

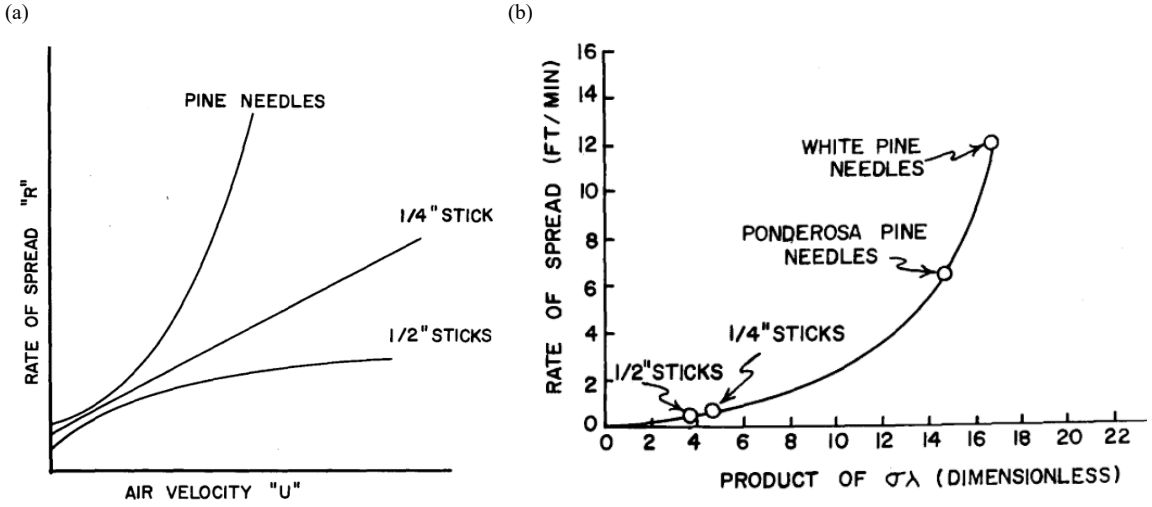


**Figure 2.11 – (a) Spread rate as a function of air velocity for three different fuel types (b) Spread rate as a function of the dimensionless parameter $\sigma\lambda$. Extracted from Rothermel and Anderson (1966)** [125]

This use of the term $\sigma\lambda$ built upon the earlier work of Curry and Fons [101], in which they attempted to explain the widely-observed increase in burning rate for more loosely packed fuel beds. This phenomenon was attributed to the greater radiation transport and increased oxygen supply afforded by the increased void space within the fuel bed. The actual absorption rate of radiation by fuel elements was considered a function of exposed fuel surface area. It was therefore proposed that spread rate was controlled by ratio of voids to fuel surface area ($\lambda$), which Curry and Fons defined as,

$$\lambda = \frac{1}{Ws} - \frac{1}{\gamma s} \tag{2.9}$$

Where $W$ is the dry fuel weight, $s$ is the fuel surface area per unit weight of fuel, and $\gamma$ is the fuel density.

For a series of quiescent flame spread experiments in various fuel types (pine needles, pine sticks and excelsior) at constant moisture content, Curry and Fons were able to explain variation in spread rate (from a point ignition source) simply as a function of the independent variables $\sigma$ and $\lambda$. This relationship is shown in Figure 2.12, which has been extracted from the publication of Curry and Fons [101].

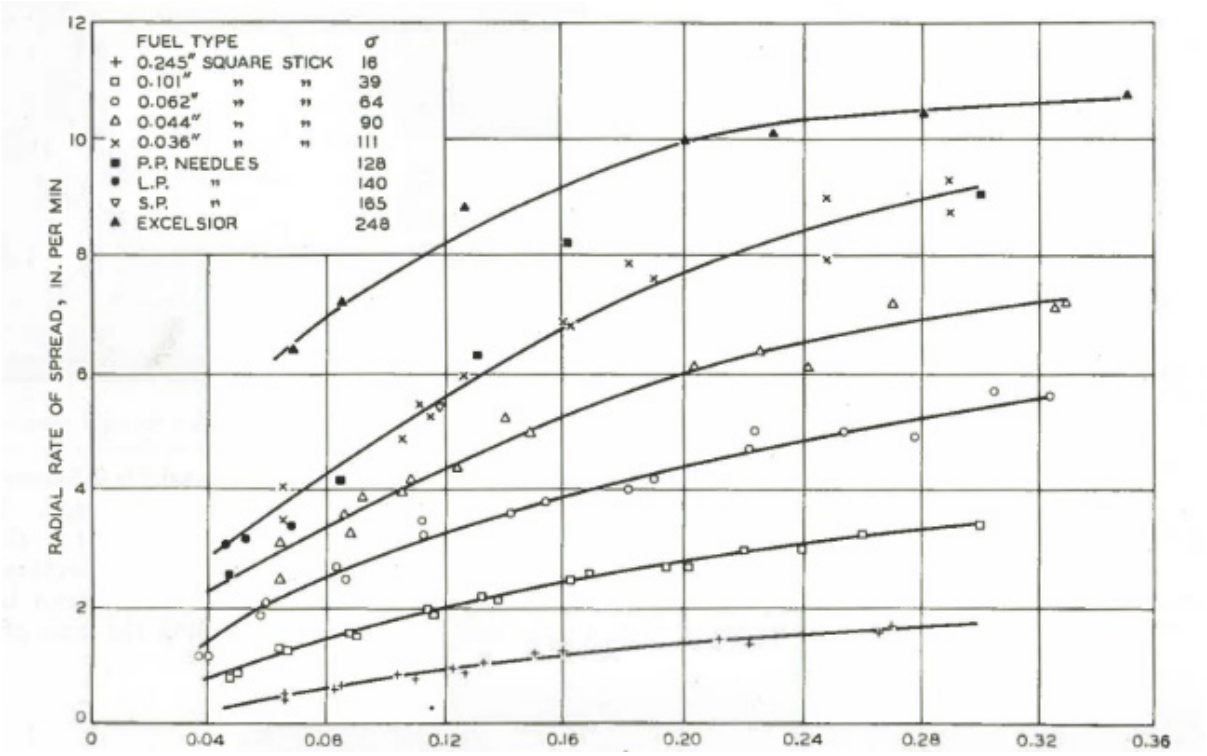


**Figure 2.12. Radial rate of spread as a function of the void voulme per surface of fuel ($\lambda$) for several fuel types with constant moisture content. (Excelsior spead rate scaled by dividing by 2.5). Extracted from Curry and Fons (1940)** [101]

In addition to Rothermel and Anderson [125], later authors have also proposed similar dimensionless terms. For example, Wilson [62,97] incorporated the optical depth of the fuel bed to define the dimensionless parameter $\sigma\beta\delta$. The development of this term, and limitations when applied to pine needle beds of varying structure (fuel loading, bulk density), is discussed further in Chapters 4 and 5. Comparison of these existing dimensionless parameters can also be drawn with the porosity factor concept used extensively in crib fire research (as discussed in Section 2.4.2.1). There remains a need to further investigate the applicability of these dimensionless terms for natural litter layers (e.g. pine needle beds) which represent an intermediate thickness between thick wood sticks and thin excelsior strands. Similarly, the applicability of the related concept of an optimum packing ratio to these natural litter layers requires further investigation, given a potential dependence on fuel loading [62,97], which may also have implications for these existing dimensionless terms.

## 2.6. Conclusions

The porous nature of wildland fuels allows for additional flow and heat transfer processes to occur within porous fuel beds, complicating efforts to extrapolate existing solid surface flame

spread theory to wildland fuel beds. A substantial volume of numerical and experimental investigation (using both natural and artificial fuels) has previously been undertaken to determine the effect of porous fuel bed structure on fire behaviour. As highlighted in this review, a number of trends between key fuel bed properties (e.g. fuel loading, fuel height, bulk density) and key fire behaviour parameters (e.g. spread rate, flame height) have been identified as a result of these systematic investigations. Yet, these observed trends have often been contradictory in nature, and we continue to lack a coherent theory to conceptually describe flame spread through porous wildland fuel beds [19].

This review has identified possible factors that may have contributed to the uncertainty around the effect of certain fuel structure parameters. Some, such as fuel height, are poorly defined as they may be altered in various manners. For example, fuel height can be altered by varying the total fuel loading for a fixed bulk density, or by altering the bulk density for a constant fuel loading. Many previous laboratory-based experiments have failed to distinguish between these two methods, and have simultaneously varied both fuel loading and bulk density, complicating efforts to understand their independent effects.

In field experiments, measuring and characterising the often largely heterogeneous fuel structure is more complicated, while fuel effects can be masked by the influence of other environmental properties (e.g. weather, topography) [85]. Where the combined effects of fuel structure and environmental properties have been studied in a controlled environment [81], an inter-dependence has been observed. This highlights the need for additional, physically linked parameters, which relate more closely to the key physical phenomena controlling flame spread in porous fuel beds (flow, heat transfer).

A number of previously proposed dimensionless parameters were reviewed, however further investigation is required to understand their applicability to natural litter layers (e.g. pine needle beds) which represent an intermediate case between very thin (high surface-to-volume ratio) excelsior and thick wood sticks used in many previous studies in which these dimensionless parameters were explored. This assessment will require further measurements of heat transfer and flow dynamics both within and above porous fuel beds, addressing identified gaps in existing datasets, as highlighted in this review and by past authors [18].

While both buoyant and entrainment flow profiles during flame spread have been investigated above porous fuel beds, there has been little examination of the in-bed flow profile in these scenarios. Previous investigation of the in-bed flow is typically limited to smaller scales and/or was conducted in the absence of flame spread. While there is an important role for studies exploring the drag profile of natural fuel beds in the absence of combustion, it is important also to investigate the feedback effect between the fuel structure, heat release rate and resulting buoyant flow profile that ultimately drives the lateral entrainment of flow.

Similarly, while dominant heat transfer mechanisms have been identified for certain fuel types and flame spread scenarios, there remains a need for great experimental evaluation of the effect of fuel structure on the relative importance of heat transfer mechanisms. As discussed in this review (and in Chapter 6), a number of past studies have measured the heat fluxes from the flame and/or combustion region, or have explored the energy released from the smouldering and/or flaming phases. Yet often these studies have focused on the effect of wind or slope, rather than systematic investigation of the effect of fuel bed structure. Additionally, a lack of consensus on measurement approaches, and the limited number of point source measurement

of heat flux, limits efforts to compare systematically the contribution of different heat sources (e.g. above-bed flame and the in-bed combustion region) in many of the existing studies.

# Chapter 3

## Methods

# 3. Methods

## 3.1. Summary

This thesis is centred upon an extensive series of laboratory-based flame spread studies conducted using a custom-built Flame Spread Table (the Table) shown in Figure 3.1. In this chapter, the basic layout of the Table is described, along with a summary of the instrumentation implemented for each of the main experimental series (discussed in Chapters 4, 5, and 6). Detailed specifications are provided for key instrumentation, along with a discussion of specific measurement techniques, analysis procedures, and uncertainties associated with the various measurements of fire behaviour and physical properties.

(a) 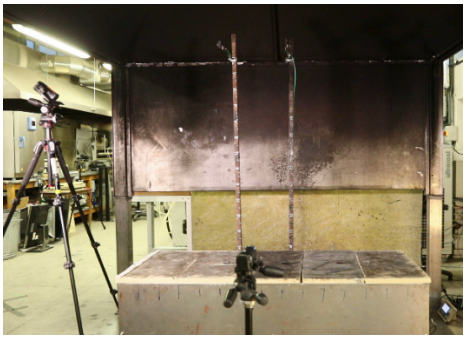 (b) 

**Figure 3.1 – (a) Typical experimental set-up of the Flame Spread Table located underneath a large calorimetry hood (b) Typical quiescent flame spread behaviour on the Flame Spread Table**

The flame-spread experiments involved fuel beds constructed using various species of pine needles and oak leaves, or a combination of the two. All of the fuel species were collected from the New Jersey Pine Pinelands National Reserve (PNR), and are typical of the fuels found within this pine-oak dominated ecosystem [241,242]. The geometric and thermochemical properties of each pine needle and oak leaf species are presented in this chapter, alongside a summary of the sampling and measurement approaches. Given the importance of the fuel bed properties (in addition to fuel element properties), the methods for fuel bed construction are also outlined. Various structural descriptors of porous fuel beds are defined, as these will be used throughout the thesis.

## 3.2. Flame Spread Table

The Flame Spread Table (the Table) consists of a 1.5 m by 0.67 m vermiculite substrate base with adjustable steel sidewalls. Fuel beds were constructed on the table surface, with the sidewalls raised to a height of 30 mm above the fuel surface to limit lateral entrainment into the fuel bed; as this has previously been shown to promote the formation of more linear flame fronts [129]. Re-radiation from the sidewalls was also limited by covering the inside surface with an insulating material (alumina-silica fibre).

The flame spread experiments were ignited across one of the short ends of the table, using a line ignition source (a 0.67 m long strip of alumina-silica fibre, soaked uniformly with 10 ml of acetone). This provided a strong ignition source intended to ensure that the resulting flame spread was independent of ignition. In a series of characterisation tests, the average burning duration of the ignition source was 61 ± 8 seconds. This resulted in the rapid formation of a linear flame front immediately after ignition, at all but the lowest fuel loadings. At these lowest fuel loadings, given the fuel sparsity, inter-element structure dominated the flame spread process.

Depending upon the experimental series, several key physical properties were measured using a variety of instrumentation: gas phase temperature (thermocouples), gas flow velocity (bidirectional pressure probes), and heat flux (heat flux gauges). By varying the sensor height, it was possible to measure these phenomena either within or above the porous fuel bed. As shown in Figure 3.2, the exact instrumentation layout in each experimental series varied, and these are described in detail within the relevant chapter for each experimental series.

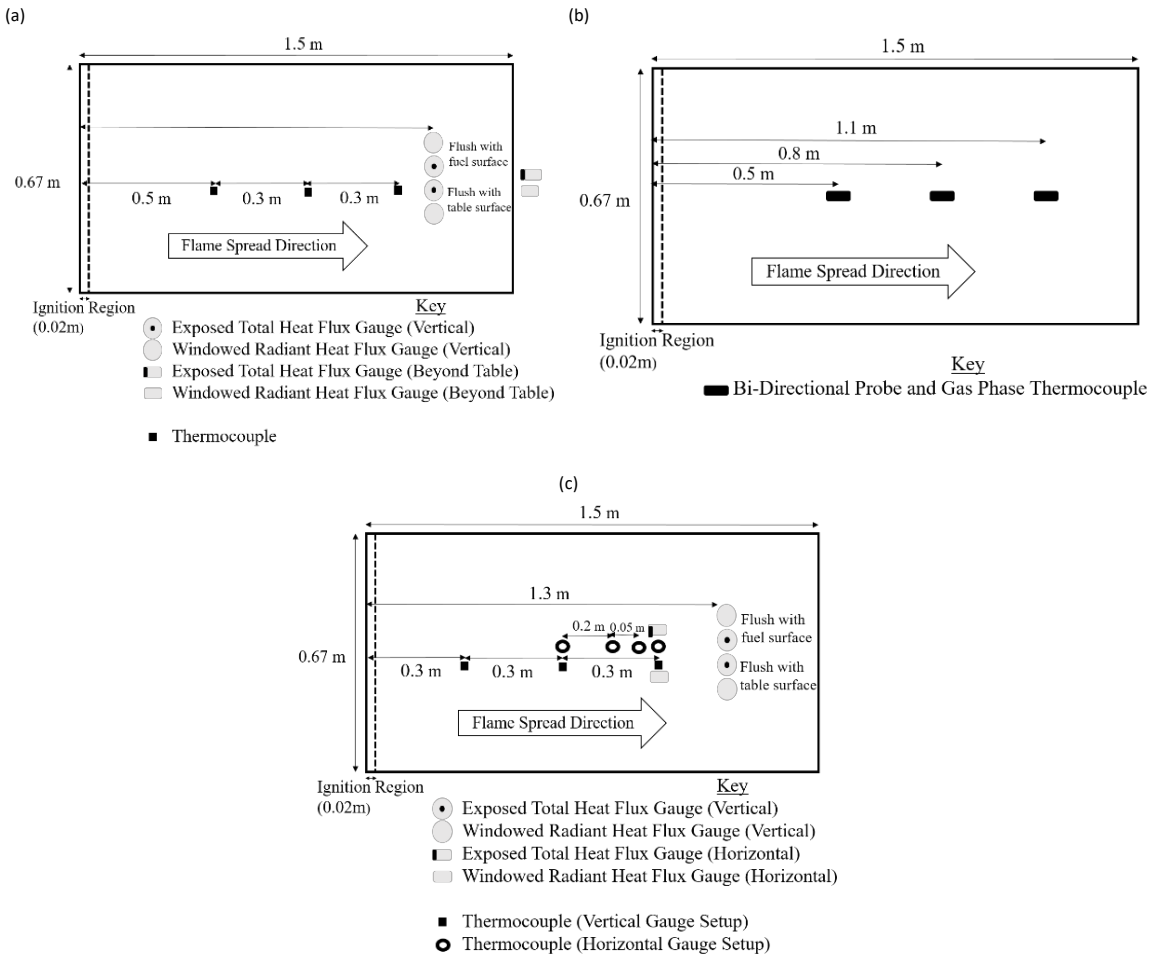


**Figure 3.2 - Schematics of the Flame Spread Table instrumentation deployed in the experimental series described in (a) Chapter 4 (b) Chapter 5, and (c) Chapter 6.**

Additional measurements of the overall fire behaviour complimented the measurements of physical properties. The Table was typically situated on a load cell, and within a furniture calorimeter, allowing continuous measurement of mass loss and heat release respectively. Experiments were filmed (using both Infrared and visual imagery) which, along with flame height and horizontal distance markers, allowed image analysis of the flame height, fire front characteristics, and rate of spread.

These fire behaviour measurements allow the global effect of fuel structure to be investigated, and may help to identify physical phenomena requiring further investigation. Additionally, the spread rate and flame height are important operational parameters, and represent common outputs of flame spread models.

The suitability of a number of existing flame spread models (when applied to a quiescent, low-intensity flame spread scenario) is assessed in this thesis, through comparison of predicted and observed fire behaviour. Where possible, the suitability of sub-models describing key physical processes was also assessed, through comparison with the measurements of physical properties (flow, heat transfer) in this study. A primary objective of this thesis is to investigate the relationship between fuel structure and these key physical processes.

## 3.3. Measurements of Physical Properties

### 3.3.1. Gas Phase Temperature

Gas phase temperatures were measured using K-Type sheathed thermocouples (TC Direct 406-473 ®), with an outer sheath diameter of 0.25 mm. Similar diameter thermocouples have been used to measure gas phase temperatures in past flame spread experiments [67,207,230,243]. Temperature measurements were logged at a rate of 10 Hz, except where indicated. This is similar [207,243], or greater than [230], the scanning rate used in a number of similar previous experiments and is suitable for the subsequent spread rate and flow velocity calculations .

#### 3.3.1.1. Temperature Uncertainty

Conduction losses can occur along the thermocouple wire, however, radiative errors are typically considered more significant for in-fire measurements [244], with the error magnitude dependent upon thermocouple surface area. To reduce this error, small diameter thermocouples (0.25 mm) were selected, and thermocouples were shielded from direct radiation where possible. Gas phase thermocouples protruded out through the Table surface, with the vermiculite surface shielding the majority of the thermocouple, but leaving the tip exposed.

For similar-sized thermocouples, Silvani and Morandini calculated (using an energy balance approach) a maximum radiative error of 10 % for thermocouples located either in the flame or in the pre-heating region ahead of the flame [245]. Therefore, in line with other subsequent authors [18], no corrections were applied to the temperature measurements reported in this thesis.

### 3.3.2. Flow Velocity

Air flow velocities (both within and above the fuel bed) were calculated from the pressure difference and gas-phase temperature measured by co-located bidirectional pressure probes [246] (20 mm diameter) and gas-phase thermocouples (0.25 mm diameter). Pressure and temperature measurements were logged at a rate of 10 Hz, except where indicated.

Pressure differences were measured using Omega PX277 ® pressure transducers. In this work, the lowest range pressure transducers (0 to 0.1 ± 0.05 inches of water) were used (approximately equal to a range of 0 to 25 Pa), with an output voltage range of 0 to 10 Volts. The manufacturer quoted accuracy, as a percentage of full scale (FS), is ± 1 %, with thermal effects of 0.02 % ± 0.0125 % FS per °C. The proof pressure[7] of 10 psi was well in excess of the pressures measured during this study.

The measured pressure difference ($\Delta P$) was converted to a gas phase velocity ($v$) according to,

[7] The proof pressure (or overpressure limit) is the maximum operating pressure to which the device can be exposed without causing permanent modification of sensor performance.

$$v = \frac{1}{K}\sqrt{\frac{2\Delta P}{\rho}} \tag{3.1}$$

Where $\rho$ is the temperature-dependent gas-phase density, and K is a correction factor dependent upon the probe geometry. The pressure probes had previously been calibrated via wind tunnel testing (Young Calibration Ltd. – Certificate No. 32217) [18] and have a correction factor of 1.08.

#### 3.3.2.1. Flow Measurement Uncertainty

Bidirectional pressure probes are a robust, durable device for the measurement of flow velocities in wildland fire scenarios [18]. While other higher-precision sensors, including those able to measure 3-dimensional flow fields are available, they may become damaged or clogged when exposed to flames, and are unsuitable for use in high temperature environments.

For bidirectional pressure probes, past studies suggest that the calibration factor can vary by as much as ± 5 % across different probes [18]. This is likely however to represent a small contribution to the overall level of uncertainty. Much of the uncertainty instead arises from the low velocity range of interest, and the pressure sensor response time. In this study, the random error was measured in the background period prior to ignition, while the variability between replicate experiments is also reported.

### 3.3.3. Heat Fluxes

Heat fluxes (both radiant and total) were measured using hybrid Schmidt-Boelter/Gardon water-cooled heat flux sensors (Hukseflux SBG01 ®) [247,248]. These gauges have a rated measurement range of 5 to 100 kW/m$^2$ and a response time of 200 ms. Heat flux measurements were logged at a rate of 10 Hz, except where indicated. A similar [207,228], or lower scanning frequency [230,245], has been used in several previous flame spread studies. This scanning rate is suitable for the overall energy comparisons undertaken in this work which does not focus on higher frequency, near-range heating effects.

The gauges measure the irradiation to a plane surface from a 180° view angle. The gauges aim to achieve directional response closely approximating that of a 'cosine response', in which the response to the radiation varies with the angle of incidence according to the cosine law. As open sensors, these gauges measure the combined radiative and convective heat flux to the cooled surface of the gauge.

Accurate measurement of heat flux within a mixed radiative and convective fire environment presents a significant challenge [245]. The gauges are initially calibrated by the manufacturer in accordance with ISO 14934-3 [249]. As a result of this initial calibration, a sensitivity value (S) is calculated based upon the thermoelectric output generated in response to a given heat flux. For the meters used in this study, the calibration heat flux was 100 kW/m$^2$, with the sensitivity ranging from $0.161 \times 10^{-6}$ to $0.166 \times 10^{-6} \pm 0.011 \times 10^{-6}$ $\frac{V}{W/m^2}$. Using this sensitivity value, the heat flux at the sensor surface ($\dot{q}$), can be calculated according to,

$$\dot{q} = \frac{V_o}{S} + \sigma(T + 273.15)^4 \tag{3.2}$$

Where the second term accounts for radiation losses emitted from the sensor, with $\sigma$ representing the Stefan-Boltzmann constant, and T the sensor temperature. If appropriately water-cooled, then this heat loss term will remain insignificant (radiation emitted at max. operating temperature of 80 °C is < 0.88 kW/m$^2$) and can be neglected.

#### 3.3.3.1. Radiative Flux Measurements

For measurements of radiative flux, a sapphire window (2.3 ± 0.1 mm thick) was placed over the sensor to block convective heat transfer. The open meters have an emissivity of up to 0.95 (given the black exterior coating of the sensor) and a flat spectral range of 0.2 to 50 µm, however this is reduced where windowed meters are used, since the applied sapphire lenses have a spectral transmission range of 0.2 - 5.5 µm.

The choice of material for use in windowed gauges is discussed in ISO 14934-4 [250], where the transmission properties of several candidate materials are compared. Sapphire windows were chosen for this study, given their wide transmission range and the lack of safety issues associated with other common window materials (e.g. the sublimation of Zinc Selenide at circa 800 °C). Sapphire lenses have previously been used as a window material in other similar laboratory and field-based studies [207,228,243,245,251]. The properties of the sapphire windows used in this study are specified in Table 3.1.

**Table 3.1 - Sapphire window specifications**

| Material | Uncoated Sapphire ($Al_2O_3$) |
|---|---|
| Abbe Number | 72.24 |
| Clear Aperture | ≥ 90 of diameter |
| Thickness | 2.3 ± 0.1 mm |
| Diameter | 25 ± 0.25 mm |
| Coefficient of Thermal Expansion | 8.8 10-6/C |
| Birefringence | 0.008 for visible light |
| Refraction Index | 1.77 |

The clear aperture of the window lens is 90 % and therefore the specified optical properties are only guaranteed across a diameter of 22.5 ± 0.25 mm; however, this is still significantly larger than the sensing area diameter (10 mm).

The proportion of incident radiative flux absorbed by the windowed gauges ($\dot{q}_w^{"}$) is dependent on both the window transmissivity ($\tau$) and the gauge emissivity ($\epsilon$),

$$\dot{q}_w^{"} = \tau\epsilon\dot{q}_{rad,inc} \tag{3.3}$$

Where $\left(\dot{q}_{rad,inc}\right)$ is the incident radiative flux.

By considering the difference between $\dot{q}_w^{"}$ and the total heat flux absorbed by the un-windowed gauge, a convective heat flux value can be estimated. This should not however be considered equal to the convective heat transfer experienced by the fuel elements, given the differences in geometry and temperature of the fuel elements.

#### 3.3.3.2. Heat Flux Measurement Uncertainty

The main types and sources of error are summarised in Table 3.2, and the overall uncertainty can be assessed in accordance with ISO 98-3 [252]. The uncertainty can be incorporated into

Equation 3.2, for example as uncertainty in sensitivity (S) (e.g. temperature dependence, instability, calibration uncertainties) and in output voltage $V_o$ (e.g. data logger voltage measurement errors).

**Table 3.2 - Summary of contributions to heat flux measurement uncertainty**

| Uncertainty Type | Description/Details |
|---|---|
| Calibration Uncertainty | Effects the uncertainty associated with the Sensitivity value (S).<br>Manufacturer quotes initial calibration error of ± 6.5% with a coverage factor of 2. |
| Variation Between Reference & Calibration Conditions | May include non-linearity effects (deviation from ideal theoretical linear voltage output across rated measurement range).<br>Manufacturer suggests non-linearity error of ± 2 % of rated measurement range which is equal to ± 2 kW/m$^2$ for the gauges in this study |
| Sensor Damage Application Errors | Suitability of sensor properties in sensing environment.<br>Sensor influence on measurement.<br>Representativeness of measurement location. |

The random error associated with the heat flux measurements was assessed in the background period prior to each experiment, with a maximum error of ± 0.12 kW/m$^2$ observed across all experiments. This effectively establishes the actual zero value of the sensor within the environmental conditions in which the experiments were conducted [253]. This measured uncertainty magnitude is similar to that observed in similar previous studies [253].

## 3.4. Fire Behaviour

### 3.4.1. Flame Spread Rate

The flame spread rate was primarily determined through video analysis of the flame front position over time. The leading edge of the flame front centreline was used to define arrival times at 0.1 m increments from the ignition line. The spread rate was then determined via regression analysis, with the standard deviation across all 0.1 m segments also calculated. The initial potentially ignition-affected region (0.3 m in length) was omitted from these spread rate calculations.

For comparison, the rate of spread was also calculated using the gas phase temperature measurements discussed in Section 3.3.1. A temperature threshold of 300 °C was assumed to indicate flame arrival at a thermocouple. The rate of spread can then be calculated based upon the time period between flame arrival at successive thermocouples (since the distance between these thermocouples is known). The same temperature threshold was used to calculate the flame residence time at each thermocouple.

### 3.4.2. Flame Height

Flame height was calculated via video analysis; with a vertical length scale (0.05 m divisions) co-located with selected measurement locations on the Table. The flame height was defined as the distance between the peak of the continuous flame region and the fuel surface [254]. This video analysis was largely manual in nature given the variation in camera angle and location, with the vertical length scales providing a reference scale for calibration.

In some cases, a slight curvature of the flame front was observed and therefore a constant region for comparison across experiments was required. The region of interest was defined as the

leading edge of the central region of the flame front, as the majority of instrumentation was located on or near the fuel bed centreline. The flame height was estimated at three different distances from the ignition line with the average value across all sample points reported.

Isolation of the flame region is possible via manual selection of colour thresholds and conversion to a binary image as shown in Figure 3.3. Part of the uppermost sections of the flame region may be lost during this thresholding process. The loss of leading, unattached flamelets was not a concern as the flame height was defined as the peak of the continuous flame region. The reflection of light onto the sidewalls was often observed as shown in Figure 3.3 however this does not hinder efforts to estimate the upper extent of the flame region.

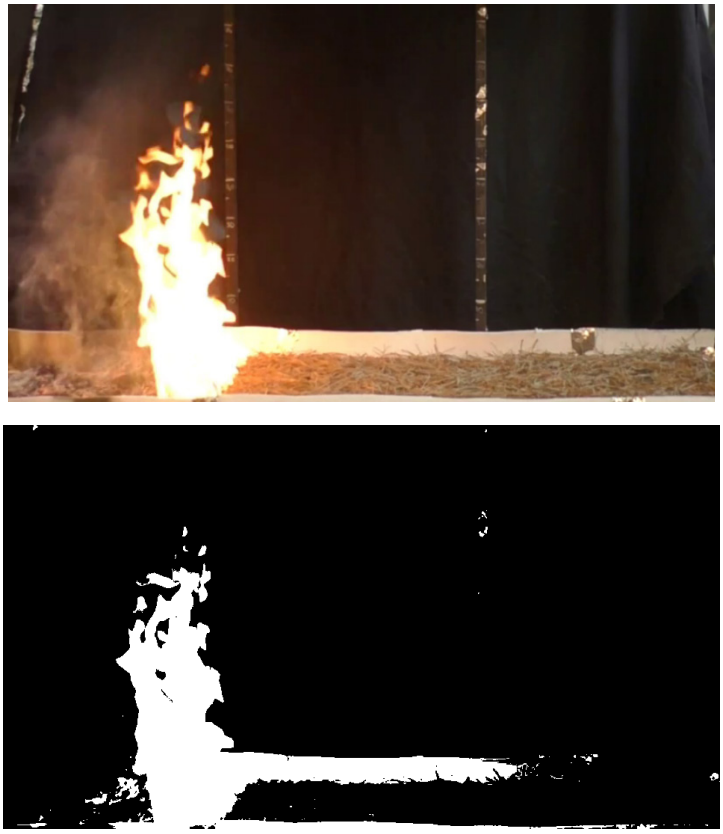

**Figure 3.3 – Example of (Top) raw and (Bottom) binary colour thresholded flame height images at first flame height marker for a fuel bed of 1.2 kg/m$^2$ and 20 kg/m$^3$**

For the experiments described in Chapter 4, the flame height was also measured using a vertical thermocouple tree. The thermocouple tree consisted of six thermocouples, arranged at irregularly spaced vertical intervals (0, 0.05, 0.1, 0.2, 0.3, 0.5 and 1 m) above the table surface. Each thermocouple was a 0.25 mm diameter, K-type thermocouple, with the irregular vertical spacing allowing greater resolution for the lower flame heights expected for the majority of the fuel bed conditions studied. Gas phase temperatures were recorded at a frequency of 10 Hz, throughout the experimental duration.

A 1 second moving average was applied to the temperature data to filter high-frequency flame fluctuations. A threshold of 300 °C was assumed to indicate the presence of a flame at a given thermocouple location, with linear interpolation used to estimate temperatures in-between thermocouple locations. The flame height was defined as the maximum vertical height at which the temperature was equal to, or greater than, the threshold value. The flame residence time at

each thermocouple was also calculated based upon the longest continuous duration for which this temperature threshold was exceeded.

### 3.4.3. Fuel Consumption

#### 3.4.3.1. Mass Loss Rate

The flame spread table was positioned upon a load cell (1 Hz sampling frequency, ± 1 g accuracy) for continuous measurement of mass loss. The mass loss rate was calculated for each time step based on the derivative of the mass over the time step period. A 5 second moving average was applied to the calculated mass loss rate. The load cell specifications, and the analysis techniques used, are similar to those in several previous studies conducted across multiple scales [74,226,255,256].

Background noise prior to ignition was filtered out by removing outliers in the mass measurements prior to ignition. Outliers were identified as values of greater than three scaled median absolute deviations from the medium, and were replaced by the nearest non-outlier value. The flame spread experiments presented in this study are characterised by a period of constant mass loss rate. Therefore, the average mass loss rate across the experimental duration (period between ignition and flameout) is reported.

## 3.5. Heat Release Rate

The Heat Release Rate (HRR) can be used to describe the fire size, and has been incorporated into various standard testing methods and past fire studies [257–259]. In this study, measurements of HRR were conducted using two different apparatus (Furniture Calorimeter and Transportable Analyser for Calorimetry Outside (TACO)), as outlined below. In both cases, the HRR was calculated using the Oxygen Consumption Calorimetry (OCC) method.

### 3.5.1. Furniture Calorimeter

In many of the experiments conducted in this study, the HRR was measured using a furniture calorimeter. The Table was positioned underneath an extraction hood, with an average flow rate of 1,000 l/s. Steel curtain walls on each side of the hood ensured full extraction of exhaust gases and prevented over-spilling. Calorimetry data was logged at a scanning frequency of 1 Hz.

#### 3.5.1.1. Exhaust Flow Rate

Measurement of the exhaust flow rate represents a significant source of the overall uncertainty of the calorimetry process [260–265]. A bidirectional pressure probe [246] (positioned on the exhaust duct centreline, with the probe axis parallel to the flow direction) measured the pressure difference within the exhaust duct. In this arrangement, the stagnation pressure is measured at the upstream tap, while the static pressure is measured at the downstream tap.

#### 3.5.1.2. Exhaust Gas Temperature

The exhaust gas temperature in the duct was measured using a 1 mm K-Type thermocouple. The temperature of the incoming airflow was calculated based on the average temperature across the 30 seconds prior to ignition. More detailed thermocouple specifications are provided in Section 3.3.1, along with a general discussion of the analysis methods and uncertainty analysis for temperature measurements.

### 3.5.2. Transportable Analyser for Calorimetry Outside (TACO)

While the Heat Release Rate (HRR) is a commonly measured variable in laboratory experiments of all scale, there has been little attempt to measure HRR in field experiments. Instead, indirect measurements such as fire line intensity (based on flame height observations) are often presented, given the greater ease of measurement in a field environment.

In a subset of the experiments in this thesis, the Transportable Analyser for Calorimetry Outside (TACO) allowed measurement of the HRR using Oxygen Consumption Calorimetry (OCC). The TACO was also used in a series of complimentary, field-based flame spread experiments that, while outside the scope of this thesis, will eventually allow more direct comparison of HRR values measured in the lab and the field.

The TACO consists of an exhaust collection hood and duct, with a gas sampling probe extracting from the exhaust duct. The exhaust gas is transported through a solid particle filter, and subsequently through a desiccant (Drierite ®) for moisture removal. Subsequent gas analysis allows the concentration of CO, $CO_2$ and $O_2$ to be determined as discussed below. The characterisation of the exhaust flow profile is also discussed in detail in subsequent sections.

As illustrated in Figure 3.4, the TACO has previously been deployed in field experiments, with the exhaust hood raised above the fuel on metal stilts, and a similar deployment was used in these laboratory experiments. The deployment height is chosen to prevent flame impingement within the exhaust hood. The measured HRR will vary as a function of the flame front location (relative to the exhaust hood centreline), with a maximum HRR measured when the flame front sits directly underneath the exhaust hood. The heat release rate per unit area can also be calculated based upon the exhaust duct cross-sectional area.

**Figure 3.4 – Example of typical field deployment of the Transportable Analyser for Calorimetry Outside (TACO)**

#### 3.5.2.1. Exhaust Flow Rate

A bidirectional pressure probe [246] was positioned on the exhaust duct centreline, with the probe axis parallel to the flow direction. In this arrangement, the stagnation pressure is

measured at the upstream tap while the static pressure is measured at the downstream tap. The support tubes of the probe were horizontally mounted and connected, with additional silicon tubing, to a differential pressure sensor (positioned at a similar height to avoid buoyancy effects).

Pressure differences were measured using a Sensiron SDP810-125 Pa ® pressure sensor. This digital pressure sensor has a calibrated pressure range of 125 Pa, with an accuracy of ± 3 %. While offering a high range, these sensors operate with a low minimum detectable pressure of 0.01 Pa and a response time of 0.5 ms.

#### 3.5.2.2. Exhaust Gas Temperature

The temperature of exhaust gases in the duct was measured using a 0.25 mm diameter K-Type thermocouple. The temperature of the incoming airflow was calculated based on the average temperature across the 30 seconds prior to ignition. More detailed thermocouple specifications are provided in Section 3.3.1, along with a general discussion of the analysis methods and uncertainty analysis for temperature measurements.

#### 3.5.2.3. Exhaust Gas Species Concentration

Within the exhaust duct, gas sampling (along with flow and temperature measurements) occurred at a distance equal to 10 times the diameter (D) from duct entrance, and at a distance from the duct exit equal to six diameters. This allows the formation of fully developed flow, prior to measurement, but avoids the influence of edge effects.

The pump-driven sampling line supplied sample gas to the analysis system at a flow rate of 1 litre/hr, with moisture removed prior to gas analysis by passage through a desiccant tube containing Drierite ®. The concentration of $CO_2$ and CO in the sample gas was measured using a Non-Dispersive Infrared (NDIR) sensor, while $O_2$ concentration was measured using an electrochemical sensor ($AO_2$ Citicel Oxygen Cell ®). All gas concentration measurements were logged to a Raspberry Pi ® at a scanning frequency of 1 Hz. The NDIR was zeroed at ambient laboratory conditions and therefore negative concentrations of CO and $CO_2$ are occasionally recorded.

### 3.5.3. Oxygen Consumption Calorimetry (OCC)

For both the Furniture Calorimeter and the TACO, the HRR was calculated using the principle of Oxygen Consumption Calorimetry (OCC). OCC is underpinned by Thornton's [266] observation that, during complete combustion, many organic liquids and gases exhibit a similar net heat release per unit of oxygen consumed. Hugget [267] later demonstrated that this also applied to many organic solids, suggesting that an average energy release of 13.1 MJ/kg of $O_2$ was appropriate in most cases (typically with an accuracy of ± 5 %).

Recently, several authors [147,159] have investigated the energy release rate of various wildland fuels. Simeoni *et al*. determined the energy constants for three different pine needle species, all of which had greater energy constants than Hugget's average value, with a maximum deviation of 11.3 % observed. For a variety of Mediterranean wildland fuels, Bartoli [147] determined an average value of 14.15 MJ/kg of $O_2$, with a similar value observed by Santoni *et al.* [227]. This value is typically assumed to provide a useful approximation for most forest fuel types [32]. While the use of this generic value contributes to the overall uncertainty of the HRR calculation [147], this is typically less significant than the uncertainty introduced during the measurement of exhaust duct flow velocities.

Given the assumption of energy constants, OCC relies upon the assumption that, to estimate the net heat release, it is necessary only to measure the oxygen consumption. This is an experimental technique that was proposed at least as far back as the 1960's, and was perhaps first practically applied in the ASTM-E84 Tunnel Test [268,269].

OCC methods have been refined over recent decades, and in this study the HRR was calculated based on the three gas ($O_2$, CO and $CO_2$) method outlined by Janssens [270], and involving the following steps:

1. Calculation of mass flow rate in exhaust duct.
2. Calculation of mole fraction of $H_2O$ in incoming air.
3. Calculation of molecular weight of incoming air.
4. Calculation of $O_2$ depletion factor.
5. Calculation of HRR.

A number of constant values were assumed throughout, and these are summarised in Table 3.3.

**Table 3.3 – Summary of constant values assumed during Heat Release Rate (HRR) calculations**

| Property | Assumed Value |
|---|---|
| Net HRR per Unit Mass of $O_2$ Consumed | 14.15 kJ/g of $O_2$ |
| Net HRR per Unit Mass of $O_2$ Consumed for CO | 17.60 kJ/g of $O_2$ |
| Molecular Weight of Dry Air | 29 kg/mol |
| Molecular Weight of $CO_2$ | 44 kg/mol |
| Molecular Weight of CO | 28 kg/mol |
| Molecular Weight of $H_2O$ | 18 kg/mol |
| Molecular Weight of $N_2$ | 28 kg/mol |
| Molecular Weight of $O_2$ | 32 kg/mol |
| Combustion Expansion Factor | 1.105 |

#### 3.5.3.1. Exhaust Gas Mass Flow Rate

Where the exhaust duct flow is measured using a bidirectional pressure probe, the relationship between the differential pressure across the probe ($\Delta P$) and the centreline velocity in the duct ($v_c$), is given by,

$$\Delta P = \frac{1}{2}\rho_e[f(Re)v_c]^2 \tag{3.5}$$

Where ($\rho_e$) is the exhaust gas density, and $f(Re)$ is a probe correction factor which is dependent upon the Reynolds number.

There the density of the exhaust gas ($\rho_e$) varies with the exhaust gas temperature ($T_e$), and can be calculated relative to the ambient conditions,

$$\rho_e = (\rho_a T_a)/T_e \tag{3.6}$$

Where $\rho_a$ is the ambient air density, and $T_a$ is the ambient air temperature. At standard conditions (1 atm.), the density of air is 1.29 kg/m$^3$ at a temperature of 273 K.

The Reynolds-dependent correction factor accounts for the variations in probe response, and this probe response is given by the ratio of the square root of the measured pressure head and the velocity head. This ratio is calculated based on the equation given by McCaffrey and

Heskestad (valid for 40 < Re < 3800, with accuracy of ± 5 %) [246], which is based on a polynomial curve fit of experimental data obtained across a range of Reynold's numbers,[8]

$$\frac{\left(\frac{2\Delta p}{\rho}\right)^{\frac{1}{2}}}{V} = 1.533 - 1.266 \times 10^{-3} Re + 1.688 \times 10^{-6} Re^2 - 9.706 \times 10^{-10} Re^3 + 2.555 \times 10^{-13} Re^4 - 2.484 \times 10^{-17} Re^5 \quad (3.7)$$

Where the Reynold's Number (Re) is given by,

$$Re = \frac{(\rho V D)}{\mu} \quad (3.8)$$

Where $V$ is the gas velocity, $D$ is the probe diameter (which is the characteristic length in this case) and $\mu$ is the dynamic viscosity.

The asymptotic value of the probe response factor (at large Reynolds numbers) is around 1.08. This is slightly higher than pitot-static tubes, which have an asymptotic response value of 1.0. In large-scale testing, it is generally assumed that the flow rate and duct diameter combination will result in Reynolds number (Re) > 3800, with Re therefore assumed to be constant (1.08), and a similar assumption is made in this analysis.

Equation 3.5 can be re-arranged in terms of the centreline velocity and converted to a volumetric flow rate, based on the duct cross-sectional area (A).

$$\dot{m}_e = \frac{A k_c}{f(Re)} \sqrt{2 \rho_e \Delta p} \quad (3.9)$$

Where $k_c$ is the velocity profile shape factor, which describes the ratio of the average velocity to the centreline velocity. This can be calculated experimentally but is often assumed to be close to 1.0, for large-scale fire tests, in which the exhaust flow in the duct is turbulent. Substituting Equation 3.6 (at standard conditions) into the above equation results in an equation of the form,

$$\dot{m}_e = 26.54 \frac{A k_c}{f(Re)} \sqrt{\frac{\Delta P}{T_e}} \quad (3.10)$$

#### 3.5.3.2. Mole Fraction of Water in Incoming Air

Water vapour is removed from the exhaust gases prior to gas species analysis, and it is therefore assumed that during analysis the only species present are $O_2$, $N_2$, $CO_2$ and CO. As a water vapour analyser was not used, the mole fraction of water vapour in the incoming air ($x^0_{H_2O}$) was calculated based upon the ambient air properties,

$$x^0_{H_2O} = \frac{RH}{100} \frac{p_s(T_a)}{p_a} \quad (3.11)$$

[8] Equation 3.7 differs slightly from that presented by Janssens [270] which appears to include a typographical error.

Where $RH$ is the Relative Humidity, $p_a$ is the air pressure, and $p_s(T_a)$ is the saturation pressure of water vapour at the air temperature $T_a$.

The saturation pressure is calculated using the full (three coefficient) version of the Antoine equation [271]. This is a semi-empirical term describing the temperature dependent vapour pressure of a pure substance, which gives the following solution to the Clausius-Clapeyron relation,

$$ln(P_s) = A - \frac{B}{C+T} \tag{3.12}$$

Where A, B and C are coefficients, equal to 23.2, 3816 and - 46 respectively, for water in the temperature range of interest.

The mole fraction of water allows the molecular weight of the incoming air ($M_a$) to be calculated,

$$M_a = M_{dry}\left(1 - x^0_{H_2O}\right) + M_{H_2O}X^0_{H_2O} \tag{3.13}$$

Where $M_{dry}$ is the molecular weight of dry air, and $M_{H_2O}$ is the molecular weight of water vapour. It is assumed that that the production of water vapour in the combustion process is negligible.

#### 3.5.3.3. Oxygen Depletion Factor

As open-system HRR measurements are made in this study, it is the flow rate of the exhaust gases that is measured rather than the flow rate of the incoming air. To relate the measured exhaust gas flow rate to the incoming airflow rate, an oxygen depletion factor ($\phi$) can be defined.

During combustion, some of the depleted oxygen in the exhaust gases are replaced by an equal or greater number of moles of combustion products. An expansion factor can be defined to describe this process but this value is dependent on the fuel composition. Janssen recommends a value of 1.105 (the actual value of methane) as a reasonable average value where the fuel composition is unknown, and this is the approach taken in this study.

The exact formulation of the oxygen depletion factor will vary according to which combustion gases are analysed, with Janssens suggesting formulations for four cases:

1. $O_2$ measured only.
2. $O_2$ and $CO_2$ measured.
3. $O_2$, $CO_2$ and CO measured.
4. $O_2$, $CO_2$, CO and $H_2O$ measured.

Only Case 3 is discussed in detail here, as this is the gas analysis combination used in this study. In this case, the oxygen depletion factor can be calculated using,

$$\phi = \frac{X^{A0}_{O_2}\left(1 - X^A_{CO_2} - X^A_{CO}\right) - X^A_{O_2}\left(1 - X^{A0}_{CO_2}\right)}{\left(1 - X^A_{O_2} - X^A_{CO_2} - X^A_{CO}\right)X^{A0}_{O_2}} \tag{3.14}$$

Where $X^A_{CO_2}$ is the mole fraction of $CO_2$ measured by the analyser, $X^{A0}_{CO_2}$ is the mole fraction of $CO_2$ in the incoming air, $X^A_{O_2}$ is the mole fraction of $O_2$ measured by the analyser, $X^{A0}_{O_2}$ is the

mole fraction of $O_2$ in the incoming air, and $X_{CO}^{A}$ is the mole fraction of CO measured by the analyser.

The mole fractions at the analyser are time-dependent, and are based on the measured gas concentration at each time step. The mole fractions of the incoming air are calculated based on an average of the pre-ignition gas analysis data (representing a background period, prior to the production of combustion gases).

#### 3.5.3.4. Heat Release Rate

The heat release rate is calculated according to,

$$\dot{q} = \left[E\phi - (E_{CO} - E)\,\frac{1-\phi}{2}\frac{X_{CO}^{A}}{X_{O_2}^{A}}\right]\frac{m_e}{1+\phi(\alpha-1)}\frac{\dot{M_{O_2}}}{M_a}\left(1 - X_{H_2O}^{0}\right)X_{O_2}^{A0} \tag{3.15}$$

Where $E_{CO}$ is the net heat energy released per unit mass of $O_2$ for $CO_2$, and $E$ is the net heat energy released in complete combustion per unit mass of $O_2$ consumed.

For the wildland fuels considered in this study, a value of 17.6 kJ/g of $O_2$ was assumed for $E_{CO}$, while for $E$ a value of 14.15 kJ/g of $O_2$ was assumed. This latter value is based on the average energy value measured by Bartoli for a range of forest fuels [147], rather than the Hugget Average (13.1 kJ/g of $O_2$) that is a typically used value for undefined fuels [267]. Bartoli's value therefore represents an increase of 8.0 % relative to Hugget's average value.

This method also assumes that all gases behave as ideal gases, with all inert gases present in the air represented by Nitrogen. All calculations are performed on a dry basis, assuming the prior removal of water vapour (by the use of a cold trap and desiccant).

Some past researchers have calculated the HRR based on the alternative principle of Carbon Dioxide Generation (CDG), however this method is not underpinned by the same universality in energy release values across species as has been demonstrated for OCC. As a result, the popularity of CDG calorimetry has diminished (particularly as the performance of oxygen analysers has improved [272]) and this approach has not been employed in this study.

The shortcomings of CDG calorimetry may otherwise have been particularly pronounced in this study given the unknown chemical composition of many of the fuel samples used. While the calcium sulphate (Drierite ®) desiccant used in both calorimeters has a tendency to absorb carbon dioxide while anhydrous, an effect that diminishes over time (as moisture is absorbed) but which may become significant for experiments of shorter duration (in which insufficient moisture is absorbed with the calcium sulphate therefore remaining anhydrous) [273].

### 3.5.4. Fireline Intensity

The fireline intensity describes the energy release rate per unit length of fire front [102], and is a commonly used descriptor of fire behaviour in wildfires, prescribed fires and field experiments. Fireline intensity ($I$) can be calculated according to,

$$I = \Delta h_c\, \Delta m\, R \tag{3.16}$$

Where $\Delta h_c$ is the heat of combustion of the fuel, $\Delta m$ is the total fuel consumption during flaming, and R is the spread rate.

18,700 kJ/kg is a commonly-used, generic value for the low heat of combustion of wildland fuels [18,274], with a variation of less than around ± 10 % for most fuel species [102,275]. However, this value may require adjustment in order to consider the effects of incomplete combustion and additional combustion phases (smouldering).

Based upon the Heat Release Rate (HRR) measurements in this study, the fireline intensity can be simply calculated by considering the flame front width ($w_f$) (typically equal to the fuel bed width),

$$I = \frac{HRR}{w_f} \tag{3.17}$$

While if the fire depth ($d_f$) is measured, the fireline intensity can be converted to an energy release per unit area of the fire front ($I_A$),

$$I_A = \frac{I}{d_f} \tag{3.18}$$

## 3.6. Fuel Properties

All fuels were collected from the Silas Little Experimental Forest in the New Jersey Pinelands National Reserve (PNR) [276–278]. The PNR is a UNESCO biosphere reserve, consisting of a mixture of upland, wetland, and aquatic areas, and was the first National Reserve in the USA. The main forest overstory components are *Pinus rigida* (Pitch Pine) and *Quercus spp*. (Oak species) with the relative dominance of each species varying throughout the region [241,242]. Shrub oaks and mountain laurel are the major midstory vegetation types (in addition to suppressed overstory species). The understory is dominated by sheep laurel, Ericaceous shrubs and a leaf litter layer [241].

The PNR is an area which has been the focus of a significant breadth of fuels and fire behaviour research [151,241,279,280]. This is due to the high frequency of wild and prescribed fire [242] within this region, and the proximity to human populations (the PNR is situated less than 60 km from both New York City and Philadelphia).

Overall, five species were studied including two types of pine needle: *Pinus rigida* (Pitch Pine*, Pinus rigida x taeda* (Pitch-Loblolly hybrid Pine), and three types of oak leaf: *Quercus stellata* (Post Oak), *Quercus alba* (White Oak), *Quercus montana* (Chestnut Oak). For each fuel type, dead, fallen fuels were collected, and stored at ambient, laboratory conditions. The fuels were allowed to air-dry during storage but were otherwise unconditioned prior to use. The geometric and thermochemical properties of each species were established through random sampling.

### 3.6.1. Geometric Properties

The geometrical properties of the pine needles were measured using the methods outlined by Thomas [32]. Geometrical properties of oak leaves were partly determined by similar methods; however, the surface area (and ultimately the surface-to-volume ratio) was determined by an alternative image analysis method described below.

#### 3.6.1.1. Surface Area

For the oak species used in this study, the leaves were broad enough to allow accurate estimation of total surface area via image analysis of their projected area. The pine species however, have characteristically thin needles and therefore it is more challenging to determine the surface area based on the projected area. Therefore, the surface area of conifer needles was not directly measured (only the surface-to-volume ratio).

For image analysis, photographs of leaves, alongside a reference object (US Penny of 19.05 mm diameter), were taken on a clear white paper background, with overhead lighting. This provided adequate contrast between both objects and the background, allowing segmentation of the foreground objects from the background. The respective pixel area of the leaf ($A_{pix,leaf}$) and the coin ($A_{pix,coin}$) were calculated, with the leaf surface area ($A_{leaf}$) then calculated based on the known surface area of the penny ($A_{coin} = 2.85 \times 10^{-4}$), multiplied by two to account for both sides of the leaf,

$$A_{leaf} = \left(\frac{A_{pix,leaf)}}{A_{pix,coin)}}\right)(2A_{coin}) \tag{3.19}$$

Multiple image segmentation methods were used:

1. Manual selection of an RGB threshold.
2. Otsu's method [281].

For segmentation by Otsu's method [281], the original images were first converted to greyscale images, then a global threshold value was calculated from the binary image histogram. A single global threshold value was calculated, based on minimisation of the intra-class variance of the background and foreground pixels, with an effectiveness value calculated at each iteration. The overall algorithm consisted of several key steps:

1. Conversion of RGB image to a greyscale image.
2. Calculation of intensity histogram.
3. Calculation of initial class probability and mean $w_i(0)$ and $u_i(0)$.
4. Calculation of all possible threshold values (t).
5. Updated values of $w_i$ and $u_i$ are calculated, along with the variance at each step, $\sigma_b^2(t)$.
6. Threshold value selected based on maximum variance.

Otsu's method is best suited to images in which the object area is small compared to the background area, which is the case for these leaf images, as shown in Figure 3.5. It is also clear that there is no excessive noise that could otherwise lead to an incorrect threshold value calculation by degrading the valley region of the histogram.

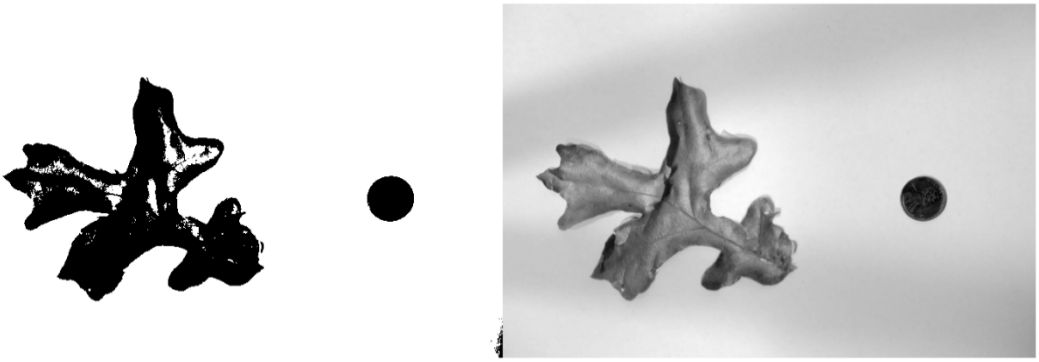

**Figure 3.5. (Left) Segmented image of oak leaf using Otsu's method (right) Original greyscale image of oak leaf**

Following segmentation, an analysis of the regions within the resulting binary images was conducted. These regions (or objects) are connected components within a binary image, and properties such as the pixel area and axis lengths can be extracted for each of these regions. As seen in Figure 3.5, the leaf and the coin represent the two largest objects in all non-distorted images. Therefore, the pixel area of the two largest regions was extracted from each image, before Equation 3.19 was used to calculate the leaf surface area. The final surface areas calculated for each oak species are shown in Table 3.4, for both segmentation methods.

**Table 3.4 - Leaf Surface Area (SA) estimates for each oak species using two different segmentation methods (Std. Dev / N)**

| **Species** | **Custom RGB SA** [$m^2$] | **Otsu SA** [$m^2$] |
|---|---|---|
| Post Oak | 0.0066 (0.0019 / 7) | 0.0064 (0.0018 / 7) |
| White Oak | 0.0061 (0.0017 / 5) | 0.0060 (0.0017 / 5) |
| Chestnut Oak | 0.0052 (0.0020 / 5) | 0.0051 (0.0021 / 5) |

#### 3.6.1.2. Density

The volume of each fuel types was determined by immersion of fuel elements in a known volume of ethanol (as described by Thomas [32]), utilising the displacement principle to calculate the fuel volume (V). Ethanol is used, rather than water, given its greater wetting properties and significantly lower surface tension at ambient conditions [32]. Since the total mass of fuel immersed in ethanol ($m_f$) was known, the effective density $(\rho_{eff})$ can then be calculated,

$$\rho_{eff} = \frac{m_f}{V} \tag{3.20}$$

However, given the porous nature of the fuels, this effective density differs from the 'true' density [32]. The true density of each fuel species was measured using helium pycnometry, performed by Merlin Powder Characterisation ®. These true densities are compared with the effective density of each fuel species in Table 3.5.

**Table 3.5 – Comparison of effective density and true density for each fuel species**

| Species | True Density [kg/m$^3$] | Effective Density [kg/m$^3$] (SD) |
|---|---|---|
| Pitch Pine | 1220 | 706 (71) |
| Loblolly Pine | 1202 | 725 (33) |
| Post Oak | 1273 | 744 |
| White Oak | 1282 | 798 |
| Chestnut Oak | 1297 | 627 |

#### 3.6.1.3. Surface-to-Volume Ratio

The Surface-to-Volume (SV) ratio of the pine needles was estimated using the methods introduced by Moro [282], and described and adapted by Thomas [32]. For pine needles growing in triplets (on a single fascicle) such as those in this study, the S-V ratio ($\sigma$) can be roughly approximated as half that of a cylinder, such that,

$$\sigma = \frac{\frac{1}{2}\pi d + d}{\frac{1}{8}\pi d^2} = \frac{4}{d} + \frac{8}{\pi d} \tag{3.21}$$

Where $d$ is the needle diameter, which was measured directly using callipers.

The needle diameter and SV ratio for both species are summarised in Table 3.6. Thomas also measured the S-V ratio of dead Pitch Pine needles collected from the New Jersey PNR [32]. The variation between the measured value in this study (5,063 ± 640 m$^{-1}$) and in Thomas' study (4,776 ± 497 m$^{-1}$) was within the observed standard deviation.

The relatively high variability associated with these SV ratio measurements is likely primarily due to natural variations in individual needle properties rather than measurement uncertainty in diameter measurements. Thomas found little variation in the standard deviation across needles of different average fuel size, or with additional measurement replications [32].

Table 3.6 also provides the S-V ratio for each oak leaf species; however, these were calculated as the ratio between the measured oak leaf surface area and volume, without measurement of the fuel diameter/thickness.

**Table 3.6 - Summary of geometric properties of each fuel species**

| Species | Dia. ($d$) [mm] (SD) | S-V Ratio ($\sigma$) [m$^{-1}$] (SD) |
|---|---|---|
| Pitch Pine | 1.31 (0.15) | 5063 (640) |
| Pitch-Loblolly Pine | 1.34 (0.12) | 4899 (446) |
| Post Oak | N/A | 11610 |
| White Oak | N/A | 16466 |
| Chestnut Oak | N/A | 9189 |

### 3.6.2. Thermochemical Properties

#### 3.6.2.1. Heat of Combustion

The heat of combustion of each fuel type was measured using bomb calorimetry [268]. As described by Janssens [268], a 1 g sample of a given fuel underwent combustion in a pure

oxygen at 30 bar pressure. The heat of combustion ($\Delta h_c$) for each fuel species is summarised in Table 3.7.

**Table 3.7 - Summary of measured Heat of Combustion ($\Delta h_c$) for each fuel species**

| Species | $\Delta H_c$ [kJ/kg] (± Max/Min) |
|---|---|
| Pitch Pine | 19670 ± 420 |
| Pitch-Loblolly Pine | 19670 ± 345 |
| Post Oak | 17850 |
| White Oak | 16950 ± 290 |
| Chestnut Oak | 17160 ± 725 |

There are well-publicised limitations to the use of bomb calorimetry data given that is it not representative of actual fire conditions [268]. The measured heat of combustion represents the upper limit of energy release, which may differ from that observed in an actual fire scenario. Therefore, the combustion efficiency within a given scenario must also be considered.

### 3.6.3. Fuel Moisture Content

The Fuel Moisture Content (FMC) was measured by oven-drying ~ 20 g fuel samples at 60 °C for 24 hours, with comparison of the initial ($m_{wet}$) and dry weight $(m_{dry})$. This method is regularly used in various areas of wildland fire science, and has been applied in numerous previous studies [32,132,135,226,228,255,283–285].

The FMC was calculated on a dry weight basis according to,

$$FMC_{Dry} = \frac{m_{wet} - m_{dry}}{m_{dry}} \times 100 \tag{3.22}$$

The dried fuel samples were weighed immediately upon removal for the oven, to avoid the rehydration of needles [135]. In each experimental series, the average FMC is reported for each fuel bed condition.

## 3.7. Fuel Bed Construction

To allow the construction of consistent, uniform fuel beds, fuels were weighed on a precision balance (± 0.01 g accuracy), and then 10 % of the overall fuel loading was distributed into each of 10 equal sub-sections of the Table surface. Within each section, needles were dropped randomly, without any effort to control the final orientation or interaction of needles, except in a small number of cases in which the effects of well-ordered fuel beds were specifically investigated. After construction, random sampling of the average fuel height was performed at 10 locations, to ensure the desired average height was achieved.

A specific focus of this study is understanding the effect of fuel bed structure on the overall fire behaviour, and the controlling physical phenomena. Therefore, the bulk fuel bed structure was systematically varied by altering (either independently or in combination) the fuel loading, bulk density and fuel bed height. Additional compaction of the fuel bed was applied in cases in which a lower fuel height (greater bulk density) was desired at a constant fuel loading. The exact variations and subsequent range of fuel structural conditions are described in subsequent chapters.

# Chapter 4

## Low-intensity flame spread – Role of Fuel Properties

# 4. Low-intensity Flame Spread – Role of Fuel Properties

*"Prescribed burning is a practice widely used to mitigate risks of damage from wildfires by reducing the amount of fuel available and modifying its structure.[…] To avoid excessive severity and minimize the potential of burns escaping, prescribed burns are generally managed to be low intensity in forests."*

***Duff et al., 2018*** [286]

## 4.1. Summary

This chapter presents the overall fire behaviour observations for a series of low-intensity, laboratory-based flame spread studies in fuel beds composed of typical pine:oak dominated forest litter layer fuels. Baseline fuel properties were established from prior sampling of natural surface fuel loadings within a pine:oak dominated area of the New Jersey Pinelands National Reserve (PNR). The effect of fuel properties on the resulting fire behaviour were investigated through a series of fuel manipulations which allowed the both the fuel structure (fuel loading, bulk density) and fuel type (pine needles only, oak leaves only, pine:oak mix) to be altered. These manipulations match those implemented in a recent, complimentary series of field experiments conducted in the PNR.[9] Initial qualitative comparisons to field observations are included, with further comparative analysis expected.

The greater environmental and fuel bed control, and the greater ease of fuel characterisation, in these laboratory experiments allows for more isolated study of the effect of fuel conditions than in a field environment. A major objective of this experimental series is therefore to provide data for the testing of physics-based models at an intermediate scale, prior to efforts to model larger, more complex field experiments. These experiments also allow further assessment of past discrepancies regarding the role of fuel structure in past field studies. The ability of existing detailed physics-based models to accurately predict fire behaviour, even in these well-controlled laboratory conditions, remains limited and further insight into the effect of fuel structure on the physical processes controlling flame spread is required. Therefore another major aim of these experiments was to inform the design of further detailed, systematic studies of fuel structure (presented in Chapters 5 and 6) by highlighting important fuel structure effects or phenomenological differences.

## 4.2. Introduction

Prescribed burning involves the controlled application of fire in the pursuit of management objectives such as the reduction or alteration of available fuels [286]. Therefore, prescribed fire science must have as a key priority, a desire for increased understanding of the effect of fire prescriptions on existing fuel strata. The effect of fuel treatments on future fires (through the alteration of the fuel properties) must also be understood if the long-term effectiveness of a prescribed fire strategy is to be assessed.

Suitable structural parameters are required for the accurate inventorying and description of the fuel properties within a chosen burn plot. Ideally, predictive tools should allow the comparison

[9] These experiments were conducted by a number of authors as part of a wider project funded by the Strategic Environmental Research and Development Program (SERDP) under the project grant RC-2641. https://www.serdp-estcp.org/Program-Areas/Resource-Conservation-and-Resiliency/Air-Quality/Fire-Emissions/RC-2641

of the potential fire behaviour for both the pre- and post-treatment fuel conditions. This will allow the selection of appropriate fuel treatments that achieve the desired fuel consumption, reduce fire risk, and meet other ecological and economic objectives.

The effect of the fuel properties are magnified at the low-intensity flame spread conditions typical of many prescribed fire scenarios [286]. Recently, the effect of fuel manipulations (of fuel structure, fuel packing, and fuel type) have been studied in a series of small-scale (100 $m^2$) field experiments [286]. The interpretation of the effect of fuel properties on the fire behaviour (and the underlying physical phenomena) is complicated in these field experiments, given the additional influence of several environmental variables (wind speed, air temperature, relative humidity, fuel moisture content) [286,287]. Therefore, in this chapter, these field experiments are complimented by a laboratory-based investigation of the effect of fuel manipulation on fire behaviour, allowing more isolated study of fuel effects on fire behaviour.

Using the flame spread table described in Chapter 3, a series of flame spread experiments were conducted. This involved a 'baseline' fuel bed (composed of 0.5 $kg/m^2$ of pine needles), which represented the natural surface fuel conditions within an area of the Pinelands National Reserve (PNR) [288]. The effect of fuel accumulation was studied using pine-needle fuel beds of greater fuel loading (1.0 and 1.5 $kg/m^2$). A key aim of prescribed burning is the reduction of this surface fuel loading, to reduce the intensity of a subsequent wildfire, increasing the likelihood of survival of the tree stand [286,289,290].

The effect of fuel packing was explored via the mechanical compaction of this highest fuel loading condition (1.5 $kg/m^2$). The effect of fuel species was studied by investigating both the fire behaviour and fuel consumption of fuel beds composed of either oak leaves or a mix of pine needles and oak leaves. Pine needle and oak leaves represent common litter layer components within the PNR and other Pine-Oak dominated ecosystems [288].

The resulting fire behaviour was measured in order to understand the effect of the applied fuel treatments upon the fire intensity and flame spread. Measurement of fuel consumption allows the burn effectiveness to be assessed for each fuel condition. These observations allow the evaluation of the suitability of existing fuel structure parameters (fuel loading, bulk density), and the development of alternative dimensionless parameters, more closely linked to underlying physical phenomena controlling the flame spread process.

Gaps in our current understanding of the effects of fuel structure on these physical mechanisms are identified. This subsequently informed the design of an extended systematic investigation of fuel structure, as discussed in Chapters 5 and 6. This eventually allowed the assessment of the performance of existing models (solid flame spread thermal models; semi-empirical porous flame spread models and simplified physics-based porous flame spread models), when applied to low-intensity flame spread scenarios of particular importance in prescribed fire science (presented in Chapters 7 and 8). Limits to the applicability of these models, and areas requiring additional research, are subsequently highlighted.

In addition to the structural properties of the surface fuel layer, the fire behaviour and fuel consumption may also be affected by the properties of neighbouring layers. Within the PNR, the surface fuel layer sits atop a sandy soil type, the properties of which (e.g. moisture, thermal conductivity) may vary spatially and temporally, and are poorly defined. In this study, fuel beds were constructed on a well-defined substrate layer (vermiculite board). However, an

initial assessment of the effect of substrate material and moisture content is also included in this chapter, with areas for further research identified.

## 4.3. Effect of Fuel Properties

### 4.3.1. Methods

#### 4.3.1.1. Baseline Fuel Properties

Baseline values for laboratory experiments were derived from measurements of natural fuel conditions at the Silas Little Experimental Forest, conducted during a recent series of field experiments [288]. The natural surface fuel loading within the Silas Little Experimental Forest was approximately 0.5 kg/m$^2$. During the field sampling, the duff layer was not collected during sampling, with only litter fuels collected. These measured fuel loadings were compared with existing fuel records for eight sites in New Jersey contained within the Natural Fuels Photo Series[10] [291].

The surface fuel loadings in the Photo Series are broken down into subcategories (Hardwood Litter, Conifer Litter, Cryptogams and Duff)[11]. As shown in Figure 4.1, there is significant variation in fuel loadings across these eight sites, however, on average, the surface fuel loading (excluding duff layer) is of a similar magnitude to those observed at the Silas Little plantation.

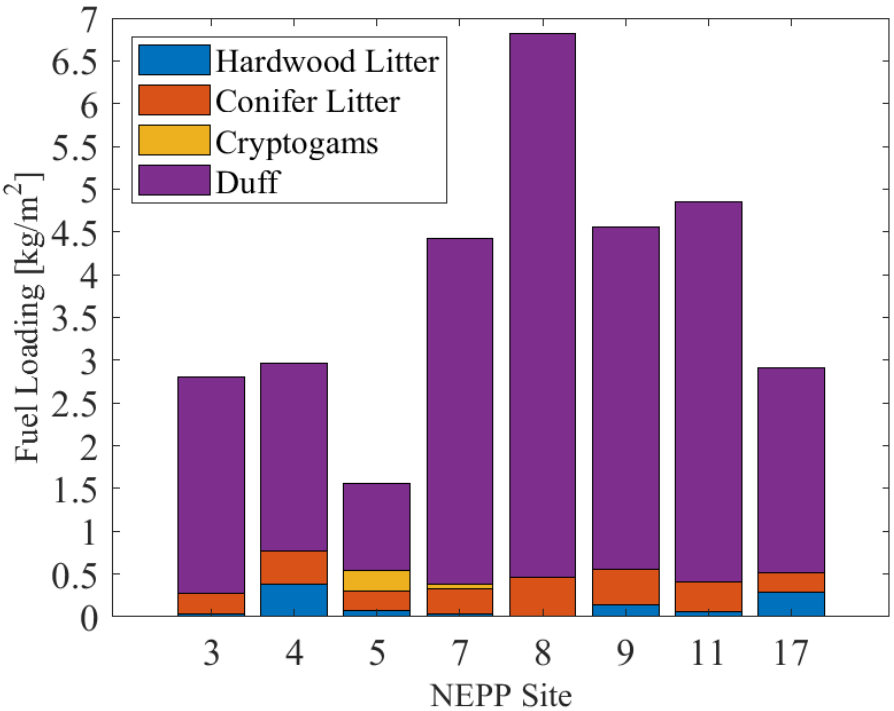


**Figure 4.1 - Surface fuel loadings by category, for Northeastern U.S. Pitch Pine (NEPP) sites in New Jersey. Based upon Natural Fuels Digital Photo Series data** [291]

[10] The National Fuels Photo Series contains photos of eight sites in New Jersey, all with pitch pine cover. https://depts.washington.edu/nwfire/dps/

[11] Tree species are generally classified as either hardwood or softwood (including conifers), both of which differ botanically. Typically hardwoods have broad leaves, with conifers usually having cones and needle-like leaves [416]. Cryptogams are a category of plants which reproduce without seed production (e.g. spore-based reproduction) and includes mosses, fungi and algae [417]. Duff describes a layer of organic material underneath the litter layer, and which has already been subject to significant decomposition [418].

A baseline fuel bed of 0.5 kg/m$^2$ fuel loading was therefore chosen for these experiments. In reality, the natural surface litter layer contains a variety of components (pine needles, pinecones, sticks, and broadleaves) however, idealized cases consisting only of either pine needles and/or oak leaves were used in this study. This omits both the duff layer and the soil layer, which would otherwise be present as a substrate layer beneath the litter layer, but likely contributes little within the flaming region in a prescribed fire. The effects of the material properties and condition of this substrate layer are investigated in Section 4.5.

#### 4.3.1.2. Flame Spread Table

Flame spread experiments were conducted using the Flame Spread Table described in Chapter 3. Fuel beds were constructed upon the vermiculite table surface, however the potential influence of the substrate material selection was investigated, as described in Section 4.5. Following the methodologies described in Chapter 3, the gas phase temperature was measured within the fuel bed at multiple distances from the ignition line (0.5, 0.8 and 1.1 m), as shown in Figure 4.2. The vertical temperature profile was measured using a thermocouple tree (also described in Chapter 3) which was located at a horizontal distance of 0.8 m from the ignition line. For a subset of experiments, heat fluxes were measured at various locations, as shown in Figure 4.2, however these measurements are mainly discussed in Chapter 8.

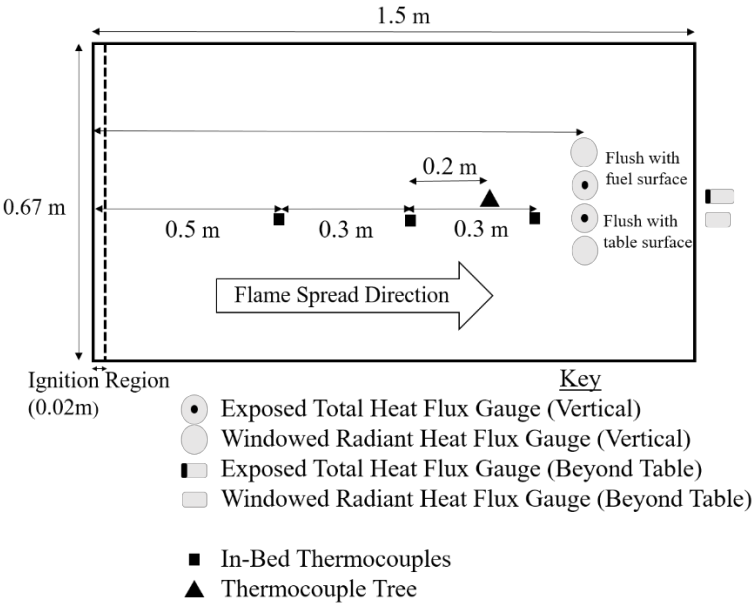


**Figure 4.2. Schematic of Flame Spread Table for flame spread experiments in Chapter 4**

The rate of spread was calculated based on the time interval between fire arrival at successive thermocouples (located within the fuel bed, as shown in Figure 4.2). The flame height was estimated from the thermocouple tree measurements as described in Chapter 3. The residence time was calculated as the maximum continuous period at which the lowest position in the thermocouple tree (0.05 m above table surface) recorded a temperature in excess of the flame threshold temperature (300 °C).

#### 4.3.1.3. Environmental Conditions

As the flame spread experiments were conducted within a laboratory, they were undertaken within a narrow range of ambient conditions. This allows greater isolation of fuel properties of interest, without the greater variability and extremes in weather conditions typical of field

experiments. Across all of the experiments, the ambient temperature within the laboratory varied within a narrow range of 11°C.

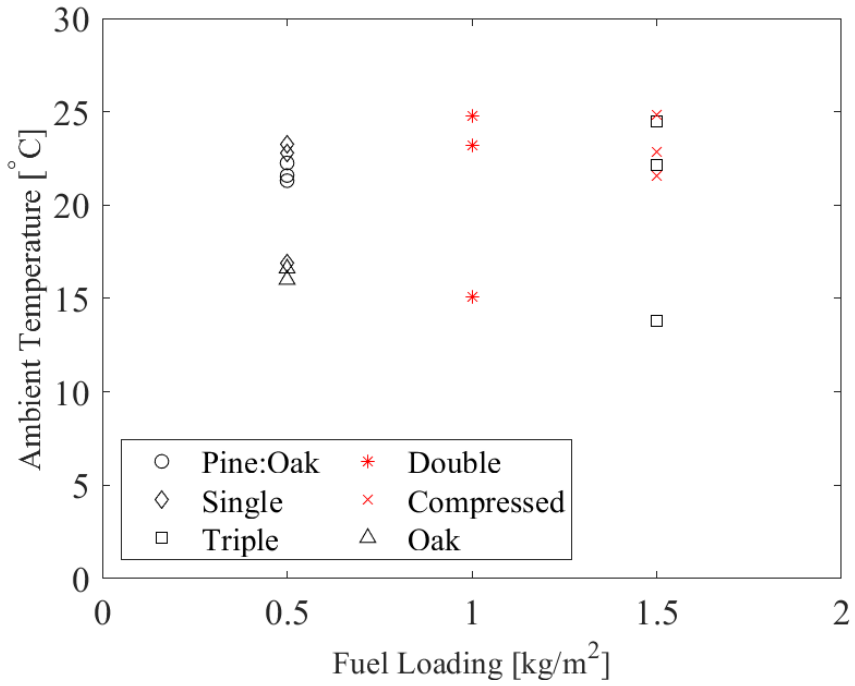


**Figure 4.3 - Background ambient air temperature in laboratory flame spread experiments**

The only fuel conditioning prior to experiments involved air-drying the fuels within the laboratory, for an extensive period post-collection. The Fuel Moisture Content (FMC) of the fuels is therefore primarily a function of the ambient conditions within the laboratory (temperature, relative humidity) although physiological differences may result in inter-species variation [93].

The average FMC for each experiment is shown in Figure 4.4, with error bars indicating the maximum error based on all the fuel samples collected for each experiment. The average FMC values varied across a range of 4.6 % on a dry weight basis. In general, the largest errors are associated with the experiments involving mixes of pine needles and oak leaves. This may partly reflect the greater variability of fuel sample composition for these mixed fuel beds.

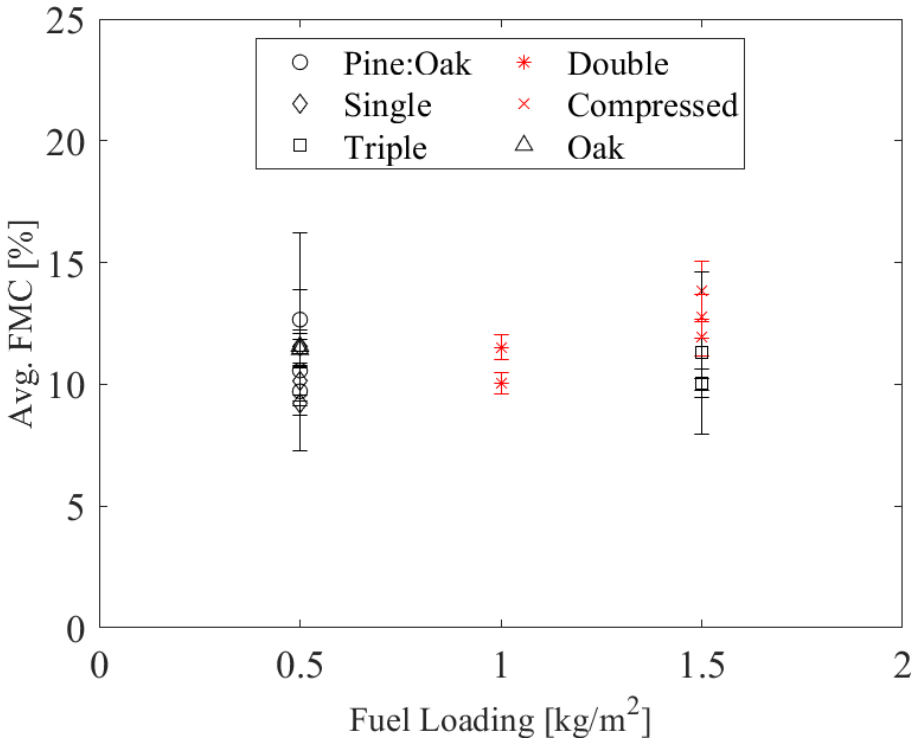


**Figure 4.4 - Average fuel moisture content in laboratory flame spread experiments**

#### 4.3.1.4. Fuel Treatments

Several fuel treatments and modifications were applied to the baseline fuel bed condition. As previously discussed, these treatments match those implemented in a complimentary series of field experiments, conducted by multiple researchers [85]. The effect of fuel loading, fuel compaction, and fuel species were explored, with the full experimental matrix shown in Table 4.1.

The effect of fuel loading was investigated using three pine needle fuel beds of different fuel loading (0.5, 1.0 and 1.5 kg/m$^2$). As no effort was made to control the fuel bed height during the complimentary field experiments, the bulk density varied slightly across these fuel loadings (varying from 22.2 to 28.6 kg/m$^3$). This bulk density variation was replicated in these Table experiments however the variation across fuel conditions is similar in magnitude to the variability observed across a given fuel bed (measured through random sampling of the fuel bed height). The effect of bulk density was investigated by compaction of the highest loading (1.5 kg/m$^2$) pine needle bed, increasing the bulk density from 27.3 to 66.7 kg/m$^3$. Finally, the effect of fuel species was explored by considering fuel beds composed of oak leaves, or a mix of oak leaves and pine needles, at the baseline fuel loading (0.5 kg/m$^2$).

**Table 4.1 - Experimental matrix for study of the effects of various fuel treatments**

| Fuel Bed Condition | Fuel Loading [kg/m$^2$] | Fuel Height ($\delta$) [cm] | Bulk Density ($\rho$) [kg/m$^3$] | Packing Ratio ($\beta$) | Porosity ($\alpha$) | $\alpha\sigma\delta$ |
|---|---|---|---|---|---|---|
| Single (Pine Needles) | 0.5 | 2.25 | 22.2 | 0.031 | 0.969 | 110 |
| Double (Pine Needles) | 1.0 | 3.50 | 28.6 | 0.041 | 0.959 | 170 |
| Triple (Pine Needles) | 1.5 | 5.50 | 27.3 | 0.039 | 0.961 | 268 |
| Pine:Oak Mix | 0.5 | 3.75 | 13.3 | 0.019 | 0.981 | 322 |
| Oak Only | 0.5 | 3.75 | 13.3 | 0.018 | 0.982 | 457 |
| Compressed | 1.5 | 2.25 | 66.7 | 0.094 | 0.906 | 103 |

While the average fuel bed properties were pre-selected (as outlined in the experimental matrix) there is inevitably variation across a given fuel bed, despite efforts to achieve uniformity. The fuel loading uniformity was improved by pre-weighing and distributing subsets of the total fuel loading into 1/10th sections of the fuel bed. No effort was made however to control the individual orientation of pine needles and therefore it is more difficult to ensure uniformity in fuel bed height (and hence bulk density). To quantify this intra-bed variation, 10 fuel bed height measurements were made at random locations throughout each fuel bed.

All the pine needles were dead *Pinus rigida* (Pitch Pine) needles, while a mix of dead oak leaves consisting of three species, *Quercus stellata* (Post Oak), *Quercus alba* (White Oak), *Quercus montana* (Chestnut Oak), was used in all cases involving oak leaves. The geometric and thermochemical properties of each fuel species are provided in Chapter 3, while the Pine:Oak mix was created on a 50:50 weight basis.

### 4.3.2. Results and Discussion

For each fuel condition, a number of fire behaviour properties were measured (spread rate, flame height, residence time) and both the average values, and the variability at a given fuel condition, were considered. An overview of key fire behaviour properties at each fuel bed condition is provided in Table 4.2.

**Table 4.2 - Summary of average fire behaviour properties for each fuel condition [N = 2 for oak only fuel bed, N = 3 for all other fuel bed conditions. Bulk density standard deviation based upon 10 random fuel bed height samples per experiment]**

| Fuel Bed Condition | Fuel Loading [kg/m$^2$] | Bulk Density [kg/m$^3$] | Spread Rate [mm/min] ± Max/Min | Flame Height [m] ± Max/Min | Residence Time [s] ± Max/Min |
|---|---|---|---|---|---|
| Single (Pine Needles) | 0.5 | 22.2 ± 5.6 | 129 ± 34 | 0.12 ± 0.08 | 11 ± 13 |
| Double (Pine Needles) | 1.0 | 28.6 ± 5.6 | 135 ± 11 | 0.23 ± 0.07 | 41 ± 7 |
| Triple (Pine Needles) | 1.5 | 27.3 ± 5.6 | 145 ± 9 | 0.80 ± 0.20 | 73 ± 13 |
| Pine : Oak Mix | 0.5 | 13.3 ± 2.7 | 199 ± 35 | 0.20 ± 0.10 | 15 ± 6 |
| Compressed (Pine Needles) | 1.5 | 66.7 ± 9.2 | 103 ± 7 | 0.33 ± 0.07 | 35 ± 2 |
| Oak Only | 0.5 | 13.3 ± 1.1 | 172 ± 13 | 0.15 ± 0.05 | 10 ± 0.4 |

#### 4.3.2.1. Rate of Spread

The observed spread rates vary significantly from some past observations from quiescent, laboratory-based studies involving other fuel types. Morandini *et al*. [67] and Silvani *et al.* [243] observed spread rates far in excess of those reported here while studying excelsior fuel loadings similar to the baseline fuel loading in this study. For excelsior fuel beds, with fuel loadings ranging from 0.4 to 0.6 kg/m$^2$, Morandini *et al*. [67] observed spread rates in excess of 1,000 mm/min. However the significantly greater height of these excelsior fuel beds (21 to 22 cm) means that they were significantly more porous (lower bulk density) than either of the pine needle beds studied here or those previously studied by Morandini *et al* [226]. The excelsior fuel bed was also larger in scale (3 m by 7m) but the surface-to-volume ratio and density of excelsior was similar to the pine needles considered in this study.

Comparison can also be drawn with spread rates observed in previous field experiments. A slightly greater spread rate (180 mm/min) was observed by Silvani and Morandini [245] in a pine needle bed of equal fuel loading to the baseline fuel bed in the present study (0.5 kg/m$^2$), and similar fuel height (3 cm). This field experiment involved a 5 m by 5 m fuel bed, and was conducted at low wind speeds (0.5 m/s) and low slope angle (- 5°), resulting in largely upright flames (90° flame angle), and therefore offers a useful comparison to the laboratory experiments conducted in this thesis. Further comparison is limited by the lack of information regarding the error or variability associated with the spread rate observations of Silvani and Morandini.

As shown in Table 4.2, variation in spread rates (as measured between thermocouple locations) occurred between repeat experiments at a given fuel condition. Similar, or even greater variability, has been observed within similar previous laboratory-based flame spread studies [81,226]. Morandini *et al*. [226] reported spread rate variations up to 37 % from the average

value at a single fuel condition (1.2 kg/m$^2$, pine needle fuel beds). In the present study, a maximum deviation from the average spread rate of 26 % was observed at any given fuel condition.

Despite the spread rate variability at a given fuel condition, a slight positive trend between fuel loading and spread rate was observed for the fuel beds composed only of pine needles, as shown in Table 4.2 and Figure 4.5. This slight trend for the pine needle beds is in line with past observations for pine needle beds in previous laboratory-based studies [81,226–228]. Tripling the fuel loading from the baseline loading of 0.5 kg/m$^2$ to 1.5 kg/m$^2$, resulted in a 12 % increase in the average spread rate. However, the variation in spread rate across the three fuel loadings was within the range of the experimental variability.

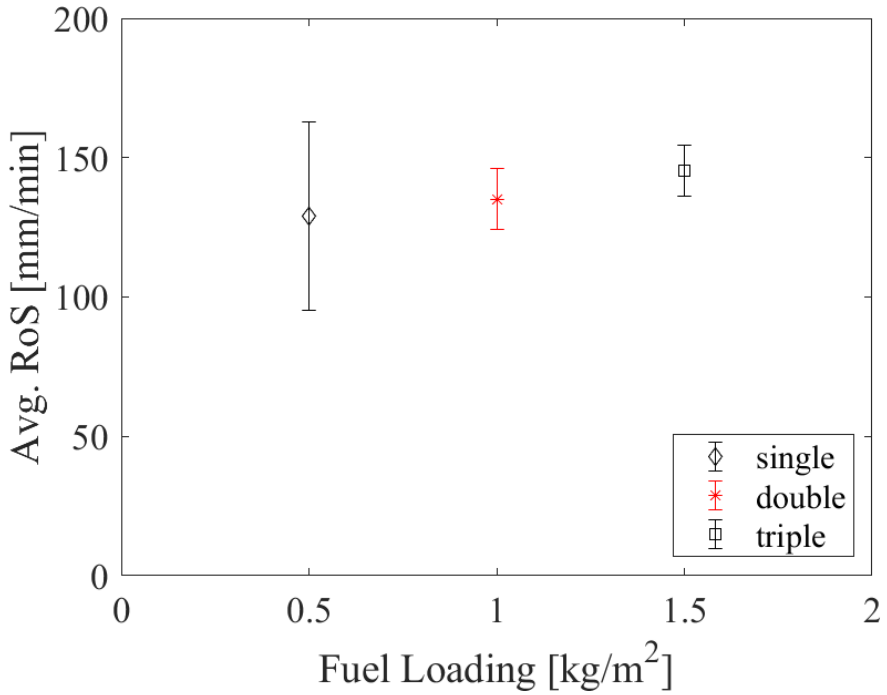


**Figure 4.5 – Effect of fuel loading on the average Rate of Spread (RoS) through fuel beds composed only of pine needles. Average spread rate at each fuel condition is shown with error bars showing the max/min deviation across all experiments at that condition.**

Dupuy [81] previously observed a power law relationship between fuel loading and spread rate in pine needle beds. This is in contrast with the linear relationship assumed in some current modelling approaches including Rothermel's [43] model. Given the small number of fuel loadings studied in this chapter, it is not possible to accurately determine the nature of this relationship and further systematic study is therefore presented in Chapters 5 and 6.

The trend between fuel loading and spread rate is not observed across all the fuel conditions (i.e. when compressed fuel beds or fuel beds containing oak are included). The slight effect of fuel loading in pine needles, and the lack of a clear trend across all fuel conditions, may partly explain discrepancies over the effect of fuel loading within previous field experiments [220,221,231]. For example, it is likely that natural fuel beds exhibit greater heterogeneity both in terms of fuel types and fuel structure. While the effect of fuel loading may be further obscured by other external factors (wind, RH, terrain, heterogeneity) during field experiments, as was observed in the complimentary field experiments [85].

In interpreting the effect of fuel loading on the fire behaviour of the pine needle beds, it is important to note that the bulk density also varied slightly across the three fuel loadings (22.2 to 28.6 kg/m$^3$), which may also affect the observed spread rate. It is therefore difficult to fully interpret the effect of fuel loading on spread rate without a greater understanding of the effect bulk density. This reiterates the previous comments of Cheney *et al*. [220], who emphasised the need to disentangle the effects of fuel height and bulk density, both of which control the fuel loading. Therefore, further systematic study of the independent effects of height, fuel loading and bulk density is required, and this is addressed by the experimental studies described in Chapters 5 and 6.

The influence of bulk density on the spread rate is demonstrated by the case in which fuel bed was compressed (increasing the bulk density). Compression of a 1.5 kg/m$^2$ fuel bed from a height of 5.5 cm to 2.25 cm (increasing the bulk density from 27.3 kg/m$^3$ to 66.7 kg/m$^3$) resulted in a 29 % reduction in the spread rate. As shown in

Figure 4.6, in this study, a general negative relationship between bulk density and spread rate was observed across all fuel bed conditions (including those involving oak leaves). This is in line with the negative relationship between spread rate and bulk density previously proposed by Thomas [292]. The variation in bulk density across fuel loadings for the single, double and triple cases is within the range of variability observed across a single fuel bed at each of these conditions. Further investigation is required to understand the independent effect of bulk density, and this is provided in Chapters 5 and 6.

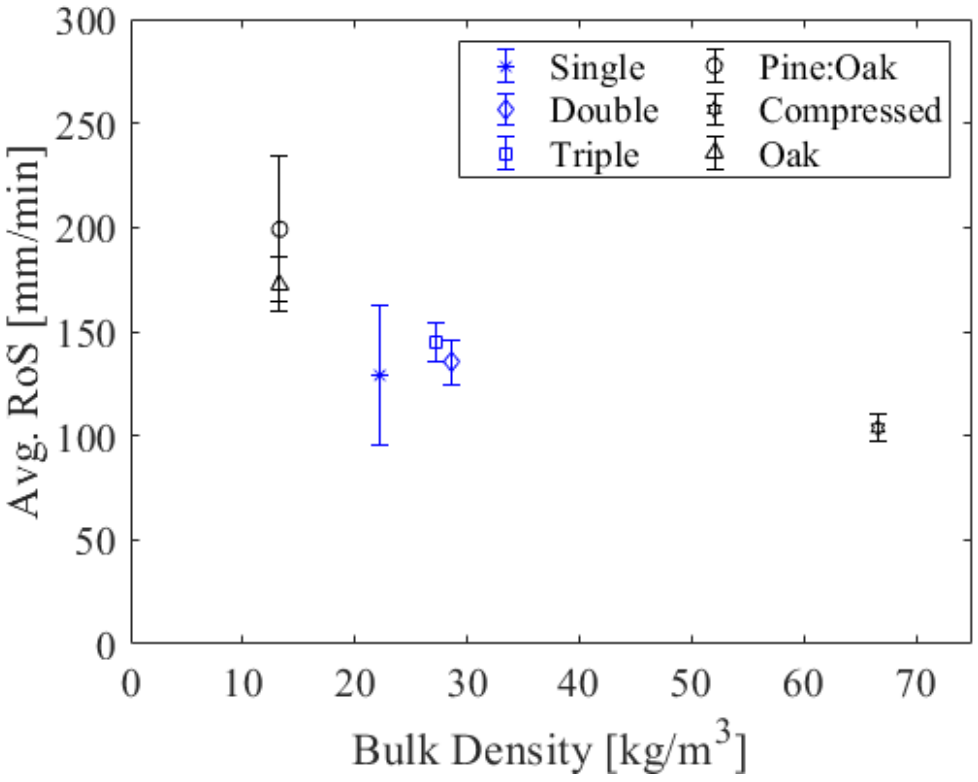


**Figure 4.6 – Comparison of average Rate of Spread (RoS) with bulk density across all fuel conditions**

The effect of fuel species is also clearly observed, with fuel beds composed of oak leaves or of a Pine:Oak mix exhibiting higher spread rates than fuel beds of equal fuel loading comprised solely of pine needles. The effect of fuel species is further emphasised by the variation in spread rates occurring between oak only and pine:oak mixed fuel beds at equal fuel loading and bulk density. In addition to any fuel species effect (e.g. chemical composition, fuel element shape) it is interesting to consider the potential influence of the different local (inter-element) structure formed within each of these fuel beds. This emphasises the need for physical parameters that are closely linked to key physical mechanisms.

As discussed in Chapter 2, various dimensionless parameters have previously been proposed to describe the structure of porous fuel beds. Often, during their development, an effort is made to link these dimensionless terms to key physical parameters affecting flame spread. In this thesis, an alternative parameter $\alpha\sigma\delta$ is introduced, which is similar to the existing terms and linked to the key physical processes of flow and heat transfer.

The parameter $\alpha\sigma\delta$ incorporates the fuel bed porosity $(\alpha)$, the fuel element surface-to-volume ratio $(\sigma)$, and the fuel bed height $(\delta)$. This term is derived from the dimensionless parameter $\sigma\lambda$ originally introduced by Curry and Fons [101] and subsequently used by Rothermel and Anderson [125]. The term $\lambda$ is the porosity which in this case is defined as the ratio of the void volume to surface area of fuel in the fuel bed. The term $\sigma\lambda$ can therefore also be expressed in terms of the solid volume fraction or packing ratio $\beta$ as $\frac{1-\beta}{\beta}$. Multiplication of this term by the packing ratio $(\beta)$, surface-to-volume ratio $(\sigma)$ and fuel bed height $(\delta)$ results in the dimensionless term $\alpha\sigma\delta$.

This parameter is introduced in an effort to describe, using a single dimensionless term, the fuel structure in a physically meaningful manner. The need for such a term is underlined by the independent effects of fuel loading and bulk density. Additionally, the effects of fuel type and fine-scale structural variations further emphasise the shortcomings of existing bulk structural descriptors and highlight the need for terms which consider both the global (e.g. fuel bed scale) and local (e.g. fuel element scale) structure.

Re-examining the observed fire behaviour at each fuel condition, through the lens of this alternative dimensionless parameter provides additional insight into the role of fuel structure. As highlighted in Figure 4.7, a general positive trend was observed between $\alpha\sigma\delta$, although there remains a need to understand the effect of fuel species and fuel compaction. This also highlights additional areas of focus within the detailed, systematic investigations described in Chapters 5 and 6. Further evaluation of this dimensionless term is presented in these subsequent chapters. The limitations associated with the use of the term $\beta\sigma\delta$ as a flame spread predictor are shown in Figure 4.7. Better agreement is observed between the spread rate and the parameter $\sigma\lambda$ however the limitations of this parameter are apparent in Chapters 5 and 6 where bulk density is systematically varied at a constant fuel loading.

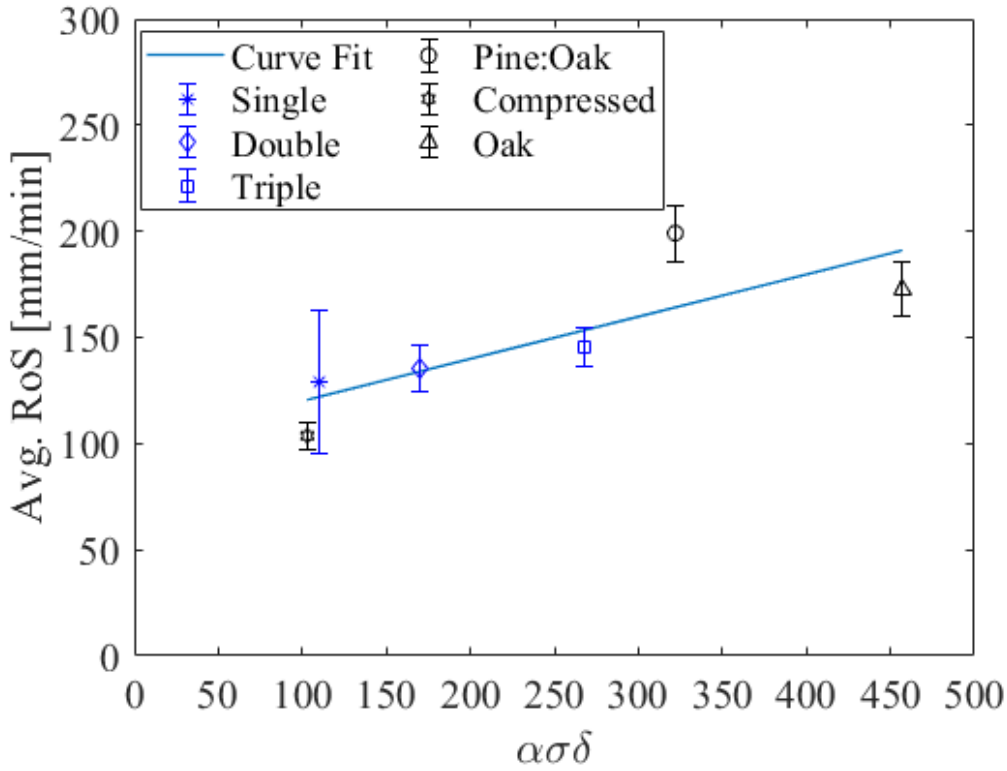


**Figure 4.7 - Comparison of average Rate of Spread (RoS) with $\alpha\sigma\delta$ across all fuel conditions ($R^2 = 0.66$)**

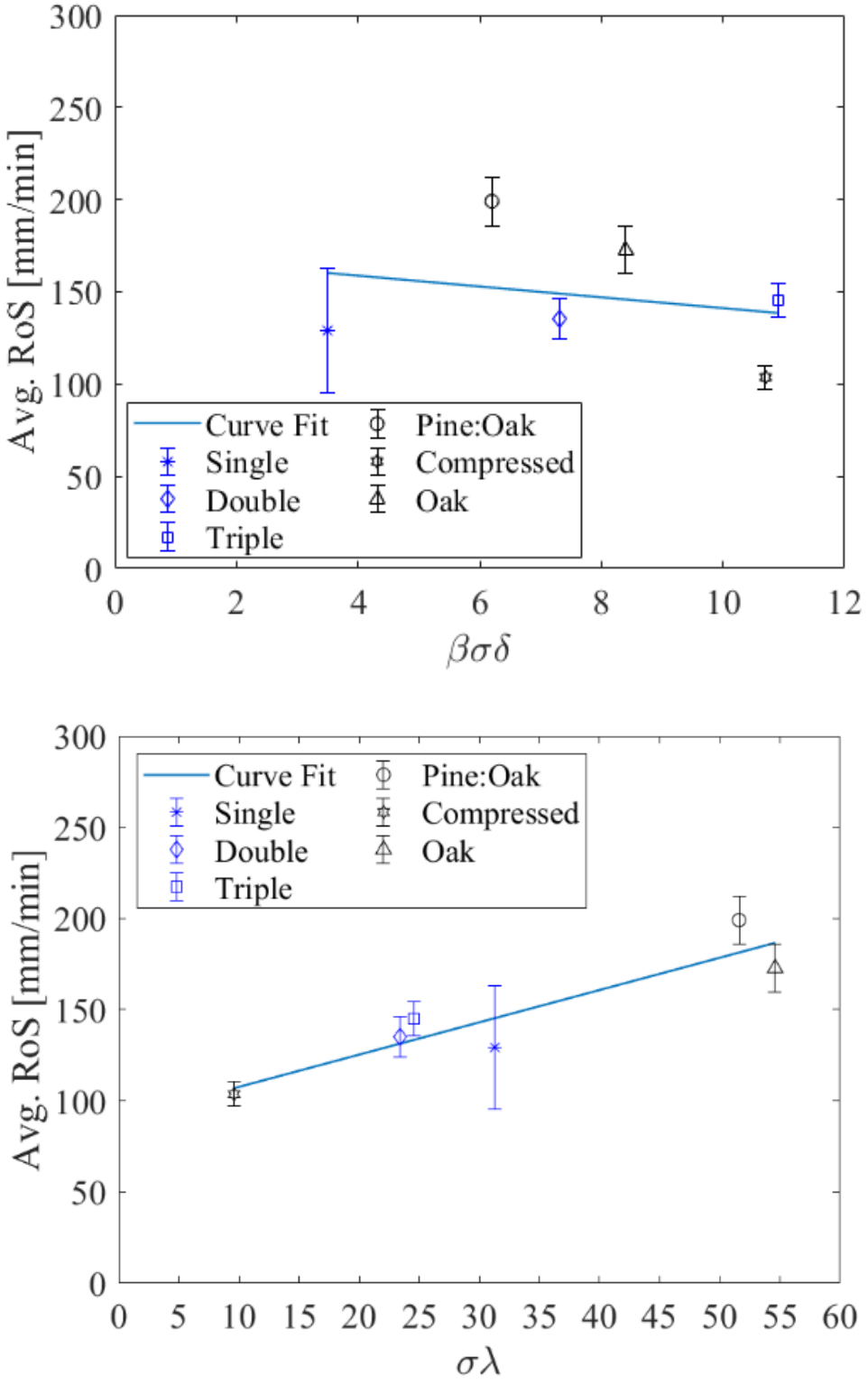


**Figure 4.8 - Comparison of average Rate of Spread (RoS) with (Top) $\beta\sigma\delta$ ($R^2 = 0.06$) and (Bottom) ($\sigma\lambda$) ($R^2 = 0.70$) across all fuel conditions**

#### 4.3.2.2. Flame Height

The flame heights reported in this study (0.12 m to 0.80 m) were similar to those observed by Morandini *et al.* [226] (0.21 m to 0.76 m) in previous laboratory experiments involving (*Pinus*

*pinaster*) pine needle beds of similar fuel loading (0.6 to 1.2 kg/m$^2$). However, in a separate study, Morandini *et al*. observed far greater flame heights (0.36 to 0.7 m) in excelsior fuel beds of similar fuel loading (0.4 to 0.6 kg/m$^2$) to the baseline pine needle bed in this study. These excelsior fuel beds had a far greater fuel height (21 to 22 cm), and hence a significantly lower bulk density, than the fuel beds studied in this chapter. Much greater flame heights in excelsior fuel beds were also observed by Silvani *et al*. [243] in a similar study.

The maximum deviation from the average flame heights observed by Morandini *et al.* [226] at a given pine needle fuel condition (43 %) was similar, but slightly lower, than the maximum deviation observed at any fuel condition in this study (67%). This maximum deviation in this present study was observed at the lowest fuel loading (single) condition, which may partly reflect the transient nature of the flame shape. The variability at other fuel conditions was mostly within the range observed by Morandini *et al.*

Comparison can also be drawn with flame heights observed in previous field experiments. A similar flame height (0.2 m) was observed in the highly relevant study of Silvani and Morandini [245] involving a pine needle bed of equal fuel loading to the baseline fuel bed in the present study (0.5 kg/m$^2$), and similar fuel height (3 cm), although the fuel species is not specified.

The close similarity of the fuel bed in Silvani and Morandini's field study allows an initial examination of the scaling effects relevant to this study. For example, the heat flux from a flame front is scale-dependent [245], which may have implications for the significance of competing heat transfer mechanisms in laboratory-scale experiments (e.g. the significance of flame radiative heating).

For the baseline fuel bed in this study, a peak radiative flux of 2.7 ± 1.3 kW/m$^2$ was measured at the fuel surface, which is significantly lower than the peak radiant flux observed for the 25 m$^2$ fuel bed in Silvani and Morandini's field study (25 kW/m$^2$). Similarly, the peak total flux at the fuel surface in this study (9.3 ± 1.6 kW/m$^2$) was significantly lower than that observed in Silvani and Morandini's field study (40 kW/m$^2$). The scale dependence of the flame heating represents a limitation of the applicability of the findings in this study. However, a key objective of this thesis is to provide the measurement data for key physical properties to understand the limitations of modelling approaches, and the role of fuel structure, at both scales.

A positive relationship between fuel loading and flame height was observed for the fuel beds composed only of pine needles, as shown in Table 4.2 and Figure 4.9. A similar trend has previously been observed in previous no-wind, no-flow, laboratory-based flame spread studies involving both excelsior [67,243] and pine needle beds [226].

Morandini *et al*. [67] previously attributed this positive relationship between fuel loading and flame height to the increased burning rate and Heat Release Rate (HRR), resulting in greater fire-generated buoyant forces. In this study, an increased HRR was observed at greater fuel loadings (as discussed in Section 4.3.2.4) however, HRR was also affected by fuel species and bulk density. Therefore, it is possible that the energy release rates are indeed controlling the flame height however further direct study of the buoyant flow regime is required to understand the relationship between HRR and buoyant flow velocity (investigated in Chapter 6).

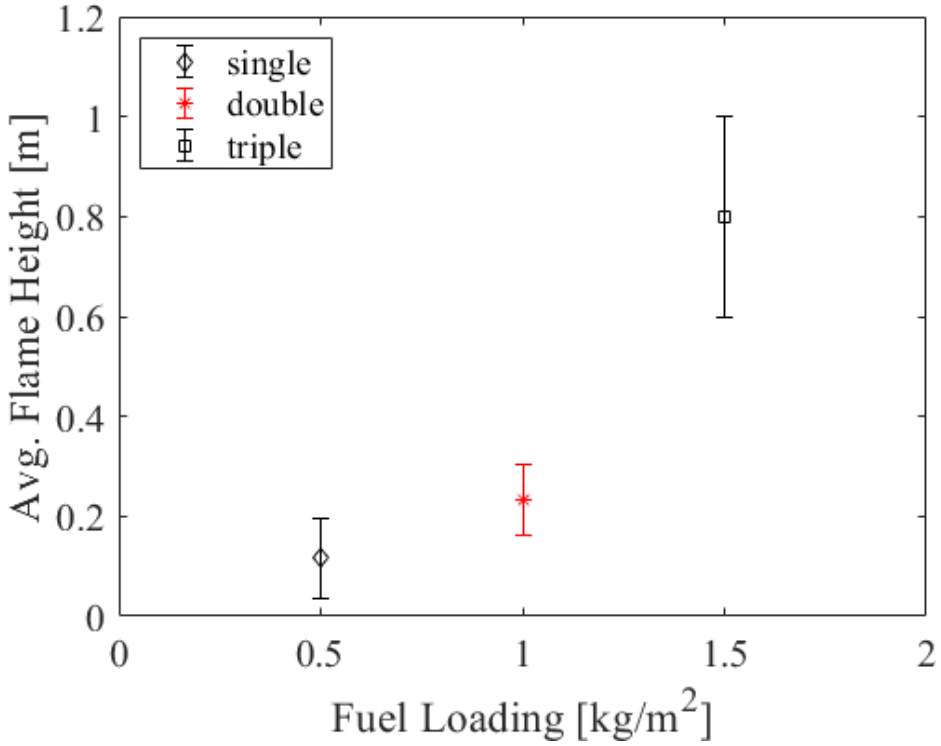


**Figure 4.9 – Comparison of fuel loading and avg. flame height at each fuel condition. (Based on thermocouple tree measurements)**

Again, the effect of bulk density is demonstrated by compression of the fuel bed. Compression of a 1.5 kg/m$^2$ fuel bed from a height of 5.5 cm to 2.25 cm (increasing the bulk density from 27.3 kg/m$^3$ to 66.7 kg/m$^3$) resulted in a 59 % decrease in the flame height. Fuel species composition of the fuel bed slightly affected the resulting flame height, but the effect was less significant than the previously discussed effect on spread rate. The variation in flame heights between the pine only, oak only and pine:oak mix fuel beds (of equal fuel loading) was within the range of experimental variability for a given fuel condition.

#### 4.3.2.3. Residence Time

The residence times measured in this study were similar to those observed in previous field experiments [18,230,293,294], including an experimental burn conducted in the New Jersey PNR and involving similar fuel types [18]. In this PNR-based experiment, residence times varied between 17 s and 34 s, for a fine surface fuel loading of 0.76 ± 0.12 kg/m$^2$, and average litter layer height of 5 ± 2 cm. Close comparison can therefore be drawn with the single and double fuel conditions in the current study, in which the residence times varied between 11s and 41 s.

As with the other parameters, comparison can also be drawn with residence time observed in the field experiment of Silvani and Morandini [245], involving a pine needle bed similar to the baseline condition in the present study. A significantly greater flame residence time (49 s) was observed by Silvani and Morandini in this field experiment. This is particularly interesting given the similarity of the measurement approach of Silvani and Morandini, which employed a 0.25 diameter K-Type thermocouple positioned at the fuel surface height.

In the present study, a clear positive trend was observed between fuel loading and residence time as shown in Table 4.2 and Figure 4.10. As the fuel loading was increased from 0.5 kg/m$^2$ to 1.5 kg/m$^2$, the residence time increased more than fivefold. This is in contrast to the previous field observations of Wotton *et al*. [293] (during bushfire experiments in eucalypt forest) in which no significant effect of fuel loading on the residence time was observed. However, given the influence of fuel size/thickness on residence time [133,295], fuel structure effects may be more complex in natural fuel stands than in laboratory fuel beds reconstructed from a single or well-controlled mix of fine fuel particles. A similar positive trend between fuel loading and residence time was observed in a series of bench-scale combustion experiments involving small pine needle bed samples [296].

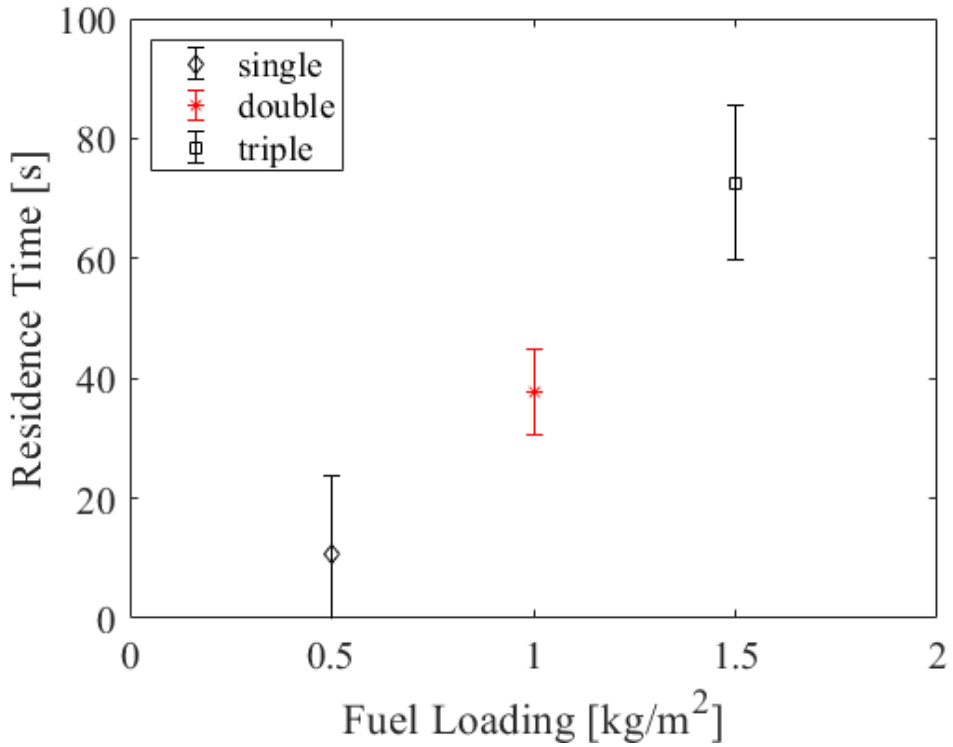


**Figure 4.10 – Comparison of residence time with fuel loading across all fuel conditions (For a thermocouple at a height of 0.05 m above the Table surface)**

The effect of bulk density was also apparent as shown in , with the compressed fuel bed resulting in a 52 % reduction in the residence time compared to the uncompressed triple fuel load case as the bulk density was increased from 27.3 kg/m$^3$ to 66.7 kg/m$^3$. This effect is again in contrast to the previous field observations of Wotton *et al*. [293] in which bulk density did not significantly affect residence time.

In laboratory-based studies involving pine needle beds, Anderson [133] noted an increase in residence time at greater porosities, which is in line with the positive trend between bulk density (and hence porosity) and residence time observed in this study. However, Anderson's observations were from a number of preliminary experiments, and therefore this effect was not subject to detailed, systematic investigation, and a description of the residence time solely as a function of fuel element size was subsequently proposed.

It is therefore important to understand the limitations of these simple formulations, which were previously observed to underestimate residence time in field experiments within Pine:Oak

dominated ecosystems [18]. Previous authors [18] have already highlighted the need for further measurement and investigation of residence time to support model development, and further analysis of the effects of fuel structure on the residence time is provided in Chapter 7.

The fuel species composition of the fuel bed appeared to have little effect on the residence time. No significant variation in the average residence time was observed for fuel beds of equal fuel loading composed of pine needles, oak leaves or a pine:oak mix.

#### 4.3.2.4. Heat Release Rate (HRR)

For the limited number of fuel conditions in which Heat Release Rate (HRR) measurements are available, the fuel loading was observed to affect the overall energy release rate. This effect was observed in HRR measurements using the Transportable Analyser for Calorimetry Outside (TACO) (described in Chapter 3), as shown in Figure 4.11. An increased HRR was observed at the greater fuel loadings, as has previously been observed in other previous no-wind, no-slope flame laboratory-based flame spread experiments involving pine needles beds [226]. As previously discussed, the increased HRR at the greater fuel loading may be responsible for the increased flame heights, however further direct measurement of the buoyant flow profile is required (and is provided in Chapter 5).

Given the difficulty of measuring HRR in field environments, indirect measurements of energy release (e.g. fireline intensity) are typically reported instead. This allows some broad comparison of overall trends between laboratory and field-based experiments, but an aim of this thesis is to contribute to the understanding of the limits to these comparisons, and to explore methods for more closely aligned measurements in both environments.

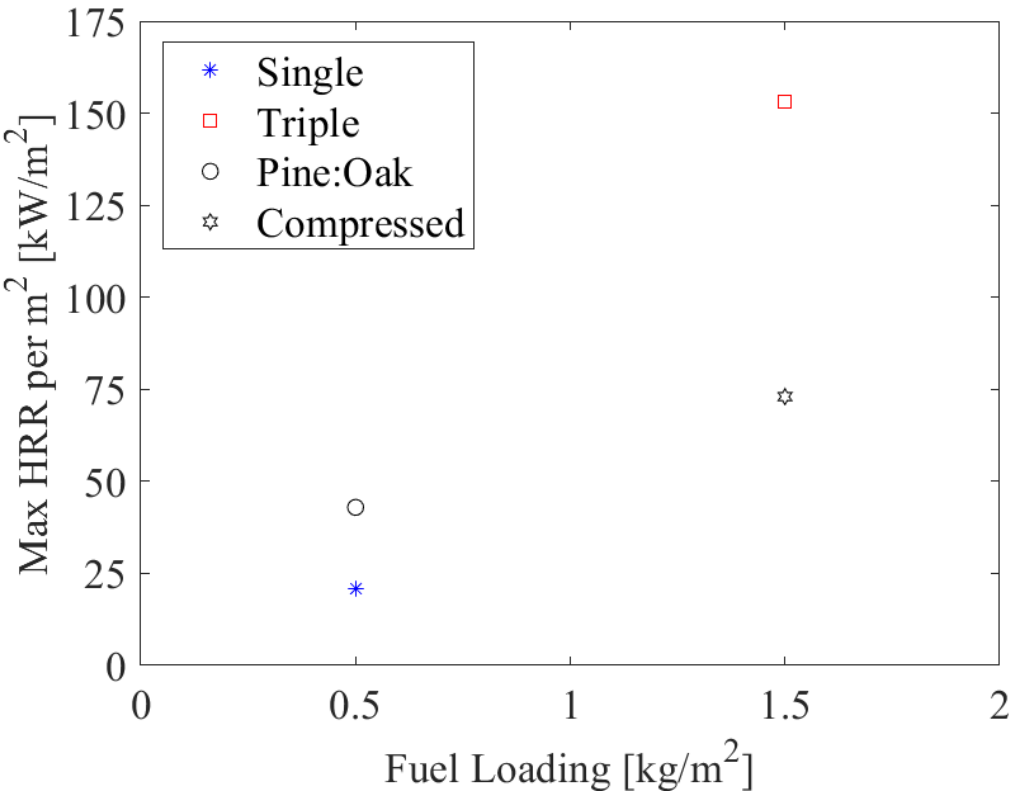


**Figure 4.11 - Comparison of Heat Release Rate (HRR) per m$^2$ with fuel loading across selected fuel conditions. Based upon Transportable Analyser for Calorimetry Outside (TACO) measurements**

#### 4.3.2.5. Fuel Consumption

Overall levels of fuel consumption were high across all fuel conditions, as shown in Figure 4.12. The average overall consumption (as a percentage of initial mass) of 92 % observed in this study was similar in magnitude to those observed in several other laboratory flame spread studies involving pine needles [81,297] and broadleaf species [297]. However much lower consumption values have also on occasion been reported for flame spread experiments involving pine needle litter layers [132].

In this study, for almost all cases, the remaining fuel (as a percentage of initial mass) was within the generic range of ash contents typically assumed for pine needles (circa. 5 to 10 % [93]). For the compressed fuel bed cases, the remaining mass exceeded this assumed ash content, with an average remaining mass of 14.3 ± 0.4 % of the initial mass. Interestingly, past studies have highlighted variations in mass consumption between different pine needle species, distinguishing between those in which only ash remained and those where partially or entirely unburnt needles remained. Dupuy *et al.* [132] suggested that this incomplete combustion is due to a lack of flame attachment at needles in direct contact with the combustion table (occurring due to their short, straight shape).

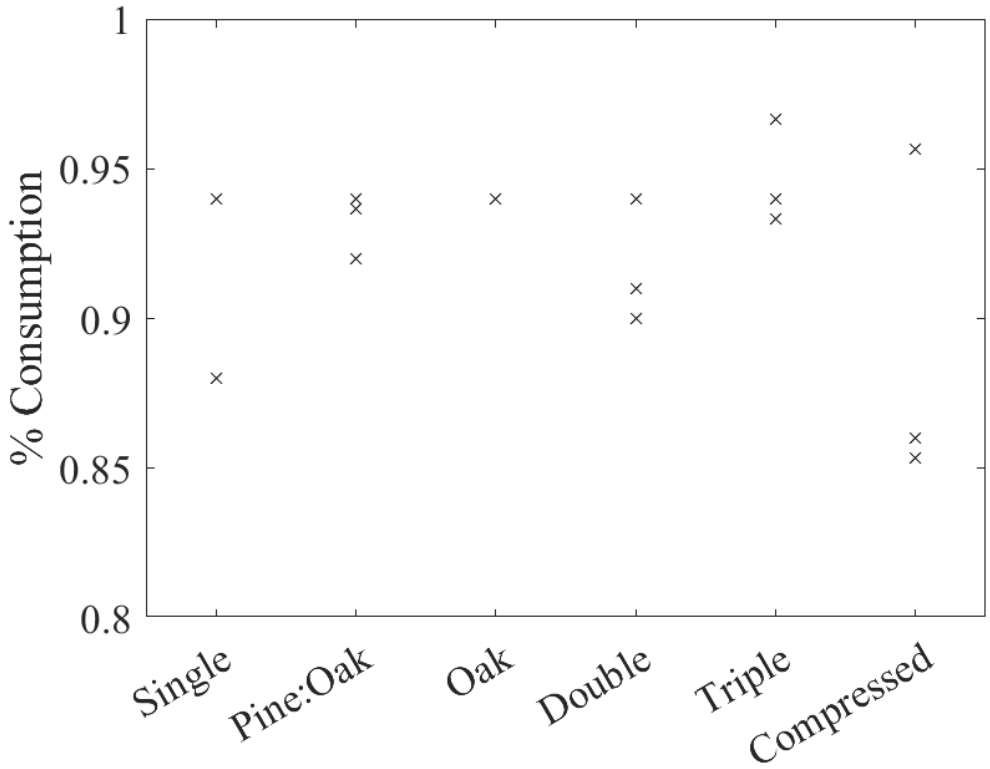


**Figure 4.12 – Effect of fuel condition on the percentage of initial fuel consumed**

**As observed in**

As shown in Figure 4.13, a strongly linear correlation ($R^2 = 0.99$) between initial fuel loading and overall mass consumption was observed, independent of the fuel species involved. The strong linear correlation between absolute consumption and initial fuel loading has also been observed in past laboratory-based flame spread studies involving natural porous fuel beds

[298], although at times this trend has been species-dependent where pine needle beds are considered [81].

The strongly linear influence of the fuel loading (on overall mass consumption of surface fuels) has also previously been observed in a number of field experiments replicating prescribed burning in the New Jersey PNR [225,299]. Indeed, this relationship between initial surface fuel loading appeared to be relatively independent of fire behaviour for the conditions studied. Mueller [18] found that thin fuels (primarily pine needles) were the greatest contributor to overall consumption, although the percent consumption of thin fuels was significantly lower than those reported in this study (average of 71 % consumption), as was the percent consumption of 1 hour fuels reported by Clark *et al.* (circa. 61 %) [225].

This strong correlation between initial fuel loading and overall consumption has not been unanimously observed at the field scale. Across a number of prescribed burns in South Carolina pine forests, Goodrick *et al.* [300] observed a much weaker relationship between initial fuel loading and fuel consumption. Although incorporating a Burning Index, greatly increased the predictive power for fuel consumption estimates.

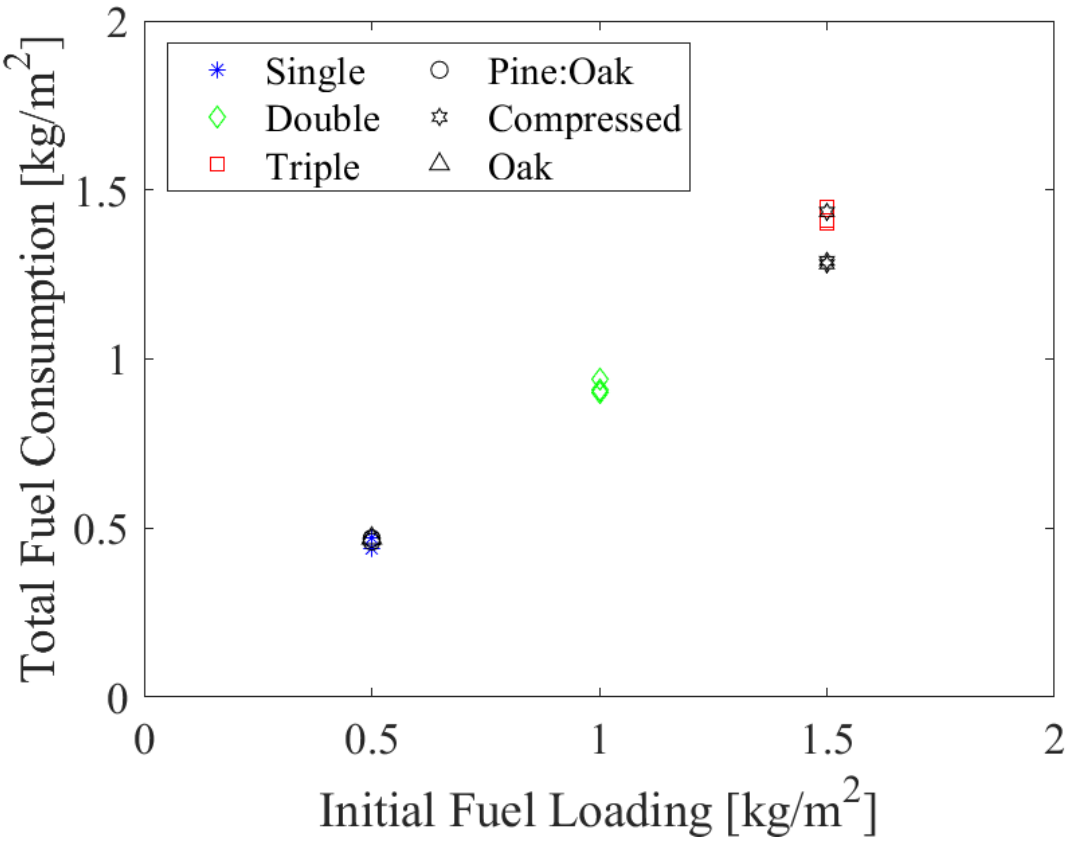


**Figure 4.13 – Effect of fuel condition on the total fuel consumption**

Some variation in mass consumption was observed for the compressed fuel bed case (with lower combustion as a percentage of the initial fuel load) however, the overall consumption remained significantly higher than at any of the lower fuel loading cases. Past comparisons of natural and reconstructed fuel beds have suggested that variations in bulk density, as a result of fuel bed compaction, may be responsible for observed variations in fuel consumption [118].

There are continuing efforts to identify the physical mechanisms responsible for this variation [56,57]. A systematic experimental study of the effect of bulk density, across a wider range of fuel conditions, is presented in Chapters 5 and 6.

No significant effect of changes in fuel composition (pine only, oak only, pine oak mix) on the overall fuel consumption was observed. This is despite the significant variations in spread rate observed across these fuel conditions. Regardless, the role of small-scale, inter-element, fuel structure may still require further investigation.

## 4.4. Implications for Systematic Study Design

The results from these initial experimental investigations indicates that both fuel loading and bulk density have an effect on fire behaviour (spread rate, flame height, residence time) and fuel consumption. However, further systematic study, with greater replicability and control of fuel bed structure than is typically possible in a field environment, is required in order to understand the independent effects of these fuel bed parameters.

A major objective of this systematic study must be contributing to an improved understanding of the effect of fuel bed structure on the key underlying physical processes controlling flame spread. This will require measurements of important physical properties (e.g. gas phase temperatures, flow velocities, and heat fluxes) in order to understand the connection between key fire behaviour properties and processes such as the pre-heating of unburnt fuel ahead of the flame front.

For example, increasing the fuel loading, or decreasing the bulk density, resulted in significant variations in flame height. However, further detailed investigation is required to understand the physical implications of this increased flame height, which may for example alter the buoyant flow regime and/or alter the relative importance of flame and in-bed heat transfer. The measurements presented in Chapters 5 and 6 will seek to address these questions by measuring both fire behaviour and key physical properties across a wider range of fuel loadings (0.2 to 1.6 $kg/m^2$) and at various bulk densities (10 to 40 $kg/m^3$). Controlling the fuel bed height will allow both these parameters to be varied independently.

As previously discussed, a major objective of this study is to provide data to support the development of physics-based models, and to allow comparison with existing field observations to contribute to the development of prescribed fire science. Therefore, it is important to understand any physical effects occurring as a result of the specific experimental set-up employed, and to understand the limitations associated with a smaller-scale, laboratory-based experiment of this nature.

While past studies have investigated the effect of fuel bed (and therefore flame front) width [132], relatively little investigation of the effect of the chosen substrate material and condition has been undertaken [59]. Understanding and characterising an effect of the substrate layer (upon which the fuel bed is constructed) is important given that substrates used in laboratory-based litter layer studies often differ greatly from the duff and soil layers typically present in a natural field environment.

## 4.5. Effect of Substrate Properties

The potential for the substrate material to influence flame spread is well acknowledged. Standard test methods for flammability and flame spread across various fields of fire safety

engineering specify compulsory substrates, or insist that the substrate reflects the actual usage condition of the tested material [301,302]. It is particularly important to consider the substrate effect when the fuel is thermally thin. In these situations, it may not be possible to test the material in a way that is independent of the testing set-up [301]. Instead, the heat losses to the substrate may become significant, affecting the burning rate of the fuel.

It is unclear whether porous fuel beds (and the individual fuel elements) are better considered as thermally thick or thin fuels. Either way, consideration of heat losses to the substrate is required, given the contact between the bottom surface of the fuel bed and the substrate layer beneath. By measuring the thermal response of appropriate substrate materials, we may also be able to gain a greater understanding of the energy transfer from the fuel bed. Several recent studies have performed inverse analysis of the substrate heat flux exposure (and/or direct heating of heat flux sensors), for the specific case of firebrands (single particles and/or accumulations) [303–306], however there seems to have been little consideration for the case of larger porous fuel beds.

Of the many laboratory-based, wildland flame spread studies, only a small minority explicitly consider, or systematically vary, the substrate properties [59,210,307]. Wolff *et al.* [59] observed a reduction in spread rate as the moisture content of the substrate was increased. In fact, the effect of the substrate moisture content was judged at least as great as that of the fuel moisture content, and it was speculatively suggested that this moisture might have a similar effect to other additives, resulting in reduced flame temperatures. However, Wolff *et al*. observed no effect from varying the substrate material (ceramic and clay substrates used) on the flame spread through a matrix of wooden `toothpicks'. McAllister *et al.* [307] found that varying the substrate colour could affect the piloted ignition of pine and fir needles, however this effect was eliminated by lightly coating the needles with graphite powder (altering the needle absorptivity/emissivity).

This section presents the methodology and results of a preliminary study of the effect of the substrate material/condition on flame spread through pine needle beds. This has important implications for understanding the similarity between substrate effects in the laboratory and field environments. The effect of substrate condition (e.g. moisture content) may also provide insight for a field environment, in which seasonal/climatic differences in substrate properties may occur.

In this study, four substrates were considered: vermiculite, aluminium, dry sand and wet sand. For the wet condition, one litre of water was added to the sand (distributed evenly across the substrate area) while the dry sand was oven-dried for 24 hours prior to use. In each of the sand cases, a layer of sand was distributed on top of the regular vermiculite board. This vermiculite board was absent for cases involving the use of an aluminium sheet. In this manner, both the substrate material and the substrate moisture content were varied, with the key properties for each of the substrate materials summarised in Figure 4.14. The sand also offers a reasonable first approximation of the sandy soil types typical of the New Jersey Pinelands National Reserve. However, the thermal properties are poorly characterised, and therefore only the substrate moisture content can be accurately defined.

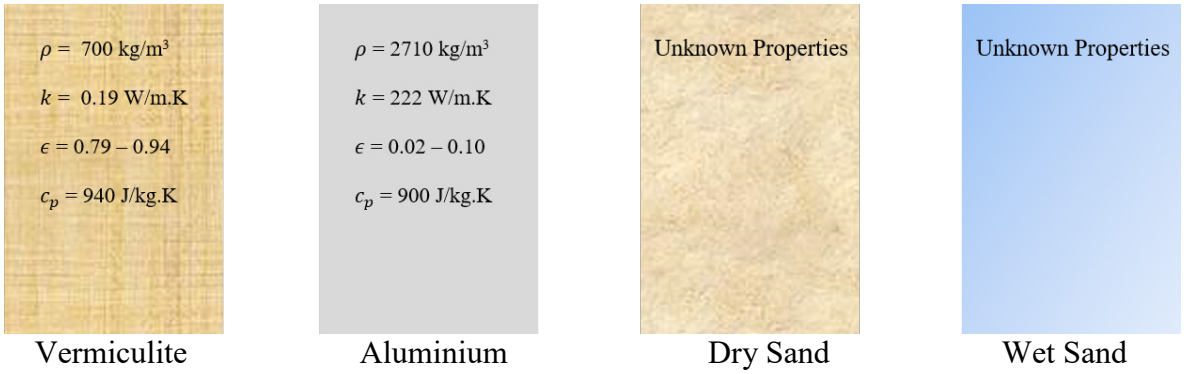


**Figure 4.14 - Properties of each substrate material. Vermiculite emissivity value extracted from Laschutza 2017** [308]

When considering the fuel beds used in this current study, the contact between the bottom surface of the fuel bed and the substrate should be considered. This contact area is likely to vary significantly from that of more discrete, thin fuel element fuel beds, of the type considered by Wolff *et al.* [59]. The thermal contact between the fuel bed and the substrate may depend on both the fuel bed and fuel element structure. A thermal contact resistance model, dependent on particle shape and surface properties, has previously been proposed for smouldering firebrands coming into contact with a fuel bed[309].[12]

There was little variation in fire behaviour and fuel consumption across most of the substrate conditions, as shown in Table 4.3. As in the previous experimental series, variation in observed fire behaviour properties occurred at each substrate condition. However, substrate effects on both fire behaviour and fuel consumption largely fell within this variability range. In cases involving dry substrate layers, the average flame height and fuel consumption for each substrate condition lie within 1.4 standard deviations of the mean. The average spread rate and peak HRR for each dry substrate lies within 1.3 standard deviations of the mean.

There was a decrease in fuel consumption (along with a small decrease in ROS) for the case involving wet sand compared to the dry sand case. This also however falls within the observed range of variability and lies within 1.2 standard deviations of the mean fuel consumption across all substrates. The average wet sand spread rate and peak HRR are within 0.4 and 0.8 standard deviations of the mean respectively. The average flame height for the wet sand substrate lies within 1.7 standard deviations of the mean across all substrates which suggests the substrate moisture content may affect the flame height. However, caution should be exercised given the limited number of substrate moistures studied and the high variability in flame height observed at the wet sand condition (± 0.13 m).

[12] The actual heat transfer to the fuel bed will also depend on the energy losses to the surroundings, and, due to evaporative losses, the fuel moisture content, however the latter is neglected in this model since mass transfer effects are not considered.

**Table 4.3 - Summary of fire behaviour for each substrate condition. [N=3 for each substrate condition]**

| Substrate Material | FMC [%] ± Max/Min | Fuel Loading [kg/m$^2$] | Fuel Consumption [%] ± Max/Min | Flame Height [m] ± Max/Min | Spread Rate [mm/min] ± Max/Min | Peak HRR [kW] ± Max/Min |
|---|---|---|---|---|---|---|
| Vermiculite | 10.3 ± 1.3 | 0.5 | 92.0 ± 4.00 | 0.12 ± 0.08 | 129 ± 34 | 28 ± 1 |
| Aluminium | 11.0 ± 1.7 | 0.5 | 93.4 ± 1.70 | 0.10 ± 0.01 | 135 ± 18 | 23 ± 2 |
| Dry Sand | 11.9 ± 0.2 | 0.5 | 93.3 ± 0.10 | 0.10 ± 0.01 | 142 ± 13 | 20 ± 5 |
| Wet Sand | 9.3 ± 2.1 | 0.5 | 91.6 ± 1.70 | 0.17 ± 0.13 | 133 ± 12 | 20 ± 3 |

In the context of this thesis, these observations support the use of the vermiculite substrate layer, despite the natural duff or soil layer present in a field environment. As a preliminary experimental investigation, there is a limit to the conclusions that can be drawn from this study. However, further systematic investigation, across a wider range of substrate moisture contents, and in different substrate materials, may be merited. Ideally, this would be accompanied with a mechanistic analysis of any significant observed moisture effect.

## 4.6. Conclusions

Fuel beds were deliberately constructed in order to replicate the field conditions in a series of complimentary field experiments. The resulting fire behaviour and fuel consumption was broadly similar to that observed in a number of past laboratory- and field-based studies. However, clearer trends between fuel properties and fire behaviour were observable given the greater control of environmental conditions than was possible in the complimentary field experiments. Comparison with past laboratory experiments involving other fuel types also emphasises the need for improved understanding of fuel effects, with significant variation observed between the spread rates and fuel heights in these pine needle beds and those observed in previous studies involving taller, excelsior fuel beds.

The use of several fuel treatments allowed an initial investigation of the role of fuel properties. Variation of fuel characteristics was observed to result in varying fire behaviour, beyond the range of variability observed at a single fuel condition. The effect of varying the fuel load was particularly pronounced in the resulting flame height, however greater variability was observed for the resulting ROS. These experiments also highlight the need to isolate changes to fuel loading or bulk density, rather than allowing both to vary simultaneously. This is further demonstrated by the significant effect of fuel bed compaction on the resulting fire behaviour and fuel consumption. By controlling the fuel bed height, it is possible to independently vary either the fuel loading or the bulk density, however this is not always employed in many existing flame spread studies, despite continuing research indicating that permeability of a fuel bed significantly affects flame spread (and is itself affected by the fuel bed packing and needle orientation).

The fuel species was also observed to affect the HRR and RoS, even where fuel bed bulk properties were held constant. This highlights the need to understand the controlling physical processes controlling the flame spread process, particularly if the roles of fuel bed and fuel

element properties are to be disentangled. Given the nature of the flame spread process observed in these experiments, efforts to improve this physical understanding must consider both the flaming and smouldering combustion phases.

Fuel consumption was high (avg. 92 % of initial mass) across all fuel conditions, matching several previous laboratory-based observations in pine needle beds. A clear positive trend between the initial fuel loading and the overall fuel consumption was observed. This is in line with past field-scale observations within the study area of interest (New Jersey Pinelands National Reserve), in which it was suggested that fine surface fuels contributed significantly to overall fuel consumption. This underlines the important role of surface flame spread in low-intensity prescribed fires.

The observations and findings in this chapter highlight the suitability and utility of the chosen experimental approach, which involves repeatable fuel beds (reflective of relevant field conditions), burned within well-controlled environmental conditions. The insight gained from the various fuel manipulations raises important considerations for land managers, but also highlights areas of limited understanding of the physical mechanisms driving variations in fire behaviour and fuel consumption. These knowledge gaps inform the systematic studies described in Chapters 5 and 6, where the relationship between fuel structure and key physical mechanisms (heat transfer, flow) controlling the flame spread process are explored in detail.

# Chapter 5

## Flow in Porous Fuel Beds

# 5. Flow in Porous Fuel Beds

## 5.1. Summary

This chapter presents measurements of the flow profiles both within and above porous (pine needle) fuel beds, in a number of laboratory-based flame spread experiments. These experiments were conducted in no wind, no slope conditions, and therefore the flame spread behaviour is buoyancy-driven. The aim was to gain a greater understanding of the effects of fuel bed structure on the Heat Release Rate (HRR) and plume flow profile, and the subsequent impact on the entrainment flow profile. The in-bed flow is further affected by the fuel structure, and resulting drag profile, which in turn affects the combustion dynamics and HRR.

Detailed measurements of the overall fire behaviour, and the physical mechanisms within and above the porous fuel bed, provide insight into the complex feedback cycle controlling the flame spread process. As in several previous studies, a positive trend between the Rate of Spread (RoS) and fuel loading and a negative trend between RoS and bulk density was observed, however neither parameter alone adequately predicted the RoS. Other existing structural descriptors were assessed, and found to be limited in their applicability to these fuel beds. An alternative structural parameter ($\alpha\sigma\delta$) is proposed, which is conceptually similar to the crib fire porosity factor, and which can be related to key physical mechanisms. A strong correlation between $\alpha\sigma\delta$ and the RoS was observed for both pine needle species studied.

A greater understanding of the physical mechanisms within the porous fuel beds was obtained through analysis of the flow profiles across a range of fuel bed structural conditions. Independent effects of fuel loading and bulk density on both the buoyant and buoyancy-driven entrainment flow were observed. Generally, increases in fuel loading resulted in increased HRR, and therefore greater buoyant flow velocity, along with an increase in the velocity of flow entrained towards the combustion region. Considerations of experimental limitations, as well as the associated measurement uncertainty, are discussed in detail.

It is hoped that the experimental data presented in this chapter will provide a useful resource in future model development and validation studies. In particular, the systematic investigation of the effect of fuel bed height (by independently controlling bulk density or fuel loading), and the measurement of in-bed flow profiles, satisfy previously identified gaps in experimental datasets. These experiments also aid our understanding of the flow conditions within the combustion region, and can inform efforts to understand the convective heating/cooling and oxygen supply within the fuel bed. These physical implications are explored further in subsequent chapters of this thesis.

## 5.2. Introduction

Quiescent flame spread is often considered analogous to opposed-flow flame spread, given the lateral entrainment of air towards the approaching flame front. Under these no-wind (or low-wind) conditions, the buoyancy force of the vertical plume (above the burning fuel) is greater than the wind inertia forces. The ratio between these forces can be expressed using the Convective Byram Number ($N_c$) [102],

$$\mathrm{N_c} = \frac{2gI}{\rho c_p T_0 \left(U_w - V_f\right)^3} \tag{5.1}$$

Where $g$ is the gravitational acceleration, $I$ is the fireline intensity, $\rho$ is the air density, $c_p$ is the specific heat capacity of air, $T_o$ is the ambient air temperature, $U_w$ is the ambient wind speed, and $V_f$ is the rate of spread.

Equation 5.1 allows the identification of two distinct flame spread regimes; wind-dominated ($N_c \ll 1$ ) and plume-dominated flame spread ($N_c \gg 1$). The quiescent flame spread scenarios described in this study therefore fall under the plume-dominated regime, with any lateral flow the result of buoyancy-driven entrainment by the plume.

The lateral airflow into the combustion zone can strongly affect the combustion dynamics and the relative importance of competing heat transfer mechanisms. In quiescent conditions, this airflow rate is controlled by the buoyancy forces of the plume that are largely dictated by the Heat Release Rate (HRR) of the fire, itself dependent upon the fuel structure which also affects the drag forces. Given the dependence of the HRR on the fuel structure (which dictates heat and mass transfer conditions) a complex feedback loop exists.

This feedback effect has been previously studied in non-porous fuels [310,311], however there is greater complexity in the case of porous fuels, where air can flow both over the surface and through the porous fuel bed itself. Despite some efforts to model the fire-induced entrainment flow in porous flame spread [46,47], there remains a lack of experimental quantification. The majority of existing experimental studies of fire-induced flow in porous fuels have focused on the flow above the fuel bed [204,243]. Further investigation is required to improve our understanding of the controlling heat transfer mechanisms within the porous fuels, and to allow the development of flow sub-models for use in physical flame spread models.

If we are to coherently describe the effect of porous fuel structure on flame spread, then it is necessary to first evaluate the flow profile as a function of fuel structure. It is the fuel bed structure that will determine various parameters controlling airflow (permeability and drag), which will subsequently influence the dominant heat transfer mechanisms (convective heating coefficient) and oxygen supply within the in-bed combustion region.

In previous quiescent flame spread experiments in porous fuel beds, several trends have emerged. Generally, an increase in fuel loading resulted in an increased rate of flame spread, along with increasing mass loss rate, flame height and HRR or fire intensity, with similar trends observed for decreases in bulk density [43,81]. In some fuels, a positive trend between fuel bed height and flame spread rate and HRR, has also been observed for cases in which either the fuel loading is kept constant [312] or alternatively the bulk density is kept constant [81,226].

Despite these observations on the effect of fuel bed structure on the fire behaviour, we continue to lack a complete theory of fire spread in porous fuel beds [19]. Many of the structural descriptors commonly applied to porous fuel beds (such as those discussed in Chapter 2) do not relate clearly to the underlying physical processes controlling flame spread.

An experimental programme was designed to investigate the effects of fuel structure on the physical mechanisms controlling flame spread in porous (pine needle) fuel beds in the absence of wind and slope. These experiments allowed the effect of fuel bed structure on the overall fire behaviour, and both the buoyant and lateral entrainment flow regimes, to be systematically investigated. This therefore seeks to address the existing gaps in understanding identified in Chapter 4, and illustrated by the fuel treatments implemented in that chapter.

In this chapter, the experimental methods are detailed, followed by overall observations of fire behaviour (spread rate, flame height, fire line intensity) across a range of fuel bed structural conditions. Identified trends are compared with those from existing studies, and the

applicability of existing structural descriptors (fuel loading, bulk density, bed height, $\sigma\lambda$, $\alpha\beta\delta$) are assessed.

An alternative structural parameter $\alpha\sigma\delta$ is proposed, and flow profiles above (buoyant velocity) and within the fuel bed are then examined. The relationship between HRR and the buoyant flow profile as well as the subsequent effect, along with fuel structure, on entrainment flow are also investigated. This is supported by analysis of the gas phase temperatures within the fuel bed from which the residence time is also calculated.

## 5.3. Methods

### 5.3.1. Instrumentation

A further series of flame spread experiments were conducted on the flame spread table described in Chapter 3. These experiments were primarily focused on investigating the flow regimes both within and above the porous (pine needle) fuel beds, and the effect of changes in fuel bed structure. The specific instrumentation deployed for these purposes is shown in Figure 5.1. Additional measurements were conducted in order to characterise the resulting fire behaviour.

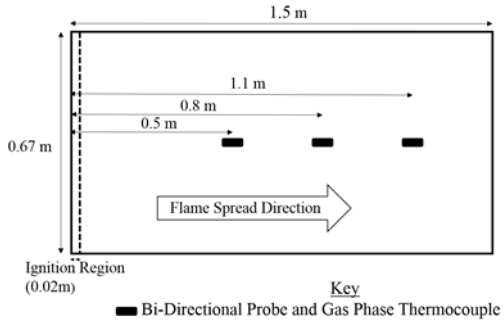


**Figure 5.1 - Schematic of the instrumented flame spread table deployed during flow regime experiments described in Chapter 5**

Flow within the fuel bed was measured using bidirectional pressure probes (and an accompanying gas phase thermocouple), from which the gas flow velocity was calculated. Located at various distances from the ignition line (0.5 m, 0.8 m and 1.1 m), both the probe centre and the thermocouple tip were positioned within the fuel bed, at a height of 10 mm above the table surface. Further specifications for the 0.25 mm K-Type thermocouples and the 20 mm diameter bidirectional pressure probes are provided in Chapter 3.

In a subset of experiments, additional measurements of the upward (buoyant) flow were recorded, using additional pressure probes positioned at a height of 1.2 m above the fuel bed. These additional probes were located at horizontal distances of 0.5 m and 0.8 m from the ignition line, and were co-located with a 0.25 mm gas phase thermocouple. Further details regarding the calculation procedure for the gas phase velocity are given in Chapter 3.

The in-bed, gas phase temperature measurements allowed calculation of the flame arrival time and residence times at each thermocouple. For both parameters, a temperature threshold of 300 °C was assumed to indicate flame presence, and the validity of this assumption is assessed further in Chapter 3.

In this chapter, the flame spread rate was calculated via video analysis of the flame front position over time, followed by a regression analysis. Video analysis was also employed in order to determine the flame height, based upon the continuous flame region [254]. Further details on all these methods are given in Chapter 3.

All experiments involved a line ignition, with 10 ml of acetone equally distributed across a 0.67 m length of alumina silica fibre. Further characterisation of this ignition source is provided in Chapter 3.

#### 5.3.2. Fuel Properties

The flame spread experiments discussed in this chapter involved fuel beds composed only of dead pine needles. Two separate experimental series, each involving a different pine needle species (Pitch Pine and Pitch-Loblolly hybrid Pine), were conducted. The physical and thermochemical properties of both pine needle species, along with the measurement and sampling methods, are given in Chapter 3.

For all experiments, pine needles were air-dried in a storage room but were otherwise unconditioned prior to use. As described in Chapter 3, the FMC of each fuel bed was established just prior to ignition via the oven drying of samples at 60 °C for 24 hours. For these experiments, the average FMC (on a dry basis) differed between the two pine needle species (10.1 % ± 0.8 % for Pitch Pine and 16.0 % ± 0.9 % for Pitch-Loblolly hybrid pine [± Std. Dev]).

Fuel bed construction methods followed those outlined in Chapter 3. In order to explore the effect of fuel structure on the flow regime (and resulting fire behaviour), both the fuel loading and the bulk density were individually varied (by controlling the fuel bed height). The properties for each fuel bed condition are summarised in Table 5.1 and Table 5.2. For the highest bulk density tests (40 kg/m$^3$), compaction of the fuel bed was required to achieve the desired fuel bed height. A minimum of one replicate experiment was conducted at each fuel bed condition, given the potential for fuel bed structural heterogeneity.

### 5.4. Results & Discussion

#### 5.4.1. Overall Fire Behaviour

As in Chapter 4, significant variations in fire behaviour were observed as the fuel bed structure was altered. Unlike in Chapter 4, in these experiments, the fuel loading and bulk density were varied independently, allowing their individual influence on flame spread behaviour (and the underlying physical phenomena) to be investigated further.

Characteristic images of the fire behaviour at selected fuel bed conditions are presented in Figure 5.2. It can be visually observed, and is confirmed in the fire behaviour measurements summarised in Table 5.1 and Table 5.2, that the flame spread rate and flame height both increased with increasing fuel loading or decreasing bulk density.

Due to the wider range of fuel loadings investigated in this experimental series, marginal burning conditions were observed at the lowest fuel loading (0.2 kg/m$^2$). At this lowest fuel loading, the flame front became discontinuous, as clearly shown in Figure 5.2, whereas at higher fuel loadings a single, continuous flame front was observed across the fuel bed width.

The greater needle-to-needle spacing at the lowest fuel loading appears to impede flame spread, with the interaction between individual needles or clusters appearing to dominate. This was particularly apparent for the Pitch-Loblolly Pine series, where fuel beds of 0.2 kg/m$^2$ were

unable to sustain flame spread across the length of the table. However, the distance from the ignition line at which flame spread ceased varied between repeat experiments. The other notable feature at these lowest fuel loadings (for both species) was the absence of the trailing smouldering region behind the main flame front. This was present at all higher fuel loadings.

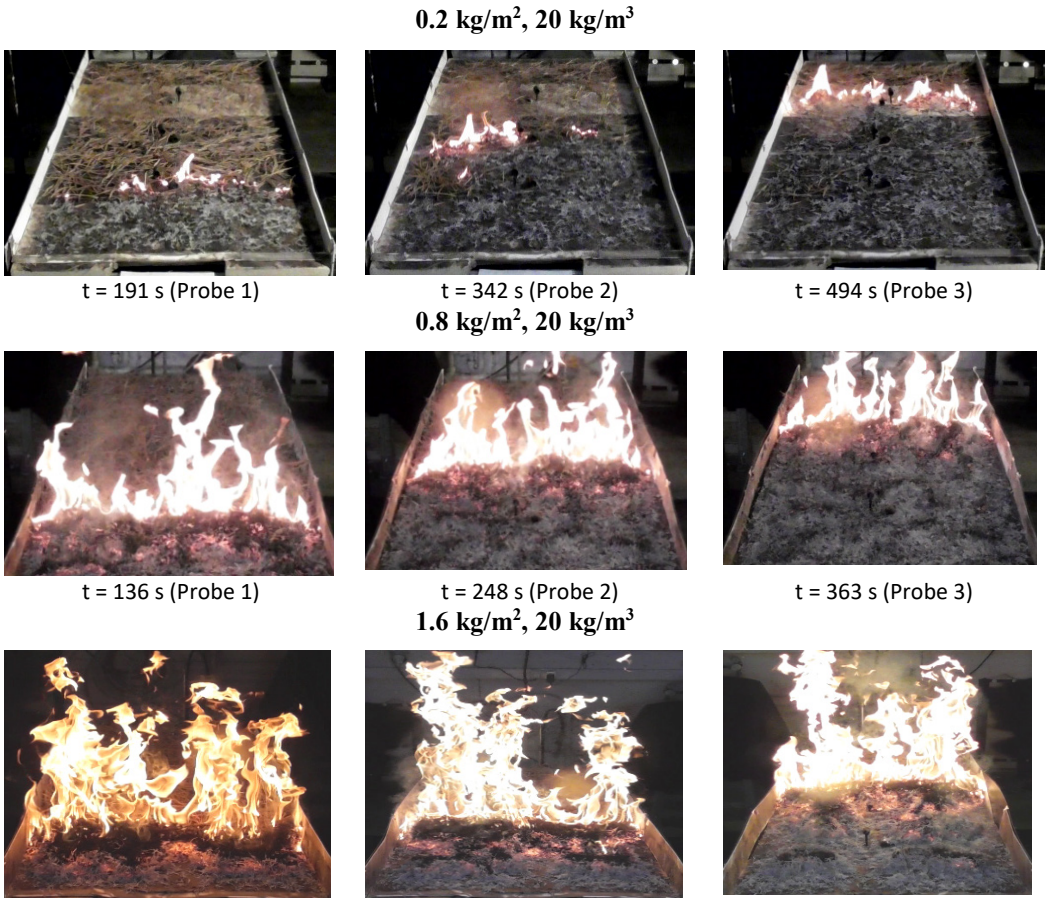


**Figure 5.2 - Representative images of the fire behaviour at selected fuel bed conditions**

The overall fire behaviour for both experimental series are summarised in Table 5.1 (Pitch Pine) and Table 5.2 (Pitch-Loblolly hybrid Pine). The values reported are the average values across repetitions at each fuel bed condition, and the standard deviation is reported. For both species, the flame spread rate increased with increasing fuel load or decreasing bulk density as shown in Figure 5.6. The flame height and steady state HRR also increases with increasing fuel load or decreasing bulk density as shown in Figure 5.3 and Table 5.1and Table 5.2. These trends are in agreement with several previously discussed trends in the existing literature, however the effect of fuel loading in previous experiments has been conflicted [43,81,226].

**Table 5.1 - Summary of fire behaviour for experiments involving Pitch Pine needle beds**

| Fuel Loading ($kg/m^2$) | Bulk Density, $\rho^*$ ($kg/m^3$) | Fuel Bed Height, $\delta$ (m) | Porosity, $\alpha$ | Fuel Moisture Content (% ± Std. Dev.) | Flame Spread Rate (mm/min ± Std. Dev.) | Steady State HRR (kW ± Std. Dev) | Residence Time (s ± Std. Dev.) | Flame Height (m ± 0.025 m) |
|---|---|---|---|---|---|---|---|---|
| 0.2 | 10 | 0.02 | 0.986 | 10.1 ± 1.1 | 108 ± 31 | 12.2 ± 3.1 | 17 ± 9 | 0.10 |
| 0.2 | 20 | 0.01 | 0.972 | 10.0 ± 1.2 | 114 ± 24 | 1.1 ± 1.1 | 18 ± 10 | 0.05 |
| 0.4 | 10 | 0.04 | 0.986 | 9.6 ± 0.8 | 144 ± 20 | 15.4 ± 1.6 | 20 ± 11 | 0.23 |
| 0.4 | 20 | 0.02 | 0.972 | 9.6 ± 0.6 | 126 ± 17 | 10.5 ± 1.5 | 29 ± 9 | 0.16 |
| 0.6 | 10 | 0.06 | 0.986 | 10.9 ± 2.1 | 180 ± 28 | 24.1 ± 3.6 | 30 ± 10 | 0.43 |
| 0.6 | 20 | 0.03 | 0.972 | 9.8 ± 0.7 | 132 ± 19 | 18.6 ± 1.8 | 33 ± 14 | 0.29 |
| 0.8 | 10 | 0.08 | 0.986 | 10.1 ± 0.5 | 210 ± 26 | 39.4 ± 2.0 | 27 ± 15 | 0.57 |
| 0.8 | 20 | 0.04 | 0.972 | 10.2 ± 0.7 | 162 ± 16 | 28.9 ± 3.6 | 46 ± 14 | 0.42 |
| 0.8 | 40 | 0.02 | 0.943 | 10.1 ± 0.9 | 126 ± 37 | N/A | 38 ± 24 | 0.33 |
| 1.2 | 20 | 0.06 | 0.972 | 11.3 ± 0.3 | 174 ± 33 | N/A | 64 ± 52 | 0.65 |
| 1.6 | 20 | 0.08 | 0.972 | 12.3 ± 1.7 | 246 ± 39 | N/A | 49 ± 23 | 0.93 |

**Table 5.2 - Summary of fire behaviour for experiments involving Pitch-Loblolly hybrid Pine needle beds**

| Fuel Loading ($kg/m^2$) | Bulk Density, $\rho^*$ ($kg/m^3$) | Fuel Bed Height, $\delta$ (m) | Porosity, $\alpha$ | Fuel Moisture Content (% ± Std. Dev.) | Flame Spread Rate (mm/min ± Std. Dev.) | Steady State HRR (kW ± Std. Dev.) | Residence Time (s ± Std. Dev.) | Flame Height (m ± 0.025 m) |
|---|---|---|---|---|---|---|---|---|
| 0.2 | 10 | 0.02 | 0.986 | 16.6 ± 1.9 | Unsustained | N/A | N/A | N/A |
| 0.2 | 20 | 0.01 | 0.972 | 16.6 ± 1.9 | Unsustained | N/A | N/A | N/A |
| 0.4 | 10 | 0.04 | 0.986 | 15.3 ± 1.2 | 114 ± 25 | 9.3 ± 2.0 | 28 ± 18 | 0.21 |
| 0.4 | 20 | 0.02 | 0.972 | 15.5 ± 0.3 | 90 ± 21 | 6.6 ± 2.1 | 15 ± 14 | 0.10 |
| 0.6 | 10 | 0.06 | 0.986 | 15.6 ± 0.3 | 156 ± 39 | 18.1 ± 2.9 | 37 ± 17 | 0.35 |
| 0.6 | 20 | 0.03 | 0.972 | 17.1 ± 0.7 | 114 ± 18 | 13.1 ± 2.5 | 23 ± 13 | 0.28 |
| 0.8 | 10 | 0.08 | 0.986 | 15.9 ± 0.6 | 162 ± 28 | 28.9 ± 3.0 | 45 ± 7 | 0.48 |
| 0.8 | 20 | 0.04 | 0.972 | 15.7 ± 2.4 | 126 ± 21 | 17.5 ± 1.6 | 45 ± 31 | 0.40 |
| 0.8 | 40 | 0.02 | 0.945 | 16.0 ± 0.8 | 96 ± 11 | 11.9 ± 1.4 | 29 ± 14 | 0.28 |

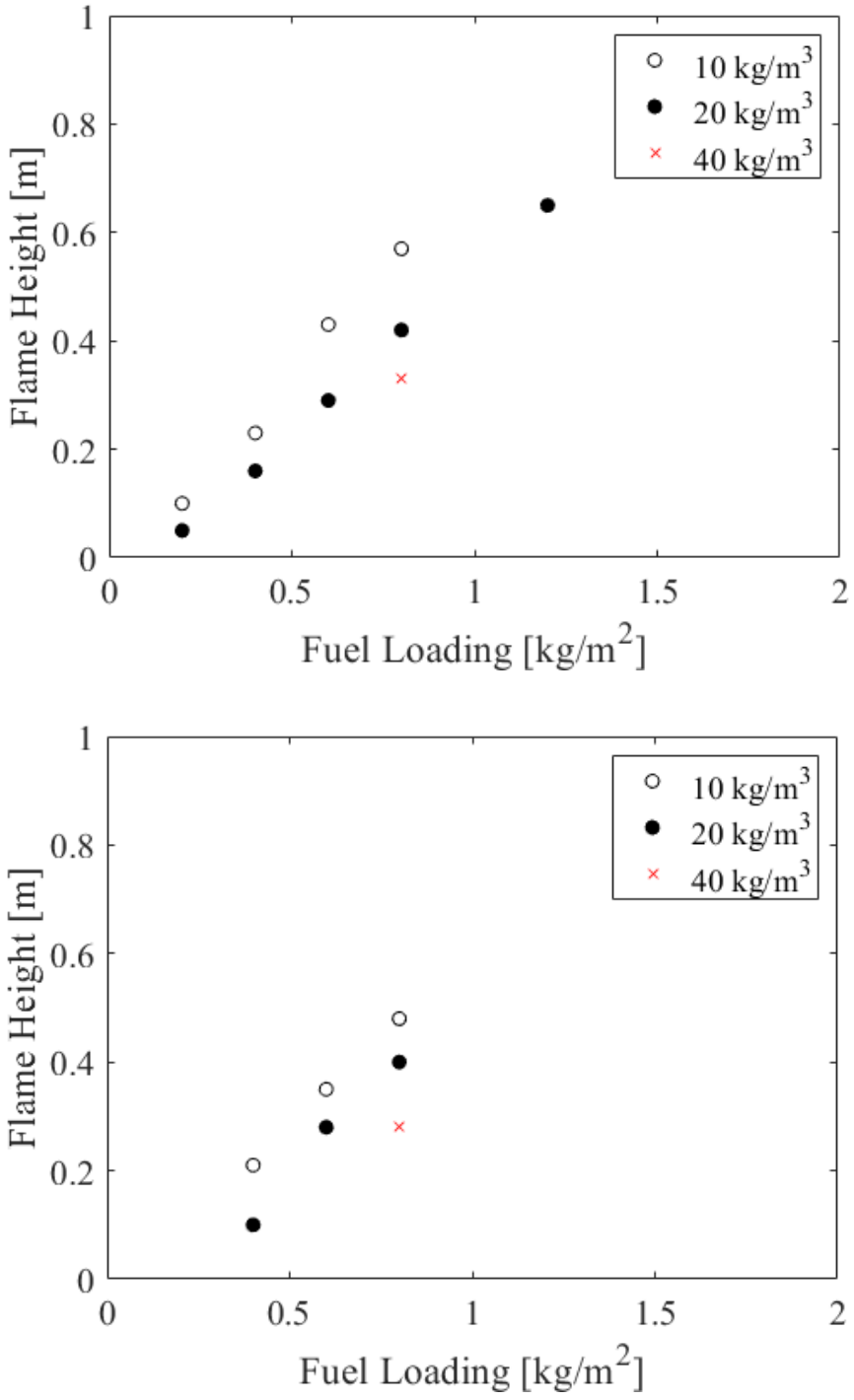


**Figure 5.3 – Comparison of flame height with fuel loading and bulk density for (top) Pitch Pine fuel beds (bottom) Hybrid Pitch-Loblolly Pine beds**

### 5.4.2. Flame Spread Rate

From video analysis, the position of the flame front over time is shown in Figure 5.4, where the ignition line represents X = 0. Through a least squares regression analysis, the degree of linearity of flame spread was evaluated for each fuel condition. A correlation coefficient of

greater than 0.99 was observed for all conditions. As in previous studies [67], this was assumed to be indicative of quasi-steady flame spread.

Despite quasi-steady flame spread occurring at all fuel conditions, in some cases a reduction in the initial spread rate occurred during the initial stages of flame spread, likely due to the influence of the ignition source. The 'ignition-affected' region appears to have a maximum length of 0.3 m, and therefore ends well before the first point measurement location (0.5 m). This is similar to the maximum propagation distance of 0.28 m that can occur during the maximum flaming duration of the ignition source (69 s),[13] at the maximum RoS (246 mm/min). This initial 0.3 m region was therefore excluded from the calculation of the flame spread rate.

[13] Further details on the characterisation of the ignition source are given in Chapter 3.

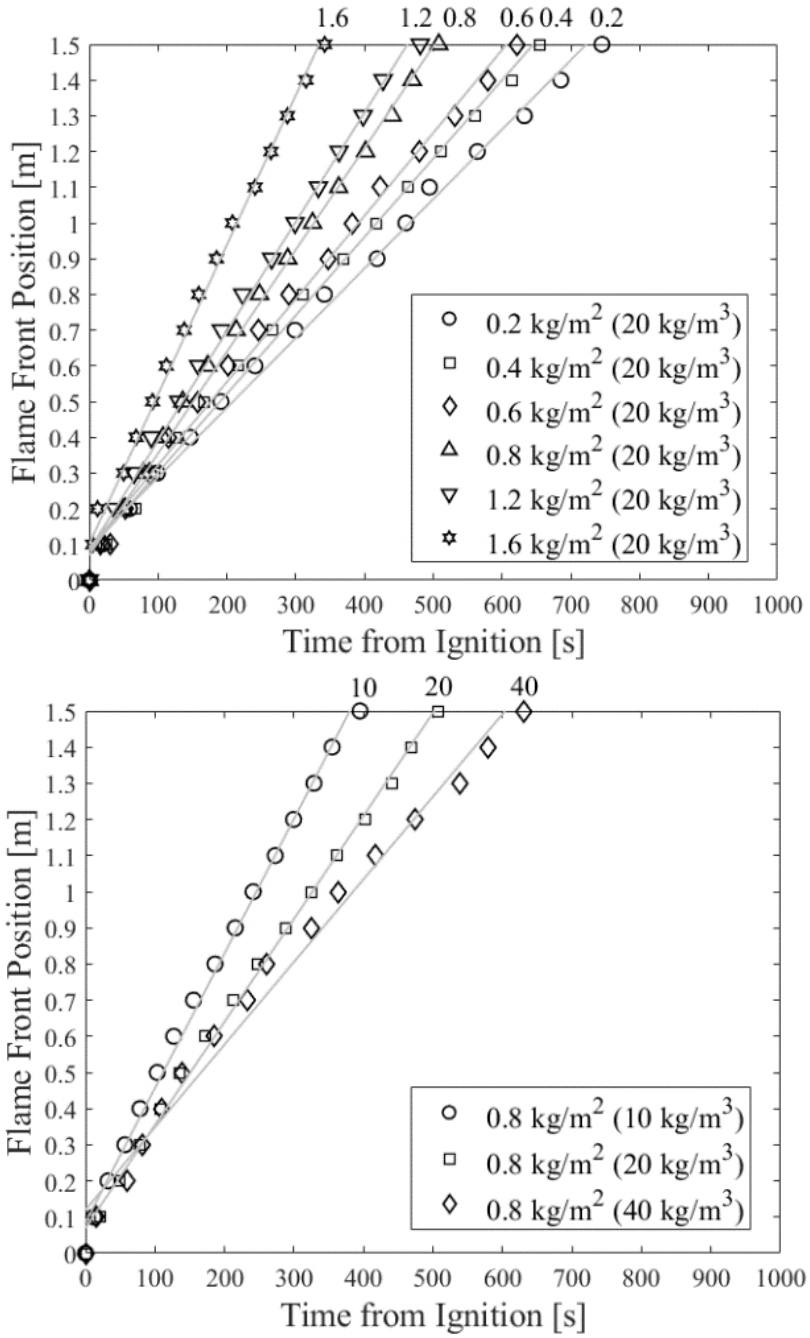


**Figure 5.4 - Flame front position vs. time from ignition for Pitch Pine beds of (top) 20 kg/m$^3$ bulk density and (bottom) 0.8 kg/m$^2$ fuel loading (Avg. of replicates at each fuel bed condition)**

Even beyond the 'ignition-affected' region, and despite the high correlation coefficients, some variability in the individual flame front position measurements can be observed, as shown in Figure 5.4. This variability is expected given the inherent heterogeneity of the fuel beds. This variability is more clearly visualised in Figure 5.5, where the flame spread rate is plotted as a function of the horizontal distance from the ignition line (excluding the 'ignition-affected' region).

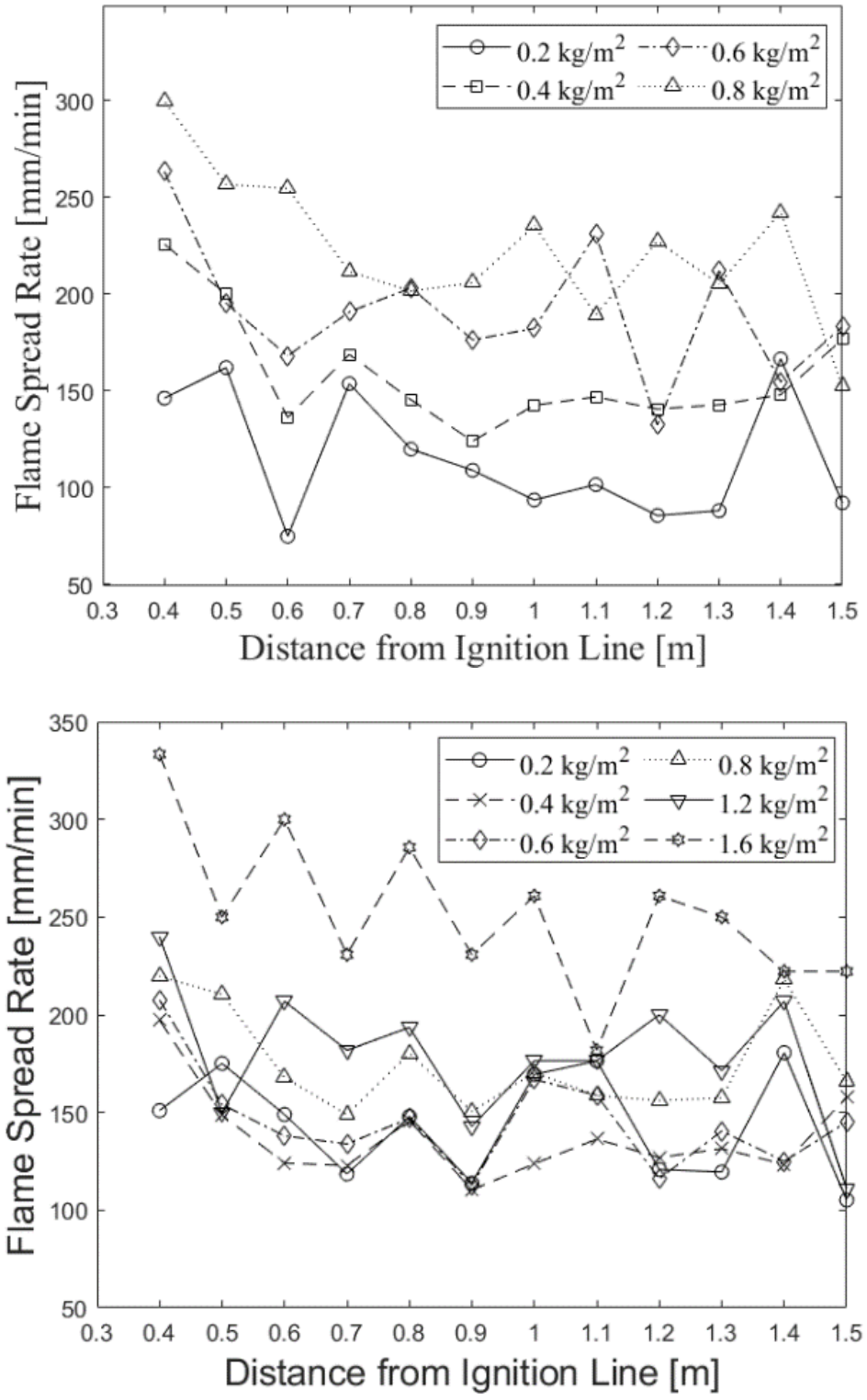


**Figure 5.5 - Flame spread rate as a function of distance from the ignition line for Pitch Pine beds of different fuel loadings at (top) 10 kg/m$^3$ bulk density, and (bottom) 20 kg/m$^3$ bulk density**

It is useful to remain aware of the inherent variability, even where considering what can properly be described as quasi-steady flame spread. However, the variability remains sufficiently low, as to allow the identification of overall trends in the average flame spread

rates across the various fuel bed conditions. As was shown in Table 5.1 and Table 5.2, the RoS increased with increasing fuel loading or decreasing bulk density, and neither parameter alone adequately described the variation in spread rate that occurs.

In Figure 5.6, the independent effects of fuel loading and bulk density, on the RoS, can be clearly observed. For example, for 20 $kg/m^3$ Pitch Pine beds a 116 % increase in RoS is observed across the fuel loading range (0.2 to 1.6 $kg/m^2$). A 67 % increase in RoS was observed across the bulk density range (40 to 10 $kg/m^3$) for 0.8 $kg/m^2$ Pitch Pine beds.

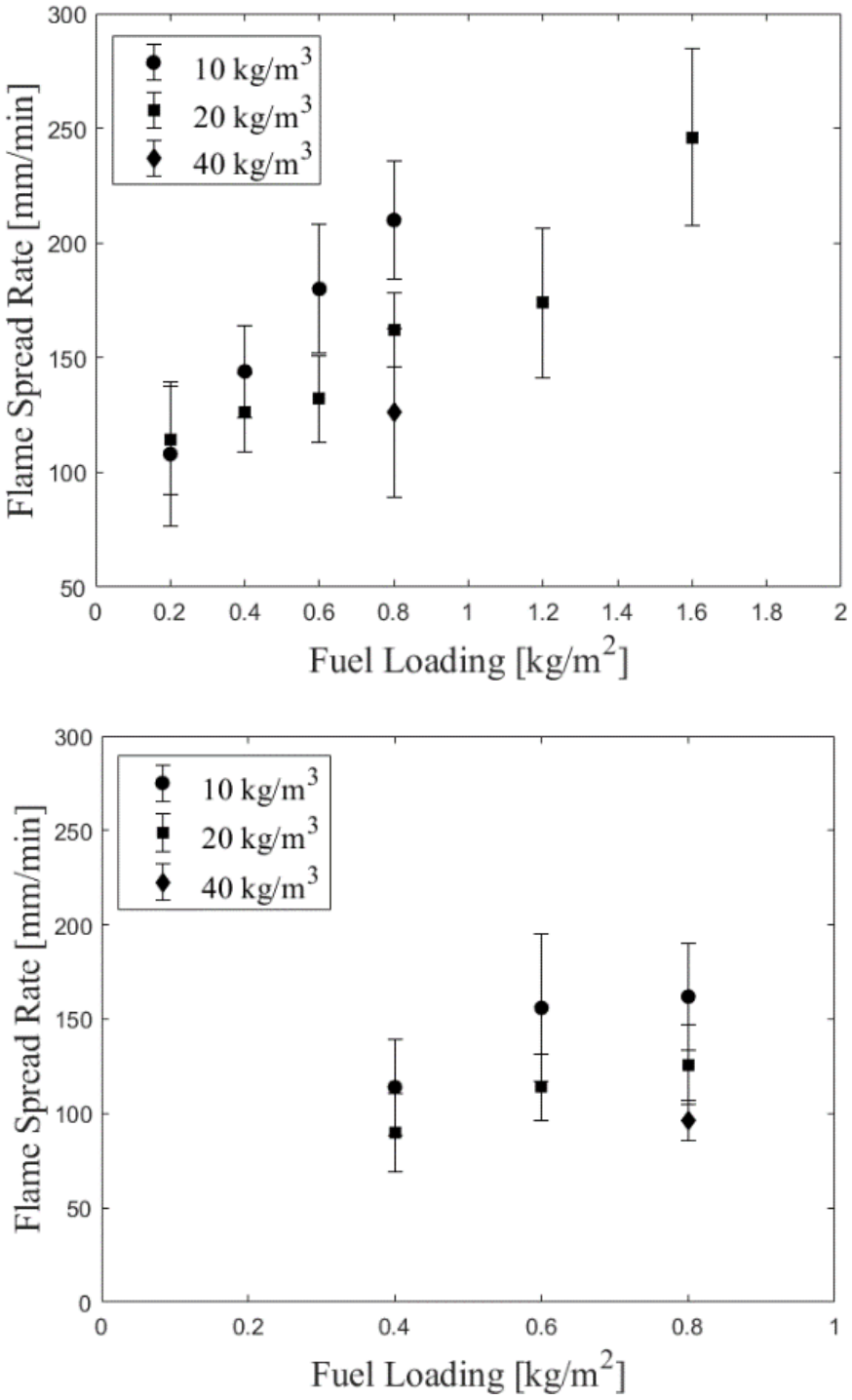


**Figure 5.6 - Comparison of flame spread rate with fuel loading and bulk density for (top) Pitch Pine (bottom) Pitch-Loblolly Pine hybrid, needle fuel beds**

If we instead assess the effect of fuel bed height, then a greater correlation with RoS is observed, as shown in Figure 5.7. This is in line with the observations of previous authors, who have highlighted the strong effect of fuel bed height on RoS [312,313]. This suggests that other aspects of the fuel bed structure, not adequately described by fuel loading and bulk density parameters, are significantly influencing the flame spread rate.

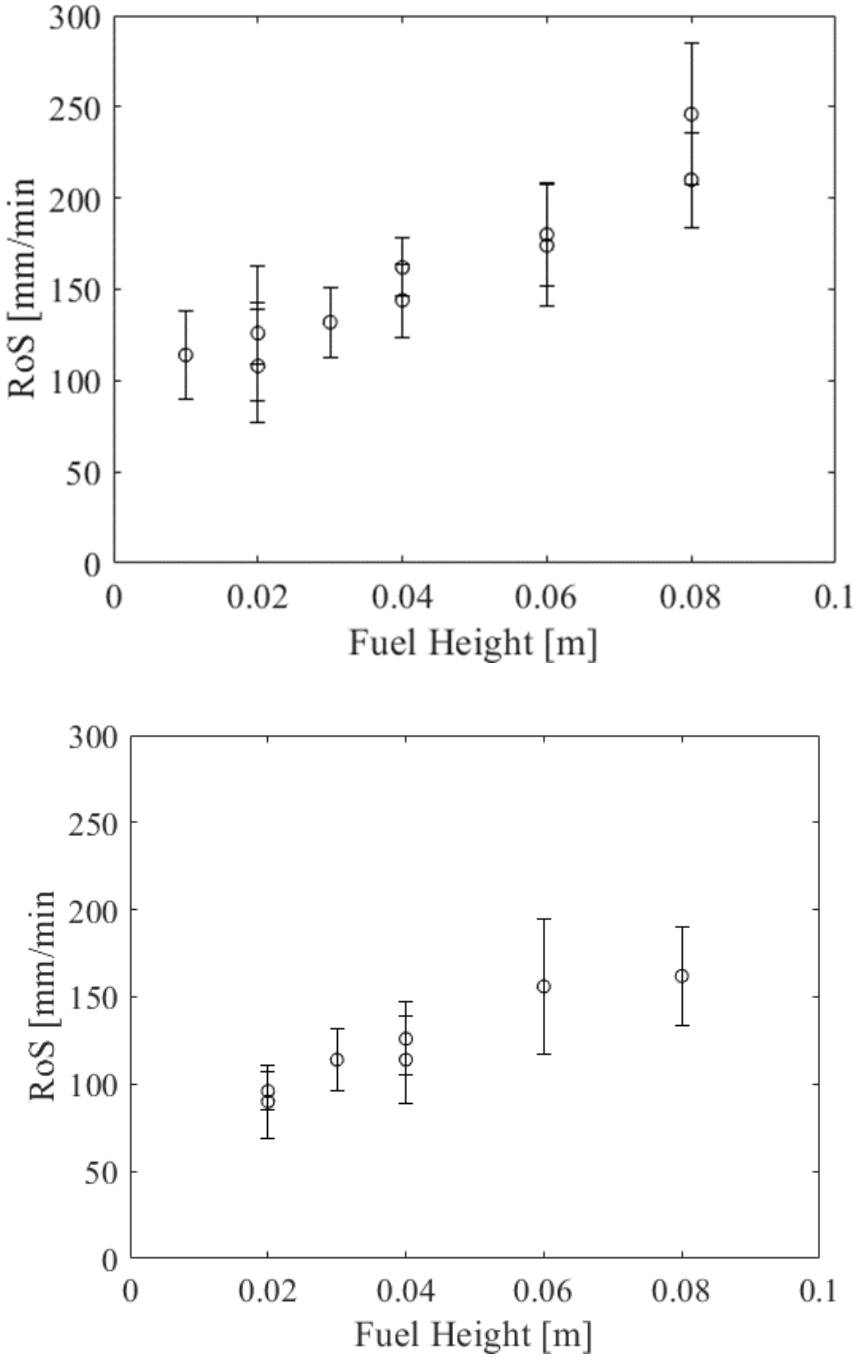


**Figure 5.7 - Comparison of flame spread rate with fuel bed height for (top) Pitch Pine [$R^2 = 0.92$] (bottom) Pitch-Loblolly hybrid Pine [$R^2 = 0.93$] fuel beds**

It is desirable to identify physically meaningful fuel structure parameters that, in addition to being well correlated with RoS, can be linked to key physical mechanisms. As shown in Figure 5.8, comparison with the experimentally observed RoS values and the dimensionless fuel bed parameter $\sigma\lambda$, proposed by Fons [111] and later Rothermel and Anderson [125], results in a high degree of correlation only once normalised by the fuel loading. This normalisation process

is similar to the manner in which the effect of wind loading was originally incorporated into this parameter however, it results in a loss of the dimensionless property.

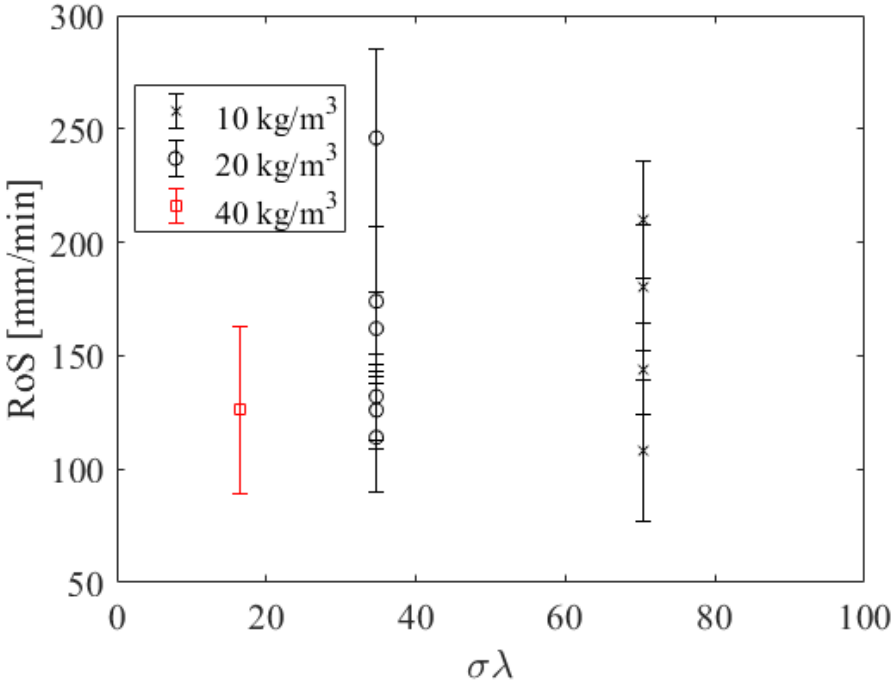


**Figure 5.8 - Correlation between $\sigma\lambda$ and flame spread rate in Pitch Pine fuel beds of various bulk densities**

The porosity ($\lambda$) was defined by Fons [111] as the ratio of the void volume to surface area of fuel in the bed. The parameter $\sigma\lambda$ can also be considered in terms of packing ratio as $\frac{1-\beta}{\beta}$, therefore multiplication by the packing ratio ($\beta$), surface-to-volume ratio of fuel elements ($\sigma$), and the fuel bed height ($\delta$), results in an alternative dimensionless parameter $\alpha\sigma\delta$, where $\alpha$ is the fuel bed porosity.

Comparison of this newly proposed term $\alpha\sigma\delta$ with RoS (as shown in Figure 5.9) shows a high correlation whilst maintaining the dimensionless properties of $\alpha\sigma\delta$. This parameter can be considered in terms of a porosity factor in a similar conceptual manner to those previously suggested for wood cribs.[14]

[14] The development of porosity factors in wood cribs is discussed in further detail in Chapter 2.

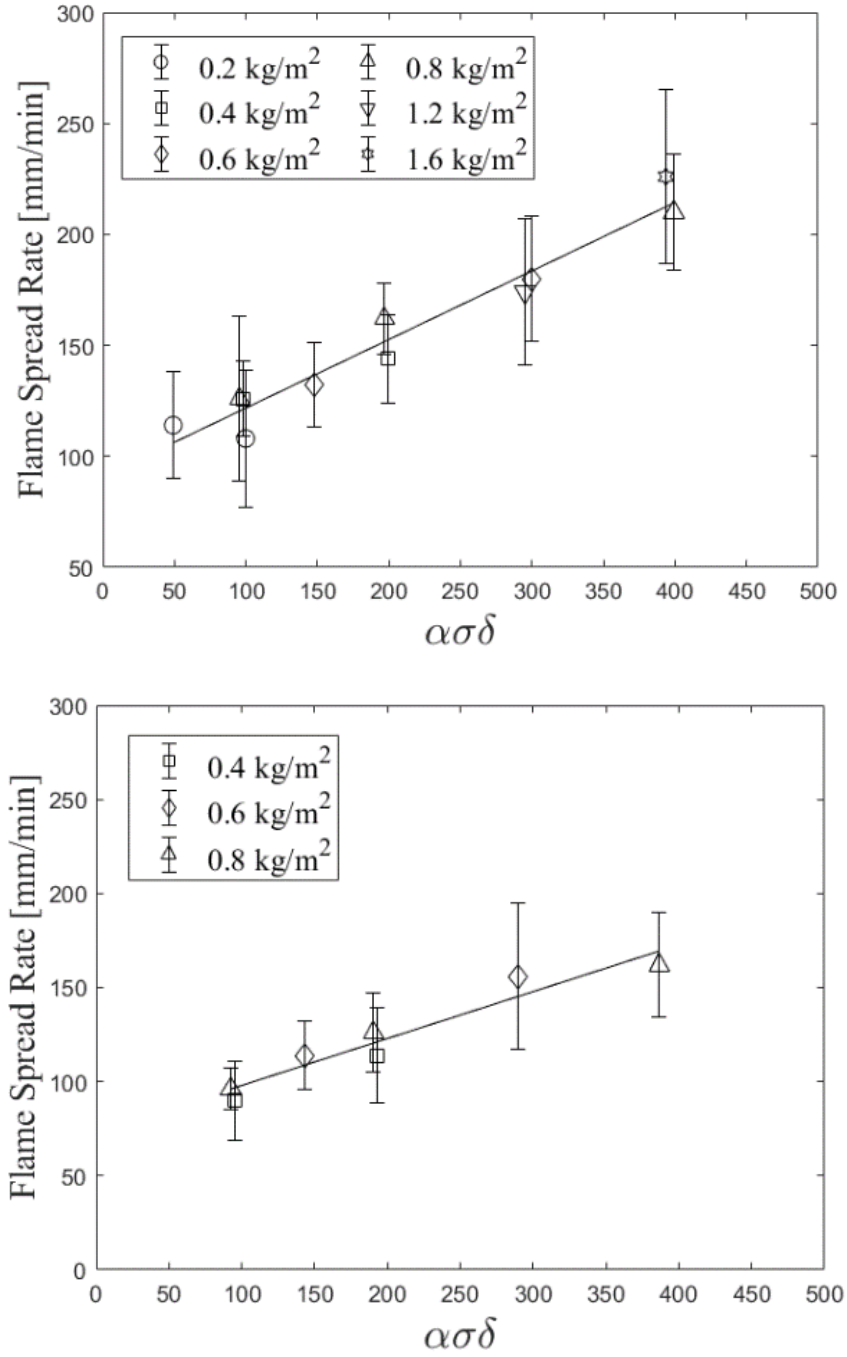


**Figure 5.9 - Correlation between ασδ and flame spread rate in (top) Pitch Pine [$R^2 = 0.91$] (bottom) Pitch-Loblolly Pine [$R^2 = 0.93$] fuel beds**

While $\alpha\sigma\delta$ appears similar to the fuel bed descriptor $\beta\sigma\delta$ previously proposed by Wilson [97] and Anderson [75], their relationship to RoS vary markedly as shown in Figure 5.10. Where $\beta\sigma\delta$ is used, a constant value is calculated for fuel beds of identical fuel load but different bulk density (fuel bed height altered), despite the clear trends between RoS and bulk density observed in this study. The constant values of $\beta\sigma\delta$ occur due to cancellation of the packing ratio ($\beta$) and fuel height ($\delta$) terms.

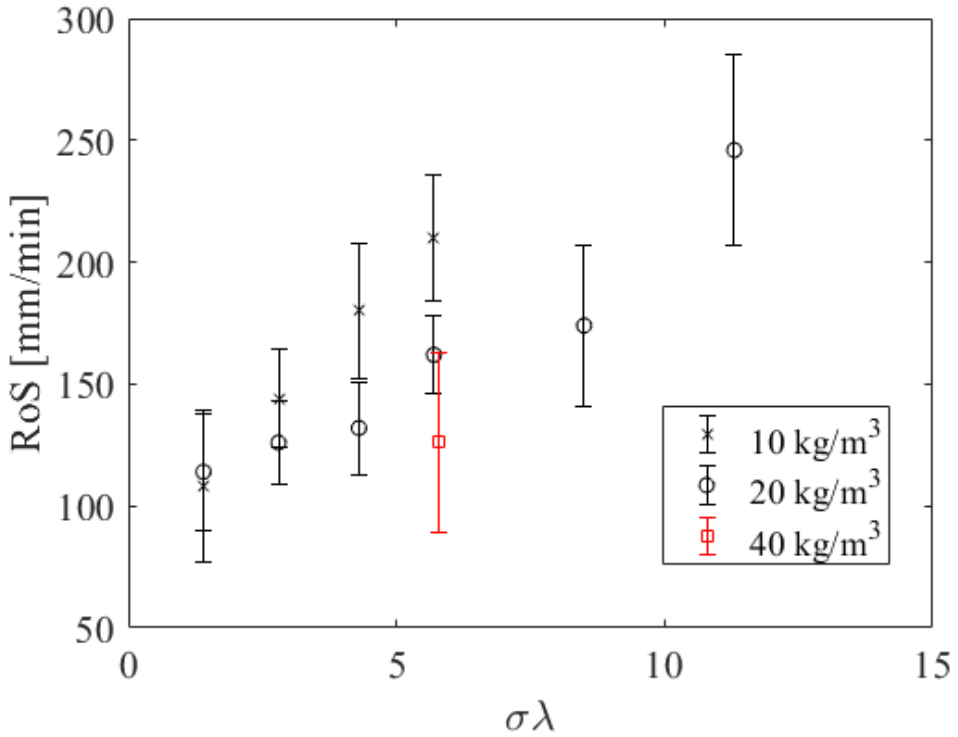


**Figure 5.10 - Correlation between $\beta\sigma\delta$ and flame spread rate in Pitch Pine fuel beds of various bulk density**

The use of $\alpha\sigma\delta$ allows fuel bed structure to be described by a single parameter, while incorporating the competing effects of bulk density and fuel loading (via fuel bed height). The correlation between $\alpha\sigma\delta$ and RoS should however be treated with caution, as its applicability has only been assessed at the limited range of fuel conditions explored in this study. The applicability of this parameter as a predictor of steady state HRR and flame height can also be assessed however a weaker correlation is observed as shown in Figure 5.11 and Figure 5.12.

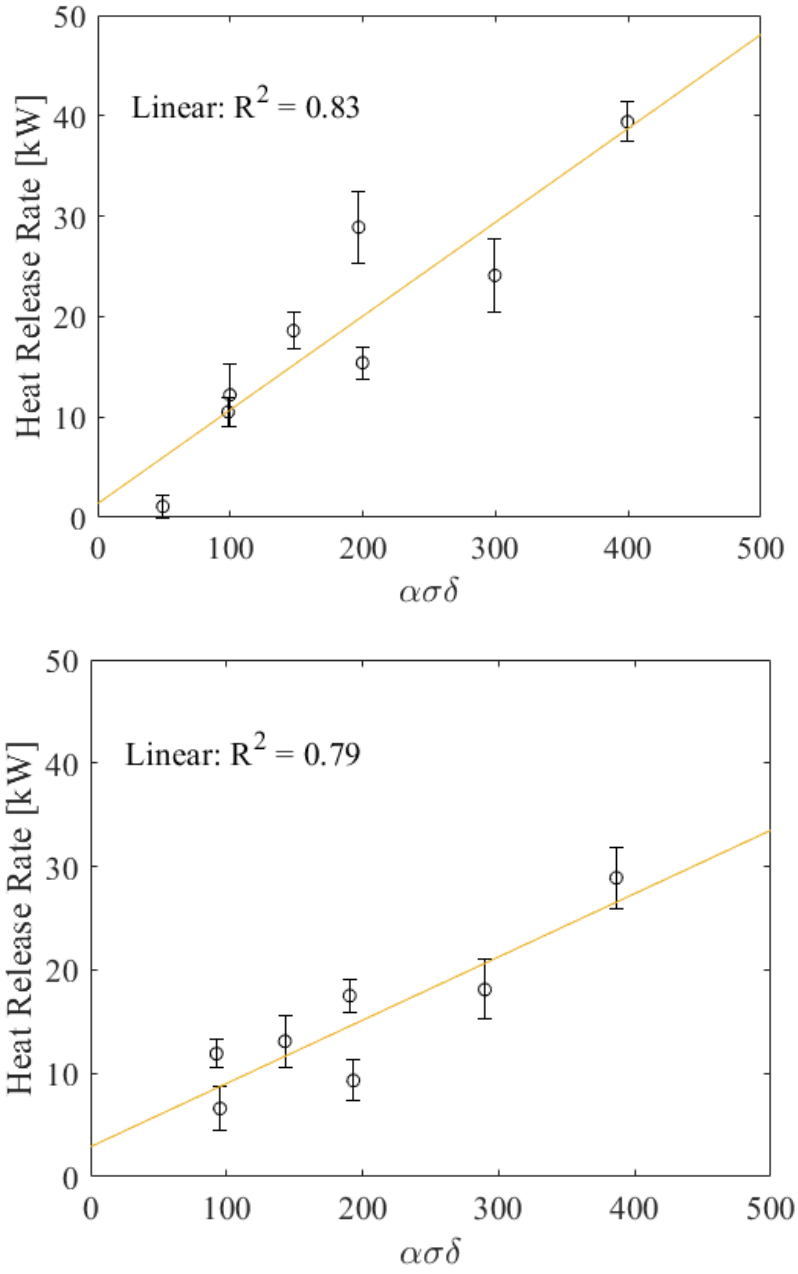


**Figure 5.11 - Correlation between ασδ and steady state Heat Release Rate (HRR) in (top) Pitch Pine $[R^2 = 0.83]$ (bottom) Pitch-Loblolly Pine $[R^2 = 0.79]$ fuel beds**

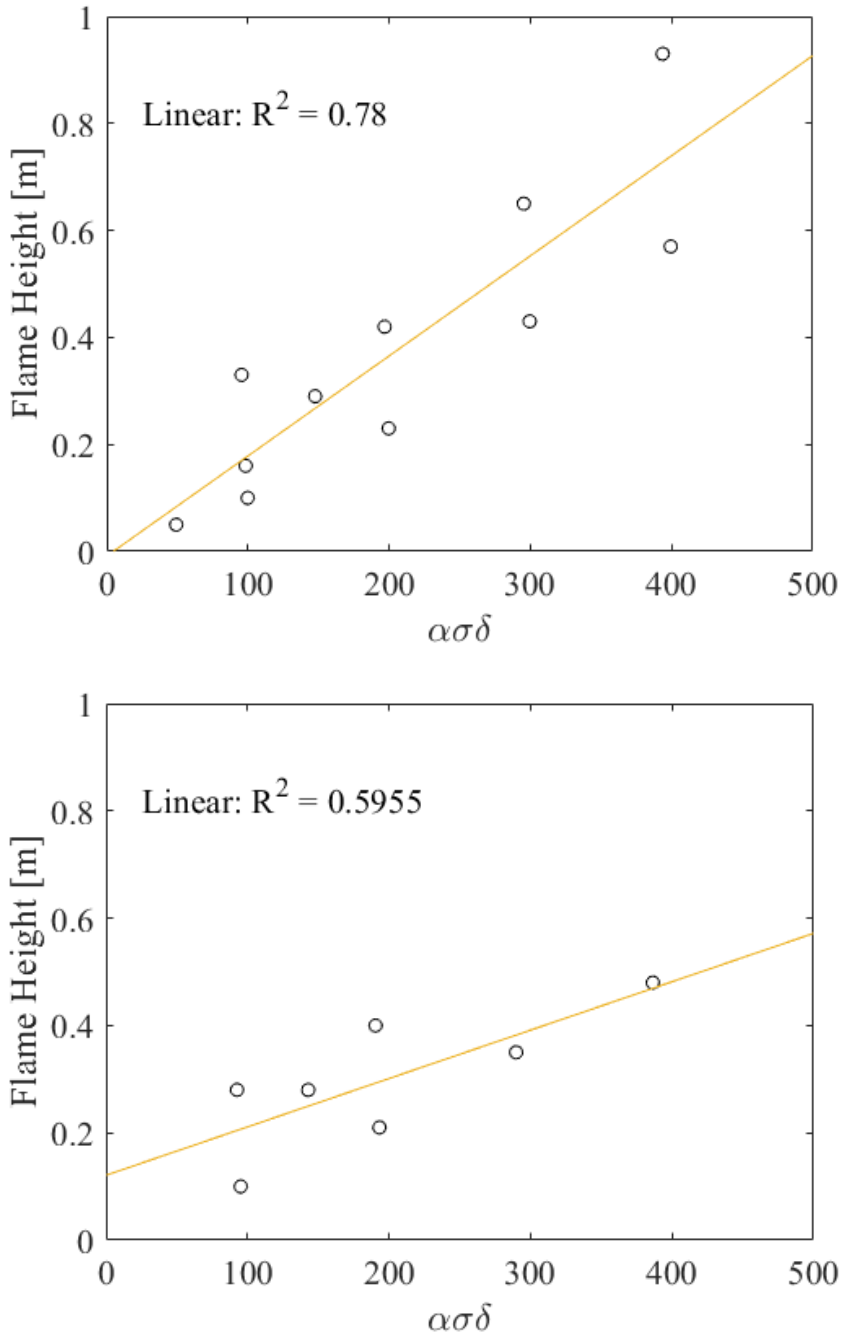


**Figure 5.12 - Correlation between αστδ and flame height in (top) Pitch Pine [$R^2 = 0.78$] (bottom) Pitch-Loblolly Pine [$R^2 = 0.60$] fuel beds**

### 5.4.3. Residence Time

For the hybrid needles, a positive linear trend ($R^2 = 0.99$ for 20 kg/m$^3$ fuel beds) was observed between fuel loading and residence time. For the Pitch Pine needles, while an initial linear trend was observed, a peak residence time was subsequently observed after which reductions in residence time occurred with further increases in fuel loading. For 10 kg/m$^3$ fuel beds, this peak residence time occurred at a fuel loading of 1.2 kg/m$^2$, and for 20 kg/m$^3$ fuel beds this occurred at a fuel loading of 0.6 kg/m$^2$.

As seen in Table 5.1 and Table 5.2, significant variations in residence time occurred as shown by the large standard deviation at several of the fuel bed conditions. This may partly be as a result of the in-bed location of the thermocouples, which leaves them exposed to both the flaming and smouldering combustion phases. The interaction between these phases is complex, with simultaneous smouldering and flaming combustion observed in some instances, along with transition (and re-transition) between phases. The interaction and relative importance of these combustion phases may also vary with fuel structure, given the previously discussed variations in combustion region characteristics at lower fuel loadings.

### 5.4.4. Buoyant Flow

To better understand the link between fuel bed structure and fire behaviour, it is necessary to investigate the physical mechanisms controlling the flame spread process. In this study, we are focused on two main phenomena, namely the flow regimes and heat transfer mechanisms. The flow regimes, both within and above the fuel bed, were explored in the present experimental series (Pitch Pine beds only), while the heat transfer mechanisms are considered further in Chapter 6.

In the quiescent (and no-slope) conditions in which these experiments were conducted, there are two main flow dynamics of interest. The buoyant plume is driven by the temperature gradient above the combustion region, which subsequently drives the entrainment flow of air towards the combustion region.

The buoyant flow profile was analysed during a 10 second window following flame front arrival at the vertical pressure probe location. Based on the minimum residence time (17 s) it was determined that this 10 second interval would allow proper measurement of the characteristic plume profile, while avoiding the inclusion of periods in which the flame front was no longer present at the pressure probe location.

During this post-flame arrival period, the maximum buoyant flow velocity increased with increasing fuel loading, as shown in Figure 5.13. As the fuel loading increased from 0.2 kg/m$^2$ to 0.8 kg/m$^2$, the maximum buoyant flow velocity increased from 1.3 m/s to 2.6 m/s. Slight variations in the maximum buoyant flow velocity at different bulk densities can also be observed in Figure 5.13, however the trend was unclear.

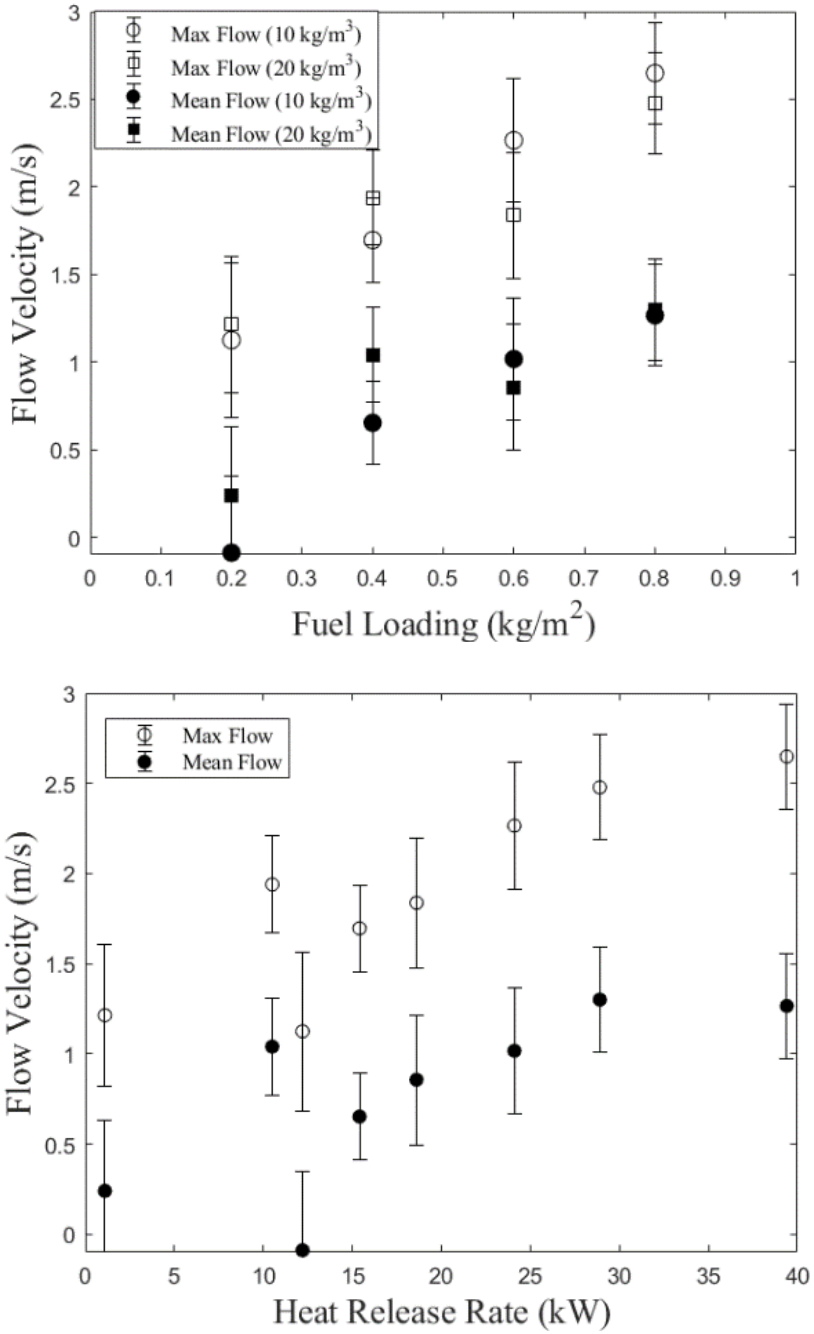


**Figure 5.13 - Comparison of (top) Fuel Loading, (bottom) Steady-State Heat Release Rate with mean and max. buoyant flow velocity at a height of 1.2 m above Pitch Pine fuel bed, in the 10 s after flame arrival**

The positive trend between fuel loading and the buoyant flow velocity (both max and mean), are in line with past observations from studies involving the use of Particle Image Velocimetry in excelsior flame spread experiments [243]. As shown in Figure 5.13, a largely positive trend between HRR and the buoyant flow velocity was also observed as expected. The HRR at the lowest fuel loadings (0.2 kg/m$^2$) should be interpreted with caution given the discontinuous nature of the flame front, since the HRR is a global measurement, while flow velocities were

measured on a point basis. As shown in Figure 5.14 the HRR generally increased with fuel loading however the effect of bulk density is also apparent.

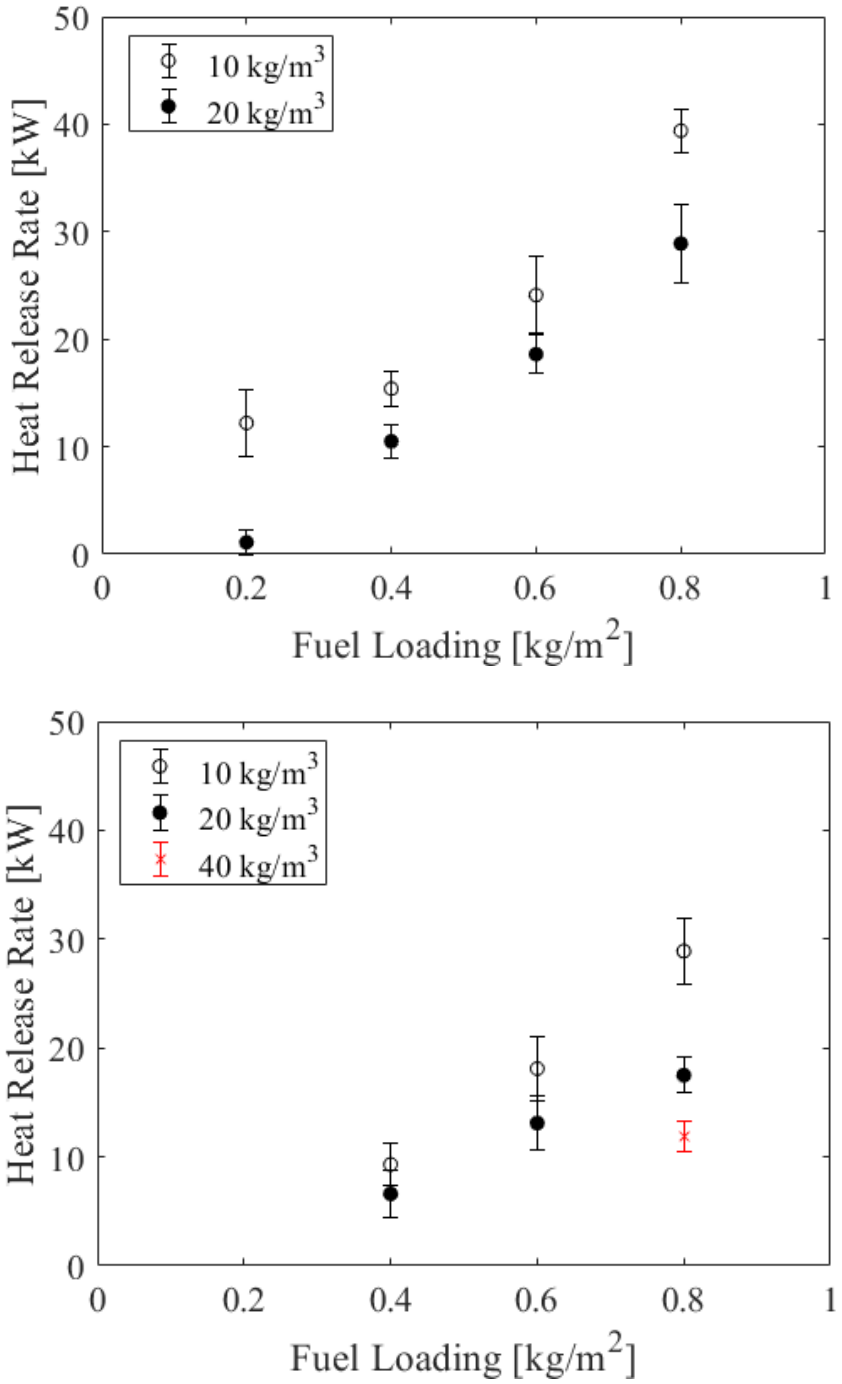


**Figure 5.14 - Comparison of Fuel Loading and Steady-State Heat Release Rate for (top) Pitch Pine fuel beds (bottom) Pitch-Loblolly hybrid Pine needle beds**

### 5.4.5. Buoyancy-Induced Flow

The buoyant flow regime promotes the lateral entrainment of air into the combustion region. This leads to a characteristic flow profile at each pressure probe in which the major flow direction is firstly towards the approaching flame front, followed by a flow reversal as air is entrained towards the departing flame front. This flow pattern is similar to those observed in

previous studies of above-bed lateral flow [204], with negative flow values indicating flow entrainment towards the approaching flame front. However, as a result of the low flow velocities of interest, significant noise is present within measured flow profiles and therefore analysis focuses on the minimum flow velocities recorded within the near-flame front region. This minimum flow velocity is therefore the peak entrainment flow (towards the approaching flame front).

From observation of the flow profiles across all tests, the onset of the measurable entrainment generally occurred at a distance of around 50 mm ahead of the flame. The magnitude of the entrainment (towards the approaching flame front) through the intact, unburned fuel was therefore calculated by investigating the flow profile over a distance of 50 mm to 10 mm between the probe and the approaching flame front, prior to flame arrival. The use of a 10 mm cut-off reduces the influence of any local flame impingement, structural heterogeneity of the fuel bed, or flow reversal ahead of the recorded flame arrival time.

Minimum and mean in-bed flow velocities were calculated for each fuel condition, and these are shown in Figure 5.15. Generally, the mean entrainment velocity increased with increasing fuel loading (and hence HRR), however the 1.2 kg/m$^2$ pitch pine fuel bed is an exception to this observed trend. Greater variations in the entrainment velocity were observed at the highest fuel loadings (1.2 kg/m$^2$ and 1.6 kg/m$^2$) as demonstrated by the larger (max-min) error bars in Figure 5.15. At these higher loadings, the peak entrainment velocity (in the opposite direction to the flame travel direction) was in some cases observed after flame arrival (and was therefore beyond the window considered in Figure 5.15).

Bulk density also appears to affect the entrainment flow profile, with variation in mean entrainment flow observed for fuel beds of equal fuel loading but varying bulk density. The increase in bulk density is, as shown in Table 5.1 and Table 5.2, accompanied by a decrease in HRR. This bulk density effect is particularly pronounced for the mean flow velocities, which may be as a result of greater averaging of the highly transient flow profile. Effects of fuel structure heterogeneity and fine scale variations in the local buoyant flow may also be greater for the measurements of minimum flow velocity.

Increases in entrainment velocity, as observed in Figure 5.15, may alter the convective heat transfer and species transport within the fuel bed. This would have implications for the convective heating and cooling of the fuel elements, particularly given the relatively thin nature of the pine needles. Additionally, the effects on oxygen supply to the combustion region requires further investigation.

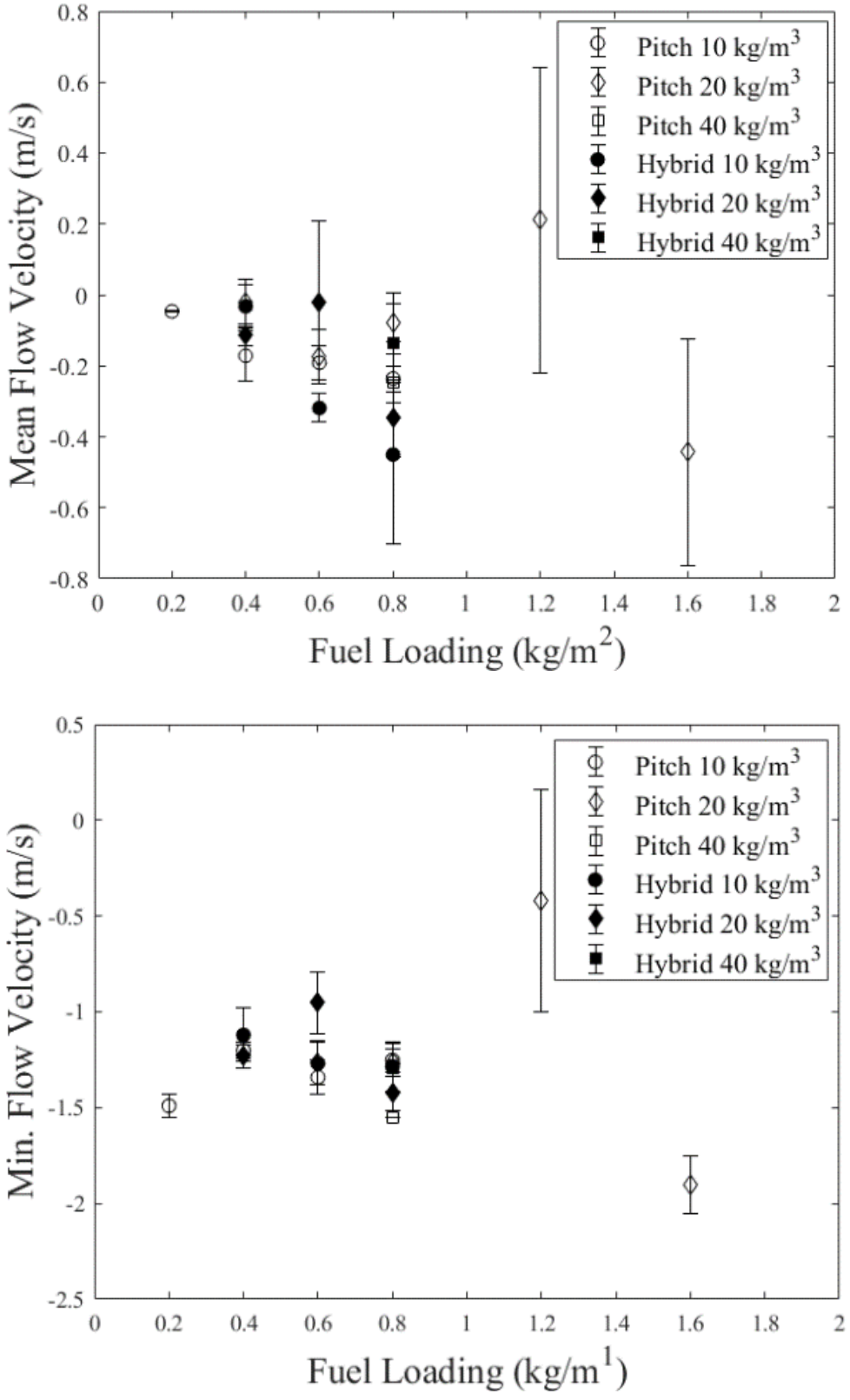


**Figure 5.15 - Mean and minimum in-bed flow velocity towards the approaching flame front (50 mm to 10 mm prior to flame arrival), in beds of different fuel loading and bulk density for beds of Pitch Pine and Pitch-Loblolly Pine hybrid respectively**

## 5.5. Conclusions

The flame spread rate (along with HRR and flame height) increased with independent increases in fuel loading or decreases in bulk density. This is consistent with many existing laboratory-based, quiescent flame spread studies in similar fuel types. However, neither of these bulk parameters alone adequately explain the variations in spread rate, and both lack explicit links to the physical processes driving flame spread. A better correlation is observed with a dimensionless fuel bed parameter $\alpha\sigma\delta$, which is more closely related to critical physical mechanisms controlling flame spread.

Independent changes in bulk density and fuel loading were observed to result in variations in the buoyant flow profile. Variations in the buoyancy-driven entrainment flow profile through the porous fuel bed were also observed as this buoyant flow profile changed. Generally, the mean entrainment velocity increased as the fuel loading (and hence HRR and buoyant flow velocity) increased. Variations in mean entrainment flow for fuel beds of different fuel loading, along with the variation between the mean and minimum entrainment velocity towards the approaching flame front, indicate the need to further quantify the role of bulk and local fuel bed structure. These findings have implications for other important physical phenomena including oxygen supply and convective heat transfer within the combustion region.

At all but the lowest fuel loadings (0.2 kg/m$^2$), the combustion region extends back beyond the trailing edge of the flame front. Within this trailing region, char oxidation/smouldering occurs within the remaining fuel load that was not consumed within the primary flame front, although charring and pyrolysis of some remaining fuel elements has occurred. The structure of the remaining fuel elements typically appears largely intact, and may therefore still exhibit a significant drag force on flow entrained into the rear of the flame front. Greater characterisation of the mass and structure of the remaining fuel region will inform further physics-based model development, particularly of fuel removal and bulk drag terms. This may help to reduce the previously identified discrepancies between predicted and observed flow velocities at the rear of the flame front which may contribute to inaccurate prediction of fire behaviour properties and flame spread extinction conditions [40].

# Chapter 6

## Heat Transfer in Porous Fuel Beds

# 6. Heat Transfer in Porous Fuel Beds

*"For any given spreading fire, different modes of heat transfer across the surface of fire inception will have different values of q associated with them. It seems logical to define the dominant spread mechanism as the one having the transfer mode that produces the largest contribution to q."*

***Forman A. Williams – Mechanisms of Fire Spread, 1977*** [92]

## 6.1. Summary

This chapter presents measurements of the heat flux and fire behaviour from a number of laboratory-based flame spread experiments involving porous fuel beds with a range of fuel bed properties. This aims to provide greater insight into the relative importance of various heat transfer mechanisms, and the effect of fuel bed structure.

The heat transfer within the fuel bed (from the in-bed combustion region) was of greater significance than the heating from the overhead flame. However, the relative importance of these two terms varied as the fuel bed structure was altered. A model based on an energy balance is presented, which incorporates the fuel bed properties and the experimentally measured heat fluxes. Spread rate predictions from this thermal model are compared to those observed experimentally.

The measurements presented here seek to address the previously identified need for more systematic measurement of heat fluxes involved in porous flame spread, as well as providing a useful dataset for future modelling efforts. To increase the utility for the modelling community, an effort has been made to describe in detail both the heat flux measurements and the fuel bed characteristics. This is supported by a detailed consideration of the measurement uncertainty associated with these measurements.

## 6.2. Introduction

In opposed-flow flame spread (in the absence of a slope), the flame is characteristically perpendicular to the fuel bed, or even slightly backwards-tilting. This generally results in lower pre-heating of unburnt fuels ahead of the flame front, and subsequently lower spread rates, than in concurrent-flow flame spread scenarios. As a result, it is particularly important to understand the effect of the fuel properties on the flame spread process, if a suitable model for the flame spread in porous wildland fuels is to be developed. In particular, this requires appropriate structural fuel descriptors, which adequately describe the thermal enthalpy required for ignition, as well as the effects of fuel bed structure on the energy transfer to the unburnt fuel.

A 'universal' flame spread equation, based upon the application of the conservation of laws to a 'surface of fire inception,' was described by Williams [92],

$$V = \frac{\dot{q}}{\rho \Delta h} \tag{6.1}$$

Where $V$ is the flame spread rate, $\dot{q}$ is the energy transfer rate across the surface of fire inception, $\rho$ is the fuel density, and $\Delta h$ is the thermal enthalpy change required for ignition.

Equation 6.1 can also be expanded to incorporate the Fuel Moisture Content (FMC) by including the heat of vaporisation of water. Similarly, energy losses can also be included, however radiative losses are generally considered negligible.

Using this framework, an important first step in the development of any flame spread theory is the determination of the dominant heat transfer mechanism across the surface of fire inception. This dominant mechanism is poorly defined for many flame spread scenarios involving porous fuels. Disagreements remain regarding the relative contribution of different energy sources e.g. relative importance of the heat transfer from the above-bed flame, compared to heat transferred through the fuel bed from the combustion region.

Determining an appropriate fuel density is also more complex for porous fuels compared to solid fuels. The complex, discontinuous structure of many porous wildland fuel beds is more difficult to characterise in bulk terms. Particularly since the pore structure will also be affected by the fuel bed packing, as well as the interaction and connectivity of fuel elements.

### 6.2.1. Porous Fuel Structure

Various approaches can be utilised to define an appropriate fuel density to describe a porous fuel bed, the simplest of which is to use the bulk density. This simple approach assumes that the fuel elements can be considered as thermally thin, and therefore that fuel elements are heated throughout their entire depth prior to flame arrival [98]. Alternatively, if the fuel elements are thermally thick, then the density term must also account for the unheated portion of the fuel elements.

This fraction of the fuel element heated prior to flame arrival was defined by Williams [92] as the product of the surface-to-volume ratio ($\sigma$) and the thickness of the heated layer. This heated layer thickness was estimated as the product of $\sqrt{\alpha}/V$ and the square root of the fuel bed heated depth ahead of the surface of fire inception. This fuel bed heated depth is dependent upon the heat transfer mechanism being considered, with a value similar to the optical depth $(1/\beta\sigma)$ proposed for radiative transfer through a porous fuel bed [97,98]. A simple flame spread equation for thermally thick fuels can thus be derived by applying this heating assumption to the universal flame spread equation,

$$V = \frac{\epsilon^2 \sigma_{SB}^2 (T_s^4 - T_i^4)^2}{\beta\sigma\alpha_{diff}\rho_s^2(\Delta h)^2} \tag{6.2}$$

This equation does not incorporate radiation from the flame above the fuel bed, or the effects of convective cooling/heating. To understand whether this model is applicable to the porous flame spread scenarios considered in this chapter, the relative importance of the different heat transfer phenomena must first be investigated.

### 6.2.2. Heat Transfer in Porous Fuel Beds

Heat transfer within porous fuel beds can occur via several different mechanisms including conduction (through fuel elements), convection (via gas flow through pores) and radiation (between fuel elements across pores). While a number of possible energy sources may also be present, with both smouldering and flaming combustion occurring.

Several previous laboratory-based flame spread studies have considered the heat transfer mechanisms involved in porous flame spread by measuring the heat flux. These studies vary widely in both the type of heat flux sensor deployed and in the deployment location of the sensor, as shown in Figure 6.1.

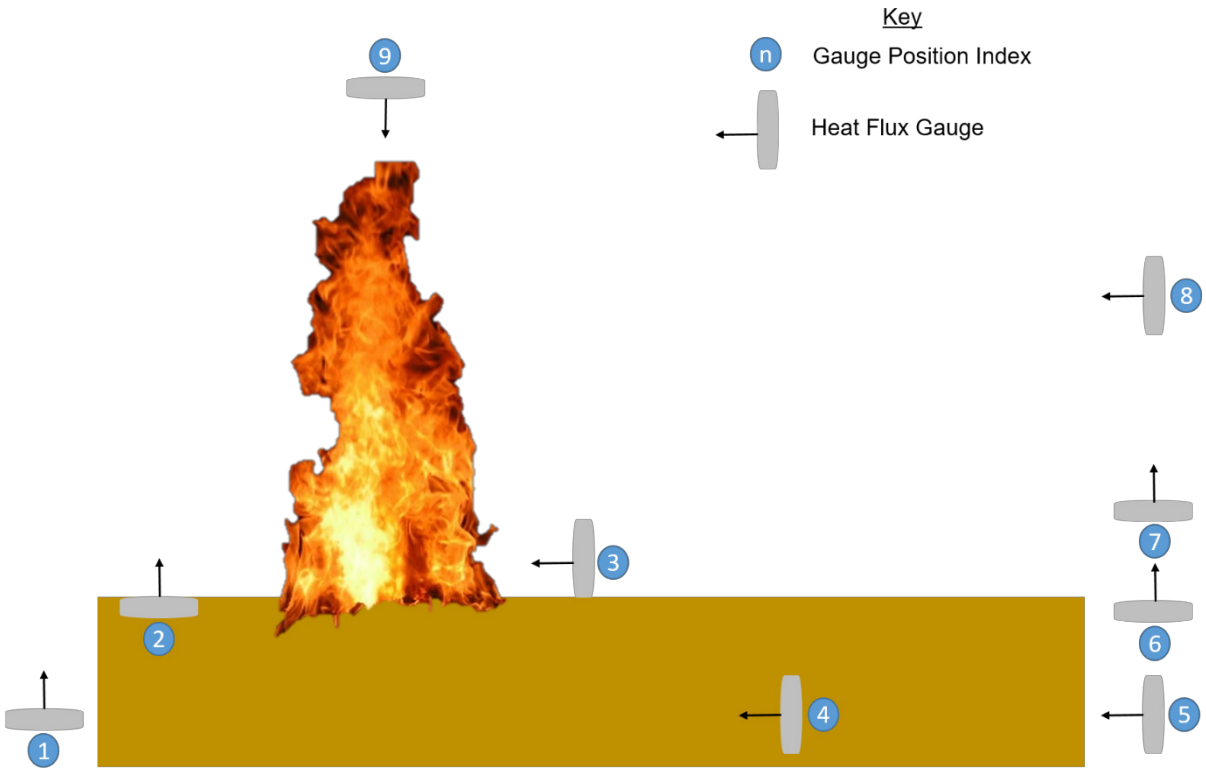


| ` | Fuel Type | Radiant Flux | Total Flux |
|---|---|---|---|
| Broido & McCarter, 1964 [115] | Wood Crib | 8 9 | |
| Thomas *et al.*, 1965 [314] | Wood Crib | 5 | 5 |
| Anderson & Rothermel, 1966 [125] | Pine Needle Bed | 8 9 | |
| Anderson 1969 [133] | Pine Needle Bed | 4 2 | |
| Konev & Sukhinin, 1977 [315] | Pine Needle Bed | 2 | |
| Ray *et al.*, 1980 [316] | PMMA | 2 | |
| Vaz *et al.*, 2004 [317] | Pine Needle Bed | 6 | |
| Morandini *et al.*, 2005 [318] | Pine Needle Bed | 6 | 6 |
| Frankman *et al.*, 2010 [71] | Excelsior on Steel Rods | 4 | 4 |
| Silvani *et al.*, 2012 [207] | Excelsior | 3 | 3 |
| Morandini *et al.*, 2013 [226] | Pine Needle Bed | 8 5 | 8 |
| Tihay *et al.*, 2014 [228] | Pine Needle Bed | 8 | 8 |
| Liu *et al.*, 2015 [129] | Pine Needle Bed | 6 | 6 |
| Jiang *et al.*, 2017 [319] | PMMA | 2 | |
| Morandini *et al.*, 2018 [67] | Excelsior | 8 | 8 |
| Silvani *et al.*, 2018 [243] | Excelsior | 7 | 7 |
| Bu *et al.*, 2021 [320] | Wooden Rods | 1 | 1 |

**Figure 6.1 - Summary of heat flux measurement approaches in previous laboratory-based flame spread studies**

The positioning of the sensor dictates which heat transfer mechanisms will be studied, both in terms of the heat sources within the sensor viewing angle, and the resulting view factor between a heat source and recipient sensor. The sensor type will determine whether the total, radiant or convective flux is measured.

The range of measurement approaches utilised in these past studies does however complicate efforts to draw comparisons between past studies, or to draw unified conclusions from this existing work. This issue has also been highlighted by past authors [71]. There also appears to have been little past attempt to systematically study the effect of the structure of natural fuel beds on the resulting heat fluxes in order to inform our understanding of the heat transfer mechanisms controlling the flame spread process.

One important heat transfer consideration, particularly in porous fuel beds, is the relative importance of the heat transfer from the flame compared to that from the in-bed combustion region. This is of particular importance in the derivation of theoretical models based on an energy balance approach, in which the significant forms of energy transfer must be included. Despite this, the effect of fuel bed structure on the dominant heat transfer mechanisms remains poorly characterised.

From largely qualitative observations, early studies suggested that the above-bed flame may be of secondary importance in porous fuels [125,197], with in-bed heat transfer mechanisms dominating. By shielding the fuel bed from the flame, Rothermel and Anderson observed sustained flame spread when the heat transfer from flame to unburnt fuel was blocked, however a 39 % reduction in spread rate occurred [125]. Past studies involving wood cribs suggested, that in this fuel type, as much as half of the radiative energy may be released from the embers in the in-bed combustion region [197,321].

Understanding the heat transfer within porous fuel beds is both of increased importance and greater difficulty in porous fuels (compared to solid fuels), given the complex, discontinuous fuel structure. As a result, the potential for conduction (through and between fuel elements), convection (by the flow of gas through pores) and radiation (between fuel elements across pores) must all be considered. Whereas classical flame spread theories for solid surface flame spread theory often consider all heat transfer within the fuel to occur via conduction, which greatly simplifies the analysis [53].

Characterising the heat transfer within the fuel bed requires knowledge of the properties of the heat source and adequate characterisation of the heat transfer paths through the fuel bed. Some past studies have suggested sub-models to describe the transfer of heat from the combustion region, particularly concerning radiative transfer from this region, where an attenuation term for the fuel bed can be incorporated. Yet there remains a lack of suitable physical measurements to allow the testing and validation of these models, or to properly explore the potential effects of fuel bed structure, which the model should incorporate.

For example, the classical formulation for fuel bed attenuation incorporates the surface-to-volume ratio of fuel elements ($\sigma$) and the packing ratio of the fuel bed ($\beta$), to determine an extinction coefficient $k_b$. However, this formulation assumes that the fuel bed is isotropic, despite the tendency of fuel elements to assume a preferential orientation within many natural fuel beds. As a result, previous bench-scale studies have suggested that this formulation may inadequately describe the relationship between fuel bed structure and the attenuation properties [139]. This suggests that for greater accuracy, alternative terms may be required to describe the

attenuation or radiation through the fuel bed in a vertical and horizontal orientation respectively.

In the experiments described in this chapter, both radiant and total heat fluxes were measured across a range of fuel bed structural conditions. Measurements of radiant heat flux provide insight into the pre-heating phase, while the total heat flux (while partly a function of the total flux gauge properties) provide insight into general heating and cooling trends. By using multiple sensor configurations, the relative importance of the above-bed and in-bed energy sources are determined across the different fuel bed conditions.

### 6.2.3. Thermal Flame Spread Models

One of the earliest theoretical models for opposed-flow flame spread was derived by De Ris [21], and described opposed-flow flame spread across the surface of a solid. De Ris considered a case involving a stationary, laminar diffusion flame, and provided solutions for both thin and semi-infinite solids. Conceptually, De Ris considered flame spread as a process in which a flame (of temperature $T_f$) heats the unburnt fuel ahead (initially at temperature $T_i$) to an ignition temperature $(T_{ig})$, thereby releasing the energy required to sustain flame spread. The heat transfer (from the flame to the fuel) can occur via conduction (gas or solid phase) or radiation however, for the thermally thin case only gas phase conduction is included.

Only gas phase combustion is considered, and the Shvab-Zeldovich diffusion flame theory [322] is applied by assuming infinite reaction rates (thereby removing several highly nonlinear kinetic terms: $\dot{m}_i'''$,$\dot{q}'''_{chem}$, $\dot{q}_{rad}$). The model solutions are therefore limited to cases in which the chemical reaction time is significantly less than the flow time of reactants. These limits of applicability, to higher Damköhler number scenarios, have subsequently been confirmed experimentally [91,316].

Several other assumptions are included within the De Ris model. The effects of both flame quenching (at the cold fuel wall) and the effects of gravity are neglected. However, the buoyancy-induced flow can be considered by adjusting the overall fluid stream velocity. The flow profile is assumed to be uniform throughout, with constant fluid properties ($k$ and $\rho u$). While in all of the conservation equations, a constant, horizontal convective mass flow is assumed.

By further assuming that vertical mass transfer occurs only via diffusion, that vaporisation does not occur ahead of the flame front, and assuming a Lewis number of unity, the following equation is derived for thermally thin fuels,

$$V = \frac{\sqrt{2k_g(T_f - T_{ig})}}{\rho c_p d(T_{ig} - T_s)} \tag{6.3}$$

And for semi-infinite fuels,

$$V = \frac{(k\rho c_p)_g u_\infty (T_f - T_{ig})^2}{(k\rho c_p)(T_{ig} - T_s)^2} \tag{6.4}$$

Where $u_\infty$ is the air velocity, $d$ is the fuel thickness, and the fuel and gas properties are described by the density ($\rho$), thermal conductivity ($k$), and specific heat capacity ($c_p$).

These solutions assume uniform properties in either the gas or solid phases. The appropriateness of such an assumption for porous fuels is however unclear, and once again raises questions regarding the appropriate definition of a characteristic density for such porous fuels. An additional complication in attempting to apply these solutions to a porous fuel, is the assumption that only conductive heat transfer occurs within the solid phase. In porous fuel beds, the presence of pores means that radiative and convective heat transfer mechanisms may be significant, while thermal conductivity may be significantly lower [92].

The complex interplay of combustion phases in porous fuel beds also complicates efforts to apply this model. In their current form, these solutions assume that combustion occurs entirely in the gas phase, and the effects of smouldering within the fuel bed are not included. Instead, it is assumed that, downstream of the flame front, fuel elements reach the vaporisation temperature and begin to vaporise at a constant rate without any further temperature rise occurring. This simplified approach avoids the need to consider the complex processes of melting or a detailed description of pyrolysis. The applicability to porous fuel beds such as pine needle beds, in which significant smouldering regions are observed behind the flame front, is therefore unclear.

Understanding the limits of applicability of existing flame spread models for solid fuels when applied to porous fuel beds is of general importance. Numerous such models have previously been proposed, and these are discussed in Chapter 2, and have been reviewed in detail by other past authors [22,323]. However, many of these models similarly consider conduction to be the only or primary heat transfer mechanism within the fuel.

In this chapter, a series of experiments are presented which provide a greater physical insight into the heat transfer mechanisms within porous fuel beds. By measuring the heat fluxes at various locations, the relative importance of heat transfer from the overhead flame can be compared to that of heat transfer from the in-bed combustion region. The effect of fuel bed structure on the underlying heat transfer is also assessed by deliberately manipulating the fuel bed structure to study fuel beds with a range of fuel loading, bulk density and hence $\alpha\sigma\delta$. These heat flux measurements are then directly used in order to assess the applicability of a thermal model (based upon the model of De Ris, and later work by Quintiere [53]) to porous fuel beds with various structural properties.

## 6.3. Methods

### 6.3.1. Instrumentation

The experiments described in this chapter were performed on the flame spread table, described in detail in Chapter 3. Two separate experimental series were conducted, each with a different instrumentation configuration (horizontal or vertical heat flux gauges respectively), as summarised in Figure 6.2. These two alternative set-ups enabled a detailed investigation of the different heat transfer mechanisms (both from the above-bed flame and from the in-bed combustion region) for fuel beds of various structure.

Each experiment involved either four vertically oriented heat flux gauges (two pairs of radiant and total gauges) or two horizontal gauges (a single pair of radiant and total gauges oriented parallel to the table surface), along with measurement of gas phase temperatures both within and above the fuel bed.

For the first experimental series (involving vertical gauges), one pair of gauges were positioned such that the sensor face was flush to the table surface, with the other pair positioned flush to the fuel bed surface. All four of these gauges were situated close to the fuel bed centreline and at a horizontal distance of 1.3 m from the ignition line.

In the second experimental series (involving horizontal gauges), the single pair of gauges were situated within the fuel bed, facing the approaching combustion front. The gauges were located at a horizontal distance of 0.9 m from the ignition line, with the midpoint of the gauge sensor positioned at a height of 12.7 mm above the table surface. The sensor element was therefore situated fully within the fuel layer at all but the lowest fuel height case (0.01 m for a fuel bed of 0.2 kg/m$^2$ fuel loading and 20 kg/m$^3$ bulk density).

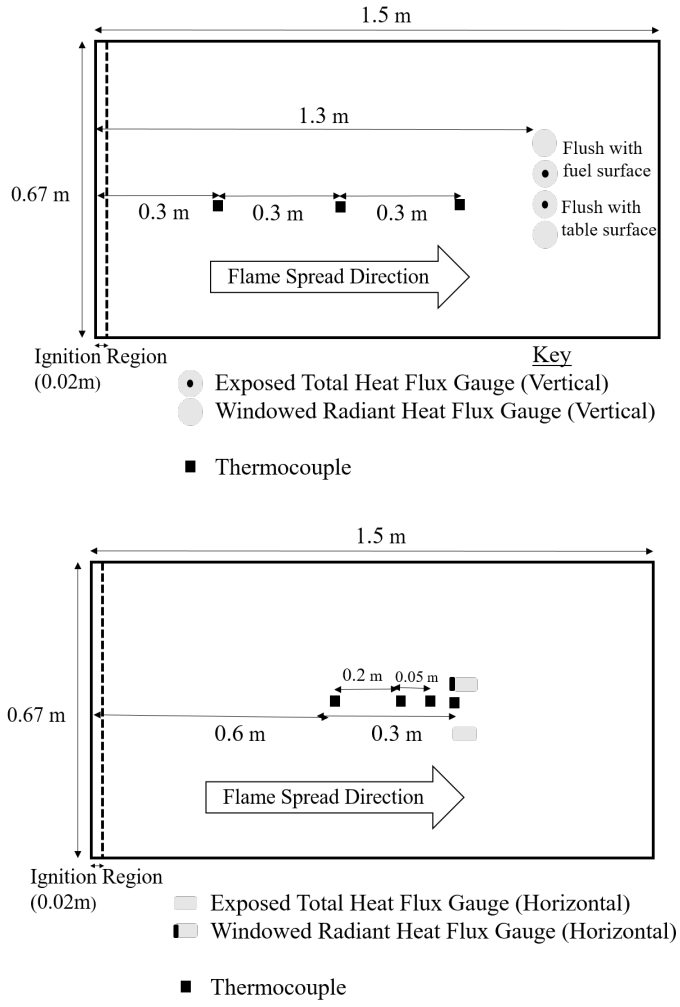


**Figure 6.2 - Schematic of table instrumentation for heat transfer experiments involving two different experimental series with (top) Vertically-oriented heat flux gauges and (bottom) horizontally-oriented heat flux gauges**

#### 6.3.1.1. Heat Flux

The heat flux was measured by the water-cooled gauges at a minimum rate of 5 Hz (24 out of 27 experiments conducted at 10 Hz). During the flame spread experiments, higher frequency heat flux fluctuations may occur, however the focus here is on the overall contributions of different heat transfer terms, rather than any intermittent heating effects. Particularly as the

measurement of these intermittent heating effects would in any case be limited by the response time of the gauges.

Radiant fluxes were measured by adding a sapphire window to these gauges (spectral transmission range of 0.2 – 5.5 μm). For both radiant and total gauges, a maximum random error of ± 0.12 kW/m$^2$ was observed during the background period prior to ignition. Full specifications for both the gauges and the sapphire windows are given in Chapter 3.

The measured heat fluxes also incorporate the effect of the view factor between each gauge and the radiator (flame and/or combustion region, depending on gauge location). Assuming that the radiator is well-approximated by a rectangle [324], the view factor can be estimated for both a parallel and perpendicular discrete element receiver (representing each of the heat flux orientations).

Figure 6.3 shows the calculated view factor for each orientation, as a function of the distance between the radiator and the gauge. The peak view factor is significantly lower for the case involving a perpendicularly aligned gauge, however at the arrival time, the parallel case may be more appropriate for both gauge configurations, given the presence of the flame or combustion region directly in front of the gauge surface.

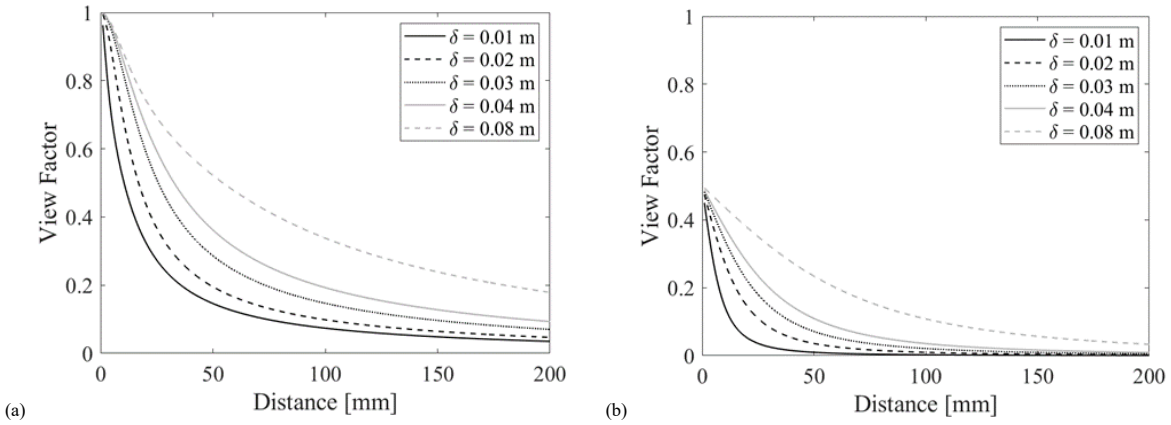


**Figure 6.3 - Estimated view factor between radiator and (a) parallel gauge (b) perpendicular gauge, for fuel beds of various height**

#### 6.3.1.2. Gas Phase Temperature

The location of gas-phase thermocouples also varied between the two experimental series. For the vertically oriented gauges, thermocouples were positioned within the fuel bed, at a height of 10 mm above the table surface, and at horizontal distances of 0.3 m, 0.6 m, and 0.9 m from the ignition line. Where the horizontal gauges were used, the thermocouples were located above the fuel bed (10 mm above the fuel bed surface) and at horizontal distances of 0.6 m, 0.8 m, 0.85 m and 0.9 m from the ignition line.

In both cases, the thermocouples were 0.25 mm diameter K-Type thermocouples, measuring at a minimum frequency of 5 Hz (21 out of 27 experiments at 10 Hz). The random error was estimated during a 30 second period prior to ignition, while potential radiation errors were also considered, as described in Chapter 3.

#### 6.3.1.3. Additional Measurements

The overall fire behaviour and flame spread were also characterised by recording each experiment, allowing video analysis of the flame height and spread rate. The spread rate was determined by linear regression analysis of the flame front position over time. The flame height was defined as the peak of the continuous flame region [254]. These analysis methods are described in detail in Chapter 3.

The heat release rate was measured using Oxygen Consumption Calorimetry (OCC) [270], and a load cell measured the continuous mass loss, from which the burning rate was calculated. Further details for this additional instrumentation are provided in Chapter 3, along with a comprehensive discussion of the analysis methods used. Each experiment was ignited using the line ignition source (10 ml acetone) described in Chapter 3.

### 6.3.2. Fuel Beds

Fuel beds were composed of *Pinus rigida* (Pitch Pine) needles, with the collection procedures and fuel properties described in detail in Chapter 3. These dead needles were stored indoors but were otherwise unconditioned prior to use, resulting in an average Fuel Moisture Content (FMC) of 13.2 % ± 4.6 % (Std. Dev. for N = 78) across all experiments. The FMC was determined on a dry basis by oven-drying samples from each fuel bed prior to each experiment as described in Chapter 3.

The fuel bed structure was deliberately varied across experiments, by altering the bulk density (10 kg/m$^3$, 20 kg/m$^3$, 40 kg/m$^3$) or the fuel loading (0.2 kg/m$^2$ to 1.6 kg/m$^2$), and the fuel bed height (10 mm to 80 mm). Controlling the fuel bed height allows the fuel loading to be altered for a constant bulk density, while similarly the bulk density can be varied by controlling the fuel loading (and allowing the fuel height to vary).

The fuel beds are also described by a single dimensionless parameter $\alpha\sigma\delta$ (introduced in Chapter 5), which incorporates the fuel bed porosity ($\alpha$), fuel element surface-to-volume ratio ($\sigma$), and fuel bed height ($\delta$). The studied fuel bed conditions are summarised in Table 6.1, with the needles having an average surface-to-volume ratio of 5063 ± 640 m$^{-1}$ (Std. Dev. for N = 10). By altering the fuel loading and/or bulk density, the $\alpha\sigma\delta$ value of the fuel bed was also deliberately manipulated as seen in Table 6.1.

**Table 6.1 - Summary of fuel bed conditions for heat transfer experiments**

| **Fuel Loading** [kg/m$^2$] | **Bulk Density** [kg/m$^3$] | $\boldsymbol{\alpha}$ | $\boldsymbol{\delta}$ [m] | $\boldsymbol{\alpha\sigma\delta}$ |
|---|---|---|---|---|
| 0.2 | 20 | 0.996 | 0.01 | 49 |
| 0.4 | 10 | 0.998 | 0.04 | 200 |
| 0.4 | 20 | 0.996 | 0.02 | 98 |
| 0.6 | 20 | 0.996 | 0.03 | 148 |
| 0.8 | 10 | 0.998 | 0.08 | 399 |
| 0.8 | 20 | 0.996 | 0.04 | 197 |
| 0.8 | 40 | 0.992 | 0.02 | 96 |
| 1.2 | 20 | 0.996 | 0.06 | 295 |
| 1.6 | 20 | 0.996 | 0.08 | 394 |

## 6.4. Results and Discussion

### 6.4.1. Overall Fire Behaviour

Key fire behaviour parameters are summarised in Table 6.2 for each fuel bed condition. As in Chapter 5, the Rate of Spread (RoS) varied significantly across the different fuel bed conditions, displaying a positive correlation with fuel loading and a negative correlation with bulk density. Both trends match the observations of several previous authors who have observed positive trends between RoS and fuel loading [81,226] and porosity [63,101,125], and a negative trend with bulk density [63].

However, Fang and Steward [63] observed no independent effect from fuel loading on spread rates through excelsior fuel beds of relatively high fuel loading (min. 0.75 kg/m$^2$). This was attributed to the negligible radiative heating contribution of the above-bed flame, and the combustion region being of sufficient thickness as to be suitably approximated as a black body.

In general, a positive relationship was observed between $\alpha\sigma\delta$ and the flame spread rate. The exception to the positive trend between $\alpha\sigma\delta$ and spread rate involves the fuel bed of $\alpha\sigma\delta = 96$, however experiments at this condition were subject to the greatest experimental uncertainty. This is shown in the maximum error values given in Table 6.2. These trends can also be observed in Figure 6.4, where the flame front position is plotted, relative to the time from ignition, for each fuel bed condition, and in Figure 6.5 where the spread rate is plotted against $\alpha\sigma\delta$ for each fuel bed condition.

**Table 6.2 - Summary of overall fire behaviour at each fuel bed condition**

| **Fuel Loading** [kg/m$^2$] | **Bulk Density** [kg/m$^3$] | $\alpha$ | $\delta$ [mm] | $\alpha\sigma\delta$ | **N** | **Flame Spread Rate** [mm/min ± Max/Min] | **Flame Height** [m ± 0.05 m] | **Peak HRR** [kW ± Max/Min] | **Burning Rate** [g/s ± Max/Min] |
|---|---|---|---|---|---|---|---|---|---|
| 0.2 | 20 | 0.996 | 10.0 | 49 | 2 | 82 ± 17 | 0.05 | 4.5 ± 2.4 | N/A |
| 0.4 | 10 | 0.998 | 40.0 | 200 | 2 | 168 ± 16 | 0.23 | 24.5 ± 5.0 | N/A |
| 0.4 | 20 | 0.996 | 20.0 | 98 | 4 | 114 ± 24 | 0.13 | 15.6 ± 1.7 | 0.38 ± 0.10 |
| 0.6 | 20 | 0.996 | 30.0 | 148 | 2 | 139 ± 20 | 0.29 | 19.5 ± 5.0 | N/A |
| 0.8 | 10 | 0.998 | 80.0 | 399 | 4 | 195 ± 37 | 0.55 | 38.3 ± 1.0 | 1.35 ± 0.03 |
| 0.8 | 20 | 0.996 | 40.0 | 197 | 5 | 149 ± 30 | 0.36 | 31.7 ± 1.8 | 0.99 ± 0.05 |
| 0.8 | 40 | 0.992 | 20.0 | 96 | 4 | 122 ± 47 | 0.34 | 20.7 ± 1.0 | 0.67 ± 0.01 |
| 1.2 | 20 | 0.996 | 60.0 | 295 | 1 | 200 ± 20 | 0.65 | 69.2 ± 6.9 | N/A |
| 1.6 | 20 | 0.996 | 80.0 | 394 | 3 | 232 ± 41 | 0.81 | 120.3 ± 12.3 | 2.43 ± 0.14 |

As in Chapter 5, the onset of steady-state flame spread was observed after the progression of the flame front beyond a short ignition-affected region. This steady-state flame spread behaviour can be observed in Figure 6.4, where linear regression indicates highly linear flame front progression.

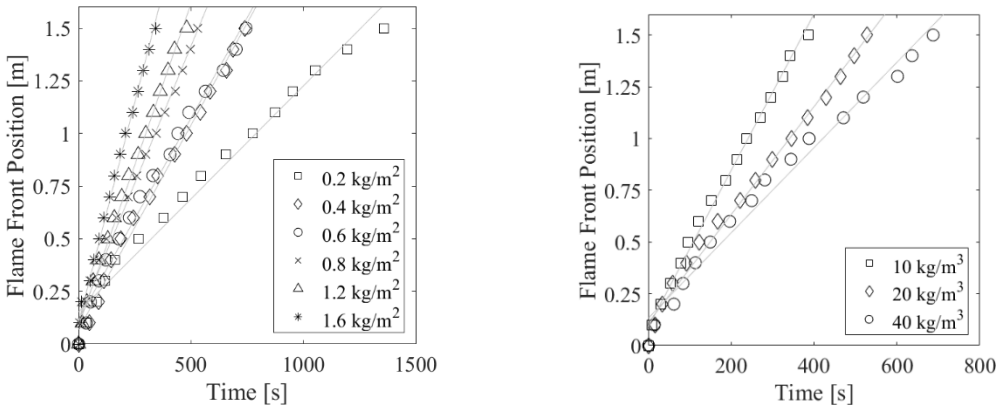


**Figure 6.4 - Flame front position over time for (left) 20 kg/m$^3$ fuel beds of different fuel loading, and (right) 0.8 kg/m$^2$ fuel beds of different bulk density**

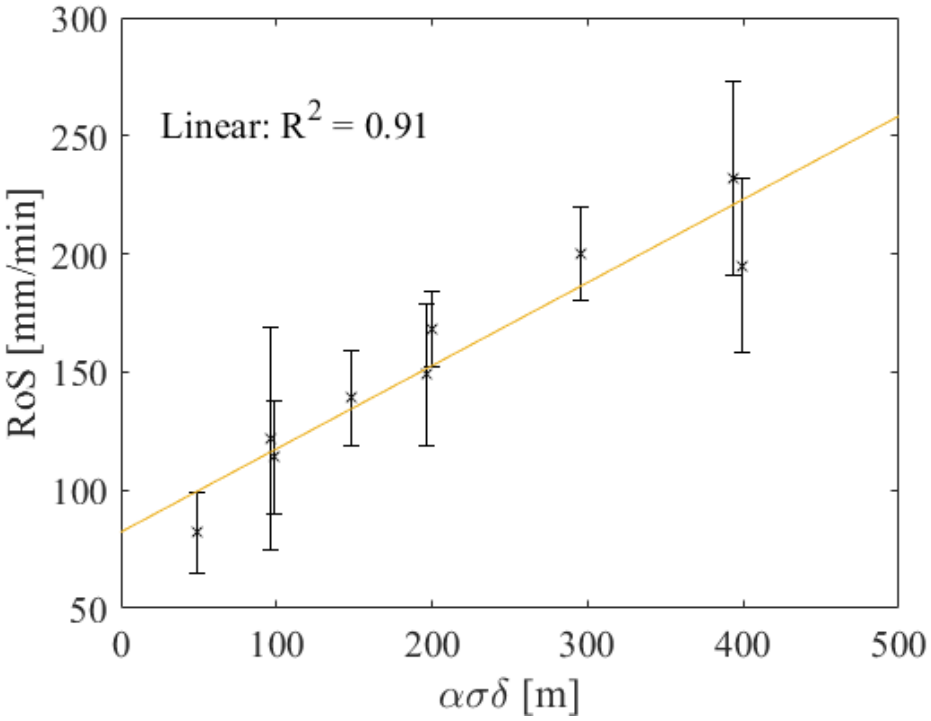


**Figure 6.5 – Experimentally observed Rate of Spread for fuel beds of various $\alpha\sigma\delta$ values**

Steady-state combustion behaviour was also indicated by the measured burning rates, with extended periods of constant mass loss rate observed (as is characteristic of steady-state behaviour [325]). This is shown in Figure 6.6, for the horizontal gauge series, where the normalised mass loss is plotted for a range of fuel bed conditions. The normalised mass loss was calculated by applying a 5-s moving average to the raw mass measurements, with outliers (greater than three scaled median absolute deviations from the median) filtered from the pre-ignition data, to remove any background noise. The average burning rate at each fuel bed condition is also given in Table 6.2.

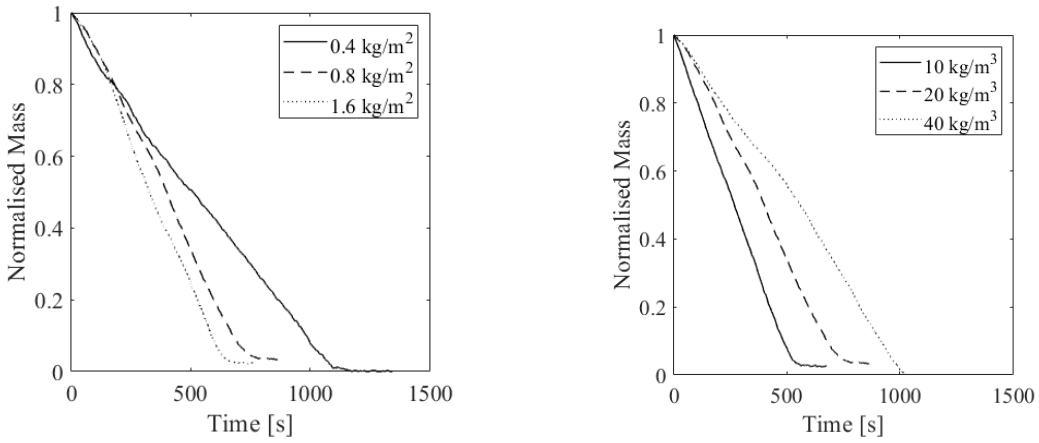


**Figure 6.6 - Characteristic normalised mass loss for (left) 20 kg/m$^3$ fuel beds of different fuel loading (right) 0.8 kg/m$^2$ fuel beds of different bulk density [5s Moving Average]**

In most cases, steady state flame spread via a single, linear flame front was observed, however the lowest $\alpha\sigma\delta$ case ($\alpha\sigma\delta = 49$) represents an exception, with unsteady flame spread behaviour observed at this condition. As in Chapter 5, at this lowest fuel loading (0.2 kg/m$^2$), a highly discontinuous flame front was visible throughout, as shown in Figure 6.8. At this lowest fuel loading, it is likely that, given the fuel sparsity, interaction between individual fuel elements or clusters begins to dominate the flame spread process.

Another notable visual feature for this lowest fuel loading condition was the absence of a smouldering region behind the flame. As shown in Figure 6.8, this region was observed for all other fuel conditions and its absence here may suggest the existence of a limiting condition for smouldering onset. Past authors have shown the existence of a critical dimension for sustained smouldering propagation in other fuel types [326].

For all other fuel bed conditions, the continuous flame front width equalled the fuel bed width (0.67 m) and as such, flame shape was a function only of flame height. In these experiments, flame height was generally positively correlated with the RoS ($R^2 = 0.86$) as shown in Figure 6.7, however, as shown in Table 6.2, exceptions to this trend were observed. This relationship between flame height and RoS is similar to that observed by Anderson (in pine needle beds involving different species), who highlighted the need to consider both the flame width and fuel structure, if the radiant heating of the fuel by the resulting flame structure is to be fully understood [327].

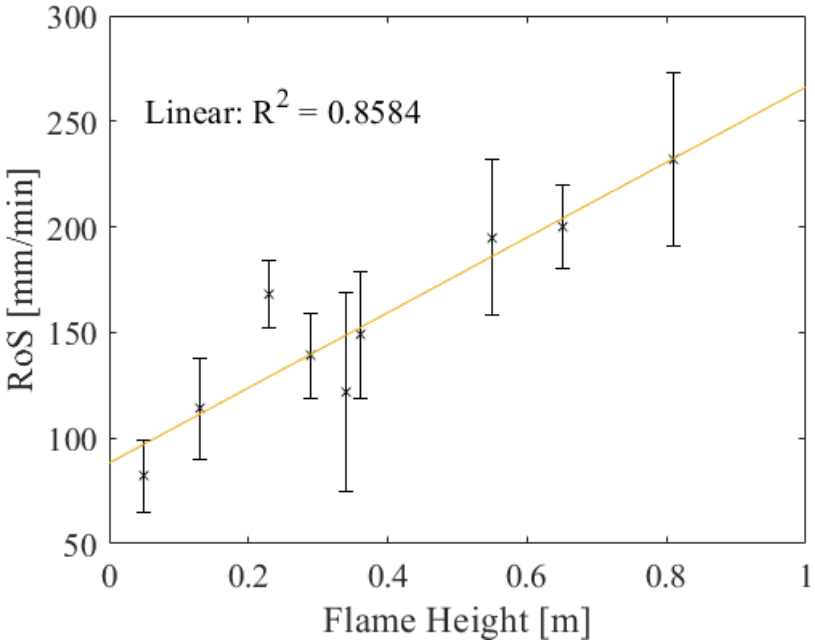


**Figure 6.7 – Comparison of Rate of Spread (RoS) with flame height for all fuel bed conditions**

For all fuel conditions, simple visual observations suggested that the flame thickness was significantly less than the critical flame thickness of 3.2 m suggested by Agueda *et al.* [328] as the threshold above which flame emissivity closely approximates that of a blackbody. Therefore, given previously observed correlations between flame thickness and emissivity, the actual flame emissivity in this study is likely significantly lower than that of a black body [328].

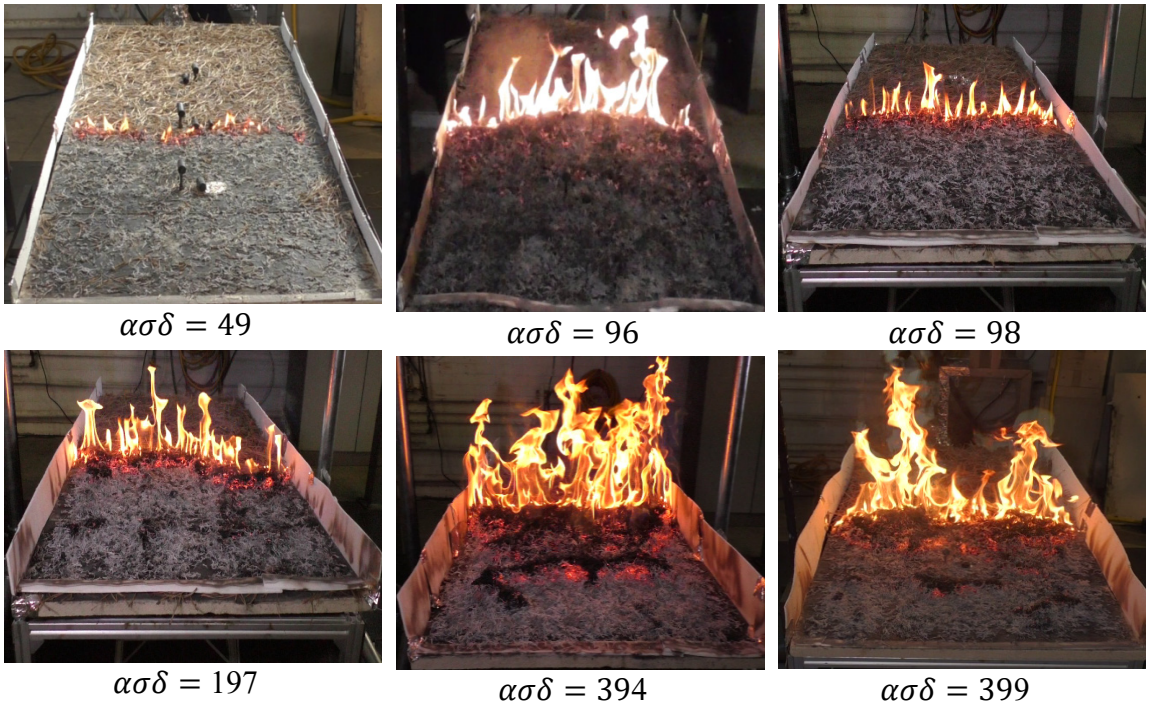


**Figure 6.8 – Representative snapshots of typical flame spread behaviour at various fuel bed conditions**

### 6.4.2. Heat Transfer

Based upon the heat flux measurements from both experimental series, it is possible to investigate the heat transfer from both the above-bed flame and the in-bed combustion region, across a wide range of fuel bed structural conditions ($\alpha\sigma\delta = 49$ to $\alpha\sigma\delta = 399$). As the fuel bed structure was altered, variations in both the heat flux magnitude and heating onset distance were observed at each of the gauge locations.

In general, greater peak (radiant and total) heat fluxes were observed for higher fuel loadings, at all gauge locations. The actual heat flux magnitude varied significantly between the different gauge locations, however a similar typical heating profile was observed across all locations. This characteristic heating profile (shown in Figure 6.9 for a range of fuel conditions) consisted of an initial period of steady heat flux growth while the flame front approached the gauge. This initial period was followed by a sharp increase in the heat flux around the time of flame arrival, followed by a period of peak-decay behaviour.

From the heating profiles shown in Figure 6.9, it can also be observed that, for both the radiant and total gauges, the peak heat flux at the top surface of the fuel bed is significantly lower than at either of the other two gauge locations. This trend was observed across all fuel bed conditions, with the ratio between the peak total heat fluxes at the bottom surface of the fuel bed to that at the top surface of the fuel bed ranging from 2.8 to 20.4. This far greater bottom surface heating suggests that the heat flux transferred through the fuel bed from the in-bed combustion region is significantly greater than the heat flux transferred from the above-bed flame.

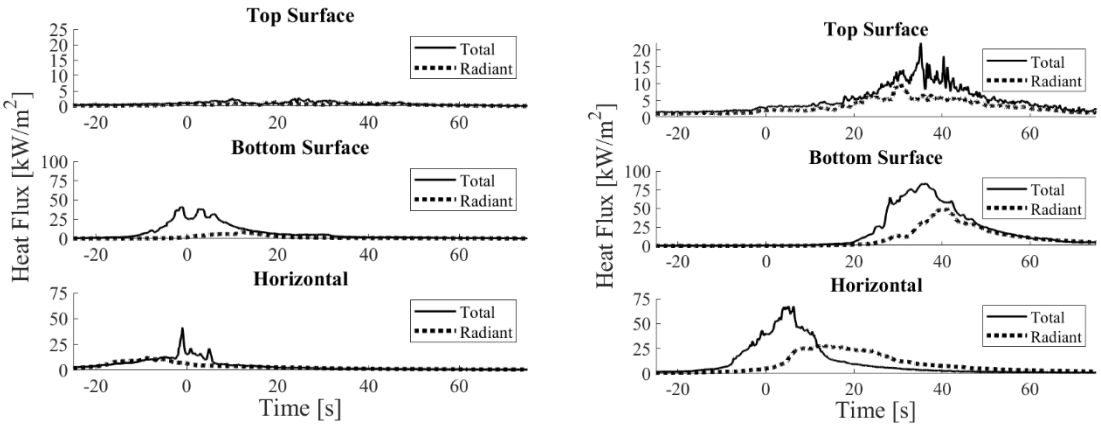


**Figure 6.9 - Characteristic total heat flux profiles at each gauge location for fuel beds of 20 kg/m$^3$ bulk density and different fuel loading. (left) $\alpha\sigma\delta = 98$, and (right) $\alpha\sigma\delta = 197$**

It is possible that the heat flux measured at the bottom surface is also affected by the deposition of burning fuel onto the gauge. However, this deposition would not occur for the horizontally oriented gauges situated within the fuel bed, and facing the in-bed combustion region. The heat fluxes measured by these horizontal gauges were also significantly higher than those measured at the top surface of the fuel bed, as shown in Figure 6.10, in which the top surface (flame heating) and horizontal flux (in-bed heating) measurements are compared.

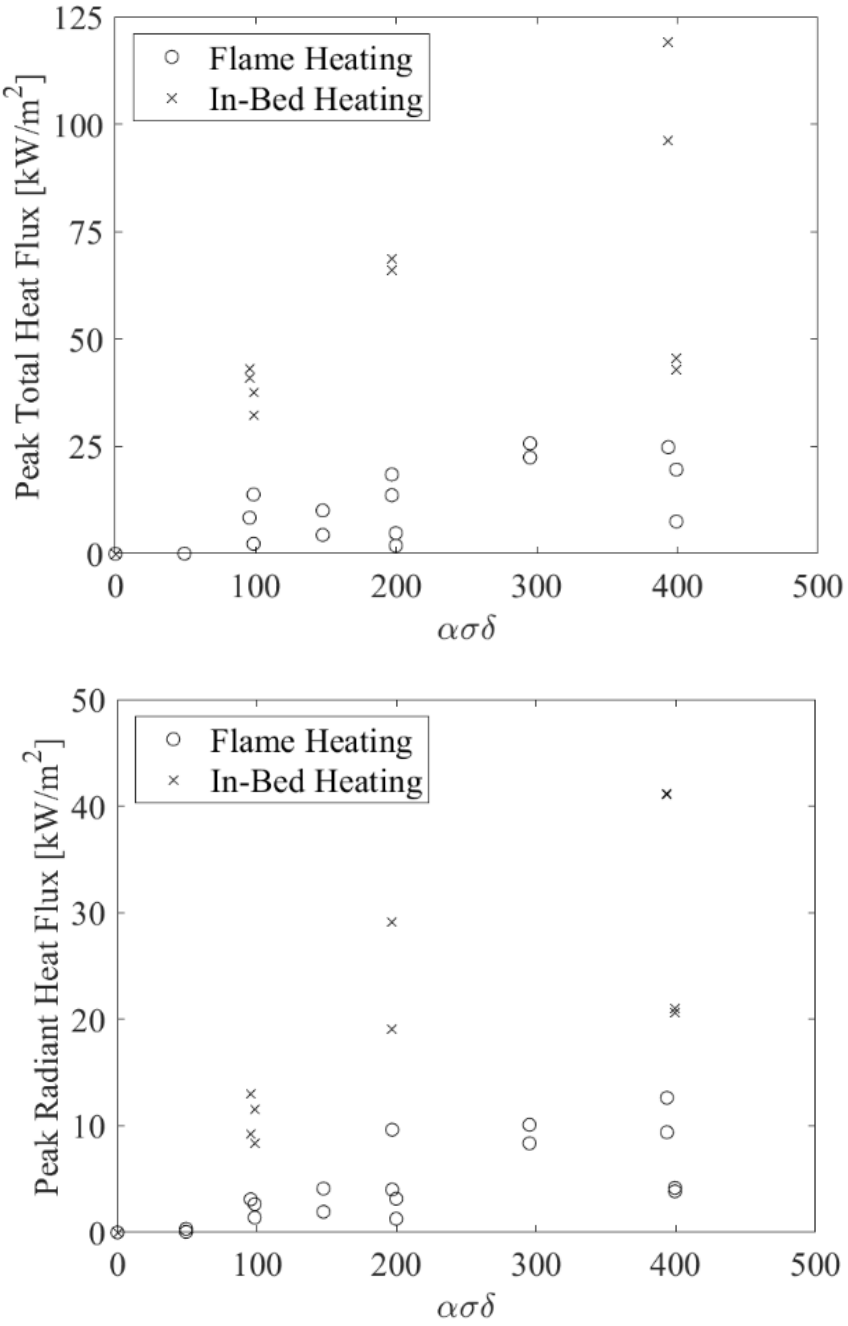


**Figure 6.10 - Comparison of peak (top) total and (bottom) radiant heat flux, from the above-bed flame (flame heating) with horizontal heat flux (in-bed heating) through the fuel beds of various structure ($\alpha\sigma\delta$)**

Where heat fluxes greater than 100 kW/m$^2$ are shown in Figure 6.10, these absolute values should be interpreted with caution, since these are beyond the calibration range of the gauges. However, where this occurs, useful comparisons between the flame heating (measured by the vertical gauge flush with the top surface of the fuel bed) and the in-bed heating (measured by the horizontal gauge within the fuel bed) can still be drawn.

Also shown in Figure 6.10 is the relationship between $\alpha\sigma\delta$ and the peak (radiant or total) heat flux at each gauge location. In general, a positive relationship between $\alpha\sigma\delta$ and the peak heat

flux was observed, with the ratio between the horizontal in-bed heat flux and the vertical overhead flame heat flux also increasing with increasing $\alpha\sigma\delta$ value. The effect of fuel loading remains apparent, with significant variation in peak heat flux observed for some fuel beds of similar $\alpha\sigma\delta$ values but differing fuel loadings. For example, this can be seen in Figure 6.10 for the two highest fuel loadings cases (0.8 kg/m$^2$ and 1.6 kg/m$^2$), where significant variations in peak heat fluxes (particularly the in-bed, horizontal total heat flux) were observed despite the similar $\alpha\sigma\delta$ values ($\alpha\sigma\delta = 394$ and $\alpha\sigma\delta = 399$).

Overall, as shown in Figure 6.10, the heat transfer from the in-bed combustion region is greater than from the overhead flame. Therefore, the heat transfer through the fuel bed region from the combustion region is the dominant heat transfer pathway in this flame spread scenario. Similar observations have previously been made in both pine needle beds [63,125] and wood cribs [115]. However, in extrapolating these findings, the scale-dependence of radiative heating must be considered, as discussed in Chapter 4.

Understanding the dominant heat transfer pathways is an important step in the development of any physically informed flame spread model. It is also important however to understand the relative importance of the different heat transfer mechanisms i.e. the relative contribution of radiative and convective heating. By calculating the ratio between the radiative and total heat flux, a qualitative indication of convective cooling or heating effects can be obtained, as shown in Figure 6.11, for the horizontal, in-bed heat flux measurements. A flux ratio of greater than one indicates the occurrence of convective cooling, while a ratio of less than one indicates convective heating is occurring.

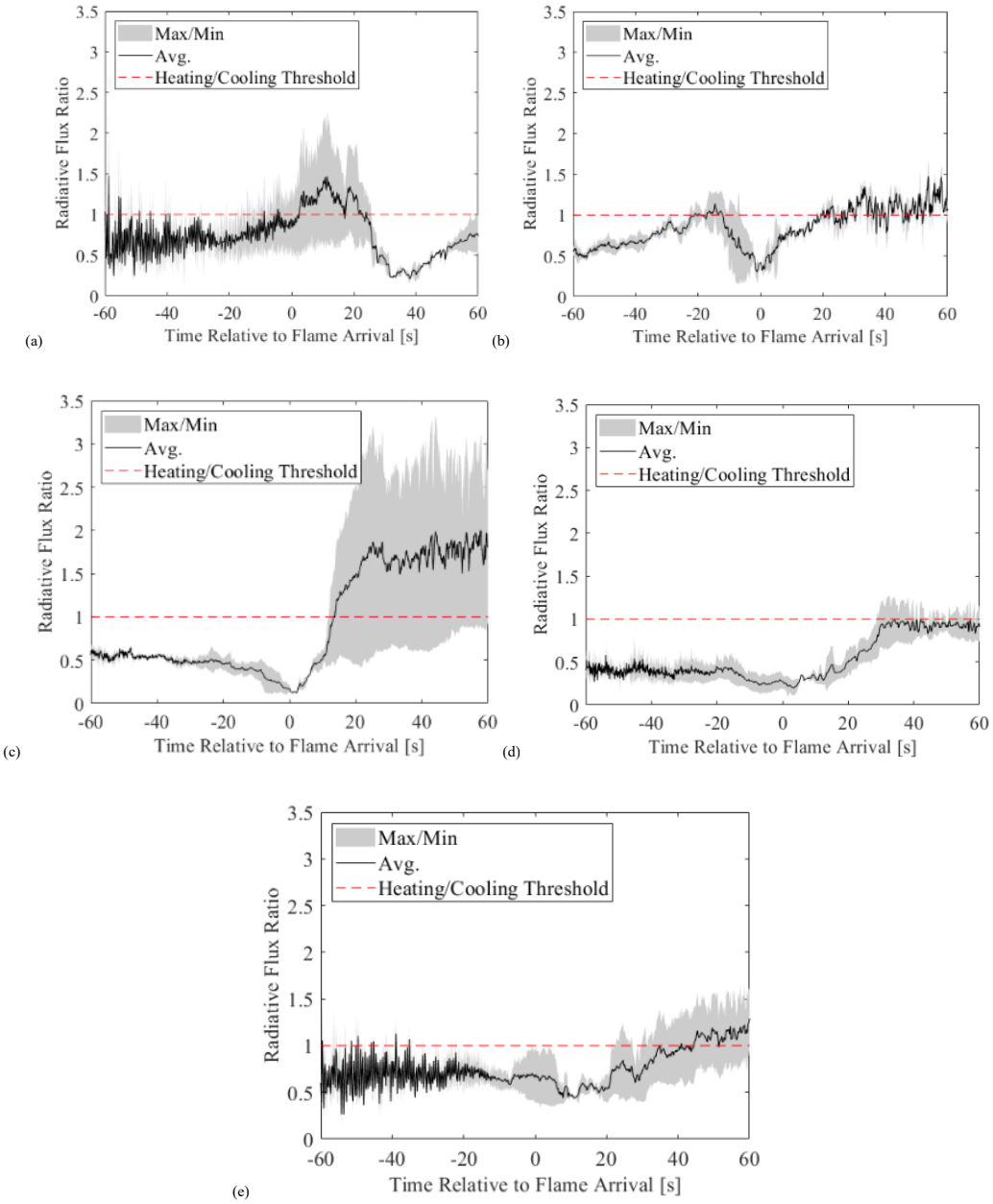


**Figure 6.11 - Instantaneous ratio of radiative:total heat flux relative to flame arrival time for fuel beds of (a) $\alpha\sigma\delta = 96$, (b) $\alpha\sigma\delta = 98$, (c) $\alpha\sigma\delta = 197$, (d) $\alpha\sigma\delta = 394$, and (e) $\alpha\sigma\delta = 399$ (Based on measurements of heat flux transferred horizontally through the fuel bed) (Avg. represents the average across all experiments at a given fuel bed condition)**

As shown in Figure 6.11, periods of both convective heating and cooling are observed throughout the experimental duration. Some convective heating of the gauges would be expected far ahead of the flame front (and also in background periods pre-ignition), since the gauges are water-cooled to a temperature below the ambient air temperature.

Across all fuel bed conditions, the radiative flux ratio reaches a minimum value around the time of flame arrival at the gauge (t = 0 s). However, the exact time at which this minimum value is reached did vary across the fuel bed conditions studied. The onset of this minimum radiative flux ratio was particularly delayed for the lowest porosity fuel bed ($\alpha\sigma\delta = 96$). In

this lowest porosity case, it is possible that the dense fuel structure may reduce the contribution of convective heating at flame arrival.

In addition to the peak heat flux, the heat flux density distribution ahead of the flame front can also be calculated, since the flame front position over time is known. Across all fuel conditions, the maximum pre-heating distance was less than 250 mm however, the peak heat flux occurred after the initial flame front arrival. This is partly due to an extended heating duration after the passage of the vaporisation front, when the trailing flaming and smouldering regions continue to propagate over the gauges. It is also difficult to determine a single arrival time given the discontinuous flame structure within the bed.

The radiant heat flux transferred through the fuel bed to the gauge varied as a function of the distance from the flame front. As shown in Figure 6.12, the normalised radiant heat flux at various distances ahead of the flame front varied with both bulk density (and hence porosity) and fuel loading, where the radiant flux at a given distance is normalised by the peak radiant flux.

Given the difficulty in establishing a single, distinct arrival time, and the effect of the trailing combustion region, it is useful to consider the heat flux measurements in the context of a surface of fire inception. It is then possible to develop a thermal model based upon the experimentally observed heat fluxes at the surface of fire inception, and the effective heating distances.

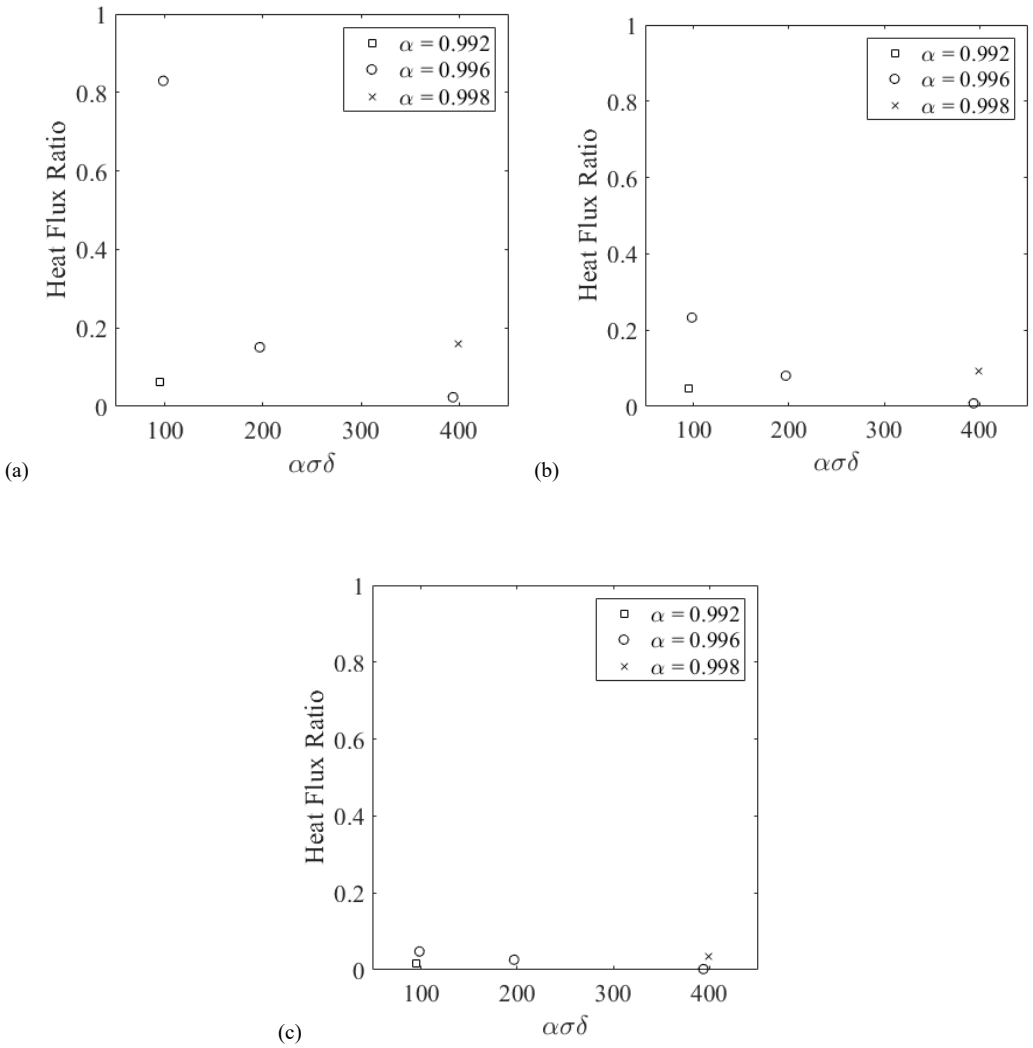


**Figure 6.12 - Ratio of instantaneous radiant heat flux: peak radiant heat flux at a distance ahead of the flame front of (a) 25 mm (b) 50 mm (c) 100 mm**

### 6.4.3. Thermal Model

A simple thermal model was proposed based upon the approach described by Quintiere [53] for thermally thin solids, which was itself based upon the model introduced by De Ris [329]. This model was adapted for application to porous fuels, of the type investigated in this study. In a similar manner to several previous theoretical models [47,70,142], these porous pine needle beds are considered as a fuel layer composed of thermally thin fuel elements.

Within the fuel bed, a control volume was defined and was considered to be fixed to the pyrolysis front ($x_p$), as shown in Figure 6.13. The conservation laws are then applied to this control volume using various assumed bulk fuel bed properties. For example, the fuel bed density is described on a volume-averaged basis, considering both the fuel element and gas phase density, thereby incorporating the inherent porosity of the fuel bed. The values assumed in this model for other fuel bed properties are summarised in Table 6.3.

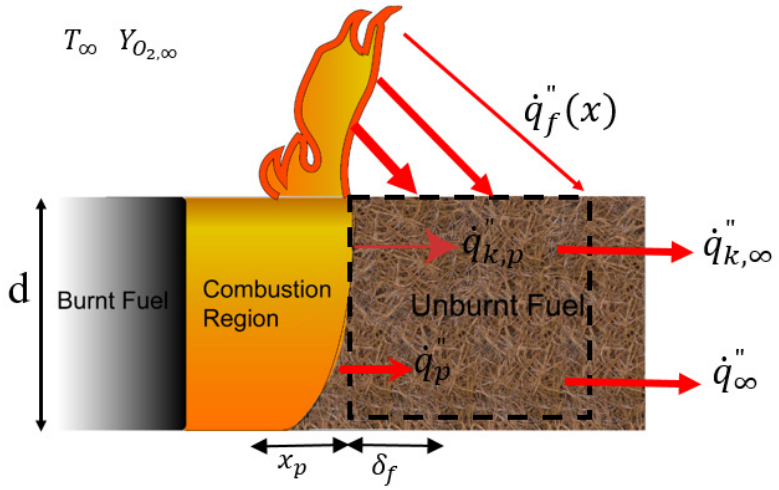


**Figure 6.13 - Schematic of control volume for thermally thin fuel bed model**

**Table 6.3. Summary of constants in thermal model**

| Property | Value |
|---|---|
| Specific Heat Capacity of Pine Needles | 2.07 ± 0.55 kJ/kg.K [32] |
| Specific Heat Capacity of Air | 1.005 ± 0.150 kJ/kg.K |
| Density of Pine Needles | 706 ± 71 kg/m$^3$ |
| Density of Air | 1.2 ± 0.6 kg/m$^3$ |
| Fuel Ignition Temperature | 573 ± 40 K |

Application of the conservation laws to the control volume results in the following equation describing the flame spread rate,

$$v_p = \frac{\int_{x_p}^{\infty} \dot{q}''_p(x)\,dx}{\rho c_p \delta (T_{ig} - T_s)} \tag{6.5}$$

Where $\dot{q}''_p$ is the heat flux into the control volume from the combustion region, which is integrated across the effective heating length. While $T_{ig}$ and $T_s$ are the ignition and initial fuel temperatures respectively.

The above equation assumes that the radiative losses from the fuel bed are negligible, and does not incorporate the effects of convective cooling. It also assumes that the heat transfer from the combustion region is dominant, as was observed experimentally in this study. However, as shown below, the influence of the above bed flame (which as observed experimentally may not be negligible) can also be incorporated into this model,

$$v_p = \frac{\int_{x_p}^{\infty} \dot{q}''_p(x)\,dx + \int_{x_p}^{\infty} \dot{q}''_f(x)\,dx}{\rho c_p \delta (T_{ig} - T_s)} \tag{6.6}$$

In the above equation, it should be noted that the effective heating length differs between these two heat transfer pathways. Both heating lengths have been measured experimentally in this

study and were calculated based upon the time delay between the onset of heating at the heat flux gauge (above a threshold of 0.5 kW/m$^2$) and the time at which the peak heat flux is recorded.

The heat flux magnitudes were also determined experimentally however for this model a 1 second moving average was applied to the raw heat flux measurements. The concept of a surface of fire inception was used, with the peak radiant heat flux, at a given fuel bed condition, integrated across the effective heating distance.

Considering radiant heat flux only from the combustion region, resulted in predicted spread rates similar to those observed experimentally. The maximum discrepancy between the predicted and experimental spread rate was 29 %, with closer agreement observed at lower $\alpha\sigma\delta$ values, as shown in Figure 6.14. As discussed in Chapter 5, for fuel beds of higher $\alpha\sigma\delta$, a greater entrainment flow velocity is expected, which may result in greater convective cooling. This may contribute to the weaker predictive performance at higher $\alpha\sigma\delta$ values since convective heat losses are not accounted for in this model.

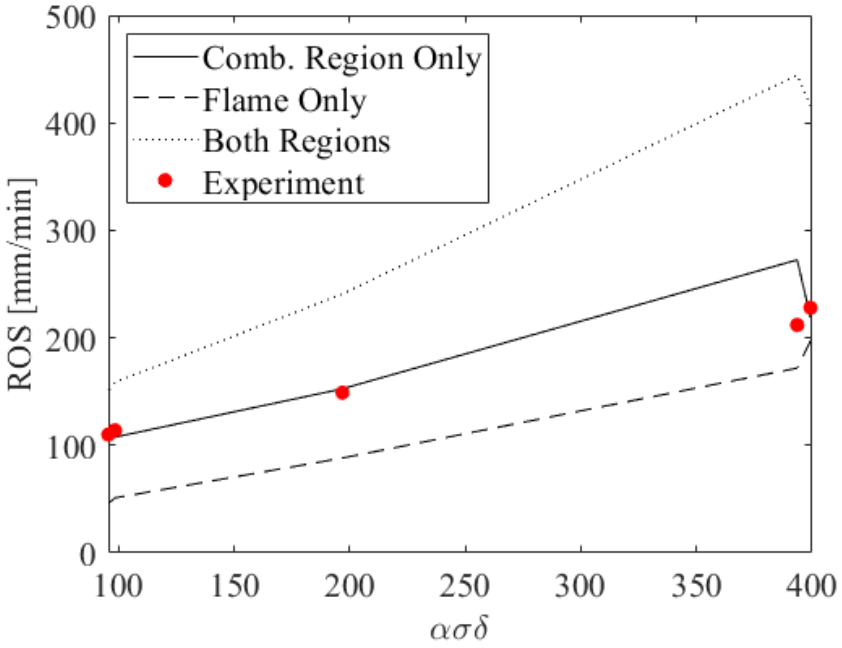


**Figure 6.14 - Comparison of experimentally observed Rate of Spread (RoS) and predicted ROS for thermal model involving either combustion region only, flame region only, or both regions**

As shown in Figure 6.14, if alternatively only the heat transfer from the overhead flame is considered, then an underestimation of the spread rate is observed. This under-prediction is greatest for fuel beds of lower $\alpha\sigma\delta$ suggesting that the relative importance of heat transfer from the combustion region increases at lower $\alpha\sigma\delta$ values. A greater radiative heat flux from the overhead flame occurs at larger $\alpha\sigma\delta$ values where the flame height is greater as shown in Figure 6.10. It is therefore possible that even greater flame heating contributions would be observed if the fuel bed width (and hence flame front width) were increased [327].

If the joint contributions of both the combustion region and overhead flame are considered then the spread rate is significantly over-predicted, as shown in Figure 6.14. Once again, this over-

prediction may partly be explained by the lack of inclusion of convective (or radiative) losses within the model. Over-estimates of experimental spread rate values has also been noted in similar past studies, in which it was concluded that heat losses should be incorporated [70,142]. In fact, the over-predictions of spread rates in this study are significantly lower than in some of these past studies. For example, De Mestre reported over-predictions of 13 times the experimentally observed spread rate [142]. The greater model performance in this study may partly reflect the inclusion of experimentally measured radiation values, which inherently incorporate the effects of the view factor and fuel bed attenuation.

The thermal model discussed here does not however distinguish between the different phases of combustion and their relative contributions to flame propagation. Both the in-bed horizontal and top-surface vertical heat flux measurements include contributions from both the smouldering/glowing and flaming phases. The current model form does not allow the relative importance of these phases, or their effective heating distance, to be independently analysed. Additionally, the combustion behaviour in each phase has been observed to vary with changes to the fuel structure, and therefore the applicability of findings beyond the studied fuel condition range should be investigated cautiously. In particular, it is necessary to consider the possible existence of an optimal fuel loading [63].

## 6.5. Conclusions

As in previous chapters, significant variations in fire behaviour were observed as the fuel bed structure (fuel loading, bulk density, $\alpha\sigma\delta$) was altered. Independent variations in fuel loading or bulk density resulted in variations in flame height, heat release rate and burning rate. The overall effect of fuel bed structure on spread rate was once again well described by the dimensionless parameter $\alpha\sigma\delta$.

Through measurement of heat fluxes (radiant and total) both above and within the fuel bed, the effect of fuel structure on the controlling heat transfer mechanisms were also observed. Radiative heating from the overhead flame was strongly correlated to the flame height. However, for all fuel bed conditions ($\alpha\sigma\delta = 49$ to $\alpha\sigma\delta = 399$), heat transfer from the in-bed combustion region was dominant however the significance of the overhead flame heating increased at higher $\alpha\sigma\delta$ values. These trends are in contrast with some previous predictions regarding heat transfer mechanisms in shallow fuel beds.

The direct measurement of heat fluxes and effective heating distances allowed the development of a simple thermal model, which was used to test the applicability of existing solid-surface, opposed flow flame spread theory to porous fuel beds. Across all fuel bed conditions, predicted spread rates varied by a maximum of 29 % compared to experimentally observed spread rates, where only radiative transfer from the in-bed combustion region was considered. Greater agreement between predicted and experimentally observed spread rates was observed for fuel beds of lower $\alpha\sigma\delta$.

The effect of including the contributions of both the in-bed and above-bed radiative heating in the thermal model was also evaluated. This led to a significant over-prediction of spread rates, and highlighted the need to consider and incorporate additional heat loss terms. The importance of understanding the short-range heat transfer mechanisms was also highlighted, and suggests that the use of a conceptual approach centred upon a surface of fire inception may be appropriately applied. As with previous chapters, the findings should be interpreted with caution when applied to fuel bed structural conditions beyond those investigated in this study.

This is particularly relevant for these experiments given the possibility of changes in flame spread regime at greater fuel loadings (and/or flame heights). While the scale-dependence of radiative heating must also be considered, with further investigation and comparison across experimental scales required.

# Chapter 7

## Applicability of the Rothermel model

# 7. Applicability of the Rothermel Model

## 7.1. Summary

This chapter introduces Rothermel's widely-used, mathematical flame spread model [43], discussing its theoretical basis, historical development, and intended usage. The key model equations and input parameters are defined, while for empirical terms, the experimental evaluation of these parameters is discussed. Rothermel's model (incorporating the modifications later suggested by Albini [330] was then implemented using MATLAB, and verified through comparison with the BehavePlus fire modelling system.

Model predictions of Rate of Spread (RoS) are compared to the RoS observations in Chapter 5. A general tendency for under-prediction of RoS is observed, with an over-sensitivity to fuel bed height (compaction), compared to the experimental observations. Physical explanations for these discrepancies are explored using the energy release and heat flux measurements introduced in Chapters 5 and 6, along with consideration of the original experimental datasets used in the model's initial development. Finally, a number of previously suggested (but not widely adopted) modifications to the Rothermel model are investigated. The effect of incorporating these modifications on model performance is assessed for the flame spread scenario considered in this study.

## 7.2. Introduction to Rothermel's Model

Published in 1972, Rothermel's mathematical model is considered semi-physical since, while having a physics-based conceptual framework, empirically derived experimental constants are included for model closure. The theoretical underpinnings build upon the earlier work of Frandsen, who applied the conservation of energy to a unit volume of fuel ahead of the flame front [43]. Empirical terms were developed based upon quiescent and wind-tunnel flame spread experiments, conducted over the course of a decade at the Northern Forest Fire Laboratory [125], alongside existing field observations from Australian grassfires [331].

The model was designed for use in continuous surface fuels (< 6 ft. above ground e.g. litter layers, shrubs, grass and logging slash [332]) and therefore application to crown fires was not intended. Neither was application to smouldering fires: since the model considers only the combustion occurring in the primary, leading-edge flame front, and not residual combustion occurring behind the main flame front. Despite these limitations, the model has seen widespread operational use, notably forming the basis of the spread rate predictions in the BEHAVE fire modelling system (released in the 1970's and deployed for field use since 1984) [333–335].

Since the introduction of Rothermel's equations, a number of validation studies have been conducted, using experimental data from a wide range of fuel types. Rothermel [332] summarised many of these early field-based studies, and this is reprinted in Figure 7.1. A number of more recent evaluation studies have since been conducted [232,336–353], however it should be remembered that these studies typically also involve the development and calibration of a new or existing fuel models. This limits the ability to validate the underlying modelling approach.

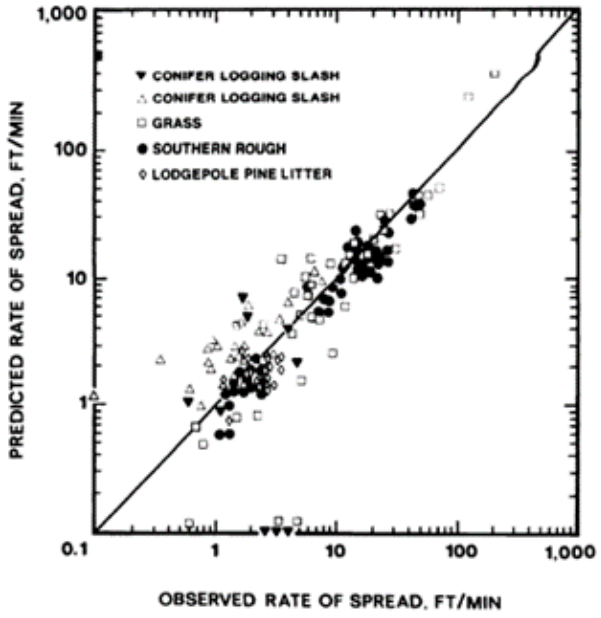


**Figure 7.1 - Summary of Rothermel model performance vs. experimental observations from various field experiments. From Rothermel (1983)** [332]

Rothermel's flame spread model [43] continues to be widely used by wildland fire practitioners. Operational use was a priority from the outset, with the model intended to be quantitative, predictable and flexible, suitable for use in fuel appraisal, fire-danger rating, and pre-suppression planning [354]. The model has since been incorporated into the United States National Fire Danger Rating System [355], the National Fire Management Analysis System (NFMAS) [356], and the Rare Event Risk Assessment Process (RERAP) [357]. Alongside current usage in several fire modelling systems [356,358–360] e.g. BehavePlus [361], NEXUS [362], FARSITE [201], FlamMap [363], and the Fire and Fuels Extension to the Forest Vegetation Simulator [364].

Despite continuing use, relatively few changes have been incorporated into Rothermel's equations since their inception. Shortly after the initial model development, Albini [330] suggested several modifications (outlined in Section 7.4) which have since been widely adopted. The original inclusion of a wind speed limit has also been re-evaluated following subsequent research and re-analysis [358]. In modern fire modelling systems, these are generally the only modifications made to the original Rothermel equations. This is despite other suggested shortcomings, including a possible over-sensitivity to fuel height, as discussed in Section 7.8.

## 7.3. Overview of Rothermel's Flame Spread Equation

In this study, Rothermel's original flame spread equations [43] are used, however the modifications suggested by Albini [330] are incorporated. To allow clearer comparison with existing studies, and to relate more closely to current management applications, the original imperial units are maintained. However, the conversion of these equations to SI units is summarised in Appendix A, using the updated constants calculated by Wilson [365]. The original Rothermel equations are now discussed in detail, followed by a summary of the modifications suggested by Albini, and adopted in this study.

Rothermel proposed a mathematical expression for flame spread in wildland fuel beds. Based upon the earlier work of Frandsen [366] and the principle of energy conservation, this equation describes the spread rate as the ratio of thermal energy transfer to the heat sink magnitude of the fuel. For homogeneous fuel beds, the RoS ($R$) is given by,

$$R = \frac{I_R \xi (1 + \phi_w + \phi_s)}{\rho_b \epsilon Q_{ig}} \tag{7.1}$$

Where $I_R$ is the reaction intensity, $\xi$ is the propagating flux ratio, $\phi_w$ and $\phi_s$ are the wind and slope correction factors respectively, $\rho_b$ is the oven-dry bulk density, $\epsilon$ is the effective heating number, and $Q_{ig}$ is the heat of pre-ignition. The physical meaning of each of these terms, and the development of mathematical descriptions, are discussed in detail below.

### 7.3.1. Reaction Intensity

#### 7.3.1.1. Physical Meaning

The reaction intensity ($I_R$) describes the heat release rate per unit area of the fire front.[15] As shown in Figure 7.2, a proportion of this heat energy (termed the propagating flux, $I_P$) is transferred to the unburnt fuel ahead of the flame front, and ultimately drives flame spread propagation. Meanwhile a significant proportion of the reaction intensity energy is transferred to the wider environment (e.g. in the convective plume), rather than to the unburnt fuel.

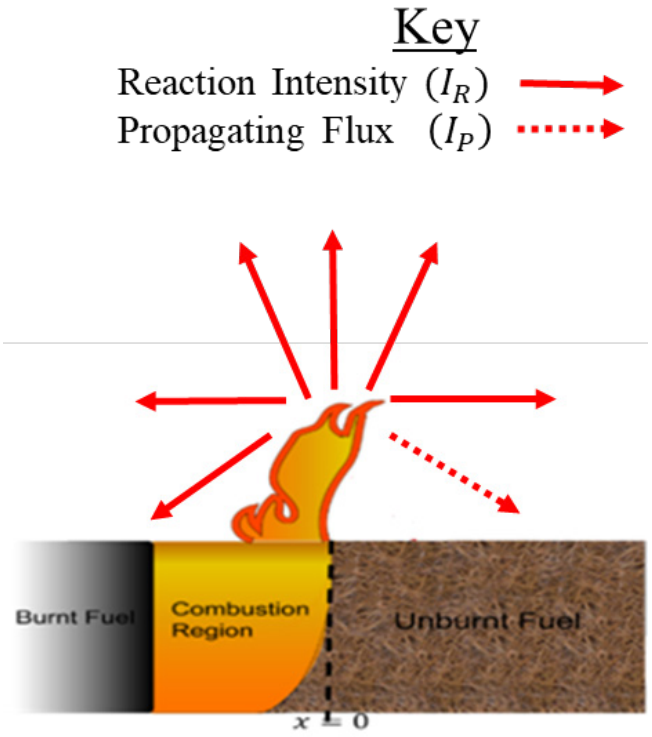


**Figure 7.2 – Flame spread schematic illustrating the key concepts of reaction intensity ($I_R$) and propagating flux ($I_P$) which underpin Rothermel's spread rate equation**

[15] It is important to note that, while similar, the reaction intensity differs from the fireline intensity (which instead describes the heat release per unit per unit length of the fire front) [419].

The reaction intensity is dependent on both the fuel consumption rate and the energy release rate of the fuel within the fire front region, and is defined physically as [43],

$$I_R = -h\frac{dw}{dt} = -\left(\frac{dw}{dx}\right)\left(\frac{dx}{dt}\right)h = -\left(\frac{dw}{dx}\right)Rh \tag{7.2}$$

Where $h_c$ is the fuel heat content, $\frac{dw}{dt}$ is the mass loss rate, and $\frac{dx}{dt}$ is the spread rate.

The fuel consumption and energy release rates may depend upon a number of factors including the fuel element geometry (size, thickness), fuel bed structure (height, fuel loading, bulk density), and the mineral and moisture content of the fuels [367].

#### 7.3.1.2. Development of Model Equation

Rothermel calculated the reaction intensity as a function of the optimum reaction velocity ($r'$), net fuel loading ($w_n$), heat content ($h$), and mineral and moisture contents. This equation is derived from the physical expression (given in Equation 7.2), which, by rearranging, can be integrated with respect to distance and weight [43],

$$I_R \int_0^D dx = -Rh \int_{w_n}^{w_r} dw \tag{7.3}$$

Where $D$ is the horizontal reaction zone depth, $w_n$ is the initial net fuel loading (net of moisture, minerals and non-combustibles) and $w_r$ is the remaining fuel load behind the flame front (as shown in Figure 7.2). Integration of Equation 7.3, gives,

$$I_R D = Rh(w_n - w_r) \tag{7.4}$$

Rothermel defined a reaction time ($\tau_R$) based upon the propagation time of the flame front across the reaction zone,

$$\tau_R = \frac{D}{R} \tag{7.5}$$

This reaction time can be substituted into Equation 7.4, such that,

$$I_R = \frac{h(w_n - w_r)}{\tau_R} \tag{7.6}$$

It is therefore clear that the maximum possible reaction intensity occurs when all combustible fuel is consumed in the flame front ($w_r = 0$). The combustion efficiency within the flame front ($\eta_\delta$) is therefore given by the ratio of the actual reaction intensity to the maximum reaction intensity. This efficiency value can be incorporated into Equation 7.6 giving,

$$I_R = \frac{w_n h \eta_\delta}{\tau_R} \tag{7.7}$$

The combustion efficiency, along with the fuel consumption rate, can be described by a single parameter: the reaction velocity ($r$). The reaction velocity is equivalent to the ratio of flame front efficiency ($\eta_\delta$) to reaction time ($\tau_R$), and incorporates the effects of mineral and moisture contents, lowering the value below that of the potential reaction velocity ($r'$),

$$r = r'\eta_M\eta_s \tag{7.8}$$

The two damping coefficients ($\eta_s$ and $\eta_M$), empirically describe the effects of mineral and moisture contents respectively. The empirical development of these damping coefficients is discussed in Sections 7.4.4 and 7.4.5.

Therefore, Rothermel's final mathematical expression for the reaction intensity is given by,

$$I_R = w_n h r'\eta_M\eta_s \tag{7.9}$$

Therefore, the reaction intensity is positively correlated with optimum reaction velocity, net fuel loading and heat content; and negatively correlated with the mineral and moisture content of the fuel. The effects of fuel element and fuel bed structure (on the mass consumption rate) are incorporated within the optimum reaction velocity calculation (as described in Section 7.4.1).

*Experimental Determination*

Rothermel obtained an empirical description for the reaction intensity by conducting laboratory-based flame spread experiments with three different fuel types (excelsior, ¼ inch wood cribs, and ½ inch wood cribs), each of differing surface-to-volume ratio. The fuel bed dimensions varied for each fuel type: excelsior (3 ft. wide, 8 ft. long, 4.5 in. height) and wood cribs (approx. 3 ft. wide, 5 ft. long, 5 to 6 in. height).

The reaction intensity was calculated using Equation 7.2, by measuring the mass loss in experiments at multiple fuel bed packing ratios for each fuel type. The measured mass loss rate ($\dot{m}$) was related to the observed spread rate ($R$),

$$\dot{m} = (w_n - w_r)RW \tag{7.10}$$

Where $W$ is the weighing platform width and R is the rate of spread.

Therefore, the combustion efficiency within the fire front can be expressed as,

$$\eta_\delta = \frac{\dot{m}}{w_n RW} \tag{7.11}$$

Such that the potential reaction velocity is given by,

$$r' = \frac{r}{\eta_M\eta_s} \tag{7.12}$$

While this experimental data informed the development of empirical model closure terms, Rothermel cautioned against direct comparison of the reaction intensities for each fuel type, as

the fuel loadings varied between fuel types. However, for each fuel type, only a single fuel bed height was studied across all fuel bed conditions (at all packing ratios studied). To achieve these different packing ratios, while maintaining a constant fuel depth, would have required alteration of the fuel loading at each condition.

It is therefore notable, that while Rothermel cautioned against the comparison of reaction intensities across fuel types (given the differing fuel loadings) no similar note of caution was included for comparisons between packing ratios (where fuel loadings also differed). Instead, an assumption is introduced that reaction intensity (and propagating flux) are linearly dependent upon the fuel height.

The calculated reaction intensities for each fuel type are shown in Figure 7.3 (reprinted from Rothermel 1972 [43]). The curves in Figure 7.3 represent the predictions from the empirically derived fitting terms proposed by Rothermel (based on a curve fit of the data from all three fuel types).

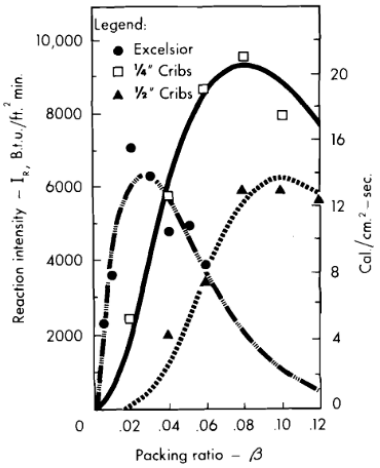


**Figure 7.3 – Empirical curve-fit of reaction intensity as a function of packing ratio for three fuel types. Extracted from Rothermel (1972)** [43]

### 7.3.2. Propagating Flux Ratio

#### 7.3.2.1. Physical Meaning

The propagating flux ratio ($\xi$) describes the proportion of the overall heat produced in the combustion zone ($I_R$) that is actually transferred to the unburnt fuel ahead in the absence of wind,

$$\xi = \frac{(I_P)_o}{I_R} \tag{7.13}$$

Where $(I_P)_o$ is the no-wind propagating flux.

As shown in Figure 7.2, much of the heat released in the combustion zone is lost to the environment, but only heat energy transferred to the fuel (the propagating flux, $I_P$) will contribute to flame spread (by providing the energy for ignition). There are two components to

this propagating flux: the horizontal heat flux through the fuel bed ($I_{xig}$) and the vertical heat transfer from the above-bed flame ($I_z$),

$$I_P = I_{xig} + \int_{-\infty}^{0} \left(\frac{\delta I_z}{\delta z}\right)_{z_c} dx \tag{7.14}$$

Where the second term on the right hand side of Equation 7.14, represents the vertical heat flux gradient across the pre-heating region (flame front leading edge to maximum end of the pre-heating distance).

The relative importance of the propagating flux terms varies depending on the flame spread scenario. The vertical heat transfer is greater in wind-driven or upslope flame spread scenarios, given the greater flame tilting towards the unburnt fuel. Rothermel assumed that there was little vertical heating at quiescent conditions [43], such that in quiescent conditions the no-wind propagating flux $(I_P)_o$ is given by,

$$(I_P)_o = R_o \rho_b \epsilon Q_{ig} \tag{7.15}$$

Where $R_o$ is the quiescent flame spread rate.

The increase in the overall energy transferred to the fuel at greater wind speeds or slope angle is accounted for by introducing empirically derived wind and slope coefficients (discussed further in Sections 7.3.3 and 7.3.4) such that,

$$I_P = (I_P)_o(1 + \sigma_w + \sigma_s) \tag{7.16}$$

*Experimental Determination*

In the same experimental series in which the reaction intensity was determined [43], the no-wind propagating flux was also calculated empirically, using Equation 7.15. The calculated no-wind propagating flux and the propagating flux ratio for each fuel type are shown in Figure 7.4 (reprinted from Rothermel 1972 [43]), including Rothermel's curve fit of the for each fuel type.

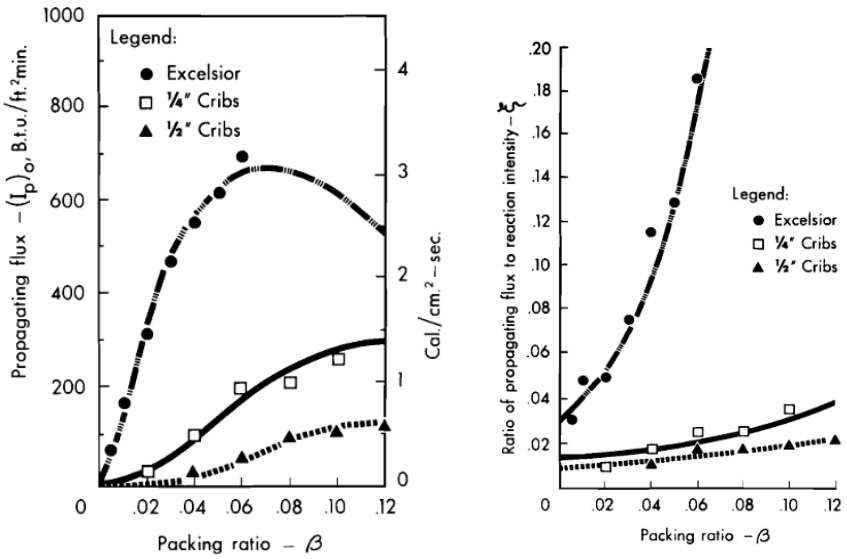


**Figure 7.4 — Experimental determination of (left) no-wind propagating flux and (right) propagating flux ratio, for 3 fuel types. Extracted from Rothermel (1972)** [43]

#### 7.3.2.2. Development of Model Equation

Using a curve fitting approach, Rothermel empirically derived an expression for the propagating flux ratio, as a function of packing ratio ($\beta$) and S-V ratio ($\sigma$), based upon the experimental data (for all three fuel types) shown in Figure 7.4,

$$\xi = (192 + 0.2595\sigma)^{-1} \exp[(0.792 + 0.681\sigma^{0.5})(\beta + 0.1)] \quad (7.17)$$

The propagating flux ratio is therefore positively correlated with surface-to-volume ratio and packing ratio, and tends towards zero as each of these decreases. The effect of increased surface-to-volume ratio is greater at higher packing ratios (more compacted fuel beds), as shown in Figure 7.5 (extracted from Burgan and Rothermel 1984 [368]). Similarly, the effect of increased packing ratio is greater at higher surface-to-volume ratios (finer fuels).

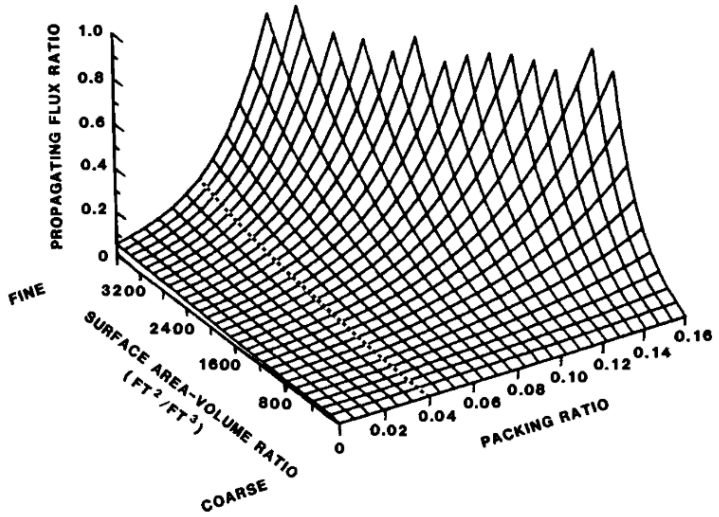


**Figure 7.5 – Propagating flux ratio as a function of surface-to-volume ratio and packing ratio. Extracted from Burgan and Rothermel (1984)** [368]

### 7.3.3. Wind Coefficient

#### 7.3.3.1. Physical Meaning

The wind coefficient ($\phi_w$) describes the effect of wind speed, with greater pre-heating (radiative and convective) occurring in concurrent flow scenarios. This heating increase occurs as a result of increased flame tilting towards the fuel bed, while additional airflow into the combustion region may also affect the combustion dynamics via increased oxygen supply. However, these physical phenomena are not explicitly considered within Rothermel's model, with an empirical correction coefficient instead applied.

By assuming that wind and slope act independently, any additional propagating heat flux in a wind-aided scenario can be attributed to the effect of wind and is represented by the wind coefficient ($\phi_w$). If there is no wind effect then the ratio of the propagating flux to the no wind propagating flux would equal unity $\left(\frac{I_P}{(I_P)o} = 1\right)$, and on this basis,

$$\phi_w = \frac{I_P}{(I_P)_o} - 1 \tag{7.18}$$

Based on Equations 7.15 and 7.16 , if the bulk density, effective heating number and heat of pre-ignition are constant, then the propagating flux is proportional to the spread rate, so that,

$$\phi_w = \frac{R_w}{R_o} - 1 \tag{7.19}$$

Where $R_w$ is the wind-aided spread rate, and $R_o$ is the no-wind spread rate.

*Experimental Determination*

In Rothermel's model, the wind coefficient ($\phi_w$) is empirically derived, based upon observations from a series of wind tunnel experiments [43], and field observations [331]. The

wind tunnel experiments were conducted by Rothermel during the model development, while the field data relied upon previous headfire spread rate observations in grassland fires [331].

McArthur's grassfire spread rate observations are summarised in Figure 7.6 (reprinted from Rothermel 1972 [43]). However, no data on fuel properties was collected for these fires, and therefore Rothermel [43] assumed fuel properties 'similar to those of a typical arid grass area in the Western United States'.[16]

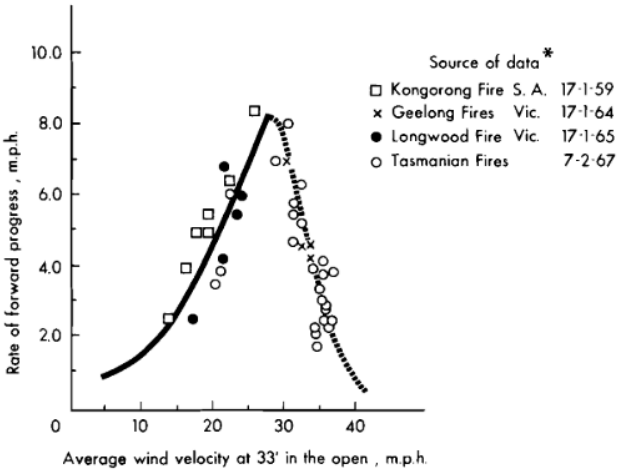


**Figure 7.6 – Rate of spread observations from previous grassland fires at various wind speeds. Extracted from Rothermel (1972)** [43]

The wind tunnel experiments were conducted in the Northern Forest Fire Laboratory wind tunnel [43] across a range of wind speeds (2, 4, 6, or 8 mph). As with the no-wind experiments, three different fuel types were studied (excelsior, ½ in. sticks, ¼ in. sticks) however, the sticks were arranged as double tripods, rather than as cribs. Various packing ratios were studied for each fuel type, and for the double tripods, the packing ratio was manipulated by varying the spacing between double tripods.

Prior to determining an appropriate wind coefficient for a given wind speed, the relationship between the wind coefficient and fuel properties (surface-to-volume ratio and packing ratio) required investigation. In determining this relationship, Rothermel used both the laboratory and field data but excluded the ½ in. stick data, as it 'did not correlate'. It was hypothesised that this lack of correlation suggested a fuel thickness limit, beyond which the assumption of constant fuel properties (used to define Equation 7.18) is no longer appropriate, due to a variation in the effective bulk density in rapid heating conditions.

The effect of both packing ratio and fuel particle size on the wind coefficient are illustrated in Figure 7.7 (re-printed from Rothermel 1972 [43]). As shown, the effect of increased wind speed is greater for higher surface-to-volume ratios (finer fuels) and at lower packing ratios (less compact fuel beds). The greater wind effect in finer fuels matched the previous experimental

[16] Rothermel [43,358] assumed values for several fuel properties: Surface-to-Volume Ratio = 3,500 ft-1; Dry Fuel Loading = 0.75 ton/acre; Fuel Depth = 1 ft.; FMC = 0.04; Heat Content = 7,500 BTU/lb; Particle Density = 25 lb/ft.; Total Mineral Content = 0.03; Effective Mineral Content = 0.01.

observations of Rothermel and Anderson [125], and the anecdotal field observations of Rothermel [43].

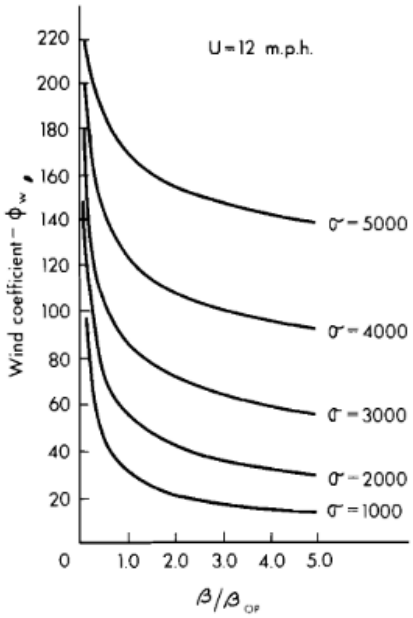


**Figure 7.7 – Experimental determination of the wind coefficient as a function of the ratio of packing ratio to optimum packing ratio ($\beta/\beta_{op}$). Extracted from Rothermel (1972)** [43]

#### 7.3.3.2. Development of Model Equation

Empirical fitting of the field and wind tunnel experimental data (again excluding the ½ in. sticks) resulted in the following empirical term for the wind coefficient ($\phi_w$),

$$\phi_w = CU^B \left(\frac{\beta}{\beta_{op}}\right)^{-E} \tag{7.20}$$

Where U is the wind speed at mid-flame height, while the correlation parameters C, B and E are a function only of fuel particle size ($\sigma$),

$$C = 7.47 \exp(-0.133\sigma^{0.55}) \tag{7.21}$$

$$B = 0.02526\sigma^{0.54} \tag{7.22}$$

$$E = 0.715 \exp(-3.59 \times 10^{-4}\sigma) \tag{7.23}$$

An upper limit is imposed on the wind coefficient, based upon the maximum spread rate observed in McArthur's grassland fire data. Based upon the previous work of Rothermel and Anderson [125], the flame angle ($\phi$) was defined relative to the ratio of the wind and fire forces,

$$\tan\phi = \frac{q\mathrm{U}}{\mathrm{I_R J}} \tag{7.24}$$

Where $q$ is the free stream dynamic pressure, U is the airflow velocity, and J is the constant of proportionality between work and heat energy. Solving for the maximum observed field spread rate (observed at a mid-flame wind speed of around 1,000 ft./min), and assuming an ambient temperature of 80 °F and elevation of 3,000 ft., gives a maximum ratio of wind speed to reaction intensity of $U/I_R = 0.9$, therefore,

$$\text{For } \frac{U}{I_R} > 0.9, \qquad \phi_w = (\phi_w)_{max} \tag{7.25}$$

Where,

$$(\phi_w)_{max} = \phi_w \quad \text{at} \quad U = 0.9\, I_R \tag{7.26}$$

However, several decades after the model's initial development, this equation was revised by Rothermel, after an error in the original analysis was identified [358]. Rothermel had originally assumed a constant free stream dynamic pressure, when this should actually vary with the square of the wind speed. Correcting this error gives a revised wind speed limit of,

$$(\phi_w)_{max} = \phi_w \quad \text{at} \quad U = 96.8\, I_R^{1/3} \tag{7.27}$$

In recent years, the upper wind limit concept has come to be viewed as overly-restrictive, but a lack of fundamental knowledge continues to complicate efforts to specify an appropriate wind limit [358]. In fact, Andrews *et al.* [358] recommended that neither the original nor the revised wind speed limits should be imposed, but that predicted spread rates should instead be limited to the mid-flame wind speed.

### 7.3.4. Slope Coefficient

#### 7.3.4.1. Physical Meaning

The slope coefficient ($\phi_s$), empirically describes the effect of slope, with greater heating of the unburnt fuel ahead of the flame front occurring in upslope flame spread scenarios. This heating increase occurs as a result of increased flame tilting towards the fuel bed, given the relative flame and fuel bed geometry. Again, it was assumed that the effects of wind and slope were not inter-related.

#### 7.3.4.2. Experimental Determination

To develop a slope coefficient, Rothermel studied the effects of slope in a series of laboratory-based, no-wind flame spread experiments. These experiments involved excelsior fuel beds of various packing ratios (0.005, 0.01, 0.02, and 0.04) and at a range of fuel bed slopes (25, 50 and 75 %). The experimental data is summarised in Figure 7.8 (extracted from Rothermel 1972 [43]).

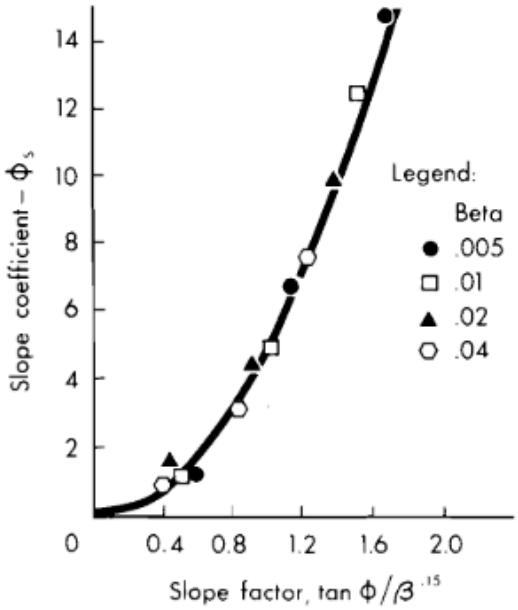


**Figure 7.8 - Experimental determination of slope coefficient as a function of the slope factor. Extracted From Rothermel (1972)** [43]

7.3.4.3. Development of Model Equation

Through curve-fitting of the experimental data (as shown in Figure 7.8), Rothermel obtained a correlation for the slope coefficient $(\phi_s)$ as a function of the slope angle $(\phi)$ and the packing ratio $(\beta)$,

$$\phi_s = 5.275\beta^{-0.3}(\tan\phi)^2 \tag{7.28}$$

7.3.5. Oven-dry Bulk Density

7.3.5.1. Physical Meaning

The bulk density $(\rho_b)$ describes the mass of fuel per unit volume of the fuel bed. The bulk density can be altered by varying the fuel loading within a given volume, or by altering the fuel volume (varying the height for a fuel bed of fixed area) for a given fuel loading.

In defining the heat sink magnitude of the fuel bed, the bulk density offers a convenient method of defining the amount of fuel to be heated per unit volume. However, since a proportion of the fuel may not be heated to the ignition temperature prior to flame front arrival, the bulk density may in fact represent an over-estimate. For this reason, in the final spread rate equation, Rothermel calculated the effective bulk density $(\rho_{be})$ by finding the product of the bulk density and an effective heating number $(\epsilon)$ (described further in Section 1.3.6).

7.3.5.2. Development of Model Equation

Rothermel used the classical equation for the oven-dry bulk density,

$$\rho_b = \frac{w_o}{\delta} \tag{7.29}$$

Where $w_o$ is the oven-dry fuel loading, and $\delta$ is the fuel height.

### 7.3.6. Effective Heating Number

#### 7.3.6.1. Physical Meaning

The effective heating number ($\epsilon$) describes the proportion of a fuel element actually heated to the ignition temperature to the arrival of the flame front [368]. This concept can also be extended to fuel bed volumes, by considering the heat distribution through the depth of the fuel bed, and defining an effective bulk density ($\rho_{be}$) [99]. The effective heating number can then be defined as the ratio of the effective bulk density ($\rho_{be}$) to the physical bulk density ($\rho_b$),

$$\epsilon = \frac{\rho_{be}}{\rho_b} \tag{7.30}$$

For thin fuels (high surface-to-volume ratio), the effective heating number will be close to one, and this value will decrease for thicker fuels (lower surface-to-volume ratio). This reflects the low thermal gradients within a thin fuel element (thermally thin at $\epsilon = 1$). Larger internal thermal gradients may occur in thicker fuels, reducing the heat penetration depth and subsequently lowering the effective bulk density. The fuel element thermal diffusivity and the presence of a moisture gradient may also affect the effective heating number, however for a simple analysis their effects can be considered to be negligible [366].

#### 7.3.6.2. Experimental Determination

The effective heating number, as a function of fuel element surface-to-volume ratio, was evaluated empirically in an earlier experimental study conducted by Frandsen [366]. These experiments were limited in scope and involved the measurement of the internal temperature profile of individual fuel elements (wood sticks) during wood crib flame spread experiments. These fuel elements were located at the crib surface.

The overall energy absorption of these fuel elements, prior to ignition, was calculated from the measured temperature profiles. Rothermel summarised these results as shown in Figure 7.9, which is re-printed from Rothermel 1972 [43]. Figure 7.9 shows the effective heating number, which was calculated as the ratio of the measured energy absorption per unit volume to the theoretical heat absorption per unit volume for uniform heating to ignition.

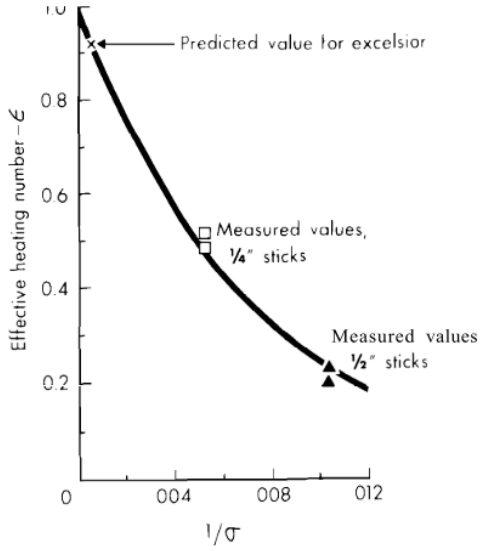


**Figure 7.9 - Experimental determination of the effective heating number as a function of the reciprocal of the surface-to-volume ratio ($1/\sigma$). Extracted from Rothermel (1972)** [43]

This experimental series involved a very limited number of conditions, with only two fuel thicknesses (or surface-to-volume ratios) tested (1/2 in. and ¼ in. sticks). Determining the effective heating number of thinner (higher surface-to-volume ratio) fuels (e.g. excelsior, pine needles) would require extensive extrapolation from these thicker fuel measurements.

Additionally, only the fuel thickness was altered in these experiments, and all fuel bed parameters (packing ratio of 0.08) were held constant. Therefore, any effect of these fuel bed properties on the effective heating number were not explored. Similarly, the experiments did not account for any variation in effective heating number that may occur for fuel elements at locations other than the fuel surface. However at the time of development of the Rothermel model, these results represented the only available experimental data for the evaluation of the effective heating number [366].

#### 7.3.6.3. Development of Model Equation

Based on a curve-fit of Frandsen's data [366], Rothermel [43] described the effective heating term as a function of the surface-to-volume ratio ($\sigma$),

$$\epsilon = \exp(\frac{-138}{\sigma}) \tag{7.31}$$

An exponential curve was chosen given the close positioning of the experimental data points to this curve. Frandsen [366] acknowledged that, given the small number of conditions studied, several possible curves could be fitted. An upper limit on the effective heating number exists for thermally thin fuels with $\epsilon = 1$ at $\frac{1}{\sigma} = 0$.

#### 7.3.7. Heat of Pre-Ignition

##### 7.3.7.1. Physical Meaning

The heat of pre-ignition $(Q_{ig})$ represents the energy per unit mass required for the fuel to reach ignition. It may depend upon several factors including FMC, heat of desorption, heat of vaporisation and ignition temperature.

##### 7.3.7.2. Development of Model Equation

Considering a cellulosic fuel, Rothermel determined the heat of pre-ignition analytically [43]. The specific heat required for a temperature rise from the ambient fuel temperature ($T_\infty$) to the ignition temperature $(T_{ig})$ was considered, along with the latent heat of vaporisation for the fuel moisture ($V$),

$$Q_{ig} = C_{pd}\Delta T_{ig} + M_f\left(C_{pw}\Delta T_B + V\right) \tag{7.32}$$

Where $C_{pd}$ and $C_{pw}$ are the specific heat capacities of wood and water respectively, $\Delta T_{ig}$ is the temperature rise to ignition, $M_f$ is the FMC ratio, and $\Delta T_B$ is the temperature rise to the boiling temperature.

Rothermel [43] used the previous solution of Frandsen [366], which assumed an ambient temperature of 20 °C, an ignition temperature of 320 °C, and a boiling temperature of 100 °C. This gives the final form of the equation specified in Rothermel's model,

$$Q_{ig} = 250 + 1{,}116M_f \tag{7.33}$$

Despite the potential effect of several factors (including FMC, heat of desorption, heat of vaporisation and ignition temperature), this equation describes the heat of pre-ignition as a function only of the FMC ratio ($M_f$).

### 7.4. Other Model Equations

#### 7.4.1. Reaction Velocity

##### 7.4.1.1. Physical Meaning

The reaction velocity ($r$) is the ratio of the flame front combustion efficiency ($\eta_\delta$) to the reaction time ($\tau_R$), and reflects the fuel consumption rate,

$$r = \frac{\eta_\delta}{\tau_R} \tag{7.34}$$

The reaction velocity is primarily a function of the fuel element size, bulk density, and the moisture and mineral content of the fuel.

##### 7.4.1.2. Experimental Determination

In Section 7.3.1, the experiments used to inform the model approach to reaction velocity are described in detail. The combustion efficiency within the fire front can be calculated experimentally, if the mass loss rate ($\dot{m}$) is measured,

$$\eta_\delta = \frac{\dot{m}}{w_n RW} \tag{7.35}$$

Where $R$ is the spread rate, $w_n$ is the net fuel loading, and W is the width of the section being weighed.

As discussed in Section 7.3.1, Rothermel defines a reaction time ($\tau_R$) based upon the flame front propagation time across the reaction zone of depth $D$,

$$\tau_R = \frac{D}{R} \tag{7.36}$$

By substituting the experimentally determined combustion efficiency into Equation 7.35, the reaction velocity can be determined,

$$r = \frac{\dot{m}}{w_n R W \tau_R} \tag{7.37}$$

From the experimentally observed reaction intensity, the potential reaction velocity can be calculated. The reaction velocity incorporates the effect of fuel mineral and moisture content, which lowers its value below that of the potential reaction velocity ($r'$),

$$r' = \frac{r}{\eta_M \eta_s} \tag{7.38}$$

Where the two damping coefficients ($\eta_s$ and $\eta_M$) empirically describe the effects of mineral and moisture contents respectively. The empirical development of these damping coefficients is discussed in Sections 7.4.4 and 7.4.5.

The potential reaction velocity must also account for the effect of the fuel properties, which requires development of an empirical correlation. The mass loss experiments described in Section 7.3.1 provide reaction velocities for a range of packing ratios for three different fuel types (excelsior, 1/2 in. stick and ¼ in. stick wood cribs). This allows the calculation of the potential reaction velocity at each fuel condition, as shown in Figure 7.10, where the curve fit assumes a modified Poisson distribution.

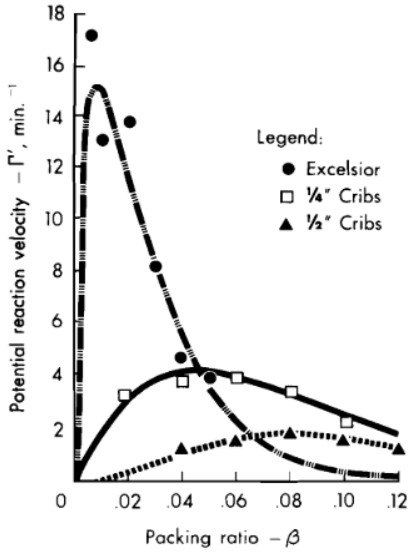


**Figure 7.10 - Experimental determination of the potential reaction velocity as a function of the packing ratio. Extracted From Rothermel (1972)** [43]

As shown in Figure 7.10, an optimum packing ratio, at which a maximum reaction velocity ($r'_{max}$) occurs, was observed for both types of wood stick cribs. This is followed by a subsequent decrease in potential reaction velocity at greater packing ratios. However, for the finer fuel (excelsior) the initial reduction in potential reaction velocity at lower packing ratios was not observed. Rothermel attributed this to the experimental challenges associated with constructing excelsior fuel beds of low fuel loading, and the low sensitivity of the load cells [43]. Rothermel instead defined an optimum packing ratio for excelsior by adding a limiting condition of $r' = 0$ at a packing ratio of zero (where no fuel is present).

As with the experimental measurements of the reaction intensity, it is important to note that the fuel loading was not held constant across the fuel bed conditions shown in Figure 7.10. This limits the ability to draw comparisons between fuel types, and also raises questions about the applicability of the concept of an optimum packing ratio, which has been criticised by subsequent authors [62,97]. The potential issues with defining an optimum packing ratio for a given fuel element size, without consideration of the effect of fuel loading, is discussed further in Section 7.4.2, and was also considered in Chapter 5.

#### 7.4.1.3. Development of Model Equation

As shown in Figure 7.11, Rothermel determined an empirical correlation for the maximum reaction velocity ($r'_{max}$) from the experimental measurements of the potential reaction velocity ($r'$). Separate equations were found, via fitting, for the optimum packing ratio $(\beta_{op})$ and maximum reaction velocity ($r'_{max}$), both as functions of the surface-to-volume ratio,

$$r'_{max} = \frac{\sigma^{1.5}}{495 + 0.0594\sigma^{1.5}} \tag{7.39}$$

$$\beta_{op} = 3.348\sigma^{-0.8189} \tag{7.40}$$

Combining both of the above equations provides an equation for the potential reaction velocity ($r'$),

$$r' = r'_{max}\left(\frac{\beta}{\beta_{op}}\right)^{A}\exp\left[A\left(1-\frac{\beta}{\beta_{op}}\right)\right] \tag{7.41}$$

Where $A$ is an 'arbitrary variable' [43],

$$A = \frac{1}{4.774\sigma^{0.1} - 7.27} \tag{7.42}$$

Rothermel [43] notes that these empirical formulations were specifically intended to constrain reaction velocity predications to physically possible values when extrapolated for use beyond the fuel conditions used in model development i.e. preventing negative or infinite values.

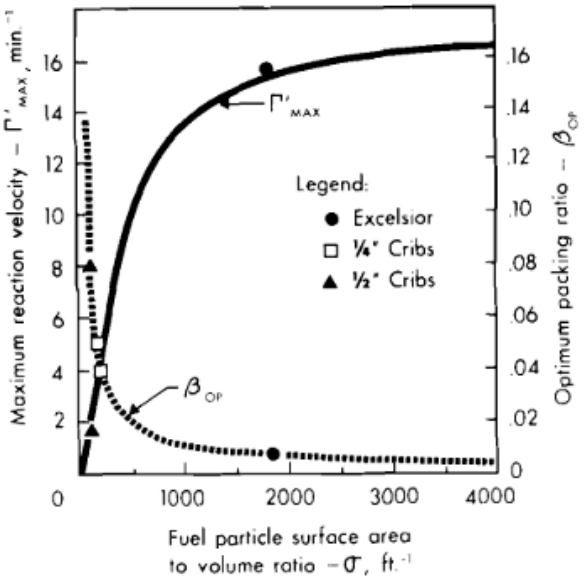


**Figure 7.11 - Experimental determination of maximum reaction velocity as a function of surface-to-volume ratio. Extracted from Rothermel (1972)** [43]

### 7.4.2. Optimum Packing Ratio

#### 7.4.2.1. Physical Meaning

As discussed in Section 7.4.1, the optimum packing ratio $(\beta_{op})$ is the fuel bed packing ratio at which the maximum reaction velocity occurs. The packing ratio $(\beta)$ describes the compactness of the fuel bed and (as discussed in Chapters 2 and 3) is commonly expressed as the ratio of the bulk density $(\rho_b)$ and the particle density $(\rho_p)$,

$$\beta = \frac{\rho_b}{\rho_p} \tag{7.43}$$

#### 7.4.2.2. Experimental Determination

As described in Section 7.4.1, the optimum packing ratio was determined from the same experimental series used to determine the reaction intensity and reaction velocity. In these experiments, mass loss measurements were obtained for three fuel types (excelsior, ½ inch stick and ¼ inch stick wood cribs) at various packing ratios. This allowed the empirical identification of the optimum packing ratio for each fuel type.

For the wood cribs, the reaction velocity initially increased with increasing packing ratio, before reaching a maximum value (at the optimum packing ratio) and subsequently decreasing at higher packing ratios. However, as discussed in Section 7.4.1, and as shown in Figure 7.10, for excelsior fuel beds, no decrease in reaction velocity was observed at lower packing ratios. Instead, an optimum packing ratio is determined only by adding the limiting case of $r = 0$ for $\beta = 0$ (no fuel present).

#### 7.4.2.3. Development of Model Equation

An empirical formulation for the optimum packing ratio ($\beta_{op}$), as a function of surface-to-volume ratio ($\sigma$), was obtained via fitting of the experimental data,

$$\beta_{op} = 3.348\sigma^{-0.8189} \tag{7.44}$$

As mentioned in Section 7.4.1, subsequent authors have questioned the suitability of the optimum packing ratio concept [62,97]. These experiments did not control for fuel loading, and the resulting empirical formulation for the optimum packing ratio is a function only of the fuel element surface-to-volume ratio. This implies that the optimum packing ratio of two fuel beds, composed of identical fuel elements, but with different fuel loadings, will have an identical optimum packing ratio, however in reality the fuel loading will also affect the optimum packing ratio (as previously discussed in Chapter 5).

### 7.4.3. Net Fuel Loading

#### 7.4.3.1. Physical Meaning

The net fuel loading ($w_n$) is the total dry fuel loading following correction for the moisture and mineral contents, and the presence of other non-combustibles.

#### 7.4.3.2. Development of Model Equation

The net fuel loading ($w_n$) was defined by Rothermel [43] as,

$$w_n = \frac{w_o}{1 + S_T} \tag{7.45}$$

Where $w_o$ is the oven-dry fuel loading and $S_T$ is the total mineral content (ratio of mineral mass to dry fuel mass).

### 7.4.4. Mineral Damping Coefficient

#### 7.4.4.1. Physical Meaning

The mineral damping coefficient ($\eta_s$) accounts for the effect of the silica-free mineral content ($S_e$) on the reaction velocity. Past studies have shown the significant effect that mineral content can have on the pyrolysis and energy content of a fuel [369–372]. The inorganic properties of wildland fuels are dependent upon a number of factors including: species; soil properties;

weather conditions (e.g. drought); plant development stage; fertilizer use; and vegetation component (e.g. needles vs branches) [373]. Defining the mineral content of a fuel is further complicated by the unequal effect of various components of ash, which limits the ability to predict pyrolysis behaviour from a bulk total mineral content value [374].

#### 7.4.4.2. Experimental Determination

Rothermel derived the mineral damping coefficient from the previous TGA experiments conducted by Philpot [374] for a variety of natural fuels. Philpot [145,374] observed an inverse relationship between the pyrolysis rate and the silica-free ash content (for $S_E$ < 12 %). This trend is shown in Figure 7.12, which is taken from a later publication by Philpot [145], as the current author was unable to access the original report cited by Rothermel [43].

Philpot observed lower pyrolysis onset temperatures and endothermic amplitudes for higher mineral content fuels, along with increased char residue [145]. However, the decomposition rate was not affected by the silica content [43].

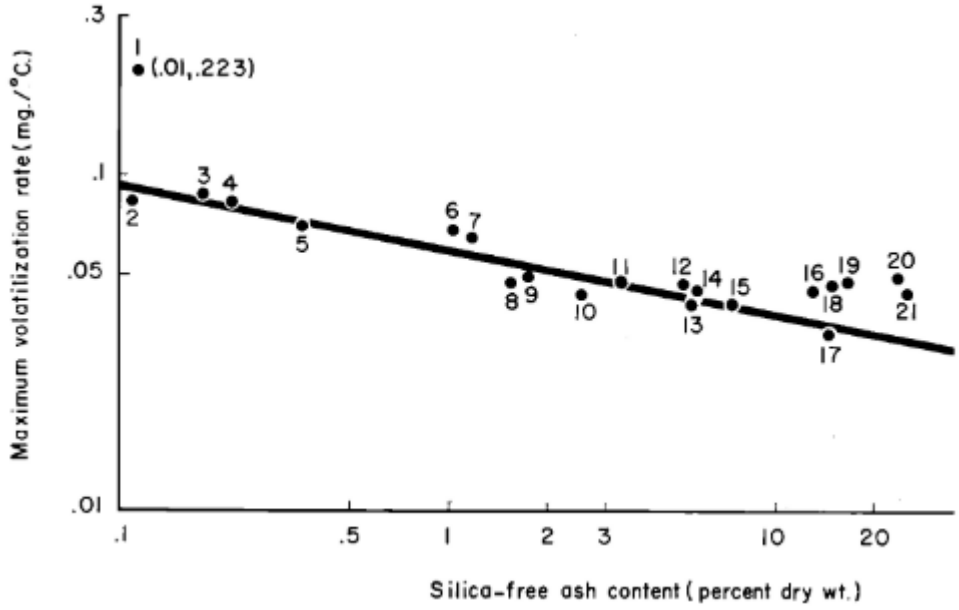


**Figure 7.12 – Relationship between maximum volatilisation rate and the silica-free ash content for a wide range of wildland fuels. Extracted from Philpot (1970)** [145]

#### *7.4.4.3. Development of Model Equation*

Rothermel [43] derived an empirical equation for the mineral damping coefficient, applying a curve fitting to Philpot's experimental data as shown in Figure 7.13. Prior to this, the decomposition rates measured by Philpott were normalised with respect to the maximum decomposition rate measured for cellulose with a mineral content of 0.0001. Rothermel [43] assumed that the mineral content would have a similar effect on the normalised reaction intensity as the observed effect on the normalised decomposition rates. Based on this assumption, a curve-fit with the following equation was obtained,

$$\eta_s = 0.174 S_e^{-0.19} \tag{7.46}$$

This considers the effective (silica-free) mineral content of fuels ($S_e$), since Philpot observed that silica had a negligible effect on pyrolysis.

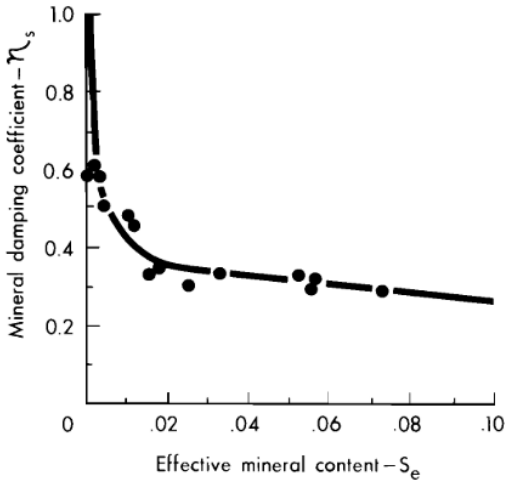


**Figure 7.13 - Determination of the mineral damping coefficient as a function of the effective mineral content. Extracted from Rothermel (1972)** [43]

### 7.4.5. Moisture Damping Coefficient

#### 7.4.5.1. Physical Meaning

The moisture damping coefficient ($\eta_M$) accounts for the effect of fuel moisture on the reaction velocity. An increased moisture content can result in a reduction in spread rate since additional energy is required for its volatilisation and removal. Moisture vapour can also inhibit flame spread if dilution of the pyrolysis gases occurs [375].

#### 7.4.5.2. Development of Model Equation

The moisture damping coefficient was empirically calculated from no-wind, no-slope flame spread experiments across a range of FMC values,

$$\eta_M = 1 - 2.59\frac{M_f}{M_x} + 5.11\left(\frac{M_f}{M_x}\right)^2 - 3.52\left(\frac{M_f}{M_x}\right)^3 \quad (7.47)$$

Where $M_f$ is the FMC ratio, and $M_x$ is the moisture content of extinction, defined as 'the dead fuel moisture content at which a fire will no longer spread with a uniform flame front and the model predicts zero spread rate' [376]. Rothermel suggested that, for dead fuels, the moisture of extinction typically ranges between 0.1 and 0.4.

## 7.5. Summary of Original Rothermel Equations

**Rate of Spread**

$$R = \frac{I_R \xi (1 + \phi_w + \phi_s)}{\rho_b \epsilon Q_{ig}} \tag{7.48}$$

**Reaction Intensity**

$$I_R = r' w_n h \eta_M \eta_s \tag{7.49}$$

**Propagating Flux Ratio**

$$\xi = (192 + 0.2595\sigma)^{-1} \exp[(0.792 + 0.681\sigma^{0.5})(\beta + 0.1)] \tag{7.50}$$

**Wind Factor**

$$\phi_w = C U^B \left(\frac{\beta}{\beta_{op}}\right)^{-E} \tag{7.51}$$

$$C = 7.47 \exp(-0.133\sigma^{0.55}) \tag{7.52}$$

$$B = 0.02526\sigma^{0.54} \tag{7.53}$$

$$E = 0.715 \exp(-3.59 \times 10^{-4}\sigma) \tag{7.54}$$

**Slope Factor**

$$\phi_s = 5.275\beta^{-0.3}(\tan\phi)^2 \tag{7.55}$$

**Oven-Dry Bulk Density**

$$\rho_b = \frac{w_o}{\delta} \tag{7.56}$$

**Effective Heating Number**

$$\epsilon = \exp(-138/\sigma) \tag{7.57}$$

**Heat of Pre-Ignition**

$$Q_{ig} = 250 + 1116 M_f \tag{7.58}$$

**Reaction Velocity**

$$r' = r'_{max} \left(\frac{\beta}{\beta_{op}}\right)^A \exp\left[A\left(1 - \frac{\beta}{\beta_{op}}\right)\right] \tag{7.59}$$

$$A = \frac{1}{4.774\sigma^{0.1} - 7.27} \tag{7.60}$$

**Maximum Reaction Velocity**

$$r'_{max} = \sigma^{1.5}(495 + 0.0594\sigma^{1.5})^{-1} \tag{7.61}$$

**Optimum Packing Ratio**

$$\beta_{op} = 3.348\sigma^{-0.8189} \tag{7.62}$$

**Net Fuel Loading**

$$w_n = \frac{w_o}{1 + S_T} \tag{7.63}$$

**Mineral Damping Coefficient**

$$\eta_s = 0.174 S_e^{-0.19} \tag{7.64}$$

**Moisture Damping Coefficient**

$$\eta_M = 1 - 2.59\frac{M_f}{M_x} + 5.11\left(\frac{M_f}{M_x}\right)^2 - 3.52\left(\frac{M_f}{M_x}\right)^3 \tag{7.65}$$

## 7.6. Modifications to Original Rothermel Equations

In this study, the only modifications applied to Rothermel's original flame spread equations were those suggested by Albini [330]. Only the modifications applicable to homogenous fuel beds were incorporated, as summarised in Table 7.1. Albini's other modifications relate to the live fuel moisture of extinction, or to mixed fuel bed weighting factors, and therefore are not relevant to this study which considers only homogenous fuel beds composed of dead fuels.

**Table 7.1 - Summary of modifications to original Rothermel flame spread equations**

| Modified Parameter | Original Rothermel | Albini Modification |
|---|---|---|
| Combustible Dry Fuel Loading ($w_n$) | $w_n = \frac{w_o}{1 + S_T}$ | $w_n = w_o(1 - S_T)$ |
| Mineral Damping Coefficient ($\eta_s$) | $\eta_s \geq 0$ | $\eta_s \leq 1$ |
| Reaction Velocity Variable (A) | $A = \frac{1}{4.774\sigma^{0.1} - 7.27}$ | $A = 133\sigma^{-0.7913}$ |

### 7.6.1. Combustible Dry Fuel Loading

Albini defined the combustible dry fuel loading ($w_n$) as,

$$w_n = w_o(1 - S_T) \tag{7.66}$$

Rather than the form suggested by Rothermel,

$$w_n = \frac{w_o}{1 + S_T} \tag{7.67}$$

Where $w_o$ is the total dry fuel loading, and $S_T$ is the total mineral content of the fuel.

Albini more accurately describes the net combustible fuel loading, since the oven-dry fuel loading $w_o$ includes the mineral content. Therefore, the net combustible fuel loading is given by the product of the oven-dry fuel loading and the non-mineral content of the fuel $(1 - S_T)$.

The difference between Rothermel and Albini's equations can be illustrated by considering a hypothetical case in which the oven-dry fuel loading is 10 lbs/ft.$^2$ and the total mineral content is 0.1,

For the original Rothermel equation,

$$w_n = \frac{w_o}{1+S_T} = \frac{10}{1+0.1} = 9.09 \text{ lbs/ft.}^2 \tag{7.68}$$

While for Albini's modified equation,

$$w_n = w_o(1 - S_T) = 10(1 - 0.1) = 9 \text{ lbs/ft.}^2 \tag{7.69}$$

### 7.6.2. Mineral Damping Coefficient

Albini imposed an upper limit of $\eta_s = 1$ on the mineral damping coefficient. Originally, no limit was imposed by Rothermel on the mineral damping coefficient, and a mineral damping coefficient of $\eta_s > 1$ would occur for $S_e < 1.5 \times 10^{-4}$.

However, (as described in Section 7.4.4) the damping coefficient was empirically determined from the normalised decomposition rate. Normalisation was with respect to the decomposition rate measured for cellulose with a mineral content of 0.0001. Therefore, physically unrealistic mineral damping coefficient estimates will be calculated within the region $1 \times 10^{-4} \leq S_e \leq 1.5 \times 10^{-4}$. For Rothermel's empirical derivation [43], no decomposition rate measurements were available for effective mineral contents lower than $1.5 \times 10^{-4}$, and therefore applying a limit of unity with the maximum normalised decomposition rate appears valid.

### 7.6.3. Reaction Velocity Variable

Albini proposed an alternative formula for the arbitrary variable A, in the reaction velocity calculation,

$$A = 133\sigma^{-0.7913} \tag{7.70}$$

Rather than the form suggested by Rothermel,

$$A = \frac{1}{4.774\sigma^{0.1} - 7.27} \tag{7.71}$$

Albini's alternative equation also fits the original experimental data but prevents negative values of $A$ from occurring (and hence reaction velocities greater than the maximum reaction velocity). Whereas in Rothermel's original equation, A has a negative value for $\sigma < 67.63$.

This modification will result in some variation in calculated spread rates between the two methods. Albini suggested that discrepancies would be greatest at high packing ratios and at surface-to-volume ratios of around 1,000 $ft^{-1}$.

## 7.7. Model Input Parameters

The model requires as inputs six fuel properties (heat content, moisture content, total and effective mineral contents, fuel density, and surface-to-volume ratio), three fuel bed properties (oven-dry fuel loading, fuel height, and moisture of extinction), and two environmental parameters (mid-flame wind speed, and slope angle) [356].

### 7.7.1. Fuel Properties

#### *7.7.1.1. Heat Content* ($h$)

In Rothermel's model, the heat content ($h$) of fuels is described by their low heat of combustion value. There is a direct, linear relationship between the assumed heat content value and the fire behaviour predictions of the model.

A generic value for forest fuels of 8,000 BTU/lb (18,608 kJ/kg) [376], is specified in all 53 of the standard fuel models [360]. However in reality, the heat content can vary across fuel species and with fuel condition [30,50]. For example, the heat content of wildland fuels can vary seasonally [369,379–381] and may depend on the level of decomposition or weathering [30,50].Numerous studies have investigated the heat content of wildland fuels, typically via

bomb calorimetry [232,369,377–379,382–384]. Measured heat contents of pine species, from a number of past studies are summarised in Table 7.2.

**Table 7.2 - Overview of heat content value for various pine needle species from previous experimental studies**

| Study | Pine Needle Species | Heat Content [BTU/lb] (Reported Range) |
|---|---|---|
| Countryman, 1964 [382] | *Pinus Ponderosa* | 9,776 |
| Hough, 1969 [369] | *Pinus taeda* | 8,895 [8,744 – 9.086] |
| Hough, 1969 [369] | *Pinus elliotti* | 9,365 [9,320 – 9,420] |
| Hough, 1969 [369] | *Pinus clausa* | 9,412 [8,751 – 9,791] |
| Hough, 1969 [369] | *Pinus banksiana* | 9,177 |
| Rothermel, 1976 [367] | *Pinus Ponderosa* | 8,821 |
| Ovington & Heitkamp, 1960 [378] | *Pinus nigra* | 8,944 [8,740 – 9,167] |
| Ovington & Heitkamp, 1960 [378] | *Pinus sylvestris* | 8,908 |

#### *7.7.1.2. Moisture Content* $(M_f)$

The moisture content $(M_f)$ is the ratio of moisture mass to the oven-dry fuel mass. The moisture content has a major influence on the heat of pre-ignition of the fuel (negative relationship), and is the main independent variable included in its calculation [43]. Higher moisture contents will also have a significant damping effect on the calculated reaction velocity, and hence the reaction intensity and overall spread rate.

#### *7.7.1.3. Total Mineral Content* $(S_T)$

The total mineral content $(S_T)$ is the ratio of the total mineral weight to the dry fuel weight. The mineral content has a significant damping effect on the calculated reaction velocity, and hence the reaction intensity and overall spread rate. However, as described in Section 7.4.4, Rothermel [43] derived the mineral damping coefficient from the previous TGA experiments conducted by Philpot [374]. During these experiments, Philpot observed that the fuel decomposition rate was unaffected by the silica content, and therefore the effective (silica-free) mineral content is considered when calculating the damping effect.

#### *7.7.1.4. Effective Mineral Content* $(S_E)$

The effective mineral content $(S_E)$ is the ratio of the silica-free mineral weight to the dry fuel weight. The effective mineral content is the independent variable considered when calculating the damping effect of mineral presence. An increase in the effective mineral content (up to around 0.12) results in a reduction in the mineral damping coefficient (and hence the reaction intensity and overall spread rate). As per the TGA results of Philpot [374], no further decrease in the mineral damping coefficient occurs for effective mineral contents greater than 0.12.

#### *7.7.1.5. Particle Density* $(\rho_p)$

The particle density $(\rho_p)$ is the ratio of the oven-dry fuel particle mass to the fuel particle volume. Variations in particle density alter the packing ratio and therefore affects each of the heat source terms in the spread rate equation. A negative trend exists between particle density and both reaction intensity and propagating flux ratio, while a positive trend exists with both the wind and slope coefficient. For quiescent flame spread, a slight negative relationship exists between particle density and the spread rate, however Rothermel did not evaluate this effect experimentally [360].

#### *7.7.1.6. Surface-to-Volume Ratio ($\sigma$)*

The surface-to-volume ratio ($\sigma$) is positively correlated with numerous model properties including: reaction intensity, propagating flux ratio, effective heating number, wind coefficient and the overall heat sink term. Generally, for loosely packed fuel beds, increases in surface-to-volume ratio will result in an increased RoS, whereas a decrease in RoS will occur in tightly packed fuel beds [376]. Andrews previously illustrated the effect of surface-to-volume ratio, for an exemplar case involving a short grass fuel bed (standard model 1) as shown in Figure 7.14.

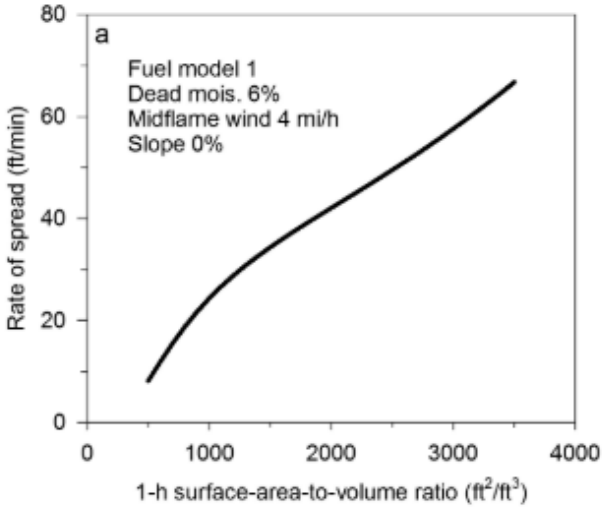


**Figure 7.14 - The effect of surface-to-volume ratio on Rothermel model predictions of spread rate. Extracted from Andrews (2018)** [360]

### 7.7.2. Fuel Bed Properties

In addition to the fuel element properties, model predictions are also affected by the fuel bed properties. Three fuel bed parameters (oven-dry fuel loading, fuel height and moisture of extinction) must be specified as model inputs.

#### *7.7.2.1. Oven-Dry Fuel Loading ($w_o$)*

The oven-dry fuel loading ($w_o$) describes the dry mass of fuel per unit area and has an influence throughout the model. Fuel loading is positively correlated with bulk density/packing ratio (for a constant fuel bed height), as well as with the magnitude of the overall heat source term. The resulting packing ratio increase for increased fuel loading at a constant fuel depth, will also increase the propagating flux ratio, and decrease the wind and slope factors (initially rapidly and then at a reduced rate as the fuel bed packing increases).

#### *7.7.2.2. Fuel Height ($\delta$)*

The fuel height ($\delta$) describes the average fuel height above the ground. The fuel height is often hard to define as a single value for real fuels and this is often seen as a weakness of the Rothermel model [360]. Burgan and Rothermel recommended that, for a litter layer, fuel height should be defined as the average fuel bed depth, ignoring protruding fuel elements [368], as shown in Figure 7.15.


**Figure 7.15 - Illustration of fuel height definition for a litter layer**

Rothermel's model has a high sensitivity to the fuel height value, despite the difficulty in characterising this property [385]. Within the model, fuel height affects the value of both the bulk density and the packing ratio, therefore affecting the overall magnitude of the fuel heat sink term, and the wind and slope factors. The propagating flux and reaction intensity will also vary with fuel height, although the effect will depend upon the proximity of the resulting packing ratio to the optimum packing ratio.

#### *7.7.2.3. Moisture of Extinction ($M_x$)*

The moisture of extinction ($M_x$) is the minimum moisture content at which flame spread is not sustained. Rothermel suggested that, for dead fuels, the moisture of extinction typically ranges between 0.1 and 0.4,[17] and assumed a constant value of 0.3 during model development [43]. This value represents the typical fibre saturation point of wood [43,386]; the point at which no free water is present, only water contained within cell walls [387]. The same value was specified in the initial 11 fuel models proposed by Rothermel, allowing the sensitivity to other model parameters to instead be explored [43,388]. In the 13 revised fuel models presented by Albini, a distinct extinction moisture value was specified for each model.

In reality, the extinction value of a fuel bed may depend upon environmental (e.g. wind, slope, RH) and fuel conditions (e.g. fuel loading, Leaf Area Index, fuel surface area, thermochemical properties, fuel species) [64,232,347,354,389,390]. Linear extrapolation of the experiments conducted at various FMC's by Rothermel and Anderson [125], suggested a moisture extinction value of 0.24 for Ponderosa Pine needle beds and 0.22 for White Pine needle beds. In a similar later study, Anderson [133] measured moisture extinction values of 0.242 for both Ponderosa Pine and Western White Pine needles. Anderson observed a lower extinction moisture for Lodgepole Pine needles, and attributed the inter-species variation to a dependence on porosity, but this was not investigated further.

Recent experimental and numerical analysis by Awad *et al.* [64] observed that the moisture extinction value (of an excelsior fuel bed) was strongly dependent on the fuel loading (before becoming independent of fuel loading at higher loadings). The extinction value was also strongly affected by the Leaf Area Index, but not by variations in bulk density; however only a single fuel bed bulk density was studied experimentally by Awad *et al.*

[17] This moisture of extinction range corresponds to the range observed by Blackmarr in a series of ignition experiments involving slash pine litter and various ignition source sizes [141]. However, confusingly Blackmarr notes that, in the field, slash pine litter may be ignited at moisture contents as high as 50 %.

The difficulty in accurately defining a suitable moisture of extinction led Wilson to propose a simplified equation for the fuel moisture damping coefficient, in which moisture damping effects were decoupled from extinction phenomena. As a result, any curve fitting of the experimental data (of the effect of FMC) when defining the moisture damping coefficient must only meet a single condition ($\eta_M = 1$ at $M_f = 0$), whereas the curve fit used by Rothermel had to also satisfy the condition: $\eta_M = 0$ at $M_f = M_x$.

The sensitivity of the Rothermel model to alterations in this moisture of extinction value are greatest for cases in which the actual FMC is similar to the extinction moisture value [376]. The predicted RoS increases as the difference between the actual FMC and the extinction moisture value increases (as fuels dry and FMC decreases), with the reverse occurring as FMC increases. Therefore, the significance of this value, on spread rate and fire intensity, is greater in 'poor burning conditions' [332] which may be of greater importance for prescribed fire applications.

### 7.7.3. Environmental Parameters

#### *7.7.3.1. Mid-flame Wind Speed*

The mid-flame wind speed represents the average wind speed at the mid-height of the flame (from the fuel surface) [385], and is specified based upon measurement or prediction of wind speeds in the area of interest. For modelling purposes, it is important to define a fixed wind speed height, given the variation in wind speed with height. However, it is often difficult to determine an appropriate mid-flame wind speed, since wind-speed measurements and predictions traditionally occur at a height of 20 ft. above the fuels [391].

Albini and Baughman therefore provided a method for calculating the mid-flame wind speed based upon this typical 20 ft. wind speed data [392]. For wind flow above a fuel layer, by assuming a logarithmic wind profile, the following relationship between 20 ft. wind speed ($U_{20+H}$) and mid-flame wind speed ($\overline{\overline{U}}$) was calculated,

$$\frac{\overline{\overline{U}}}{U_{20+H}} = \frac{1 + 0.36H/H_F}{\ln\left(\frac{20 + 0.36H}{0.13H}\right)} \left[ \ln\left( \frac{\frac{H_F}{H} + 0.36}{0.13} \right)^{-1} \right] \tag{7.72}$$

Where $H$ is the fuel height and $H_f$ is the flame height.

This method is limited by a lack of consideration of the fire-induced flow effects, a shortcoming that is shared by the Rothermel model as a whole, in which these effects are not explicitly considered. This is particularly relevant for no-wind flame spread scenarios, where the contribution of fire-induced flows are of particular importance.

#### *7.7.3.2. Slope Angle ($\phi$)*

The slope angle ($\phi$) is the angle between the fuel bed and the horizontal plane, and describes the fuel bed steepness. Therefore, a horizontal (no-slope) fuel bed has a slope angle of 0°, while upslope fuel beds have a positive slope angle between 0° and 90°. In this manner, upslope fuel beds will result in a positive slope factor, and lead to predictions of increased spread rates.

## 7.8. Fuel Height Sensitivity

The height of porous wildland fuel beds can affect the overall flame spread behaviour, as shown in Chapters 5 and 6. The fuel height depends both upon the total amount of fuel present and the compactness (or packing) of the fuel. The height can therefore be manipulated by altering either the fuel loading (for a constant bulk density) or the bulk density (for a constant fuel loading, in a fuel bed of fixed area). Increases in fuel loading (at a constant bulk density) may increase the fuel available for combustion and hence the total energy release. Decreasing the bulk density (at a constant fuel loading) results in a less compact fuel bed of greater porosity. Lower drag forces will be exerted by a more porous fuel bed, which may increase in-bed convective heat transfer, and potentially increasing oxygen supply to the combustion region.

The presence of these in-bed phenomena leads to a more complicated fuel height effect in porous fuels than is encountered in classical, solid-surface flame spread theory. Indeed, for solid fuels, conduction is typically assumed to dominate solid-surface heat transfer [53]. It is therefore important that a porous flame spread model is able to incorporate the complex effects of fuel height in any flame spread predictions. However, it has been suggested [348] that the Rothermel model may be over-sensitive to fuel height, resulting in under-predictions of spread rate in thinner fuel beds.

Cruz and Fernandes [348] reviewed several previous Rothermel model evaluation studies [349,393,394] in which large under-predictions of RoS occurred when modelling flame spread in litter fuels. An oversensitivity to fuel height was one of a number of possible explanations for this under-prediction bias. Other suggested explanations include:

- A limited ability to define the contribution of fine fuel combustion in heterogeneous fuel beds.
- A lack of consideration within the model of any fuel bed heterogeneity (e.g. varying compaction levels in fuel bed with depth).
- A lack of accurate determination of extinction moisture content.
- The presence of wind profiles outside the models limits of applicability.

Cruz and Fernandes [348] suggested that height oversensitivity may be particularly acute for matt-type fuel beds (e.g. pine needle litter beds). Cruz *et al.* evaluated the performance of the Rothermel model across 29 existing published studies involving comparison of predictions with experimental or wildfire observations [395]. They observed greater Mean Absolute Percent Errors (MAPE) for logging slash and understory fuels than in other fuel types (grassland and shrubland fuels). The increased MAPE values, and a tendency for under-prediction, were attributed to the fuel height over-sensitivity.

Poor model performance has also been observed and assessed in other fuel types. A notable study in which fuel height oversensitivity was identified is the work of Gould [342]. Gould compared predictions from the Rothermel model with observations from a series of Australian grassland fire experiments. Sensitivity of spread rate predictions to fuel height was found to be greater than the experimentally observed effect of fuel height. As a result, spread rates were under-predicted for fuel heights lower than 0.15 m, while over-predictions occurred for fuel heights greater than 0.25 m and wind speeds greater than 3.5 m/s. Similarly, the model was

observed to be oversensitive to the effect of bulk density, but both predicted and observed spread rates were unaffected by fuel loading.

However, past observations of model performance as a function of fuel height have not been in unanimous agreement. Brown [354] observed reduced model performance at lower packing ratios (higher fuel heights), which is the opposite trend to that observed in the aforementioned studies. However, Brown was studying highly discontinuous slash fuel beds, which may be expected to vary considerably in behaviour compared to the more continuous fuel beds studied in this thesis. In the latter case, high levels of fuel connectivity exist even at lower packing ratios.

Brown's study highlights the importance of understanding the effect of fuel height on a holistic, physical basis within a given scenario, even if Rothermel's model does not explicitly incorporate these physical phenomena. During the development of a second generation model, Catchpole *et al.* noted that the effect of fuel loading is dependent upon the manner in which the fuel loading ($\rho_b \beta \delta$) is changed [69]. They observed only a slight effect on spread rate of increases in fuel depth at a constant packing ratio, but at constant depth, increases in packing ratio led to a reduction in spread rate. Their observations were in contrast to the earlier findings of Wilson, who observed a positive correlation between spread rate and the square root of the fuel bed height, at quiescent conditions [62]. Catchpole *et al.* suggested that this may indicate that the effect of fuel bed depth is dependent upon the relative importance of heat transfer mechanisms (radiative vs. convective), which stresses the need for a greater understanding of these physical processes and their relationship to fuel structure.

Improving the predictive performance of the Rothermel model at various fuel heights is of great importance within prescribed fire science, given the focus on fuel manipulation and fuel load reduction. Dell'Orfano [345] conducted a sensitivity study of the BEHAVE system (in which surface spread rate predictions are based on Rothermel's model) for pine-oak forests during typical prescribed burning conditions, with over-predictions occurring as a result of oversensitivity to both fuel bed height and fine fuel surface-to-volume ratio.

## 7.9. Model Implementation

In this study, Rothermel's original mathematical equations, along with the later modifications by Albini, were incorporated into a MATLAB code (using MATLAB Version R2020a) [396]. The performance of the Rothermel model is evaluated for matt-type, pine needle fuel beds (of various fuel height, packing ratios and fuel loadings) through comparison with the experimental observations presented in Chapter 5. Comparison of model parameters with experimental observations of closely related physical properties allows further investigation into the causes for model discrepancies. Finally, the suitability of previously proposed modifications to Rothermel's model are assessed for the quiescent, low-intensity flame spread scenario considered in this thesis.

### 7.9.1. Fuel Models

For evaluation of the Rothermel model, a custom fuel model was defined with parameters chosen to represent the fuel beds studied in Chapter 5. These fuel beds were constructed from dead needles of either Pitch Pine or Pitch-Loblolly hybrid Pine, with the fuel properties specified for each species summarised in Table 7.3.

**Table 7.3. - Summary of needle properties for each pine needle species**

| Fuel Type | Dia. [in] | h [Btu/lb] | $\sigma$ [$ft^{-1}$] | $\rho_p$ [$lbs/ft.^3$] |
|---|---|---|---|---|
| Pitch Pine | 0.052 | 8000 | 1543 | 44.1 |
| Pitch-Loblolly Hybrid Pine | 0.053 | 8000 | 1493 | 45.3 |

As shown in Table 7.3, there was a minor variation in the fuel element particle density and surface-to-volume ratio ($\sigma$) of each pine needle species. Within Rothermel's model, particle density is inversely correlated with the propagating flux ratio and reaction intensity, and hence, in the absence of wind or slope, is inversely correlated with spread rate. Therefore, species-specific fuel models were constructed for each fuel bed condition studied in Chapter 5. These fuel bed conditions are summarised for each fuel species in Table 7.4 and Table 7.5.

**Table 7.4 - Summary of fuel bed properties for each fuel bed condition for Pitch Pine fuel beds**

| Wet Fuel Loading | | Bulk Density | | Fuel Height | | $\alpha\sigma\delta$ | FMC |
|---|---|---|---|---|---|---|---|
| [$kg/m^2$] | [$lbs/ft.^2$] | [$kg/m^3$] | [$lbs/ft.^3$] | [m] | [ft.] | | [%] |
| 0.2 | 0.04 | 10 | 0.62 | 0.02 | 0.07 | 100 | 10.1 ± 1.1 |
| 0.2 | 0.04 | 20 | 1.25 | 0.01 | 0.03 | 49 | 10.0 ± 1.2 |
| 0.4 | 0.08 | 10 | 0.62 | 0.04 | 0.13 | 200 | 9.6 ± 0.8 |
| 0.4 | 0.08 | 20 | 1.25 | 0.02 | 0.07 | 98 | 9.6 ± 0.6 |
| 0.6 | 0.12 | 10 | 0.62 | 0.06 | 0.20 | 300 | 10.9 ± 2.1 |
| 0.6 | 0.12 | 20 | 1.25 | 0.03 | 0.10 | 148 | 9.8 ± 0.7 |
| 0.8 | 0.16 | 10 | 0.62 | 0.08 | 0.26 | 399 | 10.1 ± 0.5 |
| 0.8 | 0.16 | 20 | 1.25 | 0.04 | 0.13 | 197 | 10.2 ± 0.7 |
| 0.8 | 0.16 | 40 | 2.50 | 0.02 | 0.07 | 96 | 10.1 ± 0.9 |
| 1.2 | 0.25 | 20 | 1.25 | 0.06 | 0.20 | 295 | 11.3 ± 0.3 |
| 1.6 | 0.33 | 20 | 1.25 | 0.08 | 0.26 | 394 | 12.3 ± 1.7 |

**Table 7.5 - Summary of fuel bed properties for each fuel bed condition for Pitch-Loblolly Pine fuel beds**

| Wet Fuel Loading | | Bulk Density | | Fuel Height | | $\alpha\sigma\delta$ | FMC |
|---|---|---|---|---|---|---|---|
| [$kg/m^2$] | [$lbs/ft.^2$] | [$kg/m^3$] | [$lbs/ft.^3$] | [m] | [ft.] | | [%] |
| 0.2 | 0.04 | 10 | 0.62 | 0.02 | 0.07 | 97 | 16.6 ± 1.9 |
| 0.2 | 0.04 | 20 | 1.25 | 0.01 | 0.03 | 48 | 16.6 ± 1.9 |
| 0.4 | 0.08 | 10 | 0.62 | 0.04 | 0.13 | 194 | 15.3 ± 1.2 |
| 0.4 | 0.08 | 20 | 1.25 | 0.02 | 0.07 | 96 | 15.5 ± 0.3 |
| 0.6 | 0.12 | 10 | 0.62 | 0.06 | 0.20 | 290 | 15.6 ± 0.3 |
| 0.6 | 0.12 | 20 | 1.25 | 0.03 | 0.10 | 144 | 17.1 ± 0.7 |
| 0.8 | 0.16 | 10 | 0.62 | 0.08 | 0.26 | 387 | 15.9 ± 0.6 |
| 0.8 | 0.16 | 20 | 1.25 | 0.04 | 0.13 | 191 | 15.7 ± 2.4 |
| 0.8 | 0.16 | 40 | 2.50 | 0.02 | 0.07 | 93 | 16.0 ± 0.8 |

As shown in Table 7.4 and Table 7.5, several fuel properties (FMC, fuel loading and fuel height) varied at each fuel bed condition. For these parameters, the average value at a given fuel condition was specified within the model. The selection of other fuel input parameters, which were held constant across all fuel conditions, are discussed below.

#### 7.9.1.1. Heat Content

The heat content of both pine needle species was measured using bomb calorimetry, as discussed in Chapter 3. The measured heat of combustion value for both pine species were similar to the standard generic value defined by Andrews [385] (8,000 BTU/lb) and this value was used throughout this analysis.

This generic value is similar to the heat contents measured for pine species in various, previous studies (shown in Table 7.2). The heating value also varies little between the two species of interest (Pitch Pine and Pitch-Loblolly Pine), with the difference within the range of experimental uncertainty.

#### 7.9.1.2. Moisture of Extinction

In this study, as in the original Rothermel model development process [43], it was not possible to determine experimentally the moisture of extinction for each fuel bed condition as this would have required extensive testing at each fuel condition. Assuming a constant value allowed a focus on the effect of other fuel bed parameters. As in Rothermel's original model development [43], a constant moisture of extinction (30 %) was assumed for all fuel beds in this study, regardless of fuel bed structure.

#### 7.9.1.3. Mineral Contents

The values for both the total and effective mineral content were based upon the values assumed within the standard fuel models ($S_T = 0.0555$ and $S_E = 0.010$) [360]. An effort was made to determine the validity of these assumed mineral content values through comparison with post-burn measurements of the remaining mass (ash and char), collected for a subset of experiments in this study (as discussed in Chapter 4). The minimum normalised remaining mass for randomly oriented fuel beds of both species was similar to the assumed total mineral content value (0.0555). For these fuel bed conditions at which maximum fuel consumption occurred, the remaining mass was visually observed to consist primarily of ash, and therefore gives some qualitative insight into the non-combustible content of the original fuel loading.

### 7.9.2. Environmental Parameters

To represent the quiescent flame spread scenario studied in Chapter 5, all model analysis assumed the absence of external wind or slope. Therefore, a mid-flame wind speed of 0 mph and a fuel slope angle of 0° were assumed throughout. As a result, both the wind factor and slope factor are also zero, and the no-wind, no-slope flame spread rate is calculated.

### 7.9.3. Model Verification

The final version of the MATLAB code (shown in Appendix B) was subject to an initial verification via comparison with the BehavePlus fire modelling system (Version 6) [397]. BehavePlus is an open-source software package containing a number of different fire models, including the Rothermel model (which underpins the SURFACE module). While there is limited ability to manipulate model variables in BehavePlus, it offers an opportunity to verify the implementation of the Rothermel equations.

For a BehavePlus run, a fuel model selection (either a default or custom model) is required along with a number of other user-defined variables[18]. For this validation study, a series of

[18] A full description of the variables for each module in BehavePlus was provided by Andrews [385]

static[19], custom fuel models (specified via fuel parameters) were used to represent the fuel beds studied in this chapter.

In BehavePlus, the FMC, surface-to-volume ratio, and fuel loading are individually specified for each fuel size (1 hr, 10 hr and 100 hr fuels), while separate values can also be specified for live and dead fuels. In this study, fuel beds consisted only of dead, 1 hour fuels (less than ¼ in. diameter), and therefore properties for single fuel size class were defined for each fuel condition.

In all cases, the Dead Fuel Moisture of Extinction was assumed to be 30 %, while a heat content of 8,000 BTU/lb was assumed for both fuel species. These values match those used in the previously described MATLAB implementation. The minimum fuel bed depth that can be specified within BehavePlus is 0.05 ft., and therefore the two fuel bed conditions with fuel bed heights below this limit (as shown in Table 7.5), were excluded from this analysis.[20]

It is not possible to alter all of the Rothermel model variables in BehavePlus. The fuel element density, and the total and effective mineral contents are specified as constant values since 'they either have a small effect over their naturally occurring range or would be very difficult for the user to determine' [368]. Values of BehavePlus constants, as outlined by Burgan and Rothermel [368], are summarised in Table 7.6.

**Table 7.6 - Summary of model constants in BehavePlus**

| Fuel Property | Constant Value (Original BEHAVE version) |
|---|---|
| Fuel Element Density | 32 lbs/ft$^2$ |
| Total Mineral Content | 0.0555 |
| Effective Mineral Content | 0.010 |
| 10 hour Surface-to-Volume Ratio | 109 |
| 100 hour Surface-to-Volume Ratio | 30 |

The total and effective mineral contents defined here equal those specified in the MATLAB analysis. The default fuel element density differs from the density of both pine needle species studied in this chapter. Since it is not possible for the user to modify this parameter within BehavePlus, this default value was also used in the Matlab script during this verification analysis.

A mid-flame wind speed of 0 mph and a slope steepness of 0 ° was also specified, since the experiments considered were conducted in no wind, no slope conditions. Therefore, while not strictly relevant, the following run options were enabled for the SURFACE module:

- Maximum effective wind speed limit imposed.
- Wind defined as blowing upslope
- Wind and spread directions were specified in clockwise degrees from upslope.
- Fire spread was in the heading direction (with wind acting in the direction of fire spread).

[19] Static fuel models involve a fixed fuel loading for each fuel category. Alternatively, dynamic fuel models can also be specified in BehavePlus, in which curing occurs and fuel can be transferred dynamically from the live herbaceous category to 1 hour timelag categories [368].
[20] In BehavePlus the valid range of fuel bed depth values is 0.05 ft to 10.0 ft (0.02 m to 3.05 m) [385].

Spread rate predictions from BehavePlus and the custom MATLAB script were compared, and agreement was observed across all fuel bed conditions. This indicates that the Rothermel flame spread equations have been implemented as intended within this custom script and provides strong verification of this implementation. The MATLAB version is therefore used in later parts of this study, to allow the evaluation of the performance of Rothermel's model in comparison to the experimental observations presented in Chapter 5.

## 7.10. Comparison of Model Predictions and Experimental Observations

Using the flame spread equations summarised in Section 7.5 and implemented in MATLAB (script shown in Appendix B), spread rate predictions were obtained for each fuel bed condition (conditions shown in Table 7.7 and Table 7.8). Predictions of spread rate and reaction intensity are now compared to experimental observations, while possible physical explanations for any discrepancies are also investigated. There is a particular focus on the role of fuel bed compaction, and the sensitivity of the model to fuel bed height.

In addition to comparisons of predicted and observed spread rates at a given fuel condition, we are also interested in the overall trends between fuel structure and predicted spread rates. This is important in assessing the physical applicability of Rothermel's model and identifying potential limitations in the description of fuel structure and its effect on fire behaviour. Therefore, it is useful to recap the key physical observations and trends presented in earlier chapters (Chapters 4, 5 and 6).

The flame spread rate (along with flame height and Heat Release Rate (HRR)) increased with either independent increases in fuel loading or decreases in bulk density. However, neither parameter alone adequately predicted the observed variations in spread rate, and in fact, a greater correlation was observed between fuel bed height and spread rate (Figure 5.7). An additional dimensionless parameter $\alpha\sigma\delta$ (incorporating porosity ($\alpha$), surface-to-volume ratio ($\sigma$), and fuel bed height ($\delta$)) was introduced and a strong correlation with spread rate observed (Figure 5.9). The observed spread rates (along with other measured fire behaviour properties) was summarised in Table 5.1 and Table 5.2, in Chapter 5.

As discussed in Chapter 5, the flow profile is dominated by the fire-induced flow, entrained towards the approaching flame front. This entrainment flow rate is controlled by the fuel bed structure and buoyant flow profile, with the buoyant flow velocity increasing with greater fuel loading and resulting in a greater HRR. Given the entrainment of ambient air ahead of the flame front, it is expected that this flow primarily results in convective cooling of unburnt fuel.

The relative importance of the various heat transfer pathways was discussed in Chapter 6, with in-bed heating providing a greater overall contribution to the propagation energy than the above-bed flame, for the fuel beds investigated in this study. Further analysis of the measured heat fluxes, along with the development of a simple thermal model, indicated that radiative heating through the fuel bed was the primary propagation mechanism at lower values of $\alpha\sigma\delta$ ($\alpha\sigma\delta \leq 200$). While for higher $\alpha\sigma\delta$ cases, an increased contribution from radiative (above-bed) flame heating was observed. These physical insights are used to inform the Rothermel model evaluation in this section.

### 7.10.1. Rate of Spread

A summary of key input parameters for each fuel bed condition (FMC ($M_f$), fuel loading ($w_n$), and packing ratio ($\beta$)) is shown in Table 7.7, along with selected intermediate values (reaction velocity ($r'$), moisture damping coefficient ($\eta_M$), propagating flux ratio ($\xi$), and reaction intensity ($I_R$)), calculated using the approaches set out by Rothermel [43]. These values also enable the final calculation of the predicted Rate of Spread (RoS) at each fuel bed condition.

**Table 7.7 - Summary of input parameters and intermediate values for each fuel bed condition**

| Fuel Type | Avg. $M_f$ | $w_n$ [lbs/ft.$^2$] | $\beta$ | $r'$ [min$^{-1}$] | $n_M$ | $\xi$ | $I_R$ [Btu/ft$^2$ min] |
|---|---|---|---|---|---|---|---|
| Pitch Pine | 0.101 | 0.04 | 0.014 | 13.8 | 0.57 | 0.039 | 929 |
| | 0.100 | 0.04 | 0.028 | 9.2 | 0.57 | 0.057 | 620 |
| | 0.096 | 0.07 | 0.014 | 13.8 | 0.58 | 0.039 | 1870 |
| | 0.096 | 0.07 | 0.028 | 9.2 | 0.58 | 0.057 | 1250 |
| | 0.109 | 0.11 | 0.014 | 13.8 | 0.56 | 0.039 | 2770 |
| | 0.098 | 0.11 | 0.028 | 9.2 | 0.58 | 0.057 | 1870 |
| | 0.101 | 0.14 | 0.014 | 13.8 | 0.57 | 0.039 | 3720 |
| | 0.102 | 0.14 | 0.028 | 9.2 | 0.57 | 0.057 | 2480 |
| | 0.101 | 0.14 | 0.055 | 3.3 | 0.57 | 0.121 | 870 |
| | 0.113 | 0.21 | 0.028 | 9.2 | 0.56 | 0.057 | 3720 |
| | 0.123 | 0.28 | 0.028 | 9.2 | 0.55 | 0.057 | 4860 |
| Pitch-Loblolly Hybrid Pine | 0.166 | 0.03 | 0.014 | 13.8 | 0.54 | 0.038 | 819 |
| | 0.166 | 0.03 | 0.028 | 9.3 | 0.54 | 0.056 | 551 |
| | 0.153 | 0.07 | 0.014 | 13.8 | 0.54 | 0.038 | 1660 |
| | 0.155 | 0.07 | 0.028 | 9.3 | 0.54 | 0.056 | 1110 |
| | 0.156 | 0.10 | 0.014 | 13.8 | 0.54 | 0.038 | 2480 |
| | 0.171 | 0.10 | 0.028 | 9.3 | 0.53 | 0.056 | 1650 |
| | 0.159 | 0.13 | 0.014 | 13.8 | 0.54 | 0.038 | 3300 |
| | 0.157 | 0.13 | 0.028 | 9.3 | 0.54 | 0.056 | 2220 |
| | 0.160 | 0.13 | 0.055 | 3.3 | 0.54 | 0.115 | 790 |

A comparison of the predicted RoS (using the Rothermel model) and the experimentally observed RoS is shown in Table 7.8 for each fuel condition. The deviation is calculated as the difference between the predicted and observed RoS, divided by the observed RoS, and therefore represents the Absolute Percent Error. A negative deviation therefore indicates a model under-prediction of RoS, and a positive value an over-prediction.

In the majority of cases, the Rothermel model under-predicted the RoS compared to the experimentally observed spread rates. The deviation between predicted and observed RoS varied across the fuel bed conditions, ranging from -75 % to 12 %. It appears that the divergence from the experimental values increase with increasing packing ratio (greater fuel bed compaction).

**Table 7.8 - Comparison of predicted and experimentally observed Rate of Spread (RoS) for each fuel bed condition**

| Fuel Type | $w_o$ [lbs/ft.$^2$] | $\beta$ | $\rho_b$ [lbs/ft.$^3$] | Predicted RoS [mm/min] | Observed RoS [mm/min] ± Std. Dev. | $\alpha\sigma\delta$ | Deviation [%] |
|---|---|---|---|---|---|---|---|
| Pitch Pine | 0.04 | 0.014 | 0.57 | 59 | 108 ± 31 | 100 | -45 |
| | 0.04 | 0.028 | 1.14 | 29 | 114 ± 24 | 49 | -75 |
| | 0.07 | 0.014 | 0.57 | 117 | 144 ± 20 | 200 | -19 |
| | 0.07 | 0.028 | 1.14 | 58 | 126 ± 17 | 98 | -54 |
| | 0.11 | 0.014 | 0.56 | 176 | 180 ± 28 | 300 | -2 |
| | 0.11 | 0.028 | 1.14 | 86 | 132 ± 19 | 148 | -35 |
| | 0.15 | 0.014 | 0.57 | 235 | 210 ± 26 | 399 | 12 |
| | 0.15 | 0.028 | 1.13 | 115 | 162 ± 16 | 197 | -29 |
| | 0.15 | 0.055 | 2.27 | 43 | 126 ± 37 | 96 | -66 |
| | 0.22 | 0.028 | 1.12 | 173 | 174 ± 33 | 295 | -1 |
| | 0.29 | 0.028 | 1.11 | 231 | 246 ± 39 | 394 | -6 |
| Pitch-Loblolly hybrid Pine | 0.04 | 0.014 | 0.54 | 46 | Unsustained | 97 | N/A |
| | 0.04 | 0.028 | 1.07 | 22 | Unsustained | 48 | N/A |
| | 0.07 | 0.014 | 0.54 | 90 | 114 ± 25 | 194 | -21 |
| | 0.07 | 0.028 | 1.08 | 44 | 90 ± 21 | 96 | -51 |
| | 0.11 | 0.014 | 0.54 | 135 | 156 ± 39 | 290 | -13 |
| | 0.11 | 0.028 | 1.07 | 66 | 114 ± 18 | 144 | -42 |
| | 0.14 | 0.014 | 0.54 | 180 | 162 ± 28 | 387 | 11 |
| | 0.14 | 0.028 | 1.08 | 88 | 126 ± 21 | 191 | -30 |
| | 0.14 | 0.055 | 2.15 | 33 | 96 ± 11 | 93 | -66 |

As shown in Table 7.8, at all fuel loadings where multiple packing ratios were investigated, a greater percentage deviation was observed at higher packing ratios. For constant packing ratios, the greatest divergence occurred at lower fuel loadings. In this study, the packing ratio was altered at a constant fuel loading by altering the fuel bed height, with an increased divergence from the Rothermel model predictions at higher packing ratios. This trend is therefore in line with previous suggestions of an over-sensitivity of the Rothermel model to fuel bed height [60].

In addition to assessing model performance relative to fuel loading and packing ratio, we can also again describe the fuel bed via a single dimensionless parameter $\alpha\sigma\delta$. As shown in Figure 7.16, the greatest divergence in predicted and observed RoS occurs at lower values of $\alpha\sigma\delta$. In particular, in the range of $\alpha\sigma\delta = 49$ to $\alpha\sigma\delta = 200$ significant under-predictions of RoS are observed.

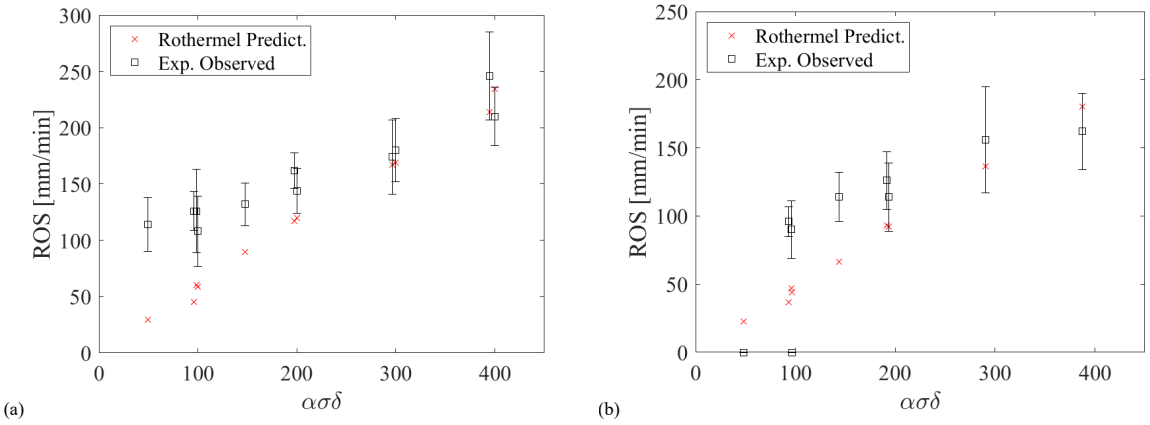


**Figure 7.16 - Comparison of Rothermel model predictions and experimental observations of spread rate for fuel beds of various $\alpha\sigma\delta$ value composed of (a) Pitch Pine needles (b) Pitch-Loblolly hybrid Pine needles**

It is interesting to note that both the model predictions and the experimental observations, indicate a strong positive trend between $\alpha\sigma\delta$ and the spread rate. Yet the significantly greater deviation (between model predictions and experimental observations) occurring at lower values of $\alpha\sigma\delta$ suggest that there is a phenomenological difference, which is not suitably being implicitly incorporated within Rothermel's model. Interestingly, the performance of the Rothermel model differs from the thermal model (discussed in Chapter 6), which in contrast displayed stronger predictive power at lower values of $\alpha\sigma\delta$ (for the model including the contribution of radiative heating through the fuel bed only).

As discussed in Chapters 5 and 6, the flame height, while not strongly correlated with the $\alpha\sigma\delta$ value, is much lower for the low $\alpha\sigma\delta$ fuel beds ($\alpha\sigma\delta = 49$ to $\alpha\sigma\delta = 200$). Therefore, a lower heating contribution from the above-bed flame (to the unburnt fuel) occurs, as shown in Chapter 6, where the performance of this simple thermal mode (considering only radiative heating from the combustion) was assessed. This model was shown to result in RoS predictions very similar to the experimentally observed spread rate for this low $\alpha\sigma\delta$ fuel bed range (see Chapter 6, Figure 6.14).

Since the spread rate can be accurately predicted at lower values of $\alpha\sigma\delta$ ($\alpha\sigma\delta \leq 200$) based only upon the radiative in-bed heating, this heat transfer regime can be assumed to dominate in these cases. Meanwhile at greater $\alpha\sigma\delta$ values, the under-predictions of this thermal model suggested that the contribution of radiative heating from the above-bed flame are of increased significance at higher $\alpha\sigma\delta$ values. This assumption is borne out by the measured heat flux magnitudes to the fuel surface, and the resulting flame heating model, discussed in Chapter 6.

If the Rothermel model is instead under-predicting the spread rate at lower $\alpha\sigma\delta$ values, then it appears that is therefore the in-bed heating contribution that is being implicitly under-

represented. Depending on the effective heating distance of this in-bed radiation and the source (primary flame front or char oxidation in trailing region), it is possible that the energy production (and the propagating component) may be under-estimated by Rothermel's model at these lower $\alpha\sigma\delta$ conditions ($\alpha\sigma\delta \leq 200$).

To better understand the variation between predicted and observed RoS, and the over-sensitivity to fuel bed compaction, it is necessary to interrogate further the intermediate model values (while understanding the inherent limitations of a semi-physical model). In Rothermel's model, a number of properties (reaction intensity, reaction velocity, propagating flux) were determined empirically from experimental observations. If we take a similar approach with the experimental data considered in this study then we can calculate the reaction intensity, reaction velocity, and propagating flux values that would result in predicted RoS values equalling those observed experimentally.

### 7.10.2. Reaction Intensity

Considering the experimentally observed spread rates, it is possible to impose these values on the Rothermel model in order to calculate the corresponding reaction intensity required to reproduce these spread rates. Since,

$$R = \frac{I_R \xi (1 + \phi_w + \phi_s)}{\rho_b \epsilon Q_{ig}} \tag{7.73}$$

If we accept that $\phi_w$, and $\phi_s$ are each equal to zero for our flame spread scenario (no wind, no slope), and that $\epsilon$ and $Q_{ig}$ are considered as intrinsic fuel/fuel bed properties, then we are left with only three variables ($I_R, \rho_b, \xi$). If the observed RoS for each fuel bed condition is inserted into the above equation (thereby fixing the value of R as the experimentally observed RoS), and all other properties (except $I_R$) are fixed (with actual $\rho_b$ specified for each fuel bed condition), then a hypothetical $I_R$ required for the observed RoS can be calculated,

$$I_R = \frac{R \rho_b \epsilon Q_{ig}}{\xi} \tag{7.74}$$

This gives an indication of the overall energy release rate in the flame front (reaction intensity), that would be required (under the Rothermel model framework) to produce the experimentally observed spread rate. However, this approach does assume that the propagating flux (the proportion of the reaction intensity energy actually transferred to the unburnt fuel) is correctly calculated for each fuel condition.

The resulting reaction intensity (based on fixing value of R as the experimentally observed RoS) is shown in Figure 7.17 and Table 7.9, along with the associated reaction velocity ($r'$) that is implied by this new reaction intensity. Since the reaction intensity ($I_R$) is also given by,

$$I_R = r' w_n h \eta_M \eta_s \tag{7.75}$$

**Table 7.9 - Summary of reaction intensity ($I_R$) and reaction velocity ($r'$) calculated based on experimentally observed ROS**

| Fuel Type | $w_o$ [lbs/ft$^2$] | $\beta$ | R (Based on Observed RoS) [mm/min] | Original Rothermel $I_R$ [Btu/ft.$^2$ min] | $I_R$ (Based on Imposed $R_{obsv}$) [Btu/ft$^2$ min] | Original $r'$ [min$^{-1}$] | $r'$ (Based on Imposed $R_{obsv}$) [min$^{-1}$] |
|---|---|---|---|---|---|---|---|
| Pitch Pine | 0.18 | 0.014 | 108 ± 31 | 929 | 1710 | 13.8 | 25.4 |
| | | 0.028 | 114 ± 24 | 620 | 2440 | 9.2 | 36.3 |
| | 0.36 | 0.014 | 144 ± 20 | 1890 | 2250 | 13.8 | 16.5 |
| | | 0.028 | 126 ± 17 | 1250 | 2680 | 9.2 | 19.6 |
| | 0.54 | 0.014 | 180 ± 28 | 2770 | 2900 | 13.8 | 14.7 |
| | | 0.028 | 132 ± 19 | 1870 | 2820 | 9.2 | 13.8 |
| | 0.73 | 0.014 | 210 ± 26 | 3720 | 3320 | 13.8 | 12.4 |
| | | 0.028 | 162 ± 16 | 2480 | 3490 | 9.2 | 13.0 |
| | | 0.055 | 126 ± 37 | 874 | 2570 | 3.3 | 9.6 |
| | 1.09 | 0.028 | 174 ± 33 | 3719.1 | 3840 | 9.2 | 9.8 |
| | 1.45 | 0.028 | 246 ± 39 | 4861.8 | 5530 | 9.2 | 10.8 |
| Pitch-Loblolly Hybrid Pine | 0.17 | 0.014 | Unsustained | 819 | N/A | N/A | N/A |
| | | 0.028 | Unsustained | 551 | N/A | N/A | N/A |
| | 0.34 | 0.014 | 114 ± 25 | 1660 | 2040 | 13.8 | 16.8 |
| | | 0.028 | 90 ± 21 | 1110 | 2220 | 9.3 | 18.3 |
| | 0.52 | 0.014 | 156 ± 39 | 2480 | 2810 | 13.8 | 15.5 |
| | | 0.028 | 114 ± 18 | 1650 | 2890 | 9.3 | 16.4 |
| | 0.69 | 0.014 | 162 ± 28 | 3300 | 2930 | 13.8 | 12.2 |
| | | 0.028 | 126 ± 21 | 2220 | 3110 | 9.3 | 12.9 |
| | | 0.055 | 96 ± 11 | 787 | 2290 | 3.3 | 9.6 |

As shown in Figure 7.17, when reaction intensity is calculated using the classic Rothermel equation, a monotonically increasing trend between packing ratio and reaction intensity is predicted (as a result of the dependence of the reaction velocity on the packing ratio). However, imposing the experimentally observed ROS, does not result in a monotonic increase, instead a maximum reaction intensity occurs at the intermediate packing ratio (0.028), with a significantly lower reduction in reaction intensity at the most compacted fuel bed condition (packing ratio of 0.055).

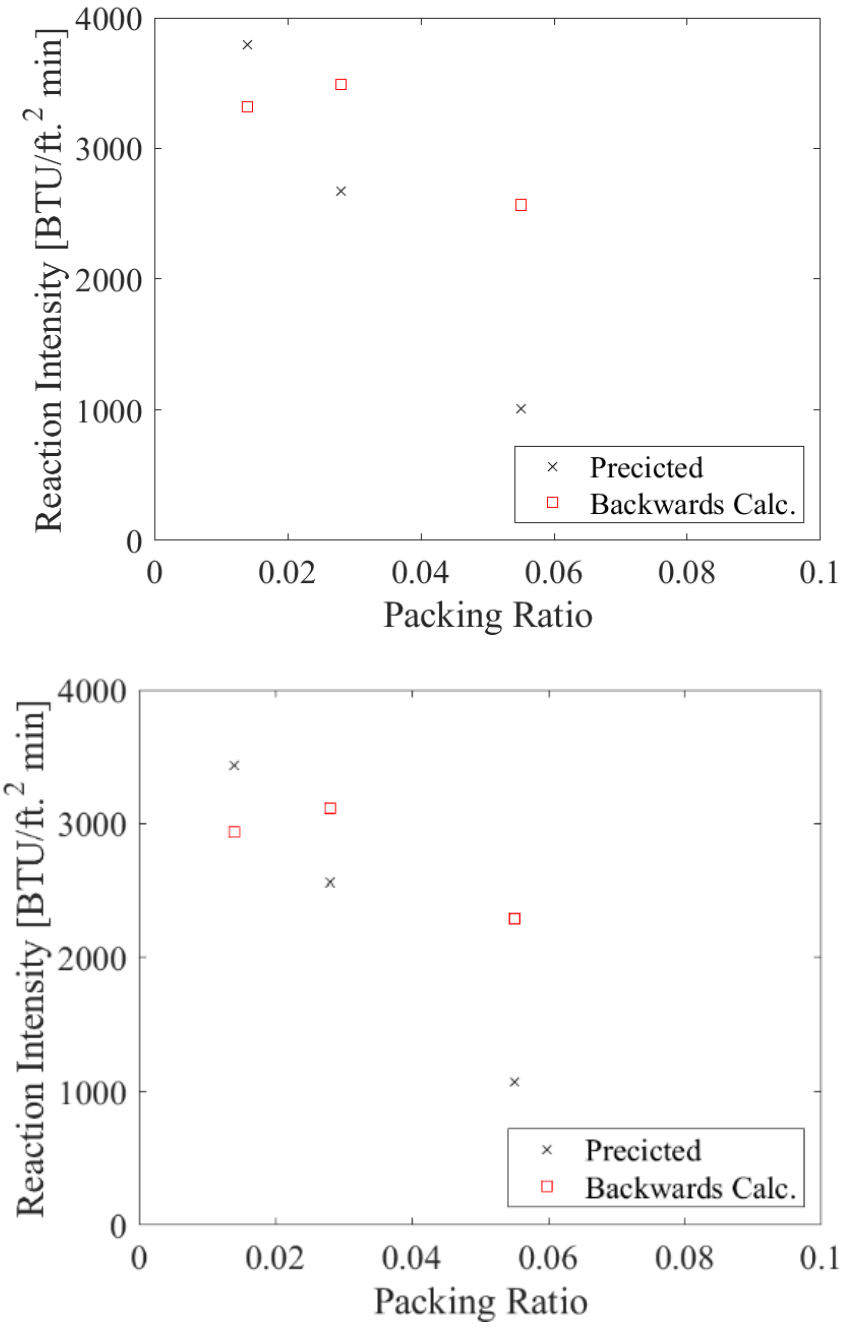


**Figure 7.17 - Comparison of trend between reaction intensity and packing ratio based upon $I_R = r'w_n h\eta_M\eta_s$ and $R = R_{obsv}$ approaches for (top) 0.73 lbs/ft$^2$ Pitch Pine (bottom) 0.69 lbs/ft$^2$ Pitch-Loblolly hybrid Pine, fuel beds**

Given this purely mathematical reasoning however it is not possible to confidently draw physical conclusions from this analysis. Instead, the relationship between reaction intensity and other directly observable physical phenomena must be explored further. This allows greater use of the experimental data presented in Chapters 5 and 6, in order to interrogate physical causes for the model discrepancies.

The reaction intensity can be straightforwardly related to the Byram Fire Intensity ($I_B$), a commonly-used descriptor of fire behaviour [102], which describes the heat release per unit

length of the fire front (rather than the heat release rate per unit area of the fire front described by reaction intensity). These concepts can therefore be related if the residence time is known, or can be estimated.

#### 7.10.2.1. Residence Time

Suitability of Existing Empirical Formulae

Anderson [133] proposed an equation for residence time ($t_r$) for surface fires in a uniform fuel bed, based upon unpublished experimental data and a review of existing studies [13,14,197,398]. Anderson determined that the residence time (of the flame at a given fuel bed location) was a function only of fuel size (fuel element diameter ($d$) or S-V ratio ($\sigma$)),

$$t_r = 8d = \frac{384}{\sigma} \tag{7.76}$$

Where $t_r$ is the residence time (minutes), and $d$ is the diameter of fuel elements (in inches) which is assumed to be related to the surface-to-volume ratio ($\sigma$) by the following relationship,

$$d = \frac{48}{\sigma} \tag{7.77}$$

This residence time is for the passage of the flame front only and does not consider the trailing combustion region. As seen in the above equation, it is assumed that the residence time is a function only of the fuel element size (S-V Ratio or diameter). Catchpole *et al.* [60] later suggested that an improved equation for residence time may be required, particularly in thicker fuels and mixed fuel beds. In particular, they suggested that an improved equation should incorporate the effect of fuel depth and packing ratio.

In this study, both the needle diameter and S-V ratio of each needle species was directly measured, as described in Chapter 3. In Table 7.10, the measured diameters for each fuel species are compared with those obtained by using Equation 7.77. This analysis indicates that the relationship between S-V ratio and diameter for fuel elements of both fuel species in this study are more accurately described by $\left(d = \frac{79}{\sigma}\right)$. The resulting residence time for predictions based upon both the measured diameter and this estimated diameter are compared in Table 7.10.

**Table 7.10 - Summary of reisdence time ($t_r$) estimates based on directly measured, and estimated fuel element diameter**

| **Species** | **Measured Dia.** [in.] (S.D.) | **Estimated Dia.** $\left(d = \frac{48}{\sigma}\right)$ [in.] | $t_r$ **Based on Measured Dia.** [s] | $t_r$ **Based on Estimated Dia.** [s] |
|---|---|---|---|---|
| Pitch | 0.052 (0.006) | 0.031 | 25 | 15 |
| Hybrid | 0.053 (0.005) | 0.032 | 25 | 15 |

Direct Measurement of Residence Time

In this study, the residence time was also measured directly using the in-bed temperature measurements, described in detail in Chapters 5 and 6. A temperature threshold of 300 °C was

assumed to indicate flame presence, with the residence time equal to the greatest continuous period over which this threshold was exceeded. The mean residence times for each fuel bed condition are shown in Table 7.11, and considerable variation with fuel structure can be observed.

**Table 7.11 - Comparison of experimentally observed residence time for various fuel bed conditions**

| Species | Fuel Loading [kg/m$^2$] | Bulk Density [kg/m$^3$] | Observed $t_r$ [s ± Std. Dev.] |
|---|---|---|---|
| Pitch | 0.2 | 10 | 17 ± 9 |
| Pitch | 0.2 | 20 | 18 ± 10 |
| Pitch | 0.4 | 10 | 20 ± 11 |
| Pitch | 0.4 | 20 | 29 ± 9 |
| Pitch | 0.6 | 10 | 30 ± 10 |
| Pitch | 0.6 | 20 | 33 ± 14 |
| Pitch | 0.8 | 10 | 27 ± 15 |
| Pitch | 0.8 | 20 | 46 ± 14 |
| Pitch | 0.8 | 40 | 38 ± 24 |
| Pitch | 1.2 | 20 | 64 ± 52 |
| Pitch | 1.6 | 20 | 49 ± 23 |
| Hybrid | 0.2 | 10 | N/A |
| Hybrid | 0.2 | 20 | N/A |
| Hybrid | 0.4 | 10 | 28 ± 18 |
| Hybrid | 0.4 | 20 | 15 ± 14 |
| Hybrid | 0.6 | 10 | 37 ± 17 |
| Hybrid | 0.6 | 20 | 23 ± 13 |
| Hybrid | 0.8 | 10 | 45 ± 7 |
| Hybrid | 0.8 | 20 | 45 ± 31 |
| Hybrid | 0.8 | 40 | 29 ± 14 |

These experimental observations of residence time vary somewhat in definition compared to the residence time predicted in Anderson's equation. As the thermocouples are located within the fuel bed, they will be subject to heating by both the primary flame front and the trailing combustion region, whereas Anderson's residence time considers only the primary flame front. There is a need to better understand the relative contribution of both of these combustion regions and the various combustion phases.

Additional insight can also be gained from the lowest fuel loading conditions (0.2 kg/m$^2$) where no extensive trailing region was observed to form behind the main flame front. The residence time in the lowest fuel load cases should therefore apply only to the primary flame front, especially at the denser (20 kg/m$^3$, 0.01 m height) fuel condition where the thermocouple tip is flush with the fuel bed surface. For the two lowest fuel loading Pitch Pine cases, residence times of 17 ± 9 s and 18 ± 10 s were observed. These are similar to those estimated using Anderson's equation, as shown in Table 7.10. However, the observed effects of fuel structure support Catchpole *et al.'s* [60] previous suggestions that an improved empirical term is required to incorporate these effects within residence time predictions.

#### *7.10.2.2. Comparison of Reaction Intensity and Fireline Intensity*

Byram's fireline intensity is a commonly used descriptor of fire size in wildland fires and field experiments [102]. Essentially, Byram's fireline intensity describes the heat release rate per unit length of flame front, and is therefore distinct from the reaction intensity, used in Rothermel's equations (which described the heat release rate per unit area of the flame front).

However, it is possible to convert between these two terms, if the Byram fireline intensity has been measured, for example by measurement of the Heat Release Rate (HRR).

The total HRR was calculated for many of the fuel bed conditions in this experimental series using Oxygen Consumption Calorimetry (OCC). The OCC method is described in detail in Chapter 3, while the resulting HRR values were presented in Chapters 5 and 6. Dividing the HRR by the flame front width (equal to the fuel bed width of 0.67m, at all but the lowest fuel loading cases), provides the Byram Fire Intensity for each fuel bed condition, and these are shown in Table 7.12 (for all conditions at which HRR was measured).

The measured Byram fireline intensity ($I_B$) can then be converted to a reaction intensity $I_R$, according to the following relationship,

$$I_B = \frac{I_R t_r R}{60} \tag{7.78}$$

Where $t_R$ is the residence time, and R is the rate of spread.

Two approaches were used to calculate this experimentally informed reaction intensity, both based upon the OCC measurements of HRR. In the first approach, experimentally observed values for both the RoS and residence time were used for each fuel bed condition. In the second approach, the average[21] estimated residence time calculated from Anderson's formulation (20 s as shown in Table 7.10) was used rather than the experimentally observed values.

Both experimentally informed reaction intensities are shown in Table 7.12 and compared with the reaction intensity predicted by Rothermel's model. Additionally, the ratio of the reaction intensity predicted by Rothermel's model to the reaction intensity calculated from the fireline intensity (for each of the approaches outlined above), is shown in Figure 7.18.

[21] This average residence time is the average value obtained from Anderson's equation using the directly measured and empirically estimated dimeters respectively.

**Table 7.12 - Comparison of predicted reaction intensity ($I_R$) (using Rothermel equations) and experimentally observed (conversion of Byram Fire Intensity) reaction intensity at each Fuel Bed Condition (N/A indicated insufficient HRR measurements at this fuel bed condition)**

| Species | Fuel Loading [kg/m$^2$] | Bulk Density [kg/m$^3$] | Byram Fireline Intensity [Btu/ft.] | Predicted $I_R$ (Rothermel Model) [Btu/ft.$^2$ min] | Observed $I_R$ (Observed $t_r$, RoS and HRR) [Btu/ft.$^2$ min] | Observed $I_R$ (Predicted $t_r$ and Observed RoS and HRR) [Btu/ft.$^2$ min] |
|---|---|---|---|---|---|---|
| Pitch | 0.2 | 10 | 5.3 | 929 | 3150 | 2680 |
| Pitch | 0.2 | 20 | 0.5 | 620 | 250 | 229 |
| Pitch | 0.4 | 10 | 6.7 | 1870 | 2540 | 2540 |
| Pitch | 0.4 | 20 | 4.5 | 1250 | 1360 | 1980 |
| Pitch | 0.6 | 10 | 10.4 | 2770 | 2120 | 3180 |
| Pitch | 0.6 | 20 | 8.0 | 1870 | 2030 | 3340 |
| Pitch | 0.8 | 10 | 17.0 | 3720 | 3300 | 4450 |
| Pitch | 0.8 | 20 | 12.5 | 2480 | 1840 | 4230 |
| Pitch | 0.8 | 40 | N/A | 870 | N/A | N/A |
| Pitch | 1.2 | 20 | N/A | 3720 | N/A | N/A |
| Pitch | 1.6 | 20 | N/A | 4860 | N/A | N/A |
| Hybrid | 0.2 | 10 | N/A | 820 | N/A | N/A |
| Hybrid | 0.2 | 20 | N/A | 550 | N/A | N/A |
| Hybrid | 0.4 | 10 | 4.0 | 1660 | 1380 | 1940 |
| Hybrid | 0.4 | 20 | 2.9 | 1110 | 2320 | 1740 |
| Hybrid | 0.6 | 10 | 7.8 | 2480 | 1490 | 2750 |
| Hybrid | 0.6 | 20 | 5.7 | 1650 | 2370 | 2730 |
| Hybrid | 0.8 | 10 | 12.5 | 3300 | 1880 | 4230 |
| Hybrid | 0.8 | 20 | 7.6 | 2220 | 1470 | 3300 |
| Hybrid | 0.8 | 40 | 5.1 | 790 | 2030 | 2940 |

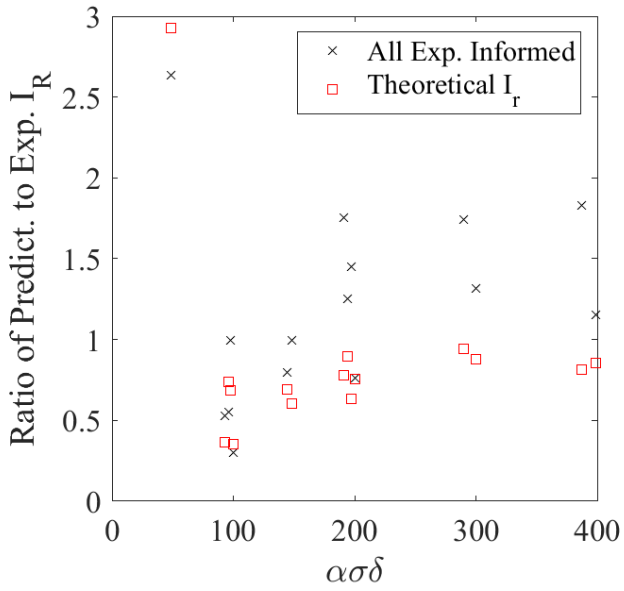


**Figure 7.18 - Ratio of predicted reaction intensity ($I_R$) (from Rothermel's model) to the calculated reaction intensity based on the experimentally observed Byram intensity, for each fuel bed condition.**

As shown in Figure 7.18, the effect of including either the theoretical (based on Anderson's observations) or the experimentally measured residence time, on the resulting reaction intensity is significant. As previously discussed, this may be because of the location of the thermocouples (within the fuel bed) and the resulting exposure to heating from both combustion phases (primary flame front and trailing smouldering region). This would also explain the greater divergence between these reaction intensity values at greater values of $\alpha\sigma\delta$ at which higher residence times were measured, and longer trailing combustion regions were observed.

In Figure 7.18, a ratio of greater than one indicates that the Rothermel prediction of reaction intensity over-predicts the experimentally determined value. Where the experimentally observed residence time is used, significant over-predictions are observed at many of the higher $\alpha\sigma\delta$ cases ($\alpha\sigma\delta \geq 200$). Again, this is likely indicative of an overestimate of the spatial distribution of the energy release (overestimate of the size of the flame front region) where the in-bed measurements of residence time are used.

Over-predictions of the reaction intensity by the Rothermel model are not observed (except at the lowest $\alpha\sigma\delta$ value which may represent a marginal burning condition) where Anderson's equation is used. Instead, the model performance improves at higher values of $\alpha\sigma\delta$, with under-predictions of reaction intensity observed at lower $\alpha\sigma\delta$ cases ($\alpha\sigma\delta \leq 200$). This range in which under-prediction occurs is very similar to the range at which significant under-predictions of RoS occur, as was previously shown in Figure 7.16. It therefore appears that the energy released in the primary flame front region in fuel beds of lower $\alpha\sigma\delta$ value, may currently be under-predicted by Rothermel's model (except at the most marginal condition).

## 7.11. Effect of Model Modifications

### 7.11.1. Wilson

Wilson suggested several modifications to the Rothermel model, in two separate publications released in 1982 [97] and 1990 [62] respectively, and involving a large number of additional laboratory experiments to complement those used in the initial model development. In the first of these studies, Wilson observed experimentally the apparent validity of Rothermel's original assumption that the reaction intensity is linearly related to the fuel loading. However, additional investigation was required for thin fuels at low fuel loadings.

Similarly, Rothermel's empirical relationships for the propagating flux ratio, while generally adequate, appeared to result in an under-prediction for thin fuels at high fuel loadings. A new relationship for the propagating flux (as a function of the optical density) was therefore proposed, however it was noted that further development was required.

Wilson's alternative equation for the propagating flux ratio was based on an expanded set of laboratory experiments (involving excelsior and cribs of two different stick thicknesses). This new curve fit included all of the experimental data (> 250 experiments) presented by Wilson [62],

$$\xi = 1 - \exp(-0.17\sigma\beta) \tag{7.79}$$

Where the S-V ratio ($\sigma$) is specified here in $cm^{-1}$, and where ($\sigma\beta$) represents the optical density of the fuel bed, and is the dominant factor controlling the propagating flux ratio. The value 0.17

represents the 'physical skin thickness' of the particle and is similar to the effective heating coefficient defined by Frandsen [366]. Wilson also cautions against extrapolation of this relationship to other fuel bed types (beyond those involving essentially one-dimensional, long narrow particles in which the optical length is a function of the particle cross-sectional area), in which the extinction length may vary significantly.

A comparison of the propagating flux ratio estimated by the original Rothermel equation and the equation proposed by Wilson is shown in Figure 7.19.

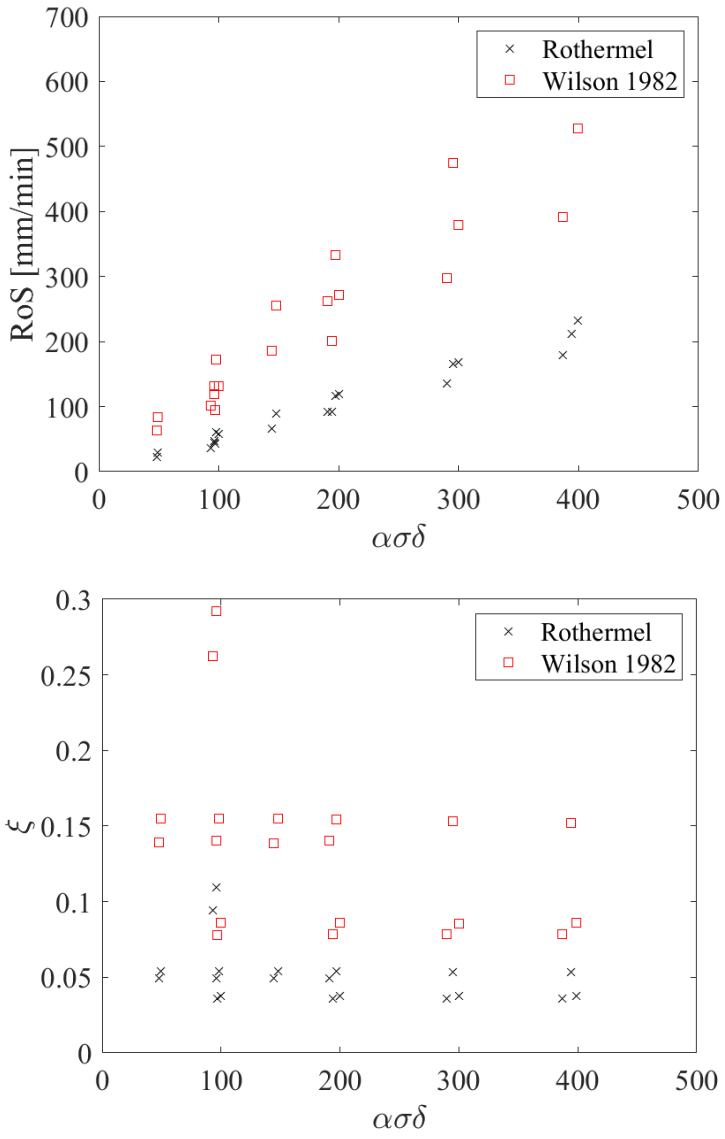


**Figure 7.19. - Comparison of original Rothermel model and Wilson (1982)** [97] **predictions of (top) Rate of Spread (ROS), (bottom) propagating flux ratio, for fuel beds of various ασδ**

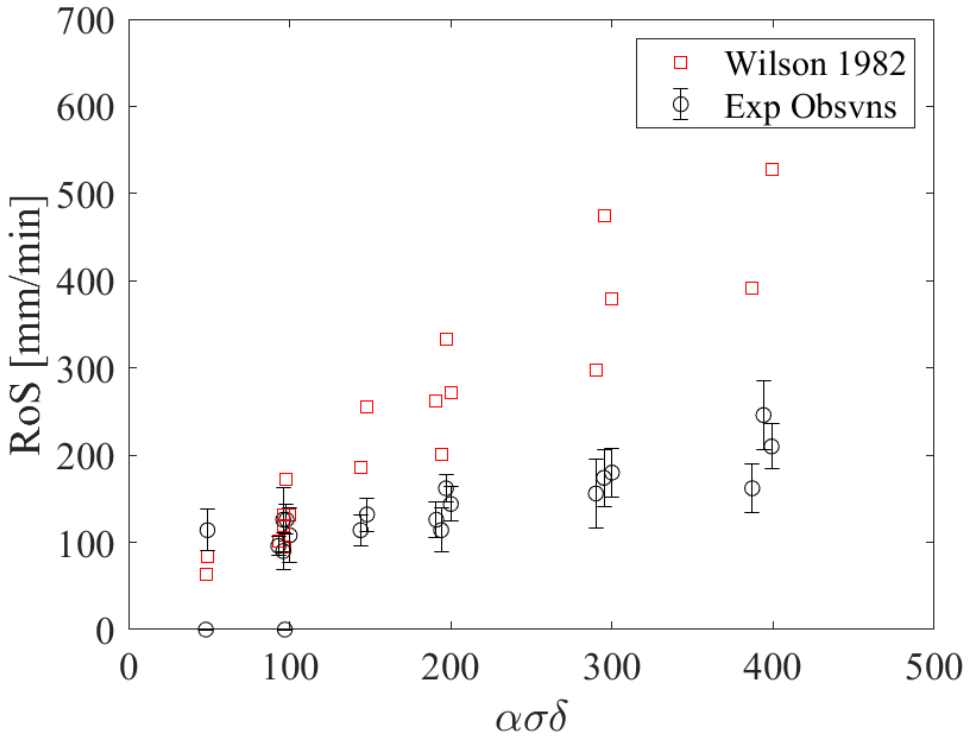


**Figure 7.20. - Comparison of experimental observations and Wilson (1982)** [97] **predictions of Rate of Spread (RoS) for fuel beds of various ασδ (For experimental observations a spread rate of zero indicates unsustained flame spread)**

Wilson also proposed alternative equations for the reaction velocity ($r$) and moisture damping coefficient ($\eta_M$), which were incorporated into the original form of the RoS equation given by Rothermel,

$$R = \frac{\xi h_v w_o r \eta_M}{\rho_b \epsilon \left(Q_f + M_f Q_w\right)} \tag{7.80}$$

Where $h_v$ is the heat of combustion of the vaporised fuel, $w_o$ is the dry fuel loading, $\rho_b$ is the bulk density, and $M_f$ is the dry basis FMC. The effective heating number ($\epsilon$) follows the original, experimentally-determined value, previously suggested by Frandsen [366] (which differs slightly from the equation used in the original Rothermel equations),

$$\epsilon = \exp\left(\frac{1}{0.22\sigma}\right) \tag{7.81}$$

$Q_w$ is the heat of vaporisation of water, which is given by,

$$Q_w = 4.18(100 - T_{amb} + 540) \tag{7.82}$$

$Q_f$ is the heat of pyrolysis where,

$$Q_f = \int_{amb}^{400} (dQ/dT)dT \tag{7.83}$$

The newly proposed reaction velocity has a similar form to the original Rothermel value but the concept of an optimum packing ratio was removed. Instead, based upon experimental observations, the reaction velocity depends upon overall fuel loading and/or total fuel surface area. The original Rothermel model assumes a parabolic relationship, in which the reaction velocity increases with reduced packing ratio (increased fuel bed height) to a maximum value at the optimum packing ratio and subsequently decreases. Wilson instead predicted a negative trend between reaction velocity and packing ratio, until fuel sparsity dominates. At high fuel sparsity, the flame front becomes discontinuous, and ultimately leads to extinction.

A new fire extinction probability function $P_f$ was introduced by Wilson to describe this marginal burning behaviour, and this acts as a limit on the maximum reaction velocity,

$$P_f(\eta_x) = \frac{1}{\left(1 + \exp(-\pi(\eta_x - \overline{\eta_x})/1.2\sqrt{3})\right)} \tag{7.84}$$

Where the value 1.2 and $\overline{\eta_x}$ are fuel-specific constants that calibrate the distinction between 'good' and marginal burning conditions. The typical value of $\overline{\eta_x}$ for cellulosic woody fuels is 3, and choosing a higher value will push the extinction threshold towards higher fuel loadings or lower fuel moisture. While $n_x$ is the extinction index (described in an earlier Wilson publication [399]), which describes the energy balance in marginal burning conditions, and provides the cut-off between 'good' and 'bad' burning conditions,

$$n_x = \frac{\ln(\sigma\beta\delta h_v/Q_w)}{\left(M_f + Q_f/Q_w\right)} \tag{7.85}$$

This was then incorporated into Wilson's reformulation of the reaction velocity ($r$) equation,

$$r = 0.34\sigma(\sigma\beta\delta)^{-\frac{1}{2}} \exp\left(-\frac{\sigma\beta}{3}\right) P_f(\eta_x) \tag{7.86}$$

Where $0.34\sigma$ has a similar effect to the residence time equation previously proposed by Anderson (8d). The exponential term $\frac{\sigma\beta}{3}$ describes the effective heating distance through the fuel bed from the combustion region. The inclusion of $\sigma\beta$ and $\beta\delta$ terms reduces the reaction velocity at higher, denser fuel beds. Aside from very marginal conditions, the probability term $P_f(\eta_x)$ will have a limited effect and can be removed.

Finally, Wilson proposed a much simpler formulation for the moisture damping coefficient ($\eta_M$), which unlike Rothermel's original equation, did not consider extinction phenomena (since these were considered separately by Wilson in the previously discussed extinction probability function),

$$\eta_M = \exp(-M_F/M_c) \tag{7.87}$$

Where $M_c$ is the characteristic moisture content for a given fuel bed.

A comparison of the RoS estimated by the original Rothermel equation and the equation proposed by Wilson is shown in Figure 7.19. The spread rate predictions from Wilson's model are roughly twice those of the Rothermel model, and this effect seems to be largely as a result of the increased propagating flux (which is also roughly double Rothermel's estimate).

### 7.11.2. Sandberg *et al.*

Several modifications to the Rothermel model were suggested by Sandberg *et al*. Three of the suggested modifications were adopted and these are summarised in Table 7.13.

**Table 7.13 - Summary of modifications incorporated from Sandberg *et al.*** [400]

| Parameter | Original Rothermel Model | Sandberg *et al.* Modified Form |
|---|---|---|
| Propagating Flux Ratio $(\xi)$ | $\xi = (192 + 0.2595\sigma)^{-1} \exp[(0.792 + 0.681\sigma^{0.5})(\beta + 0.1)]$ | $\xi = 0.03 + 2.5\beta_{\epsilon}$ |
| Effective Heating Number $(\epsilon)$ | $\epsilon = \exp\left(-\frac{138}{\sigma}\right)$ | $\epsilon = 1$ [for $r < 0.085$ cm] |
| Optimum Packing Ratio $(\beta_{op})$ | $\beta_{op} = 3.348\sigma^{-0.8189}$ | $\beta_{op} = 0.022$ [for $r < 0.085$ cm] |

A comparison of the original Rothermel predictions of RoS, with those predicted following these three modifications, is shown in Figure 7.22. Also shown is a comparison of the propagating flux ratio estimated by the original Rothermel equation and the equation proposed by Sandberg *et al.*

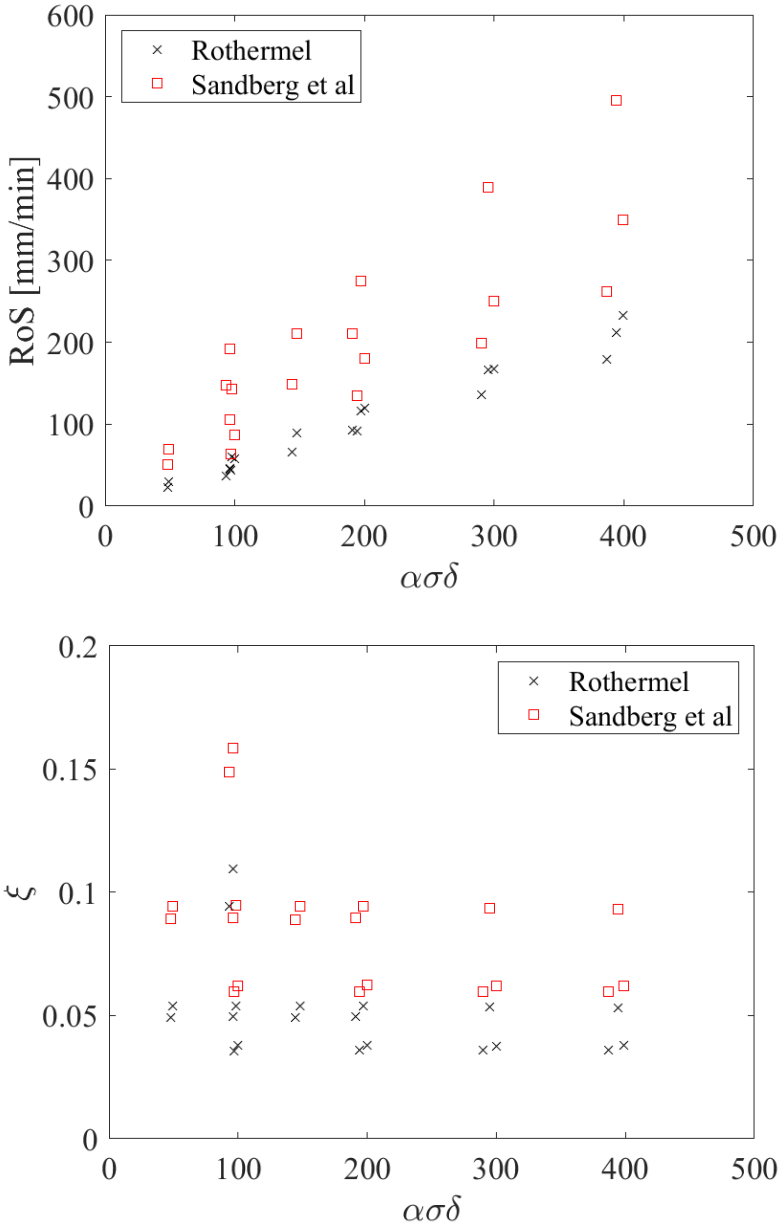


**Figure 7.21 - Comparison of original Rothermel model and Sandberg *et al.* [400] predictions of (top) Rate of Spread (RoS), and (bottom) propagating flux ratio, for fuel beds of various $\alpha\sigma\delta$**

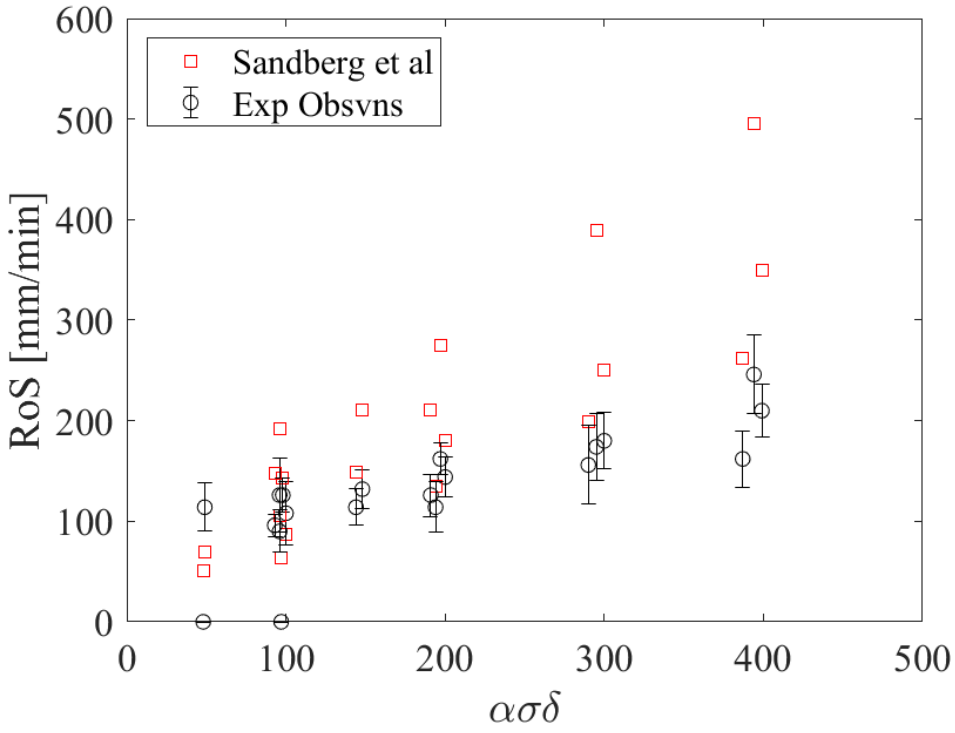


**Figure 7.22 - Comparison of experimental observations and Sandberg *et al.* [400] predictions of Rate of Spread (RoS)**

The propagating flux ratio calculated using the method suggested by Sandberg *et al*. is almost double the value calculated in the original Rothermel model. It is questionable whether the use of a single curve fit for all three fuel classes studied by Rothermel (excelsior, ¼ inch and ½ inch cribs) will improve predictions of the propagating flux in the thin fuel element, matt-type fuel beds used in this present study compared to use of the original equation derived by Rothermel based on individual curve fittings for each fuel class.

Mathematically, the value of the propagating flux ratio can range from zero (no heat transfer to the unburnt fuel) to one (all heat released is transferred to the unburnt fuel). However, Burgan and Rothermel [368] suggested that in reality the propagating flux ratio is generally in the range of 0.01 to 0.2. The basis for this claim is unclear, but we may guess that it was informed by the past experimental observations of both authors, and indeed this range matches the experimental data previously presented by Rothermel [43], and shown in Figure 7.4. However, it is clear from Figure 7.4, that this typical limit ($\xi < 0.2$) would quickly be exceeded if excelsior fuel beds with packing ratios higher than those studied by Rothermel were included. This may have important implication for the fine fuels studied in this thesis.

Figure 7.23 (extracted from Sandberg *et al*.) demonstrates that this simplified, single curve-fit over-predicts the propagating flux for the thin fuel element (excelsior) fuel beds compared to experimental observations (particularly at intermediate packing ratios). However, since the relationship between the propagating flux ratio and the underlying physical mechanisms is not explicit, it is difficult to understand how this would extend to these pine needle fuel beds.

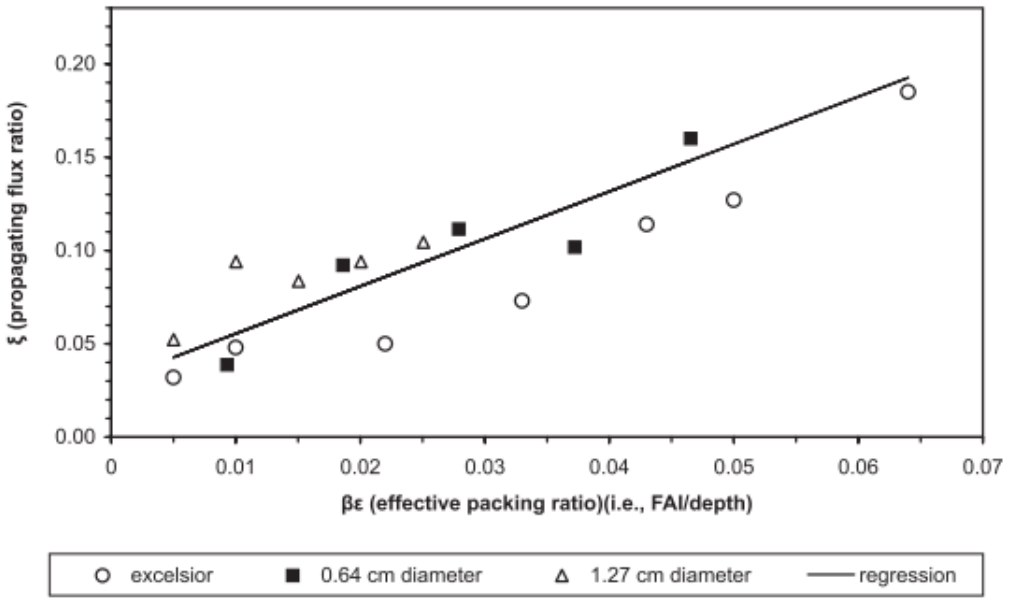


**Figure 7.23 – Relationship between propagating flux ratio and effective packing ratio, based upon the simplified curve-fit proposed by Sandberg et al.** [400] **and applied to the original experimental data of Rothermel** [43]**. Extracted from Sandberg et al. (2007)** [400]

The modified equation for the optimum packing ratio suggested by Sandberg *et al.* may also not lead to increased accuracy for these pine needle fuel beds. This is because, as with the original equation proposed by Rothermel, the optimum packing ratio remains a function only of fuel element S-V ratio.

## 7.12. Conclusions

The performance of the widely used Rothermel flame spread model was assessed when applied to the laboratory flame spread experiments described in Chapters 5 and 6. In general, Rothermel's model under-predicted the rate of spread (RoS) compared to experimental observations. The greatest divergence between model predictions and experimental RoS occurred for fuel beds of lower fuel loadings and higher packing ratio (higher bulk density), and in the lower range of $\alpha\sigma\delta$ value fuel beds ($\alpha\sigma\delta = 49$ to $\alpha\sigma\delta = 200$). These observations support previous suggestions that the Rothermel model may be over-sensitive to fuel bed height (and the effects of fuel bed compaction).

Comparison with the thermal model predictions (presented in Chapter 6) highlight an implicit under-representation of the in-bed radiative heating contributions at these lower $\alpha\sigma\delta$ values ($\alpha\sigma\delta \leq 200$). In contrast to this simple thermal model, the predictive performance of the Rothermel model was greater at higher $\alpha\sigma\delta$ values, at which the contribution of radiative heating from the above-bed flame is increased.

Within this low $\alpha\sigma\delta$ range ($\alpha\sigma\delta = 49$ to $\alpha\sigma\delta = 200$), the predicted reaction intensity also under-predicted those observed experimentally. This suggests that the model is under-predicting the energy release in these cases and mischaracterising the proportion of combustion occurring in the primary flame front. The experimentally observed reaction intensities (with HRR converted to fireline intensity and then reaction intensity) were very sensitive to the residence time.

Experimentally observed residence times (based upon in-bed temperature measurements) are affected by both the primary and trailing combustion regions, and their effects are difficult to disentangle. However, by analysing cases in which thermocouples were positioned above-bed, or where the low fuel loading led to the absence of a significant trailing combustion region, residence times were observed to closely match those predicted by existing formulations in which residence time is considered only as a function of fuel element size. However, modifications to existing relationships between fuel element diameter and surface-to-volume ratio were required for the pine needle fuels considered in this study. Existing formulations do not allow for the effects of fuel bed properties despite the effects observed in this and other studies.

Several potential model modifications, suggested by previous authors but not widely adopted, were assessed for the flame spread scenario considered in this study. Estimates of the propagating flux ratio are approximately doubled if the modifications of Sandberg *et al.* [400] or Wilson [62,97] are incorporated, yet the physical justification for their simpler curve-fitting approach is unclear, and the resulting over-predictions for thin fuel elements may preclude its suitable application to pine needle beds.

# Chapter 8

## Implications for simplified physics-based models

# 8. Implications for Simplified Physics-Based Models

*" as these [simplified physics-based] models tend not to consider the combustion process, characteristics of the flame must often be prescribed a priori, as determined from experimentation … This places limits on their purely predictive capacity, though such empirically-imposed constraints are not unique to this class of model.*

***Eric V. Mueller, 2016*** [18]

## 8.1. Summary

This chapter introduces a class of models categorised as simplified physics-based models, and briefly charts their historical development. Unlike the semi-empirical models discussed in Chapter 7, these models explicitly define terms for separate heat transfer mechanisms and exchange pathways. Developed for various porous fuel types and flame spread scenarios, these flame spread models differ in their key assumptions and in their selection of significant heat transfer mechanisms.

In this chapter, common modelling approaches for several important physical processes (above-bed flame heating, in-bed heat transfer, ember radiation) are discussed. Relevant existing formulations are introduced and their suitability is assessed via comparison with the physical measurements presented in Chapters 4-6. Certain commonly applied assumptions for radiation transport are found to be of limited applicability to matt-type fuel beds such as the pine needle beds investigated in this thesis. This chapter aims to address a historic lack of suitable physical measurements for the testing, validation and development of sub-terms in simplified physics-based models, and to highlight areas for further research. This may in turn benefit the development of sub-models for detailed physics-based models, particularly regarding descriptions of fuel structure effects (occurring at the sub-grid scale).

## 8.2. Introduction

Semi-empirical models, such as the Rothermel model [43], have a theoretical basis and are under-pinned by a conservation of energy approach [99]. However these models require empirically derived terms to close the model and do not distinguish between the individual heat transfer mechanisms (radiation, convection and conduction) [18]. A more complex class of models, typically described as simplified physics-based models, do allow these separate heat transfer mechanisms to be distinguished. However, unlike the more complex, detailed physics-based models, these models typically do not include combustion chemistry nor do they explicitly resolve the flow.

Simplified physics-based models have not seen widespread operational use but the inclusion of explicit equations for physical processes means that they are of great potential value for research use. This is particularly true for those physical phenomena which are affected by the fuel structure, since development of modelling capabilities in these areas can support and aid the development of simple sub-model terms for detailed physics-based models (in which the detailed structure of many porous fuel layers (e.g. pine needle beds) often exists at the sub-grid scale [18]).

Continued experimental investigation can support the further development of simplified physics-based models. While separate heat transfer mechanisms are considered within these

models, dominant heat transfer mechanisms are typically identified at the outset in order to simplify model development. This can represent a significant limitation for this class of model if applied to a scenario in which the assumptions regarding dominant heating mechanisms are no longer applicable [93]. However, through comparison of theoretical expressions with experimental observations, these models may allow assessment of our theoretical understanding of porous flame spread and the effect of factors such as fuel structure.

This chapter begins with an introduction to simplified physics-based models, and a discussion of the approaches taken during their development. The historical development of physics-based models has been reviewed in detail by past authors [100,401]. These previous reviews provide clear and concise summaries of the key theoretical approaches and mathematical formulations underpinning these models developed over recent decades. The aim of this section is not therefore to provide a comprehensive review of these studies but instead simply to establish a broad timeline of the key developments for this model class.

In doing so, the main objective is to identify and discuss the key physical assumptions relevant to the flame spread scenario studied in this thesis. Common approaches to incorporating the key physical phenomena and/or the effects of fuel structure within these models are highlighted. This will allow the evaluation of these existing approaches, and their applicability to fuel conditions representative of actual field conditions using the measurements of fire behaviour and key physical properties presented in earlier chapters of this thesis.

Finally, the majority of existing physical models describe a steady-state flame spread process. However, a small number of dynamic models have been proposed [402,403], in which unsteady flame spread can be considered, often employing a moving boundary value (Stefan problem) approach [100]. These dynamic models may be particularly relevant when considering the fire growth stage or an unsteady flame spread process. However, the flame spread experiments presented in this thesis were observed to display quasi-steady flame spread behaviour, and models describing this regime will be primarily considered within this chapter.

## 8.3. Development of Simplified Physics-Based Models

In 1946, Fons [111] presented what is widely believed to be the first detailed attempt to develop a mathematical model of wildland flame spread [18,47,404]. Beginning with a flame spread description for discrete vertical fuel elements (similar to those described in Section 2.4.2.2.2), Fons subsequently extended this model for application to both homogeneous and heterogeneous natural fuel beds. While physical properties, such as the film conductance for convection, were included, empirical closure terms were still required.

Fons also discussed the importance of the surface-to-volume ratio on the relative significance of radiative and convective heating. Understanding this balance between competing heat transfer mechanisms, and the specification of a dominant heating mechanism(s) (for a given flame spread scenario), is an important starting point in most physics-based modelling efforts [92].

### 8.3.1. Conduction

Conduction is often assumed to be negligible given the high porosity, and hence low effective thermal conductivity, of natural porous fuel beds [93]. This is in clear contrast to the typical approaches taken within non-porous solid surface flame spread models, in which conduction is significant for flame spread in thick fuels [22,93]. A relative outlier amongst existing

simplified physics-based models, is that of Fujii *et al*. [403], in which in-bed radiation is treated as non-linear conduction. This is in contrast to the manner in which Fujii *et al.* consider flame heating, where a more standard radiative transfer approach is taken, and the result is a complex model which has been criticised by subsequent authors [100]. Therefore, conductive heating is typically neglected during the construction of most existing simplified physics-based models.

### 8.3.2. Convection

Relatively few existing models allow for a scenario in which convective heating dominates [18,45]. Vogel and Williams [46] developed a flame spread model (informed by experimental investigation) to describe flame spread through a matchstick array (of the type discussed in Section 2.4.2.2.2). Based upon previous experimental observations, the model was developed under the assumption that convective heating was the dominant pre-heating mechanism (with radiative heating offset by radiative losses and therefore neglected).

The dynamic flame spread model proposed by Cekirge [402] also allows for convection (heating and cooling) and can be applied to either linear or radial propagation. Both the heating and cooling terms were dependent upon the in-bed flow velocity, which, as observed in this thesis, will vary with fuel structure. The in-bed flow velocity was defined as a proportion of the wind velocity, with an arbitrary coefficient of proportionality chosen, without experimental investigation. Inclusion of convection within the model led to greater agreement with experimental data than was achieved with a radiation-only model however, the experimental fitting of the in-bed velocity coefficients limits the ability to draw physical insights from these results.

The model of Pagni and Peterson [47] identified flame radiation as the dominant heating mechanism at low wind speeds, with convective heating becoming dominant at higher wind speeds. This is similar to the two flame spread regimes (wind-driven and plume-dominated) identified by past authors [33] (and discussed in Chapter 2). Pagni and Peterson also suggested that in-bed convective heat transfer may be of greater significance than surface convection for very porous fuels [47]. However, description of the in-bed flow profile is complicated by the drag forces exerted by the fuel bed elements, which may vary with fuel bed structure.

Pagni and Peterson [47] described the in-bed gas phase velocity, as a function of the distance ahead of the flame front,

$$V_{gi}(y) = U_w - 5\nu_g l_c N_c y \qquad \text{for} \quad 0 \leq y \leq U_w/5\nu_g l_c N_c \tag{8.1}$$

$$Re_c = U_w D_c/\nu_g < 10 \tag{8.2}$$

Where $U_w$ is the ambient flow velocity, $\nu_g$ is the gas phase kinematic viscosity, $l_c$ is the equivalent cylindrical length of the fuel elements, and $N_c$ is the number of fuel elements per unit volume.

However, given the applicable range of this formula, if the ambient flow velocity is strictly applied as a no-flow condition ($U_w = 0$) then no solution is possible. However, in reality some low ambient flow value likely exists, which near to the flame will be dominated by the fire-induced flow. Given that, the term $5\nu_g l_c N_c y$ represents the fuel bed drag force (with fuel

elements represented as cylinders), the in-bed flow velocity can be evaluated if the above-bed velocity is known.

While a limited number of formulations have previously been suggested for the description of this in-bed flow [47,405], there appears to remain a lack of experimental data for testing and development of these formulations. The flow measurements presented in Chapter 5 represent novel measurements of the in-bed flow profile within pine needle fuel beds with various structural properties.

Even at higher (non-quiescent) wind speeds, this induced flow may have important implications for the combustion dynamics. Particularly ahead of the flame front, entrained fresh air may alter the oxygen supply rate and combustion region temperature [93]. Further experimental investigation of the variation between in-bed and above-bed horizontal flow profiles during spreading fires is required, alongside continued efforts to measure the pressure drop through fuel beds in a non-combustion scenario [83]. This thesis contributes to these required physical investigations for a wide range of fuel bed conditions.

#### 8.3.3. Radiation

In 1963, Emmons [52] presented an early, physically-informed flame spread model which assumed that in-bed radiation (from burning fuel elements) was the primary heating mechanism. This model was similar to that described in the 1961 report of The Committee on Fire Research [8], with the attenuation of radiation through the fuel bed described by an exponential term, described in detail in Section 8.5.1. The development of this exponential term was later described in detail by Hottel and Sarofim [406], and has been incorporated into several subsequent models [100,407].

As shown in this thesis (Chapter 6), and as discussed elsewhere [191], the assumption of dominant in-bed radiative heating is particularly applicable to low-intensity and/or no-wind flame spread scenarios. Despite acknowledging the lack of consensus over the relative importance of various heating mechanisms, Van Wagner [44] developed a radiation-dominated flame spread model, which considered only radiative heating from the flame. While Van Wagner suggested that ember radiation from the combustion zone could be incorporated within this model, this analysis was not conducted.

The consideration only of radiative flame heating considerably limits the applicability of Van Wagner's model. In the same year, Albini [407] presented a model for flame spread through brush,[22] which while also considering radiation as dominant, included consideration of several other physical processes including flame bathing and attachment. Such phenomena are of considerable current interest given the recent work of Finney *et al*. [72,216] on intermittent flame heating (as discussed in Chapter 2). Meanwhile, the radiation sub-model used by Albini was the same as that used previously by Hottel *et al* [408]. Notably, a rudimentary term was included to describe the effect of wind, in which the flame angle was described by the Froude number.

Hottel (and colleagues) [408] presented their own set of flame spread models in 1965, evaluated, rather unsatisfactorily [61], against observations from experiments involving newspaper and cardboard. Four different models, involving respectively a linear or non-linear

[22] Brush describes a fuel system dominated by shrubs.

cooling term for both infinitely thin and thick slabs, were presented. All four models incorporated radiative flame heating and ember heating, as well as local convective heating (with turbulent eddy transport described by a Gaussian distribution [19]), while also allowing for an external radiation source. These models included one of the earliest detailed considerations of the view factor between the flame and the fuel bed [229].

These models were revisited by Kwentus [61] who developed a surface fire model based upon the same slab concept. A linear heat loss approach was adopted, given the unsatisfactory performance (in comparison to experimental observations) of the more complex non-linear approach. Predictions from Kwentus' refined model still deviated from experimental observations. This modified version also incorporated heat sink terms for pyrolysis and mass transport, while flame radiation was determined to be of greater significance (relative to the externally imposed radiation) than had originally been assumed. Kwentus represented the flame as a series of line radiation sources, rather than the vertical black plane assumed by Hottel *et al.* [408], however the planar assumption has been used in a number of other models [44,47,70,142,409,410].

In a similar manner to Hottel *et al*. [408], Van Wagner [44] considered the flame as a planar source transferring radiation to the surface of a fuel bed (considered to be thermally thin). A simple view factor was defined using the general solution for radiation between a radiating strip of infinite length and a small receiving element. This surface heating approach, employed also by Hottel *et al*. [408] and various others [402,403,411], has since been criticised. De Mestre *et al.* [142] argued that this approach (which essentially treats the fuel surface as a solid surface) is inapplicable to highly porous fuel beds (such as pine needle beds) which are in fact semi-transparent. As such, De Mestre *et al*. [142] instead determined the radiant energy transferred to a small rectangular fuel volume, with attenuation through the semi-transparent fuel bed described by an exponential decay term.

The view factor is scenario dependent and the majority of existing models consider linear flame spread scenarios, in which the flame front progresses in a single linear direction across a fuel bed. However, the view factor between the flame and unburnt fuel would vary significantly during radial propagation (e.g. from a point source as shown in Figure 2.5), which may favour increased spread rates in this radial scenario [402]. One of the few models to determine a view factor for this radial scenario was provide by Cekirge [402], in which a cylindrical flame was assumed.

In subsequent sections, common underlying assumptions for radiative flame heating and in-bed heat transfer are evaluated through comparison with the experimental observations from previous chapters. In particular, the applicability of existing view factor formulations are assessed based upon the heat fluxes measured during the experiments described in Chapter 4. The common conceptual basis for the description of radiative attenuation through porous fuel beds is also discussed in terms of its applicability to pine needle beds.

## 8.4. Above-Bed Flame Heating

### 8.4.1. Buoyant Plume Region

Many of the approaches to determining the flame emissive power require the selection of a representative flame temperature and flame shape however, these are difficult to determine experimentally. By revisiting the flame spread experiments presented in Chapter 4, it is

possible to examine further the temperature distribution and flame dimensions above the fuel bed.

Based on the thermocouple tree measurements (described in Chapters 3 and 4), Figure 8.1 shows the maximum temperature at any thermocouple location (irregularly spaced from 0.05 m to 1 m above the table surface) for each fuel bed condition. These temperatures therefore represent the maximum instantaneous temperature measured within the buoyant plume at each fuel bed condition.

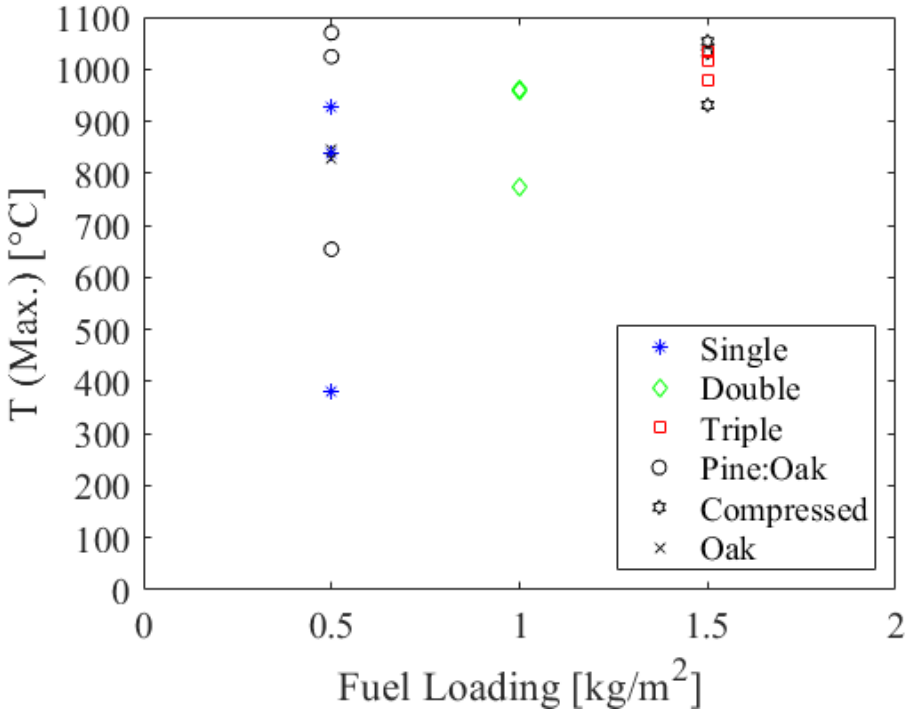


**Figure 8.1 - Maximum plume temperature for flame spread experiments conducted with six different fuel bed conditions as presented in Chapter 4.**

As seen in Figure 8.1, a wide range of maximum temperatures (382 °C to 1070 °C) was observed. This significant variation, even at a given fuel bed condition, may reflect the spatially and temporally transient nature of the flame envelope, as shown in Figure 8.2. Therefore, it is possible that, in a given experiment, none of the thermocouples will be engulfed in flame for a significant period. If only the maximum temperature at any single thermocouple is considered for each fuel bed condition (across all replicates) then the range narrows considerably (847 °C to 1070 °C). The temperatures indicated by this second, shorter range, are similar to the flame temperatures observed or assumed in other previous forest fuel studies by a number of past authors [47,133].

**Figure 8.2. Images from high-speed videos of flame shape during a demonstration with a 0.8 kg/m$^2$, 10 kg/m$^3$ Pitch-Loblolly hybrid Pine needle bed**

If the midpoint of this shorter range is calculated, then an approximate average maximum temperature of 960 °C is obtained. However, caution is required when interpreting this value, as the accuracy of mean temperature values are limited by the available description of the overall statistical variability [93].

The period over which the maximum local temperature occurs can also be relatively short. This is illustrated in Figure 8.3, where the effect of smoothing (moving averages of 1 s and 5 s) are investigated for a single temperature measurement at each pine needle fuel bed loading. A more systematic investigation would be required for a quantitative comparison but it is interesting to observe the sharp reduction in maximum temperature measured by the thermocouple if significant smoothing is applied, highlighting the short heating period that can occur. This is also observable (over a much wider dataset) in the characteristic curve of the thermocouple temperature profile which is characterised by a period of slow heating as the flame approaches, followed by a sharp spike in temperature at flame arrival.

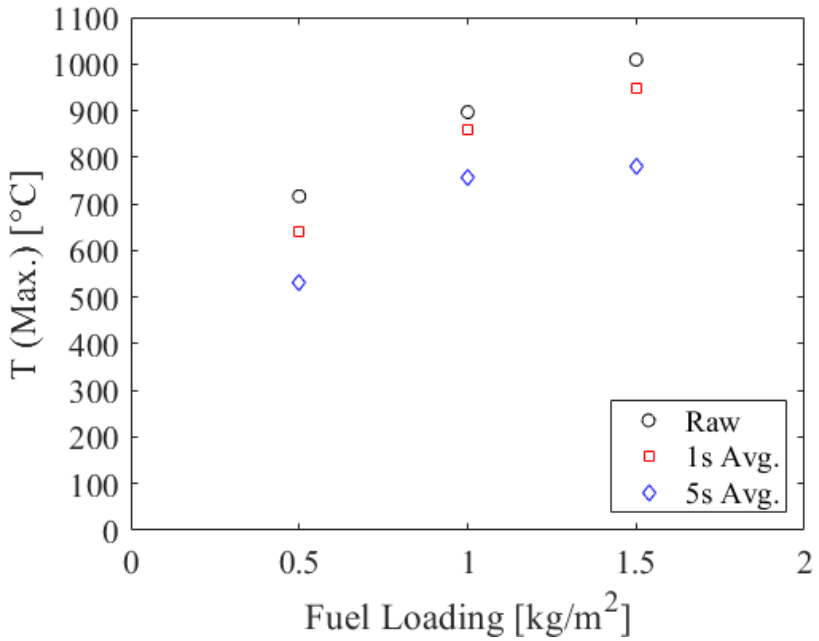


**Figure 8.3 - Qualitative example of the effect of time-averaged smoothing and the low period of maximum temperature for each pine needle bed fuel loading in Chapter 4. Raw temperatures are the maximum temperatures during the 10 Hz sampling duration. Maximum values following the application of a 1 second and 5 second moving average are also shown.**

This analysis also assumes a uniform flame temperature throughout the flame envelope however, in this study, significant variation in flame temperature with vertical height was observed, as shown in Figure 8.4. This figure shows the maximum flame temperature (at any time) recorded at each thermocouple location, for each replicate experiment at a given fuel condition. The time at which this maximum temperature is measured may therefore vary at each thermocouple location. Alternatively, the plume vertical temperature distribution at a single point in time (flame arrival at the bottom thermocouple) is shown in Figure 8.5.

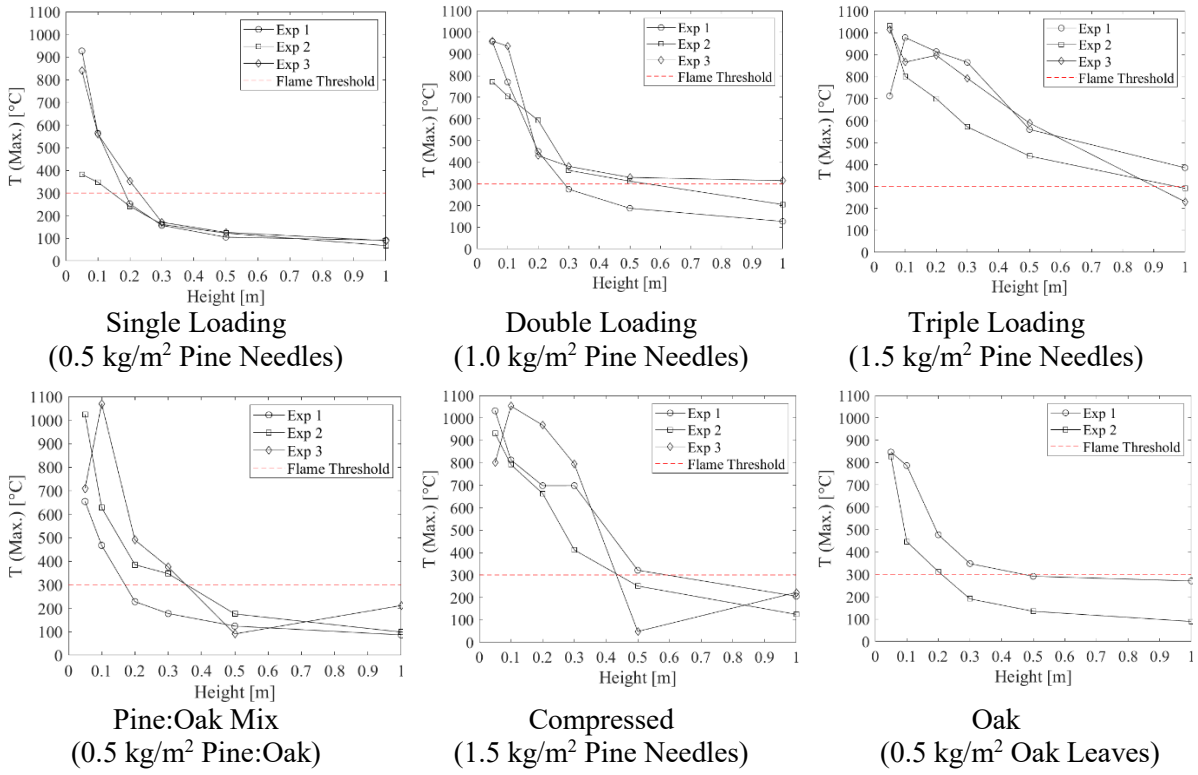


**Figure 8.4 - Vertical distribution of maximum convective plume temperature relative to the height above the table surface. Maximum temperature recorded at any point in experimental duration is shown for each thermocouple. Each line represents a replicate experiment at that condition.**

As shown in both Figure 8.4 and Figure 8.5, generally the temperature decreases with increasing vertical distance in the buoyant plume. This provides insight into the flame dimensions at each fuel bed condition. As discussed in Chapter 4, and as shown in Figure 8.4 and Figure 8.5, a temperature threshold of 300 ° can be assumed to indicate flame presence at a given thermocouple. This allows a flame height to be estimated, as well as a flame area, since the flame width was equal to the fuel bed width at all fuel conditions studied in Chapter 4. As previously discussed this will not however account for the transient flame shape effects (e.g. flame flickering) that occur.

Finally, an interesting feature of Figure 8.5 is the slight initial increase in temperature with vertical height in some of the higher fuel loading fuel beds (double and triple loading). A number of these experiments display a slightly greater flame temperature at a height of 0.1 m than at the lower measurement location (0.05 m). This may be as a result of the more sustained flame presence at this height, but may also reflect some slight forward tilting of the flame.

However, for the triple loading case, this analysis is complicated by the greater fuel bed height (5.5 cm). The lowest thermocouple (0.05 m above table surface) is therefore located just within the fuel bed, rather than in the above-bed flame envelope, at this fuel condition.

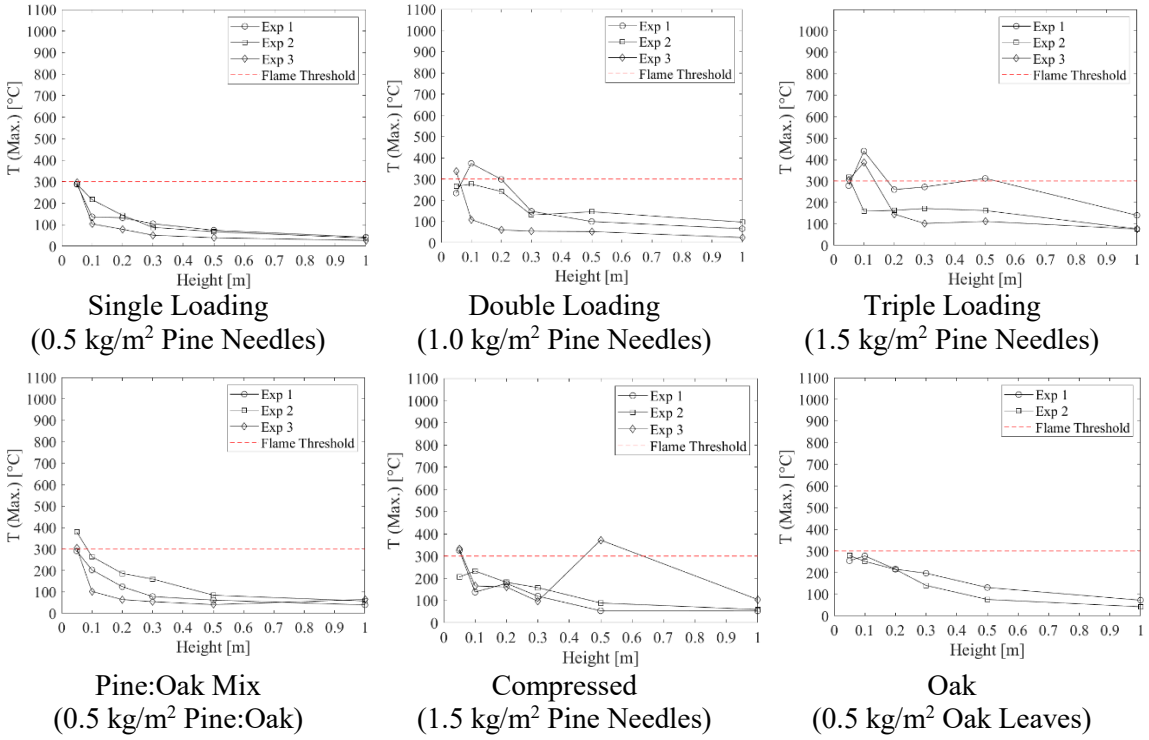


**Figure 8.5 - Vertical distribution of convective plume temperature relative to the height above the table surface, at the time of flame arrival at the bottom thermocouple location (Arrival defined as first measurement > 300 °C or max. temp if max temp < 300°C). Measurements from all thermocouples recorded simultaneously. Each line represents a replicate experiment at that condition.**

These measured temperatures highlight the difficulty in selecting a single representative flame temperature. Significant temperature variability was observed across fuel conditions and within a given flame envelope. Radiative emissions from the flame region are greatly influenced by the chosen flame temperature given the dependence on $T_f^4$. Small adjustments to the chosen flame temperature can therefore easily allow prediction of the desired emissive power but the basis for these adjustments is often unclear.

### 8.4.2. View Factor

Using the heat flux measurements for the flame spread experiments described in Chapter 4, the actual radiative transfer between the overhead flame and a gauge at the fuel surface can be investigated. The radiant heat flux from the flame (measured at the fuel surface) is shown for three different fuel loadings in Figure 8.6. In this figure, the radiant heat flux profile at the fuel surface is shown for each replicate experiment. As in Chapter 6, the radiant heat flux from the flame increases with increasing fuel loading, despite the slight variation in bulk density that exists across these three fuel beds (representing the fuel manipulations studied in a recent field study [85]).

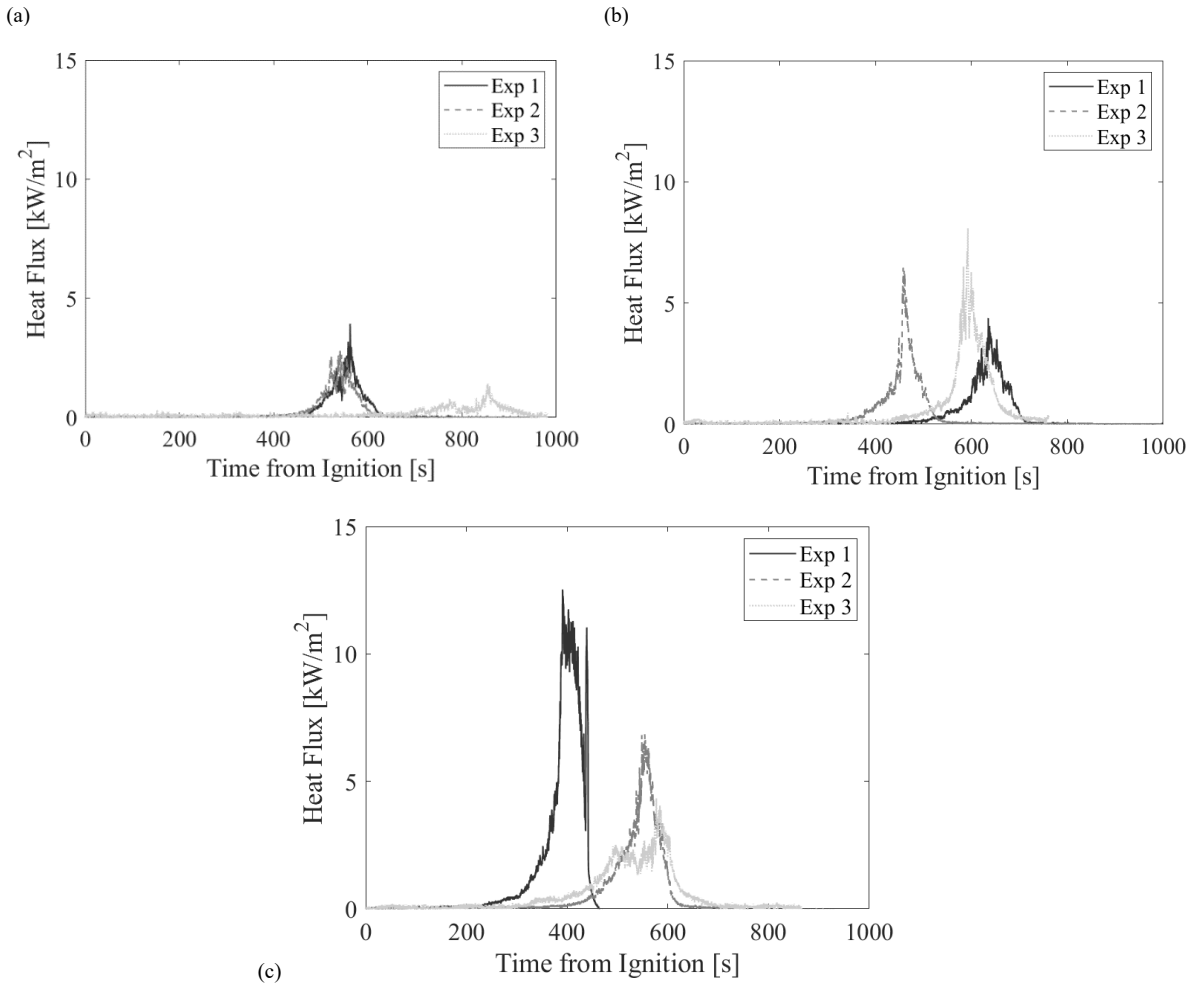


**Figure 8.6 - Radiative flux at the top surface of the fuel bed for the (a) single (0.5 kg/m$^2$), (b) double (1.0 kg/m$^2$) and, (c) triple loading (1.5 kg/m$^2$), pine needle fuel beds described in Chapter 4. Each line represents a separate replicate experiment**

The radiative flux measured at the fuel surface depends not only on the emissive power of the flame but also on the relative geometrical relationship between the flame and the fuel bed. This relationship can be described by the view factor (or configuration factor). In Figure 8.7, the ratio of the instantaneous radiative flux (measured at the fuel surface) to the maximum radiative flux (also measured at the fuel surface) is shown for the three fuel loadings studied in Chapter 4. This maximum irradiation represents the flame arrival point, at which the flame front sits directly above the gauge, and can be considered as the flame flux. The ratio at any time represents the proportion of this flame flux that has been transferred to and received by the gauge.

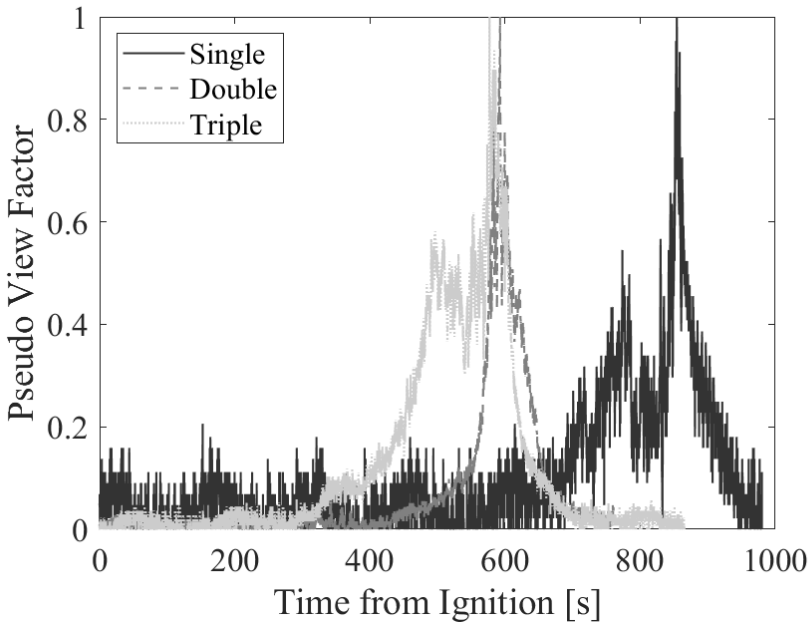


**Figure 8.7 - Ratio of the instantaneous radiant heat flux measured at the fuel bed surface to the maximum radiant heat flux measured at the fuel bed surface. For a single (0.5 kg/m$^2$), double (1.0 kg/m$^2$) and, triple loading (1.5 kg/m$^2$), pine needle fuel bed**

As shown in Figure 8.7, this ratio of the instantaneous surface radiant heat flux to the maximum surface radiant heat flux remains low throughout the majority of the experimental duration. Even during the heating period, this ratio remains low (typically significantly less than 0.5) until a short spike, indicative of flame arrival, occurs.

The radiative heating distribution ahead of the flame front can be further explored by plotting the radiative flux measured at the fuel surface as a function of the distance ahead of the flame front. This is shown Figure 8.8 for each of the three fuel loadings, where x=0 was determined based upon flame arrival at the gauge.

This measured radiative heating distribution can be compared with the predicted profiles obtained using commonly used view factor approaches. Multiple previous physical models have described this view factor using the crossed-string method [47,407,408], as introduced by Hottel [8] and subsequently described in detail by Hottel and Sarofim [406].

The exact notation of the resulting view factor as a function of distance from the flame front V(z) varies between authors. Generally however, the flame is represented by a black radiator, and a typical formulation was given by Pagni and Peterson [47],

$$V(z) = \frac{1}{2}\left[1 + Z(1+Z^2)^{-\frac{1}{2}}\right] \tag{8.3}$$

Where,

$$Z = \tan\theta - \frac{z}{L\cos\theta} \tag{8.4}$$

Where $z$ is the distance ahead of the flame front and $\theta$ is the flame tilt angle (from the vertical), and $L$ is the flame length. Therefore, for vertical flames where the flame tilt angle is zero,

$$Z = -\frac{z}{L} \tag{8.5}$$

The applicability of this term was evaluated for the three fuel loadings described in Chapter 4, each of which had a different average flame height, as shown in Section 8.4.1. The measured radiative flux for each experiment at a given condition is plotted (as a function of distance of the flame front from the gauge) against the predicted profile (using Equation 8.3) in Figure 8.8.

As shown in Figure 8.8, this theoretically calculated view factor cannot be sensibly compared with the initial radiative flux measured at the gauge position (x = 0 mm). The radiative flux measured at this location is received when the flame is positioned directly above the gauge, and therefore the radiator and receiver are essentially aligned in parallel rather than perpendicularly. This represents the view factor, which considers the radiator and receiver to be perpendicular at all times, is therefore half of the actual measured flame flux.

Greater attention can be afforded to the heat flux decay ahead of the flame (measured from the gauge location in Figure 8.8). For cases such as in this study, in which the flame is essentially perpendicular to the fuel bed surface, this view factor (expressed as a function of distance from the flame front) is dependent only upon the flame length. For each fuel bed condition in Figure 8.8, the view factor was calculated according to the average flame height measured at each condition as presented in Chapter 4 (Single: 0.12 m, Double: 0.23 m, Triple: 0.80 m). As seen in Figure 8.8, this theoretical view factor most closely represented the actual flame radiation decay for the lower flame height cases, such as the single loading fuel bed (0.5 kg/m$^2$ fuel bed with average flame height of 0.12 m). At higher flame heights, the exponential decay observed experimentally was not predicted accurately.

A sharp spike in the peak radiant heat flux ratio was observed for a single experiment for the triple fuel loading (1.5 kg/m$^2$) case. This likely represents a secondary heating phase as a result of either the passage of a secondary flame front or deposition of burning fuel elements onto the heat flux gauge. As seen in Figure 8.8, the peak radiant flux ratio quickly reverts to a similar decay trend to that observed in the other replicate experiments, after this short spike occurs.

Therefore, while this classical approach to the flame spread view factor may be applicable in certain cases, it appears to be less applicable in scenarios involving greater flame heights. In these situations, the predicted decay profile (of the flame flux as a function of distance from the flame front) is under-predicted by this crossed-string method approach. The greater discrepancies at greater flame heights is of particular significance given the greater importance of flame heating in these cases, as shown in Chapter 6. Further comparison should be undertaken with the complimentary field experiments in order to understand the implications of flame front scaling on these observed trends.

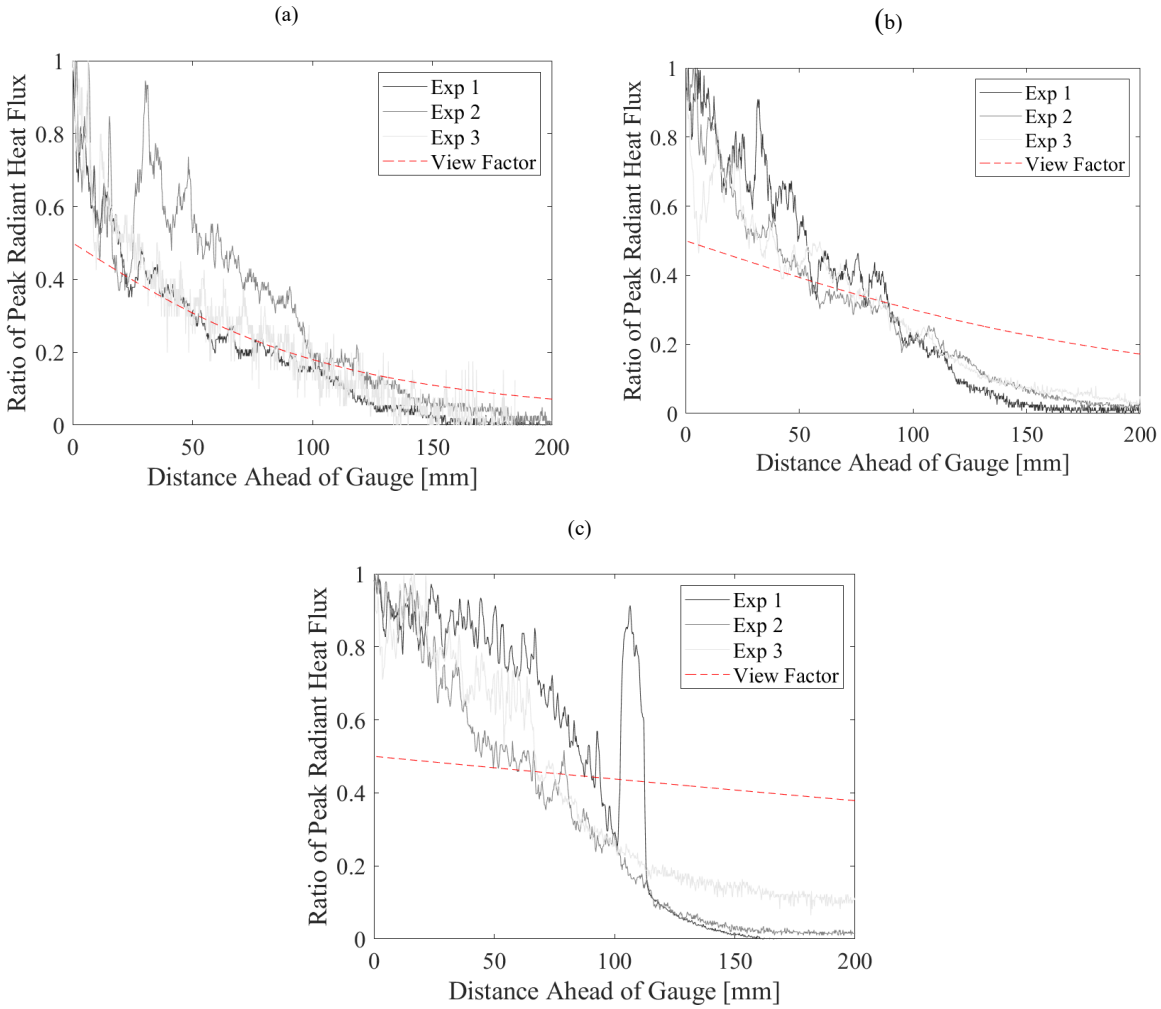


**Figure 8.8 - Comparison of crossed-string method view factor (red -- line) and the measured radiative fluxes (for each replicate experiment) to the top surface gauge as a function of distance from the flame. Comparison shown for the fuel beds described in Chapter 4 of (a) single fuel loading (0.5 kg/m$^2$) (b) double fuel loading (1.0 kg/m$^2$) (c) triple fuel loading (1.5 kg/m$^2$). Three replicate experiments plotted at each condition**

## 8.5. In-Bed Heat Transfer

The detailed heat transfer study presented in Chapter 6 highlighted the important role of in-bed heat transfer in quiescent, porous flame spread, particularly at lower values of $\alpha\sigma\delta$. The experiments presented in Chapter 6 included heat fluxes measured during and after flame arrival at the heat flux gauge, in addition to heat fluxes measured during the pre-heating phase. In order to isolate this pre-heating phase, an additional series of experiments were conducted across a smaller range of fuel conditions (Fuel Loading: 0.4 to 0.8 kg/m$^2$, Bulk Density: 10 to 40 kg/m$^3$). As in past studies [226,228], in these additional experiments the heat flux gauges were positioned beyond the end of the table (and therefore were not engulfed in the flame at any time). Separate measurements of total heat flux from the flame and fuel bed combustion regions were conducted.

As shown in Figure 8.9, the total heat flux from the combustion region appears to be significantly higher than the total heat flux of the overhead flame. This is in line with the observations presented in Chapter 6. The actual measured flame heat fluxes will be affected by the transient and spatially dependent behaviour of the flame as shown previously in Figure 8.2.

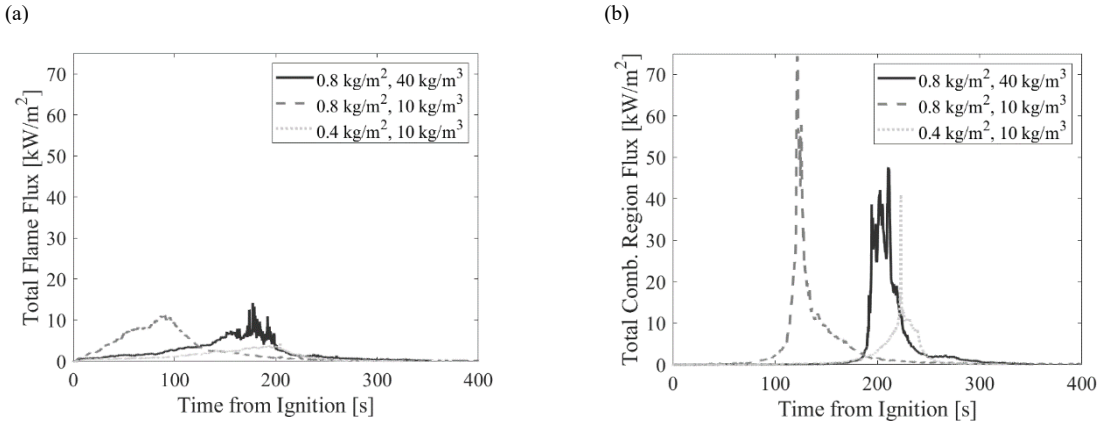


**Figure 8.9 – (a)Total fluxes, measured just beyond table, for overhead flame (gauge centred at 25 cm above table surface) (b) Total fluxes, measured just beyond table, for combustion region (gauge centred at 1 cm above table surface), for fuel bed of different fuel loading and bulk densities (Pitch-Loblolly hybrid Pine needles)**

Accurate representation of the in-bed heating mechanisms within simplified physics-based models is therefore of great importance. This is particularly true in the quiescent flame spread scenarios considered in this thesis, in which the convective heating contribution is reduced. Stefan-Boltzmann's law can provide an initial estimate of the emissive power of embers within the combustion region, assuming an accurate ember temperature and emissivity can be defined [93]. However, to describe the heat transfer from the combustion region to the unburnt fuel, the attenuation by intervening fuel particles must also be suitably described.

### 8.5.1. Fuel Bed Attenuation

The attenuation profile of a porous media is dependent upon its structure and the relative volumes and arrangements of air and the solid elements. As radiation travels through a medium with obstructions, a reduction in radiation can occur because of scatter and dissipation (also known as absorption). The absorption can be related to the emissivity via Kirchoff's Law [406], and classical attenuation theories are well-developed. An attenuation profile for wildland fuel beds can be defined from classical theory, with Hottel (in a 1961 Committee on Fire Research report) [8] suggesting a suitable form for randomly oriented fuel beds.[23] While the Committee on Fire Research described a simple theoretical example, the transmission of radiation through brush fuel beds was described in further detail shortly after by Kwentus [61].

The Committee on Fire Research [8] initially presented simple definitions of the absorptivity coefficient (defined as the fraction of the heat flux $Q(x)$ absorbed per unit length in the x-direction perpendicular to the flame front) for a simple, 2-D fire front, in an 'idealised forest'. As shown in Figure 8.10, this idealised forest is composed of a statistically homogenous set of

[23] Also discussed in further detail in the subsequent book titled 'Radiative Transfer' co-authored by Hottel and Sarofim [406].

randomly distributed fuel elements of height $h$. The heat flux $Q(x)$ describes the heat transfer mechanism responsible for the pre-heating in the pre-heating region ahead of the advancing flame front, and may represent radiative (from embers or flame region) or convective heating.

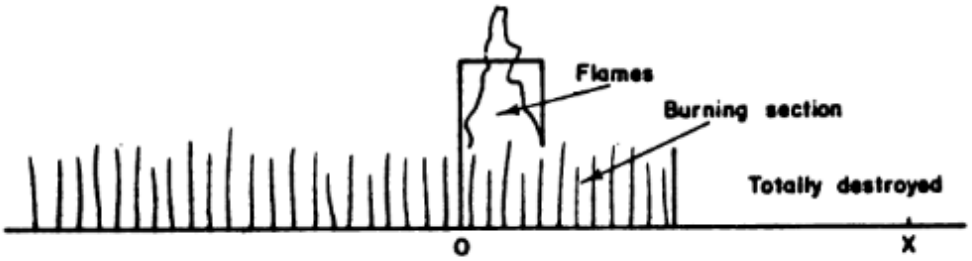


**Figure 8.10. Schematic of idealised forest. Extracted from 1961 report of the Committee on Fire Research [8]**

If $Q(x)$ is chosen to represent horizontal radiation, and assuming all fuel elements are vertical cylinders of diameter D, the absorptivity coefficient $\alpha$ is described by the product of the fuel element diameter ($D$) and the number of fuel elements per unit area ($n$),

$$\alpha = nD \tag{8.6}$$

This idealised scenario is effectively describing the attenuation through a series of simplified, hypothetical 'trees', and can be described as the 'tree blockage statistics' [8]. Similar equations can be derived for fuel elements of different shapes through consideration of their radiation geometry, particularly the ratio of random projected area ($A'$) to surface area ($a'$). This can then be used to describe the emitted radiant energy by a fuel particle at position x,

$$dQ' = \alpha\epsilon\sigma T_b^4\, dx = \alpha q dx \tag{8.7}$$

Where $\epsilon$ is the fuel element surface emissivity, $\sigma$ is the Stefan-Boltzmann constant, and $T_b$ is the burning temperature of the fuel element.

Additional assumptions and simplifications would be required to derive similar terms, relating Q and $\alpha$, for flame radiation and convective heating by turbulent eddy effects. If these additional terms are ignored, and only horizontal radiation from burning fuel elements is considered, the radiative energy received at the origin, from a fuel particle burning at position x, is given by,

$$dQ = dQ' e^{-\alpha x} \tag{8.8}$$

This accounts for absorption by intervening fuel elements. The total radiative energy through the origin (and into the pre-heating region) is given by,

$$Q = \int_0^c \alpha Q^0 e^{-\alpha x}\, dx = Q^0(1 - e^{-\alpha c}) \tag{8.9}$$

Where the burning region limits are the fire front origin, and the trailing edge of the burning section (Point c) as shown in Figure 8.11. From this formulation, and by considering the energy required for fuel particle ignition, a simple energy balance could be constructed. However, we will focus here on the further derivation of the transmission properties of a fuel bed, provided by Hottel and others [8].

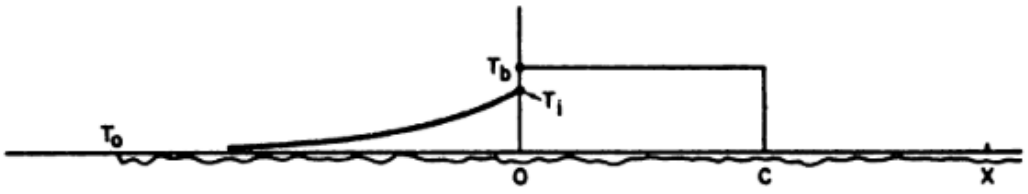


**Figure 8.11 – Temperature distribution in a forest fuel bed. Extracted from 1961 Committee on Fire Research Report [8]**

Hottel, and the Committee on Fire Research [8], described transmission of a radiant beam ($\tau$), for the specific case of 'the penetration of radiation through randomly oriented obstructions' using,

$$\tau = e^{-nA'L} \tag{8.10}$$

Where $n$ is the particle concentration, $A'$ is the capture cross-section and their product is equal to the attenuation coefficient $k$, while $L$ is the length over which the beam travels. The mean free path is given by the reciprocal of the attenuation coefficient. This equation therefore represents the classical equation derived initially by Bouguer and subsequently by Lambert [406].

This equation applies to cases in which the particle concentration and capture cross-section are constant along the path (constant attenuation coefficient). Alternative equations can also be derived for non-particulate obstructions. For example, the transmittance of rod-like obstructions along lines of random orientation, with aggregate length per unit volume of space of $I$, is given by,

$$\tau = e^{BIL} \tag{8.11}$$

Where B is the mean projected area of a rod per unit length. For these equation to be valid, element surfaces must be complete absorbers (black body absorption), there must be negligible interference ($\sqrt{A'} > \lambda$ or $\sqrt{B} > \lambda$), and the path length must be of sufficient length to allow a continuum treatment ($L \gg \sqrt[3]{1/c}$ or $L \gg \sqrt{1}/B$).

Therefore, the capture diameter or cross-section must be determined for the fuel elements of interest within a given fuel strata. As before, the fractional radiation intensity decrease along a path with obstructions is,

$$\frac{dI}{I} = a\, dx \tag{8.12}$$

Where $dI$ is the magnitude of absorption of a collimated beam of monochromatic radiation of intensity $I$, and $a$ is the total projected area per unit volume (product of projected area per particle and the number of particles, divided by the volume), which is dependent upon the fuel particle shape.

Where particles are randomly positioned, some overlapping of particles will occur causing some shadowing. Therefore, complete interception of radiation will not occur and instead $\frac{1}{e}$ of the radiation will be transmitted. For randomly oriented, convex particles (in which particle orientation is random but no part of the surface views another part of the surface) on an average basis, half the surface will be illuminated by the incident beam. A simple relationship for the projected area of a particle, with illuminated surface $dA$, and with a normal angle to the radiation of $\theta$ is given by $dA\cos\theta$.

An average projected area can then be calculated by weighting this projected area term ($dA\cos\theta$) by the solid angle about the normal ($\sin\theta\, d\theta d\backslash\psi$) and integrating over the entire hemisphere, giving,

$$dA_{av} = \int_{\theta=0}^{\frac{\pi}{2}} \int_{\psi=0}^{2\pi} \frac{dA\cos\theta\, sin\theta\, d\theta\, d\psi}{2\pi} = \frac{dA}{2} \tag{8.13}$$

Where $\theta$ is the polar angle, and $\psi$ is the azimuth angle. This applies only to black particles with characteristic dimensions much greater than the radiation wavelength. Since only half the element is illuminated, the effective area of interception is $\frac{dA}{4}$, and therefore an attenuation factor of $\frac{a}{4}$ is derived. The random projected area, for an element with three finite dimensions, is the mean projected value across $4\pi$ steridians. This is not unexpected, since the element has an equal chance of orientation throughout $4\pi$ steridians, and can therefore be considered to behave similar to part of the surface of a sphere.

The Committee on Fire Research report listed the radial geometry of a number of element shapes and these are presented in Table 8.1. For sphere, long circular rods, and thin long strips, the random projected area is equal to ¼ of the superficial area, and it was suggested that this also applies adequately to randomly oriented forest fuels.

**Table 8.1 – Radiative geometry for various fuel element shapes [As given in 1961 report of the Committee on Fire Research [8]]**

| Shape | Characteristic Dimensions | Volume | Surface Area (a) | Normal Projected Area ($a'$) | Random Projected Area ($A'$) | $\frac{A'}{a'}$ |
|---|---|---|---|---|---|---|
| Sphere | Diameter | $\pi D^3/6$ | $\pi D^2$ | $\pi D^2/4$ | $D^2/4$ | ¼ |
| Long round rods | Diameter Length | $\pi D^2 L/4$ | $\pi DL$ | $DL$ | $(\pi/4)DL$ | ¼ |
| Long square rods | Side Diameter Length | $D^2 L$ | $4DL$ | $1.122\ DL$ | $0.881DL$ | 0.22 |
| Thin flat sheets | Area Thickness | $a'W/2$ | $a'$ | $a'/2$ | $a'/4$ | ¼ |
| Long thin strips | Width Thickness Length | $DWL$ | $2DL$ | $(2/\pi)DL$ | $DL/2$ | ¼ |

The approach which has just been described is well-used throughout existing modelling approaches [93,100]. However, as has been shown, this approach assumes that the fuel elements are randomly oriented, and that the resulting fuel beds therefore display isotropic radiation properties. A casual glance however, of a pine needle fuel bed will indicate a preferential orientation of fuel elements, with a tendency to align more closely to an orientation parallel to the substrate layer beneath. This preferential angle may vary with the fuel structure, and logically, for a fuel bed of fixed fuel loading, the needles must assume an increasingly vertical alignment as the bulk density is lowered (fuel height increased).

This variation in attenuation properties is important, with previous experimental and theoretical studies identifying a negative trend between absorption coefficient (for a constant S-V ratio) and the spread rate, despite an increase in ember radiation [61,101]. Where greater fuel bed attenuation occurs, the overall magnitude of the fuel bed heat sink is increased.

Additionally, the directional dependence of the fuel bed radiation attenuation properties may have important implications for the relative importance of different heat transfer paths. For example, Telisin [411] described a quiescent/opposed flow flame spread model in which radiative flame heating could be considered to extend vertically into the fuel bed to a distance equal to the mean free path, below which only horizontal heat transfer would occur. In such a model, greater vertical attenuation will therefore increase the relative contribution of the in-bed heating (both flaming and smouldering combustion occurring within the in-bed combustion region).

Simeoni *et al.* [223] and Vaz *et al*. [139] previously observed that fuel beds, of the type studied here, may be anisotropic. However, more detailed investigation is required before a full, quantitative description of the attenuation properties can be derived, perhaps using an approach similar to that previously introduced by Vaz *et al.* [139].

## 8.6. Conclusions

Various simplified physics-based models were reviewed, highlighting several common approaches that underpin many of these existing models. Unlike the semi-empirical model investigated in Chapter 7, these models explicitly define individual heat transfer terms.

However, experimental investigation is required to test and develop these individual terms, while individual account must be taken of the significant heat transfer mechanisms in a given scenario. The suitability of existing heat transfer terms and modelling approaches was evaluated for the pine needle beds used in this study, for which the heat transfer mechanisms were explored in detail in Chapter 6.

The dominance of in-bed heating for the flame spread scenario studied in this thesis was described in this previous chapter and reaffirmed by further analysis in this chapter. This scenario was therefore well suited to a number of existing simplified physics-based models, which have often focused on radiative heating. Conduction was considered negligible in many existing simplified physics-based models, and was typically excluded from analysis. Only a very few existing models allow for significant convective heat transfer, despite the need to incorporate convective cooling terms even in quiescent scenarios.

Where convection has previously been considered in detail, there are often limits to the applicability of existing terms when applied to the flame spread scenario and fuel beds used in this thesis. Relevant models were often either developed in very different fuel types (e.g. highly discrete fuel elements) or do not explicitly account for fire-induced flow, limiting application in quiescent conditions. Further development of in-bed flow (and resulting convective heat transfer) terms is required to support the future use of this class of model. A useful starting point would be additional comparison of in-bed and above-bed horizontal entrainment profiles in a flame spread scenario. Along with ongoing efforts to measure the drag profile of vegetative fuel structures, this would also support the development of convective heat transfer modelling within detailed physics-based models.

For radiative heating, existing models typically define separate formulations to describe the flame and in-bed radiative heating contributions. The difficulty in determining the emissive power of a flame (even *a posteriori*) is well known, and was demonstrated through analysis of the flame properties in the flame spread experiments described in this thesis. The transient flame shape and spatial variability of the plume temperature was shown, even in this quiescent flame spread scenario. Based upon the heat flux measurements from these flame spread experiments, limitations were identified with the popular 'crossed-string' approach to view factor calculation. While the view factor predictions closely matched the observed radiative heating profile (at the fuel surface) for low flame heights (0.12 m) occurring at the baseline fuel loading (0.5 kg/m$^2$), significant variations occurred for the taller flame heights (0.23 m and 0.80 m) occurring at larger fuel loadings (1.0 and 1.5 kg/m$^2$).

Finally, existing approaches to modelling of in-bed heating, which was shown in Chapter 6 to be a significant contributor to the propagating flux, were also evaluated. Past authors have suggested that a classical Stefan-Boltzmann law approach can more easily be applied to estimate the emissive power of the in-bed ember region, than is possible with the above-bed flame. However, even if the emissive power is accurately predicted, the resulting heat transfer to an unburnt fuel particle can only be accurately determined if the attenuation by intervening particles can also be adequately described. Past authors have questioned the suitability of an isotropic radiation assumption for natural fuel beds, and analysis of classical approaches has highlighted a potential lack of applicability to pine needle beds. Possible future research directions have been outlined in order to address the issues that occur because of the preferential angle of inclination of pine needles. This should also take into account the effect

of fuel structure, as (at a constant fuel loading) variations in fuel height will alter this average angle of inclination.

# Chapter 9

## Conclusions

# 9. Conclusions

*...In that Empire, the Art of Cartography reached such Perfection that the map of one Province alone took up the whole of a City, and the map of the Empire, the whole of a Province. In time, those Unconscionable Maps did not satisfy, and the College of Cartographers set up a Map of the Empire which had the size of the Empire itself and coincided with it point by point. Less Addicted to the Study of Cartography, Succeeding generations understood that this Widespread Map was Useless, and not without Impiety they abandoned it to the Inclemencies of Sun and of the Winters. In the deserts of the West some mangled Ruins of that Map lasted on, inhabited by Animals and Beggars; in the whole country there are no other relics of the Disciplines of Geography.*

***Jorge Luis Borges – On Rigor in Science*** [412]

## 9.1. Summary

This chapter provides a summary of the main research outcomes, and outlines the contribution to the nascent field of prescribed fire science, and to wildland fire science more generally. These outcomes include the systematic measurement of key physical properties (flow, heat transfer, energy release) for a wide-range of fuel conditions relevant to field applications. This thesis addresses existing gaps in the availability of experimental data for key physical processes, and will aid the continuing development of physics-based flame spread models. It also allows further investigation of previously identified issues with the semi-empirical Rothermel model by providing physical insight into the cause of model oversensitivity to fuel height.

Additional analysis of the experiments in this thesis has identified key physical phenomena and controlling mechanisms for a low-intensity flame spread scenario (typical of prescribed fire use) and illuminated the role of fuel structure on these underlying physical processes. The ability of existing modelling approaches to accurately predict this flame spread behaviour, and to represent the effects of fuel structure on these complex physical phenomena, has been assessed. These efforts have provided insight for (prescribed) fire science research efforts including the introduction of alternative descriptors of fuel bed structure; identification of current model limitations; and the identification of areas requiring further experimental investigation.

## 9.2. Thesis Aims

It is useful to revisit the study aims, outlined at the outset of this thesis, in order to provide greater context for the concluding remarks in this chapter. The main objective of this thesis was to evaluate and describe the effect of fuel bed structure on flame spread processes in natural porous fuel beds. This required initial evaluation of the existing literature in order to understand previously observed trends between fuel structure and fire behaviour and to identify the physical mechanisms believed to account for these effects, but for which experimental investigation had thus far been limited. Assessment of the applicability of existing structural parameters, proposed for various porous fuel types, was also required, and the need for more physically relevant dimensionless parameters was established.

The primary thesis objective was then met by undertaking a detailed, systematic study of the effect of fuel structure on fire behaviour (flame spread, heat release rate, flame height, residence time, burning rate) and the underlying physical processes (heat transfer, fluid flow). To provide insight for ongoing (prescribed) fire science efforts, this study focused on a low-intensity flame spread scenario, with fuel conditions established based upon prior sampling of a study site within an area of active prescribed fire use and research. The aim throughout these experimental studies was to provide accurate measurement of physical processes required for further development of detailed physics-based models; to provide insight into the controlling mechanisms of low-intensity flame spread (and the role of fuel structure); and to allow the assessment of existing semi-empirical models (e.g. Rothermel model) and simplified physics-based modelling approaches.

## 9.3. Research Outcomes

Several key research outcomes are summarised below:

- Both fuel loading and bulk density independently affect the fire behaviour. Systematic variation of each parameter, achieved by controlling the fuel bed height, is required to understand these independent effects.

- A lack of independent variation of fuel loading and bulk density in several existing studies complicates efforts to understand the role of fuel bed height.

- Several existing dimensionless parameters fail to account for the role of fuel loading, which alters the optimum porosity.

- The dimensionless parameter $\alpha\sigma\delta$ (incorporating the fuel bed porosity ($\alpha$), surface-to-volume ratio ($\sigma$), and fuel height ($\delta$)) was strongly correlated with the rate of spread.

- Both the buoyant and fire-induced entrainment flow were affected by the fuel bed structure. Generally, a positive trend was observed between the fuel loading and the flow velocity magnitude.

- Increases in the buoyant flow velocity at higher fuel loadings were driven by the greater heat release rates. This has important implications for the flame angle and overall flow regime.

- In-Bed heat transfer was observed to be the dominant heating mechanism for all the fuel beds studied. However, the significance of flame heating was greater for fuel beds with higher $\alpha\sigma\delta$ values (at which taller flame heights were typically observed).

- A simple thermal model, incorporating only the in-bed radiative heating, accurately predicted the spread rate across all fuel conditions (max. variation = 29 %), with greater accuracy for lower $\alpha\sigma\delta$ fuel beds ($\alpha\sigma\delta < 200$).

- The inclusion of radiative flame heating in the thermal model led to over-predictions of spread rate highlighting the importance of the inclusion of cooling terms.

- Existing simplified physics-based models rarely allow for explicit calculation of the in-bed flow (and hence convective/cooling terms). Recommendations for further work to support the experimental data provided in this thesis have been outlined.

- The over-sensitivity to fuel height of Rothermel's flame spread model has been confirmed for the matt-type fuel beds studied in this thesis. Increased divergence in spread rate predictions was observed at lower values of $\alpha\sigma\delta$ ($\alpha\sigma\delta = 49$ to $\alpha\sigma\delta = 200$).

A more detailed discussion of the contributions of this thesis and the relevance for prescribed fire practice is provided in the sections that follow. This is accompanied by recommendations for further work to address identified gaps in the theoretical understanding of low-intensity wildland flame spread and issues identified with existing modelling approaches.

### 9.3.1. Experimental Observations

An initial series of laboratory-based flame spread experiments provided a broad assessment of the role of fuel structure and condition. The initial studied fuel conditions were chosen to represent the typical surface fuels within an area of the New Jersey Pinelands National Reserve (PNR), which plays host to significant prescribed burning and fire research activity [413]. The effect of fuel properties was assessed through the application of various fuel treatments, which altered the fuel loading, level of compaction, and fuel species composition.

The experiments were conducted as part of a wider multi-scale project (SERDP-RC2641), with similar fuel conditions studied in a recent series of complimentary field experiments [85]. The laboratory experiments offer additional insight, particularly into the role of fuel structure, given the greater level of control and measurement of fuel properties and environmental conditions (e.g. wind, ambient temperature) that is achievable within this environment. These laboratory-based experiments represent an additional resource for future model development efforts, addressing a need for further detailed physical measurements to support numerical investigations of flame spread, and the effects of fuel structure [18,40].

Initially, the effect of fuel condition on the overall fire behaviour were assessed, followed by the effects on the overall fuel consumption. The observations in this initial study highlighted the importance of fuel loading to the fire behaviour of porous pine needle beds, despite an existing lack of agreement regarding the effect of fuel loading in other fuel types (e.g. grasses) [219]. A positive trend was observed between fuel loading and spread rate, flame height, and heat release rate. However, for spread rate this fuel loading effect was slight and within the range of experimental variability. The effect of fuel loading on fuel consumption was also apparent, with a linear trend observed between initial fuel loading and overall fuel consumption, as previously observed in field experiments involving similar fuel types [18].

A clear effect of bulk density on the fire behaviour and fuel consumption was also observed for these pine needle fuel beds. Compression of a 1.5 kg/m$^2$ fuel bed from a height of 5.5 cm to 2.25 cm (increasing the bulk density from 27.3 kg/m$^3$ to 66.7 kg/m$^3$) resulted in a 29 % reduction in the spread rate. This highlights the importance of adequately controlling, and independently varying, the fuel loading and bulk density by controlling the fuel bed height. A similar conclusion was previously reached regarding many existing bench-scale studies, motivating recent research efforts with constant mass fuel samples [32]. The lack of

independent study of these variables (fuel loading and bulk density) represents a significant limitation of many existing studies, and this is an issue that this thesis addressed.

The effect of fuel species was also apparent, as determined by investigating flame spread in fuel beds involving other fuel species (oak leaves, pine-oak mix). This has important management implications for the pine-oak dominated ecosystem in which the baseline fuel conditions for this study were established. There remains a need to understand the relative importance of chemical and physical effects that result in these inter-species variations as both the chemical and geometrical properties of these fuel species differed.

The initial experimental series also provided the motivation for the systematic study of the independent effects of these fuel structure properties on key physical phenomena (flow and heat transfer) controlling low-intensity flame spread, presented in subsequent chapters (Chapters 5 and 6). An initial analysis of fire behaviour in these experiments further highlighted the independent effects of fuel loading and bulk density, with neither parameter alone able to adequately explain the variation in fire behaviour (e.g. spread rate, flame height). This emphasises the need for accurate inclusion of these fuel structure effects within flame spread models, along with the development of additional fuel structure parameters with a closer link to key physical phenomena.

A review of previously proposed structural descriptors highlighted limits to their applicability to natural porous fuel beds, and particularly a failing to account for the effect of fuel loading on the optimum fuel bed packing. In an effort to address these issues, a modified dimensionless parameter, $\alpha\sigma\delta$ was proposed. This parameter incorporates the fuel bed porosity ($\alpha$), fuel element surface-to-volume ratio ($\sigma$), and fuel bed height ($\delta$). A strong correlation between $\alpha\sigma\delta$ and the spread rate through pine needle fuel beds of various structural conditions was observed. As with past dimensionless parameters, $\alpha\sigma\delta$ is linked to the key processes of fluid flow (and hence $O_2$ supply and convection), radiative transport, and fuel element energy absorption. However, it was apparent that more detailed measurement and understanding of the effect of fuel structure on these key physical processes was required. Further experimental work was therefore conducted in order to characterise the flow regimes and heat transfer above and within porous fuel beds with a broad range of structural properties.

Measurement of both the buoyant and fire-induced entrainment flow allowed characterisation of the buoyancy-dominated flow regime associated with low-intensity flame spread. By measuring the in-bed flow velocity, the effect of porous fuel structure (which exerts a drag force) was incorporated. The fuel structure was also observed to influence the buoyant flow profile within the convective plume above the fuel bed. A positive trend between fuel loading and the buoyant flow velocity was observed, along with a similar trend between the fuel loading and the heat release rate. This has important implications for the resulting flame spread behaviour, given past identifications of two separate flame spread regimes (plume-driven and wind-driven), the onset of which is determined by the ratio of buoyant to inertial forces. However, the onset conditions for these regimes remain poorly characterised by existing dimensionless parameters [226]. These observations emphasise the need to consider fuel loading effects on buoyancy forces in other flame spread scenarios (e.g. wind-aided, or up-slope spread) and may have implications for flame tilting and the resulting flame heating [228].

Changes to the buoyant flow profile also have implications for the fire-induced entrainment flow. Generally, the mean entrainment flow through the fuel bed was observed to increase with

increasing fuel loading. Variations in the in-bed flow velocity across different bulk densities highlight the important role of fuel bed structure. The observed entrainment flow trends provide a useful resource for continuing model development, especially given previously observed discrepancies in observed flow velocities (from preliminary experiments in this thesis) and predicted flow velocities behind the main flame front (using the Wildland Fire Dynamics Simulator) [40].

In particular, the work presented in this thesis provides additional clarification and quantification of the role of fuel structure within the complex feedback cycle that controls the overall flow regime. However, prediction of resulting in-bed flow velocities requires greater characterisation of the vegetation drag profile, which may vary over time as fuel degradation and consumption occurs. The development of appropriate drag profile terms has been aided by recent small-scale wind tunnel studies of natural fuel beds [56,83] in the absence of fire including those examining fuel conditions complimentary to those studied in this thesis [83].

For detailed physics-based models, particular further investigation is required to understand the drag forces associated with the remaining fuel structure behind the flame front (of fuel not consumed in the fire front). In this thesis, at all but the lowest fuel loadings (0.2 kg/m$^2$), significant volumes of remaining (unconsumed) fuel were observed in the large smouldering/char oxidation region behind the primary flame front. Further characterisation of the mass and structure of fuel within this trailing region is required to ensure adequate modelling of fuel removal and selection of appropriate bulk drag terms within detailed physics-based models. These bulk descriptors are required, as these structure effects will occur at the sub-grid scale for many detailed physics-based model applications.

Characterisation of the trailing smouldering/char oxidation region is also important when describing the heat transfer mechanisms driving flame spread, particularly in the low-intensity scenarios considered in this thesis. Measurements of heat flux (radiant and total) allowed investigation of the effects of fuel structure on these underlying heat transfer mechanisms. This allowed the identification of controlling heat transfer mechanisms; an important starting point in any flame spread model development effort. While in-bed heating was observed to dominate, the significance of flame heating increased for fuel beds of greater $\alpha\sigma\delta$, at which greater flame heights were typically observed.

The effects of fuel structure on heat flux were also systematically investigated, with a general positive trend between $\alpha\sigma\delta$ and the radiant heat flux (from either the flame or the combustion region). The effects of fuel loading and bulk density were also observed, and these effects were even more prominent for the measured total heat fluxes. Periods of both convective heating and cooling were observed throughout these flame spread experiments. Although extrapolation of convective heat transfer analysis to fuel elements is limited by the reliance upon geometry and temperature history of the fuel elements, which will likely differ significantly from the gauge.

### 9.3.2. Modelling Implications

This thesis aimed to use the experimental observations described in early chapters (Chapters 4 - 6) to inform the evaluation of existing models (semi-empirical, simplified physics-based, and detailed physics-based models). Suggestions of existing limitations for certain models informed this process, for example, a previously suggested over-sensitivity of the Rothermel model to fuel height was investigated in detail. Similarly, numerical simulation

of preliminary experiments from this thesis, were conducted by Mueller *et al.* [40], identifying limited ability of existing detailed physics-based models (Wildland Fire Dynamics Simulator) to accurately predict the effect of fuel bed manipulations on the flame spread through the model fuel beds used in this thesis.

A detailed approach to the evaluation of various modelling approaches was followed within this thesis. As discussed in Chapter 6, in-bed heat transfer through these pine needle beds was identified as the dominant heat transfer mechanism in this low-intensity, quiescent flame spread scenario. The construction of a simple thermal model allowed additional analysis of the relative importance of the various heat transfer mechanisms. This thermal model adapted previous approaches for solid surface flame spread [53,329], highlighting the increased complexity of defining the bulk properties of porous fuel beds.

The thermal model also provided insight into the role of fuel bed structure. Across all fuel bed conditions, predicted spread rates varied by a maximum of 29 % compared to experimentally observed spread rates, where only radiative transfer from the in-bed combustion region was considered. Greater agreement between predicted and experimentally observed spread rates was observed for fuel beds of lower $\alpha\sigma\delta$ ($\alpha\sigma\delta \leq 200$). Significantly greater flame heights were observed for higher $\alpha\sigma\delta$ fuel beds, and the significance of flame heating appears to be greater in these cases (as indicated by comparison with the predictions of the thermal model in which only flame radiation was considered). Where both flame and in-bed radiation were considered, significant over-predictions of the observed spread rates occurred at all fuel bed conditions. This reiterates the need to include appropriate heat loss and cooling terms (both radiative and convective), with further investigation of in-bed flow and convective heat transfer properties of fuel elements required.

In addition to the simple thermal model, the performance of the Rothermel model was assessed in terms of its applicability to the low-intensity flame spread scenario described in this thesis. As one of the most widely used flame spread models, the performance of the Rothermel model was evaluated in comparison to the experimental observations presented in Chapter 5. Rothermel's model generally under-predicted spread rates compared to experimental observations of flame spread. Performance was greater for fuel beds of higher $\alpha\sigma\delta$ however, performance was weaker at lower fuel loadings and higher packing ratios, resulting in increased divergence at lower values of $\alpha\sigma\delta$ ($\alpha\sigma\delta = 49$ to $\alpha\sigma\delta = 200$).

This study also confirmed a previously identified [342] over-sensitivity of the Rothermel model to fuel height. The increased under-predictions of spread rate for low fuel heights or low $\alpha\sigma\delta$ values appears in part due to an under-prediction of the reaction intensity in these more compact fuel beds. The Rothermel model predicted a largely linear decrease in reaction intensity with fuel height for the fuel bed condition with the largest range of fuel heights (0.8 kg/m$^2$ fuel beds). However, calculating the reaction intensity by using the observed spread rates resulted instead in a non-monotonic trend, with a much lower decline in the reaction intensity for the lower height fuel beds.

Since the Rothermel model only considers combustion occurring in the primary flame front, further work is required to understand and characterise the effect of fuel structure (specifically height and compaction) on the combustion wave profile. This will help to establish whether significant energy release within the trailing smouldering region is currently unaccounted for despite contributions to the propagating flux. Characterisation of the combustion wave and

further comparison with experimentally observed reaction intensities (derived from fireline intensity measurements) may also require the development of new formulations to describe the residence time. Existing empirical formulae do not account for the observed effects of fuel structure, and are instead functions only of fuel element thickness.

In addition to the evaluation of Rothermel's model, existing approaches within simplified physics-based models were also assessed. Unlike Rothermel's semi-empirical model, this class of model explicitly considers individual heat transfer mechanisms. A historical review of the development of these models highlighted several key assumptions that continue to inform the design of models of this type.

A key simplification during the model development process is often the identification of a dominant heat transfer mechanism(s). Many of the existing models reviewed in this thesis consider a flame radiation-dominated flame spread scenario. As demonstrated by the thermal model in Chapter 6, this approach may be well suited to the low-intensity, quiescent flame spread scenario considered in this thesis. However, the thermal model analysis also highlighted the importance of incorporating adequate cooling terms, while the heat flux measurements in Chapter 6 confirm the occurrence of convective cooling and heating within this flame spread scenario. Few of the existing simplified physics-based models account for this convective phenomena [46,47], and further development of appropriate sub-models describing the in-bed flow profile (and resulting convection) is important not only for this class of model, but also for the continued development of detailed physics-based models.

In terms of the modelling of radiant heat transfer mechanisms, limitations were observed in certain key assumptions underpinning many existing simplified physics-based models. The lack of applicability of common approaches to flame heating was observed for the laboratory-based experiments in this thesis, involving fuel beds representative of relevant field fuel conditions. Where the crossed-string method was used to determine the flame view factor, resulting predictions poorly described the flame heat transfer (to fuel bed surface) for cases involving larger flame heights.

In the experiments described in Chapter 6, the in-bed heating was observed to be dominant, and this was an important consideration when evaluating the suitability of existing simplified physics-based models. An examination of the theoretical basis behind existing approaches to fuel bed attenuation highlights a reliance upon an isotropic fuel bed assumption. As discussed by past authors [139], this may limit applicability to pine needle beds in which a preferential angle of inclination of fuel elements may occur. Further systematic study is required to develop suitable terms to describe the effects of fuel structure on the attenuation profile of the fuel bed. This must also consider the variations in the preferential angle of orientation of the needles, which must occur as the bulk density is varied (at a fixed fuel loading).

## 9.4. Recommendations for Further Work

Throughout this thesis, several areas for future work have been identified, alongside the contributions that address previously identified research gaps. With almost any research project of this nature there is a general desire for further investigation of a wider range of conditions, and of additional variables. The findings presented in this thesis arise from the consideration of a specific low-intensity, quiescent flame spread scenario. Different phenomena may be observed in other flame spread regimes, or where significantly different fuel types are studied.

The design of this study, as part of a wider multi-scale research project (SERDP RC-2641), will allow further future investigation of these limitations by enabling comparison across environmental conditions, experimental scale, and flame spread regimes. The benefits of this approach, particularly in the context of prescribed fire sciences, are discussed further in Section 9.5. However, when describing areas for further research, the focus will instead be on identifying specific research activities that may address the identified development areas for existing modelling approaches.

There is a need for further measurements of the mass loss rate profiles of porous fuel beds, as a function of $\alpha\sigma\delta$ and fuel height, in order to understand the distribution of mass consumption relative to the distance from the flame front. This will allow greater characterisation of the combustion wave, and further investigation of the suitability of considering propagating fluxes emerging only from the primary flame front. This will support the further development of the Rothermel model or its replacement, allowing more accurate application to lower $\alpha\sigma\delta$ cases, and addressing an over-sensitivity to fuel height.

Development of improved residence time predictive methods will also be required if further comparison of predicted and observed reaction intensities is to occur. This may involve greater investigation of the interaction between the primary and trailing combustion regions, which is linked to the improved understanding of the energy release within these regions. As with other fire behaviour properties, the residence time was observed to be influenced by the fuel bed structure. This is not suitably incorporated within existing empirical terms, which consider residence time as a function only of fuel element thickness.

Future systematic study of the effects of fuel bed structure on the residence time are required to support this development. Further systematic study of fuel structure effects is also required in order to characterise the moisture of extinction for pine needle fuel beds. The relationship between this extinction value and the fuel bed structure is currently unclear. This could be informed by a systematic study (similar to those presented in Chapters 5 and 6) in which the fuel structure is deliberately altered at a variety of fuel moisture contents in order to develop an empirical relationship for the extinction moisture content as a function of fuel structure.

For simplified physics-based models, there is a need for further exploration of convective heating within porous fuel beds, and development of sub model terms to describe the in-bed flow profile and resulting convective heating/cooling. A previous need for further model development, and accompanying experimental measurement of these physical processes, was previously identified as a research priority for detailed physics-based models [18]. Radiative heating sub-models within these simplified physics-based models also require further development to address issues with commonly used assumptions.

Given the importance of in-bed heating within the flame spread scenario considered in this thesis, it is important that the radiative transport through pine needle beds can be accurately described by this model class. An initial theoretical assessment of the radiation attenuation properties of pine needle beds has suggested that these fuel beds are anisotropic. A systematic study should be conducted to allow the development of attenuation terms that incorporate this anisotropic behaviour. This study should consider, and systematically investigate, the effect of the preferential angle of inclination of the fuel bed, which will vary with bulk density (for a constant fuel loading).

Finally, initial efforts [40] to numerically model preliminary experiments from this thesis have shown poor model accuracy in predicted spread rates and behaviour. Simulations conducted using the Wildland Fire Dynamics Simulator (WFDS) highlighted significant variation between the predicted and observed flow profiles behind the flame front, which may reflect issues regarding the representation of the vegetation drag profile [40]. The observations within this thesis have highlighted the large volume of fuel which remains (unconsumed) behind the main flame front, prior to later consumption during the smouldering/char oxidation phase. Further characterisation of the transient mass and structure of this remaining fuel region is required in order to allow the selection of appropriate bulk drag terms in detailed physics-based models. This may have important physical implications for convective heating and cooling, as well as the oxygen supply to the combustion region.

## 9.5. Relevance to Prescribed Fire Science

The experimental observations presented in this thesis have provided insight into suitability of several current modelling approaches. A number of areas for further model development and supporting experimental investigation have also been outlined. These observations and suggestions contribute to efforts to improve our ability to model the behaviour and effectiveness of prescribed fires. The implications of this work, in the context of prescribed fire science, are described in detail in this section.

Given the importance of conducting a safe and effective burn, prescribed fires are often conducted during calmer weather conditions, often aiming to deliver a low-intensity flame spread scenario. The effect of fuel structure on fire behaviour and fuel consumption may be particularly significant in this low-intensity flame spread scenario given the reduced impact of environmental factors e.g. lower ambient wind speeds. This thesis highlights the important role of fuel structure (fuel loading, bulk density) and fuel species in low-intensity flame spread scenarios. Independent effects were identified not only on the overall fire behaviour (spread rate, flame height, intensity) and fuel consumption, but also on the underlying physical processes (heat transfer, fluid flow).

Measurement and understanding of the controlling physical phenomena is vital for the further development of prescribed fire modelling tools. The continuing need for development has been emphasised by the limitations identified in existing semi-empirical (namely the Rothermel model) and simplified physics-based models when applied to this low-intensity flame spread scenario across a range of fuel bed conditions. Model performance may be suitable for some current uses in which lower fidelity, larger scale predictions are required, and where expectations around accuracy and precision are lower. However, the greater planning time afforded in prescribed burn operations is likely to drive increased demands for greater spread model accuracy, particularly where coupling to other models is desired (e.g. models of emissions generation, smoke production, soil heating).

An example of these specific challenges emerging within a prescribed fire modelling framework is given by the limitations of existing residence time formulations discussed in this thesis. Common existing formulae may provide sufficient accuracy for modelling approaches in which only the primary flame front is considered, but additional study of the inter-relationship between the primary and trailing combustion regions is required. Considering both these phases will also require greater consideration of the effect of fuel bed structure on the residence time (as observed in this thesis), with current approaches considering residence time

as a function only of fuel element thickness. In the quiescent flame spread scenario considered in this thesis, the trailing smouldering region may contribute to the overall propagating flux, but even where this contribution to flame front propagation is negligible, improved prediction of residence time will allow more accurate prediction of fuel consumption and fire effects.

The effects of scaling must be considered during these model development efforts, and where conducting experiments using reduced-scale model fuel beds. The experiments presented in this thesis compliment those conducted at multiple other scales as part of a wider research project (SERDP RC-2641). The flame spread experiments presented in Chapter 4 match the baseline fuel conditions, and subsequent fuel treatments, within a complimentary series of field experiments conducted at a slightly increased scale (10 m by 10 m) [85]. This will allow further future analysis of both scaling effects and the relative importance of fuel structure effects in quiescent and field environments through comparison of these experimental studies.

This cross-scale and multi-environment crossover enables the evaluation of modelling approaches and the limits of applicability of common modelling assumptions. The work in this thesis contributes to these efforts, with further comparative analysis expected to occur in the future. This represents a particular opportunity for the evaluation of simplified physics-based models that have not yet seen significant operational use. The testing and development of specific sub-models within these models may provide greater insight into the key processes at different scales and can offer a powerful diagnostic research tool. Additionally, continuing development of these simplified physics-based models may also allow the improvement of existing sub-modelling terms within detailed physics-based models.

## 9.6. Final Remarks

*"That's another thing we've learned from your Nation," said Mein Herr, "map-making. But we've carried it much further than you. What do you consider the largest map that would be really useful?"*

*"About six inches to the mile."*

*"Only six inches!" exclaimed Mein Herr. "We very soon got to six yards to the mile. Then we tried a hundred yards to the mile. And then came the grandest idea of all! We actually made a map of the country, on the scale of a mile to the mile!"*

*"Have you used it much?" I enquired.*

*"It has never been spread out, yet," said Mein Herr: "the farmers objected: they said it would cover the whole country, and shut out the sunlight! So we now use the country itself, as its own map, and I assure you it does nearly as well. Now let me ask you another question. What is the smallest world you would care to inhabit?"*

***Lewis Carroll - Sylvie and Bruno*** [414]

As has been highlighted throughout this thesis, it is important to realise the multiple scales at which structural properties exert an influence and at which different physical phenomena occur. As with any laboratory-based study of this type, this issue of scaling represents a limitation of

this work. However, by closely mirroring the fuel types, instrumentation and ethos of complimentary field experiments of various scale, it is hoped that further comparison will allow these scaling challenges to be embraced, generating additional insight.

Various recommendations for the development of empirical and physics-based models have been provided based upon the observations in these laboratory flame spread experiments. Simplified-physics based models in particular seem to have an important role to play, by providing greater insight into shortcomings of current empirical models, and by aiding in the development of sub-models for detailed physics-based models. If these models represent our map of the forest, then only by understanding these effects of scale and environment, can we avoid maps that bear either no resemblance or which are overwhelmingly descriptive of a single fire scenario. This is the path to a future in which effective prescribed burns can be planned and conducted safely, with accurate predictive tools supporting the expertise and decision-making of land managers and fire agencies.

## References


[1] Z.H. Rahman, In the Light of What We Know, Macmillan, 2014.

[2] J.K. Hiers, J.J. O'Brien, J.M. Varner, B.W. Butler, M. Dickinson, J. Furman, M. Gallagher, D. Godwin, S.L. Goodrick, S.M. Hood, A. Hudak, L.N. Kobziar, R. Linn, E.L. Loudermilk, S. McCaffrey, K. Robertson, E.M. Rowell, N. Skowronski, A.C. Watts, K.M. Yedinak, Prescribed fire science: the case for a refined research agenda, Fire Ecol. 16 (2020) 11. doi:10.1186/s42408-020-0070-8.

[3] M.A. Finney, The wildland fire system and challenges for engineering, Fire Saf. J. 120 (2021). doi:https://doi.org/10.1016/j.firesaf.2020.103085.

[4] T. Egan, The big burn: Teddy Roosevelt and the fire that saved America, Houghton Mifflin Harcourt, 2009.

[5] D.M. Smith, Sustainability and Wildland Fire: The Origins of Forest Service Wildland Fire Research, FS-1085. Washington, DC US Dep. Agric. For. Serv. 120 P. (2017).

[6] D. Strauss, L. Bednar, R. Mees, Do one percent of the forest fires cause ninety-nine percent of the damage?, For. Sci. 35 (1989) 319–328.

[7] P.M. Fernandes, H.S. Botelho, A review of prescribed burning effectiveness in fire hazard reduction, Int. J. Wildl. Fire. 12 (2003) 117–128. doi:10.1071/WF02042.

[8] The Committee on Fire Research, A Study of Fire Problems, Washington D.C., 1961.

[9] W.G. Berl, ed., International Symposium on the Use of Models in Fire Research, in: National Academy of Sciences - National Research Council, Washington D.C., 1961. doi:10.17226/20284.

[10] H.. Emmons, The Growth of Fire Science, Fire Saf. J. 3 (1981) 95–106. doi:https://doi.org/10.1016/0379-7112(81)90036-9.

[11] The Committee on Fire Research, The Committee on Fire Research Final Report, Washington D.C., 1962.

[12] W.L. Fons, H.D. Bruce, W.Y. Pong, S.. Richards, Project Fire Model Summary Progress Report, Berkeley, California, 1960.

[13] W.L. Fons, H.B. Clements, E.R. Elliot, P.. George, Project Fire Model - Summary Progress Report II, Macon, Georgia, 1962.

[14] G.M. Byram, H.B. Clements, M.E. Bishop, R.M. Nelson Jr., Final Report. Project Fire Model - An experimental study of model fires, Macon, Georgia, 1966.

[15] M. McNamee, B. Meacham, P. van Hees, L. Bisby, W.K. Chow, A. Coppalle, R. Dobashi, B. Dlugogorski, R. Fahy, C. Fleischmann, J. Floyd, E.R. Galea, M. Gollner, T. Hakkarainen, A. Hamins, L. Hu, P. Johnson, B. Karlsson, B. Merci, Y. Ohmiya, G. Rein, A. Trouvé, Y. Wang, B. Weckman, IAFSS agenda 2030 for a fire safe world, Fire Saf. J. 110 (2019). doi:10.1016/j.firesaf.2019.102889.

[16] Society of Fire Protection Engineers, Research Needs for the Fire Safety Engineering Profession, (2017). https://www.sfpe.org/research/research-roadmap (accessed 18 October 2020).

[17] P.F. Steblein, R.A. Loehman, M.P. Miller, J.R. Holomuzki, S.C. Soileau, M.L. Brooks, M. Drane-Maury, H.M. Hamilton, J.W. Kean, J.E. Keeley, J. Mason, R.R., A. McKerrow, J.R. Meldrum, E.B. Molder, S.F. Murphy, B. Peterson, G.S. Plumlee, D.J. Shinneman, P.J. van Mantgem, A. York, U . S . Geological Survey Wildland Fire Science Strategic Plan , 2021 – 26 Circular 1471, 2021. doi:https://doi.org/10.3133/cir1471.

[18] E.V. Mueller, Examination of the underlying physics in a detailed wildland fire behavior model through field-scale experimentation, The University of Edinburgh, 2016. http://hdl.handle.net/1842/22039.

[19] M.A. Finney, J.D. Cohen, S.S. Mcallister, W.M. Jolly, On the need for a theory of wildland fire spread, Int. J. Wildl. Fire. 22 (2013) 25–36. doi:10.1071/WF11117.

[20] U.S.D. of the Interior, U.S.D. of Agriculture, D. of Energy, D. of Defense, D. of C.U.. E.P. Agency, F.E.M. Agency, N.A. of S. Foresters, Review and Update of the 1995 Federal Wildland Fire Management Policy, 2001.

[21] J.N. De Ris, Spread of a Laminar Diffusion Flame, Symp. Combust. 12 (1969) 241–252. doi:10.1016/S0082-0784(69)80407-8.

[22] A.C. Fernandez-Pello, The Solid Phase, in: G. Cox (Ed.), Combust. Fundam. Fire, 1st ed., Academic Press, 1995: pp. 34–96.

[23] W.F.E. Council, The National Strategy. The Final Phase of Development of the National Cohesive Wildland Fire Management Strategy, 2014.

[24] V. Masson-Delmotte, P. Zhai, A. Pirani, S.L. Connor, C. Pean, S. Berger, N. Caud, Y. Chen, L. Goldfarb, M.I. Gomis, M. Huang, K. Leitzell, E. Lonnoy, J.B.. Matthews, T.K. Maycock, T. Waterfield, O. Yelekci, R. Yu, B. Zhou, Climate Change 2021: The Physical Science Basis. Contribution of Working Group 1 to the Sixth Assessment Report of the Intergovernmental Panel on Climate Change, 2021. doi:10.1080/03736245.2010.480842.

[25] J. Williams, L. Hamilton, R. Mann, R. Marc, L. Herman, D. Orville, B. Dave, S. Mann, The Mega-Fire Phenomenon: Toward a more effective management model, Brookings Inst. – CPPE. (2005) 1–19.

[26] W.J. De Groot, M.D. Flannigan, A.S. Cantin, Climate change impacts on future boreal fire regimes, For. Ecol. Manage. 294 (2013) 35–44. doi:10.1016/j.foreco.2012.09.027.

[27] M. Flannigan, A.S. Cantin, W.J. de Groot, M. Wotton, A. Newbery, L.M. Gowman, Global wildland fire season severity in the 21st century, For. Ecol. Manage. 294 (2013) 54–61. doi:https://doi.org/10.1016/j.foreco.2012.10.022.

[28] Y. Liu, S. L. Goodrick, J. A. Stanturf, Future U.S. wildfire potential trends projected using a dynamically downscaled climate change scenario, For. Ecol. Manage. 294 (2013) 120–135. doi:https://doi.org/10.1016/j.foreco.2012.06.049.

[29] M.P. Girardin, A.A. Ali, C. Carcaillet, S. Gauthier, C. Hély, H. Le Goff, A. Terrier, Y. Bergeron, Fire in managed forests of eastern Canada: Risks and options, For. Ecol. Manage. 294 (2013) 238–249. doi:https://doi.org/10.1016/j.foreco.2012.07.005.

[30] J.E. Halofsky, D.L. Peterson, B.J. Harvey, Changing wildfire, changing forests: the effects of climate change on fire regimes and vegetation in the Pacific Northwest, USA, Fire Ecol. 16 (2020). doi:10.1186/s42408-019-0062-8.

[31] M.D. Flannigan, B.J. Stocks, B.M. Wotton, Climate change and forest fires, Sci. Total Environ. 262 (2000) 221–229. doi:https://doi.org/10.1016/S0048-9697(00)00524-6.

[32] J.C. Thomas, Improving the Understanding of Fundamental Mechanisms that Influence Ignition and Burning Behavior of Porous Wildland Fuel Beds, University of Edinburgh, 2016.

[33] M. El Houssami, Development of a Numerical and Experimental Framework to Understand and Predict the Burning Dynamics of Porous Fuel Beds, The University of Edinburgh, 2016.

[34] A. Simeoni, Experimental Understanding of Wildland Fires, in: C.M. Belcher (Ed.), Fire Phenom. Earth Syst., 1st ed., John Wiley & Sons, Oxford, 2013: pp. 35–52. doi:10.1002/9781118529539.ch3.

[35] H.E. Anderson, Burnout of Large-Sized Woody Fuels, in: R.G. Hickman, C.A. Meier (Eds.), 17th Asilomar Conf. Fire Blast Eff. Nucl. Weapons, Pacific Grove, California, 1983: pp. 164–169.

[36] S.B. Show, E.I. Kotok, Cover Type and Fire Control in the National Forests of Northern California, Washington, 1929.

[37] J.R. Curry, W.L. Fons, Rate of Spread of Surface Fires in the Pondersoa Pine Type of California, (1938).

[38] S.B. Show, Climate and Forest Fires in Northern California, J. For. 17 (1919) 965–979. doi:10.1093/jof/17.8.965.

[39] W.G. Berl, Fire Research Abstracts and Reviews, Volume 1, 1958. doi:10.17226/18850.

[40] E. V. Mueller, Z. Campbell-Lochrie, W. Mell, R.M. Hadden, Numerical simulation of low-intensity fire spread in pine litter, in: D.X. Viegas (Ed.), Adv. For. Fire Res. 2018, 2018. doi:https://doi.org/10.14195/978-989-26-16-506_162.

[41] W. Mell, A. Maranghides, R. McDermott, S.L. Manzello, Numerical simulation and experiments of burning douglas fir trees, Combust. Flame. 156 (2009) 2023–2041. doi:10.1016/j.combustflame.2009.06.015.

[42] Y. Nakamura, T. Yamazaki, Smoldering Combustion, Encycl. Wildfires Wildland-Urban Interface Fires. (2019) 1–12. doi:10.1007/978-3-319-51727-8_63-1.

[43] R.C. Rothermel, A Mathematical Model for Predicting Fire Spread in Wildland Fuels, USDA Forest Service. Research Paper INT-115, 1972.

[44] C.E. Van Wagner, Calculations on forest fire spread by flame radiation, Can. Dept. For. Report N° (1967) 18. http://cfs.nrcan.gc.ca/pubwarehouse/pdfs/24717.pdf.

[45] E. Planas, J. Arnaldos, E. Pastor, L. Za, Mathematical models and calculation systems for the study of wildland fire behaviour, 29 (2003) 139–153. doi:10.1016/S0360-1285(03)00017-0.

[46] M. Vogel, F.A. Williams, Flame propagation along matchstick arrays, Combust. Sci. Technol. 1 (1970) 429–436.

[47] P.J. Pagni, T.G. Peterson, Flame spread through porous fuels, Symp. Combust. 14 (1973) 1099–1107. doi:10.1016/S0082-0784(73)80099-2.

[48] J. Williams, Exploring the onset of high-impact mega-fires through a forest land management prism, For. Ecol. Manage. 294 (2013) 4–10. doi:10.1016/j.foreco.2012.06.030.

[49] P.M. Attiwill, M.A. Adams, Mega-fires, inquiries and politics in the eucalypt forests of Victoria, south-eastern Australia, For. Ecol. Manage. 294 (2013) 45–53. doi:10.1016/j.foreco.2012.09.015.

[50] W.L. McCaw, Managing forest fuels using prescribed fire – A perspective from southern Australia, For. Ecol. Manage. 294 (2013) 217–224. doi:https://doi.org/10.1016/j.foreco.2012.09.012.

[51] M. Busse, R. Gerrard, Thinning and Burning Effects on Long-Term Litter Accumulation and Function in Young Ponderosa Pine Forests, For. Sci. 66 (2020) 761–769. doi:10.1093/forsci/fxaa018.

[52] H.. Emmons, Fire in the Forest, in: Fire Res. Abstr. Rev. Vol. 5, National Academies Press, 1963. doi:10.17226/18854.

[53] J.G. Quintiere, Fundamentals of Fire Phenomena, 2006. doi:10.1002/0470091150.

[54] I.S. Wichman, Studies of Flame Spread in an Opposed Flow Over Surfaces of Solid Fuels, Princeton University, 1983.

[55] D. Ward, Combustion chemistry and smoke, For. Fires Behav. Ecol. Eff. (2001) 55–77. doi:10.1016/B978-012386660-8/50005-2.

[56] S. Figueroa, J. de D. Rivera, W. Jahn, Influence of Permeability on the Rate of Fire Spread over Natural and Artificial Pinus radiata Forest Litter, Fire Technol. 55 (2019) 1085–1103. doi:10.1007/s10694-019-00824-w.

[57] S. Fehrmann, W. Jahn, J. de Dios Rivera, Permeability Comparison of Natural and Artificial Pinus Radiata Forest Litters, Fire Technol. 53 (2017) 1291–1308. doi:10.1007/s10694-016-0631-1.

[58] D.R. Weise, G.S. Biging, Effects of wind velocity and slope on flame properties, Can. J. For. Res. 26 (1996) 1849–1858. doi:10.1139/x26-210.

[59] M.F. Wolff, G.F. Carrier, F.E. Fendell, Wind-Aided Firespread Across Arrays of Discrete Fuel Elements. II. Experiment, Combust. Sci. Technol. 77 (1991) 261–289. doi:10.1080/00102209108951731.

[60] E.A. Catchpole, W.R. Catchpole, R.C. Rothermel, Fire Behavior Experiments In Mixed Fuel Complexes, Int. J. Wildl. Fire. 3 (1993) 45–57. doi:10.1071/WF9930045.

[61] G.K. Kwentus, Fuel Preheating in Free Burning Fires, Massachusetts Institute of Technology, 1967.

[62] R.A. Wilson, Reexamination of Rothermel Fire Spread Equations in No-Wind and No-Slope Conditions, 1990.

[63] J.B. Fang, F.R. Steward, Flame spread through randomly packed fuel particles, Combust. Flame. 13 (1969) 392–398. doi:10.1016/0010-2180(69)90108-4.

[64] C. Awad, D. Morvan, J.L. Rossi, T. Marcelli, F.J. Chatelon, F. Morandini, J.H. Balbi, Fuel moisture content threshold leading to fire extinction under marginal conditions, Fire Saf. J. 118 (2020). doi:10.1016/j.firesaf.2020.103226.

[65] J. Lozano, W. Tachajapong, D.R. Weise, S. Mahalingam, M. Princevac, Fluid dynamic structures in a fire environment observed in laboratory-scale experiments, Combust. Sci. Technol. 182 (2010) 858–878. doi:10.1080/00102200903401241.

[66] W.H. Frandsen, R.C. Rothermel, Measuring the energy-release rate of a spreading fire, Combust. Flame. 19 (1972) 17–24. doi:10.1016/S0010-2180(72)80082-8.

[67] F. Morandini, X. Silvani, J.L. Dupuy, A. Susset, Fire spread across a sloping fuel bed: Flame dynamics and heat transfers, Combust. Flame. 190 (2018) 158–170. doi:10.1016/j.combustflame.2017.11.025.

[68] P.J. Murphy, Rates of fire spread in an artificial fuel, Montana State University, 1963.

[69] W.R. Catchpole, E.A. Catchpole, B.W. Butler, R.C. Rothermel, G.A. Morris, D.J. Latham, Rate of spread of free-burning fires in woody fuels in a wind tunnel, Combust. Sci. Technol. 131 (1998) 1–37. doi:10.1080/00102209808935753.

[70] F.A. Albini, Wildland Fire Spread by Radiation—a Model Including Fuel Cooling by Natural Convection, Combust. Sci. Technol. 45 (1986) 101–113. doi:10.1080/00102208608923844.

[71] D. Frankman, B.W. Webb, B.W. Butler, Time-resolved radiation and convection heat transfer in combusting discontinuous fuel beds, Combust. Sci. Technol. 182 (2010) 1391–1412. doi:10.1080/00102202.2010.486388.

[72] M.A. Finney, J. Forthofer, I.C. Grenfell, B.A. Adam, N.K. Akafuah, K. Saito, A study of flame spread in engineered cardboard fuelbeds: Part I: Correlations and observations, in: Proc. Seventh Int. Symp. Scale Model., 2013.

[73] P.H. Thomas, Fire Spread in Wooden Crins: Part III The Effect of Wind, (1965).

[74] S. McAllister, M. Finney, Burning Rates of Wood Cribs with Implications for Wildland Fires, Fire Technol. 52 (2016) 1755–1777. doi:10.1007/s10694-015-0543-5.

[75] H.E. Anderson, Relationship of Fuel Size and Spacing to Combustion Characteristics of Laboratory Fuel Cribs, USDA Forest Service. Research Paper INT-424, 1990.

[76] S. McAllister, M. Finney, The Effect of Wind on Burning Rate of Wood Cribs, Fire Technol. 52 (2016) 1035–1050. doi:10.1007/s10694-015-0536-4.

[77] S. McAllister, The Role of Fuel Bed Geometry and Wind on the Burning Rate of Porous Fuels, Front. Mech. Eng. 5 (2019) 1–9. doi:10.3389/fmech.2019.00011.

[78] M.J. Gollner, C.H. Miller, W. Tang, A. V Singh, The effect of flow and geometry on concurrent flame spread, Fire Saf. J. 91 (2017) 68–78. doi:10.1016/j.firesaf.2017.05.007.

[79] J.M.C. Mendes-Lopes, J.M.P. Ventura, J.M.P. Amaral, Flame characteristics, temperature-time curves, and rate of spread in fires propagating in a bed of Pinus pinaster needles, Int. J. Wildl. Fire. 12 (2003) 67–84. doi:10.1071/WF02063.

[80] H.E. Anderson, R.C. Rothermel, Influence of moisture and wind upon the characteristics of free-burning fires, Symp. Combust. 10 (1965) 1009–1019. doi:10.1016/S0082-0784(65)80243-0.

[81] J.L. Dupuy, Slope and fuel load effects on fire behaviour :Laboratory experiments in pine needles fuel beds, Int. J. Wildl. Fire. 5 (1995) 153–164. doi:10.1071/WF9950153.

[82] C. Walker-Ravena, Z. Campbell-Lochrie, R.M. Hadden, The Influence of Structure on the Flammability of Wildland Fuels under Radiative Heating, in: 6th Int. Fire Behav. Fuels Conf., International Association of Wildland Fire, 2019.

[83] E. V Mueller, M.R. Gallagher, N. Skowronski, R.M. Hadden, Approaches to Modeling Bed Drag in Pine Forest Litter for Wildland Fire Applications, Transp. Porous Media. 138 (2021) 637–660. doi:10.1007/s11242-021-01637-8.

[84] W.E. Heilman, K.L. Clark, X. Bian, J.J. Charney, S. Zhong, N.S. Skowronski, M.R. Gallagher, M. Patterson, Turbulent Momentum Flux Behavior above a Fire Front in an Open-Canopied Forest, Atmosphere (Basel). 12 (2021) 956. doi:10.3390/atmos12080956.

[85] K. Clark, M. Gallagher, N. Skowronski, M. Patterson, W.E. Heilman, X. Bian, J.J. Charney, J. Hom, E. Mueller, R. Hadden, Z. Campbell-Lochrie, C. Walker-Ravena, R. Kremens, Intermediate-scale Fire Behaviour Measurements in the Field: Bridging the Gap Between Laboratory Experiments and Management-scale Prescribed Fires, in: Proc. 6th Int. Fire Behav. Fuels Conf., International Association of Wildland Fire, 2019: pp. 615–620.

[86] G. Di Cristina, N.S. Skowronski, A. Simeoni, A.S. Rangwala, S. Im, Flame spread predictions over linear discrete fuel arrays using an empirical B-number model and stagnation point flow, Combust. Flame. 234 (2021) 111644. doi:https://doi.org/10.1016/j.combustflame.2021.111644.

[87] G. Di Cristina, S. Kozhumal, A. Simeoni, N. Skowronski, Forced convection fire spread along wooden dowel array, Fire Saf. J. (2020) 103090. doi:10.1016/j.firesaf.2020.103090.

[88] H.T. Gisborne, Measuring Forest-Fire Danger in Northern Idaho, 1928.

[89] D. Drysdale, An introduction to fire dynamics, 3rd ed., John Wiley & Sons, Ltd, 2011. doi:10.1016/0379-7112(86)90046-9.

[90] G. Rein, Smouldering Combustion Phenomena in Science and Technology, Int. Rev. Chem. Eng. 1 (2009) 3–18. doi:http://hdl.handle.net/1842/2678.

[91] A.C. Fernandez-Pello, S.R. Ray, I. Glassman, Flame Spread in an Opposed Flow: The Effect of Ambient Oxygen Concentration, Symp. Combust. 18 (1981) 579–589. doi:10.1016/S0082-0784(81)80063-X.

[92] F.A. Williams, Mechanisms of fire spread, Symp. Combust. 16 (1977) 1281–1294. doi:10.1016/S0082-0784(77)80415-3.

[93] C. Chandler, P. Cheney, P. Thomas, L. Trabaud, D. Williams, Fire in forestry. Volume 1. Forest fire behavior and effects. Volume 2. Forest fire management and organization., John Wiley & Sons, Inc., 1983.

[94] C. Sanchez Tarifa, A. Muñoz Torralbo, Flame propagation along the interface between a gas and a reacting medium, Symp. Combust. 11 (1967) 533–544. doi:10.1016/S0082-0784(67)80178-4.

[95] R. Friedman, A survey of knowledge about idealized fire spread over surfaces, in: Fire Res. Abstr. Rev., 1968: p. 1.

[96] A.C. Fernandez-Pello, T. Hirano, Controlling mechanisms of flame spread, Combust.

Sci. Technol. 32 (1983) 1–31. doi:10.1080/00102208308923650.

[97] R.A. Wilson, A Reexamination of Fire Spread in Free-Burning Porous Fuel Beds, US Forest Service: Research Paper INT-289, 1982.

[98] F.A. Williams, Urban and wildland fire phenomenology, Prog. Energy Combust. Sci. 8 (1982) 317–354. doi:10.1016/0360-1285(82)90004-1.

[99] W.H. Frandsen, Fire spread through porous fuels from the conservation of energy, Combust. Flame. 16 (1971) 9–16. doi:10.1016/S0010-2180(71)80005-6.

[100] R.O. Weber, Modelling fire spread through fuel beds, Prog. Energy Combust. Sci. (1991). doi:10.1016/0360-1285(91)90003-6.

[101] J.R. Curry, W.L. Fons, Forest-fire behavior studies., Mech. Eng. 62 (1940) 219–225.

[102] G.M. Byram, Combustion of Forest Fuels, in: K.P. Davis (Ed.), For. Fire Control Use, McGraw-Hill, New York, 1959: pp. 61–89. doi:10.2307/1932261.

[103] J.S. Barrows, Fire Behaviour in Northern Rocky Mountain Forests, 1951.

[104] W.L. Fons, Use of Models to Study Forest Fire Behaviour, in: 10th Pacific Sci. Congr., Hawai, 1961.

[105] P.H. Thomas, Some aspects of the growth and spread of fire in the open, Forestry. 40 (1967) 139–164. doi:10.1093/forestry/40.2.139.

[106] P. Thomas, D. Simms, H. Wraight, Fire spread in wooden cribs, 1964.

[107] B.A. Adam, N.K. Akafuah, M.A. Finney, J. Forthofer, K. Saito, Fire and explosion - a study of flame spread in engineered cardboard fuel beds part II: Scaling Law approach, in: Prog. Scale Model. Vol. II Sel. from Int. Symp. Scale Model. ISSM VI ISSM VII, 2015: pp. 85–95. doi:10.1007/978-3-319-10308-2_6.

[108] J.-L. Dupuy, M. Larini, Fire spread through a porous forest fuel bed: a radiative and convective model including fire-induced flow effects, Int. J. Wildl. Fire. 9 (1999) 155. doi:10.1071/WF00006.

[109] F. Morandini, P.A. Santoni, J.H. Balbi, Fire Front Width Effects on Fire Spread Across a Laboratory Scale Sloping Fuel Bed, Combust. Sci. Technol. 166 (2001) 67–90. doi:10.1080/00102200108907820.

[110] P. Santoni, F. Morandini, T. Barboni, Steady and Unsteady Fireline Intensity of Spreading Fires at Laboratory Scale, Open Thermodyn. J. 4 (2010) 212–219. doi:10.2174/1874396X01004010212.

[111] W.L. Fons, Analysis of Fire Spread in Light Forest Fuels, J. Agric. Res. 72 (1946) 93–121.

[112] F. Folk, Experiments in Fire Extinguishment, Q. Natl. Fire Prot. Assoc. 31 (1937) 115–126.

[113] D. Gross, Experiments on the burning of cross piles of wood, J. Res. Natl. Bur. Stand. Sect. C Eng. Instrum. 66C (1962) 99. doi:10.6028/jres.066c.010.

[114] G. Heskestad, Flame Heights Of Fuel Arrays With Combustion In Depth, Fire Saf. Sci. 5 (1997) 427–438. doi:10.3801/iafss.fss.5-427.

[115] R.J. McCarter, A. Broido, Radiative and Convective Energy from Wood Crib Fires, in: Combust. Inst. West. States Sect. 1964 Spring Meet., 1964. doi:10.1017/CBO9781107415324.004.

[116] J.A. Block, A Theoretical and Experimental Study of Nonpropagating Free-Burning Fires, Proc. Thirteen. Symp. Combust. 13 (1971) 971–978.

[117] M. Boboulos, M.R.I. Purvis, Wind and slope effects on ROS during the fire propagation in East-Mediterranean pine forest litter, Fire Saf. J. 44 (2009) 764–769. doi:10.1016/j.firesaf.2009.03.006.

[118] A. Ganteaume, M. Jappiot, T. Curt, C. Lampin, L. Borgniet, Flammability of litter sampled according to two different methods: Comparison of results in laboratory experiments, Int. J. Wildl. Fire. 23 (2014) 1061–1075. doi:10.1071/WF13045.

[119] R.D. Schuette, Preparing Reproducible Pine Needle Fuel Beds, US Forest Service Research Note INT-36, 1965.

[120] W.R. Beaufauit, Characteristics of Backfires and Headfires in a Pine Needle Fuel Bed, US Forest Service Research Note INT-39, 1965.

[121] H.E. Anderson, Mechanisms of Fire Spread Research Progress Report No. 1, Ogden, Utah, 1964.

[122] R.C. Rothermel, C.E. Hardy, Influence of Moisture on Effectiveness of Fire Retardants, U.S. Forest Service Research Paper INT-18, 1965.

[123] H.E. Anderson, R.D. Schuette, R.W. Mutch, Timelag and Equilibrium Moisture Content of Ponderosa Pine Needles, USDA Forest Service. Research Paper INT-202, 1978.

[124] D.S. Stockstad, Spontaneous and Piloted Ignition of Pine Needles, USDA Forest Service Research Note INT-194, 1975.

[125] R.C. Rothermel, H.E. Anderson, Fire Spread Characteristics Determined In The Laboratory, US Forest Service Research Paper INT-30, 1966.

[126] C.E. Van Wagner, Fire behaviour mechanisms in a Red Pine plantation: field and laboratory evidence., Canadian Department of Forestry and Rural Development; Departmental publication 1229, 1968.

[127] C.G. Rossa, D.A. Davim, D.X. Viegas, Behaviour of slope and wind backing fires, Int. J. Wildl. Fire. 24 (2015) 1085–1097. doi:10.1071/WF14215.

[128] Z. Yang, H. Zhang, L. Zhang, H. Chen, Experimental Study on Downslope Fire Spread over a Pine Needle Fuel Bed, Fire Technol. 54 (2018) 1487–1503. doi:10.1007/s10694-018-0740-0.

[129] N. Liu, J. Wu, H. Chen, L. Zhang, Z. Deng, K. Satoh, D.X. Viegas, J.R. Raposo, Upslope spread of a linear flame front over a pine needle fuel bed: The role of convection cooling, Proc. Combust. Inst. 35 (2015) 2691–2698. doi:10.1016/j.proci.2014.05.100.

[130] J.L. Dupuy, J. Maréchal, Slope effect on laboratory fire spread: Contribution of radiation and convection to fuel bed preheating, Int. J. Wildl. Fire. 20 (2011) 289–307. doi:10.1071/WF09076.

[131] H.E. Anderson, Sundance Fire: An Analysis of Fire Phenomena, USDA Forest Service Research Paper INT-56, 1968.

[132] J.L. Dupuy, J. Maréchal, D. Portier, J.C. Valette, The effects of slope and fuel bed width on laboratory fire behaviour, Int. J. Wildl. Fire. 20 (2011) 272–288. doi:10.1071/WF09075.

[133] H.E. Anderson, Heat transfer and fire spread, USDA Forest Service Research Paper INT -69, 1969. doi:10.5962/bhl.title.69024.

[134] F. Morandini, X. Silvani, A. Susset, Feasibility of particle image velocimetry in vegetative fire spread experiments, Exp. Fluids. 53 (2012) 237–244. doi:10.1007/s00348-012-1285-5.

[135] T. Marcelli, P.A. Santoni, A. Simeoni, E. Leoni, B. Porterie, Fire spread across pine needle fuel beds: Characterization of temperature and velocity distributions within the fire plume, Int. J. Wildl. Fire. (2004). doi:10.1071/WF02065.

[136] P.A. Santoni, T. Marcelli, E. Leoni, Measurement of fluctuating temperatures in a continuous flame spreading across a fuel bed using a double thermocouple probe, Combust. Flame. 131 (2002) 47–58. doi:10.1016/S0010-2180(02)00391-7.

[137] H. Wang, P.J. Van Eyk, P.R. Medwell, C.H. Birzer, Z.F. Tian, M. Possell, X. Huang, Air Permeability of the Litter Layer in Broadleaf Forests, Front. Mech. Eng. 5 (2019) 1–15. doi:10.3389/fmech.2019.00053.

[138] Y. Bebieva, K. Speer, L. White, R. Smith, G. Mayans, B. Quaife, Wind in a Natural and Artificial Wildland Fire Fuel Bed, Fire. 4 (2021) 1–10.

[139] G.C. Vaz, J.C.S. André, D.X. Viegas, Estimation of the radiation extinction coefficient of natural fuel beds, Int. J. Wildl. Fire. 13 (2004) 65–71. doi:10.1071/WF03009.

[140] H.E. Anderson, Moisture and Fine Forest Fuel Response, Fire For. Meteorol. (1985) 192–199.

[141] W.H. Blackmarr, Moisture content influences ignitability of slash pine litter, USDA Forest Service Research Note SE-173, 1972.

[142] N.J. De Mestre, E.A. Catchpole, D.H. Anderson, R.C. Rothermel, Uniform Propagation of a Planar Fire front Without Wind, Combust. Sci. Technol. 65 (1989) 231–244. doi:10.1080/00102208908924051.

[143] E. Ormeño, B. Céspedes, I.A. Sánchez, A. Velasco-García, J.M. Moreno, C. Fernandez, V. Baldy, The relationship between terpenes and flammability of leaf litter, For. Ecol. Manage. 257 (2009) 471–482. doi:10.1016/j.foreco.2008.09.019.

[144] R.A. Dewhirst, N. Smirnoff, C.M. Belcher, Pine Species That Support Crown Fire Regimes Have Lower Leaf-Level Terpene Contents Than Those Native to Surface Fire Regimes, Fire. 3 (2020) 17. doi:10.3390/fire3020017.

[145] C.W. Philpot, Influence of Mineral Content on the Pyrolysis of Plant Materials, For. Sci. 16 (1970).

[146] P. Reszka, J.J. Cruz, J. Valdivia, F. González, J. Rivera, C. Carvajal, A. Fuentes, Ignition delay times of live and dead pinus radiata needles, Fire Saf. J. 112 (2020). doi:10.1016/j.firesaf.2020.102948.

[147] P. Bartoli, Feux de forêt : amélioration de la connaissance du couplage combustible-flamme, Universite de Corse-Pacal Paoli - University of Edinburgh, 2011.

[148] P. Mindykowski, A. Fuentes, J.L. Consalvi, B. Porterie, Piloted ignition of wildland fuels, Fire Saf. J. (2011). doi:10.1016/j.firesaf.2010.09.003.

[149] C.F. Schemel, A. Simeoni, H. Biteau, J.D. Rivera, J.L. Torero, A calorimetric study of wildland fuels, Exp. Therm. Fluid Sci. 32 (2008) 1381–1389. doi:10.1016/j.expthermflusci.2007.11.011.

[150] N. Mofidi, J. Hashempour, M.T. Timko, A. Simeoni, Soot Characterization of Burning Wildland Porous Fuel Bed, in: 11th U.S. Natl. Combust. Meet., Western States Section of the Combustion Institute, Pasadena, California, 2019.

[151] J.C. Thomas, A. Simeoni, M. Gallagher, N. Skowronski, An Experimental Study Evaluating the Burning Dynamics of Pitch Pine Needle Beds Using the FPA, Fire Saf. Sci. 11 (2014) 1406–1419. doi:10.3801/IAFSS.FSS.11-1406.

[152] P.A. Santoni, P. Bartoli, A. Simeoni, J.L. Torero, Bulk and particle properties of pine needle fuel beds – influence on combustion, Int. J. Wildl. Fire. 23 (2014) 1076–1086. doi:10.1071/WF13079.

[153] J.C. Thomas, J.N. Everett, A. Simeoni, N. Skowronski, J.L. Torero, Flammability Study of Pine Needle Beds, in: Proc. Seventh Int. Semin. Fire Explos. Hazards, 2013. doi:10.3850/978-981-08-7724-8.

[154] M. El Houssami, J.C. Thomas, A. Lamorlette, D. Morvan, M. Chaos, R. Hadden, A. Simeoni, Experimental and numerical studies characterizing the burning dynamics of wildland fuels, Combust. Flame. (2016). doi:10.1016/j.combustflame.2016.04.004.

[155] T. Fateh, F. Richard, J. Zaida, T. Rogaume, P. Joseph, Multi-scale experimental investigations of the thermal degradation of pine needles, Fire Mater. (2016) 654–674. doi:10.1002/fam.2407.

[156] A. Ganteaume, J. Marielle, L.M. Corinne, C. Thomas, B. Laurent, Effects of vegetation type and fire regime on flammability of undisturbed litter in Southeastern France, For. Ecol. Manage. 261 (2011) 2223–2231. doi:10.1016/j.foreco.2010.09.046.

[157] M.L. Ramadhan, J. Carrascal, A.F. Osorio, J.P. Hidalgo, Experimental Study on the Flammability and Burning Behaviour of Live and Dead Eucalyptus Saligna Foliage Experimental Study on the Flammability and Burning Behaviour of Live and Dead Eucalyptus Saligna Foliage, (2019). doi:10.18720/spbpu/2/k19-74.

[158] C.F. Schemel, Transport Effects on Calorimetry of Porous Wildland Fuels, The University of Edinburgh, 2008.

[159] A. Simeoni, P. Bartoli, J.L. Torero, P.A. Santoni, On the role of bulk properties and fuel species on the burning dynamics of pine forest litters, in: Fire Saf. Sci., 2011. doi:10.3801/IAFSS.FSS.10-1401.

[160] F.X. Jervis, G. Rein, Experimental study on the burning behaviour of Pinus halepensis needles using small-scale fire calorimetry of live, aged and dead samples, Fire Mater. 40 (2015) 385–395. doi:10.1002/fam.

[161] L.. Markwardt, H.D. Bruce, A.D. Freas, Brief Descriptions of Some Fire-Test Methods Used for Wood and Wood-Base Materials, USDA Forest Service Report No. 1976, 1954.

[162] H.. Eickner, Surface Flammability Measurements for Building Materials and Related

Products, in: I.M. Kolthoff, P.J. Elving, F.. Stross (Eds.), Treatise Anal. Chem., 1977.

[163] H.D. Bruce, Experimental Dwelling-Room Fires, USDA Forest Service Report No. 1941, 1959.

[164] H.D. Bruce, V.. Miniutti, Small Tunnel Furnace Test for Measuring Surface Flammability, USDA Forest Service Report No. 2097, 1957.

[165] A.J. Kelly, Atmospheres from fires in rooms with little ventilation. Part 1, Fire Research Note No. 494, 1962.

[166] J.S. Kristensen, G. Jomaas, Experimental Study of the Fire Behaviour on Flat Roof Constructions with Multiple Photovoltaic (PV) Panels, Fire Technol. 54 (2018) 1807–1828. doi:10.1007/s10694-018-0772-5.

[167] T.Z. Harmathy, A new look at compartment fires, part I, Fire Technol. 8 (1972) 196–217. doi:10.1007/BF02590544.

[168] M.J. O'Dogherty, R.A. Young, Miscellaneous Experiments on the Burning of Wooden Cribs, Fire Research Note No. 548, 1964.

[169] U. Laboratories, UL 1715, 1203 (1997).

[170] B.S. Institute, BS 5852, 2006.

[171] B.S. Institute, BS 6807, 2006.

[172] BSI 8414, BS 8414-1:2020, (2020).

[173] I. Móder, Á. Varga, P. Geier, B. Vágó, E. Rajna, Brief summary of the Hungarian test method (MSZ 14800-6:2009) of fire propagation on building façades, MATEC Web Conf. 46 (2016). https://doi.org/10.1051/matecconf/20164601002.

[174] J.F. Christian, Mass-Fire Control Test, US Army Corps of Engineers Report 1531-TR, 1958.

[175] J.B. Davis, D.L. Dibble, C.B. Phillips, Firefighting Chemicals, USDA Forest Service Miscellaneous Paper No. 57, 1961.

[176] T.R. Truax, The Use Of Chemicals In Forest Fire Control, USDA Forest Service Report No. 1199, 1956.

[177] H.D. Tyner, Fire-Extinguishing Effectiveness of Chemicals in Water Solution, Ind. Eng. Chem. 33 (1941) 60–65. doi:10.1021/ie50373a011.

[178] P.H. Thomas, M. Law, Experiments on the Spread of Fire, Report on Forest Research for the year ended March 1965, 1965. doi:10.1038/218315c0.

[179] P.G. Smith, P.H. Thomas, The rate of burning of wood cribs, Fire Technol. 6 (1970) 29–38. doi:10.1007/BF02588857.

[180] P.H. Thomas, Behavior of fires in enclosures-Some recent progress, Symp. Combust. 14 (1973) 1007–1020. doi:10.1016/S0082-0784(73)80091-8.

[181] M.A. Delichatsios, Fire growth rates in wood cribs, Combust. Flame. 27 (1976) 267–278. doi:10.1016/0010-2180(76)90028-6.

[182] C.T. Webster, M. Raftery, P.G. Smith, The Burning of Well Ventilated Compartment

Fires Part III - The Effect of the Wood Thickness, Fire Research Note No. 474, 1961.

[183] P.A. Croce, Y. Xin, Scale modeling of quasi-steady wood crib fires in enclosures, Fire Saf. J. 40 (2005) 245–266. doi:10.1016/j.firesaf.2004.12.002.

[184] A. Lönnermark, H. Ingason, The effect of air velocity on heat release rate and fire development during fires in tunnels, Fire Saf. Sci. (2008) 701–712. doi:10.3801/IAFSS.FSS.9-701.

[185] H. Ingason, Y.Z. Li, Model scale tunnel fire tests with longitudinal ventilation, Fire Saf. J. 45 (2010) 371–384. doi:10.1016/j.firesaf.2010.07.004.

[186] H. Ingason, A. Lönnermark, Effects of longitudinal ventilation on fire growth and maximum heat release rate, in: Proc. from Fourth Int. Symp. Tunn. Saf. Secur. Ger., 2010: pp. 395–406.

[187] S. Zhang, X. Ni, M. Zhao, J. Feng, R. Zhang, Numerical simulation of wood crib fire behavior in a confined space using cone calorimeter data, J. Therm. Anal. Calorim. 119 (2015) 2291–2303. doi:10.1007/s10973-014-4291-4.

[188] D. Gross, A.F. Robertson, Experimental fires in enclosures, Symp. Combust. 10 (1965) 931–942. doi:10.1016/S0082-0784(65)80236-3.

[189] T.Z. Harmathy, Experimental study on the effect of ventilation on the burning of piles of solid fuels, Combust. Flame. 31 (1978) 259–264. doi:10.1016/0010-2180(78)90138-4.

[190] J. Grumer, A. Strasser, Uncontrolled fires- Specific burning rates and induced air velocities, Fire Technol. 1 (1965) 256–268. doi:10.1007/BF02588468.

[191] G.M. Byram, H.B. Clements, E.R. Elliot, P.. George, An Experimental Study of Model Fires: Technical Report 3, 1964.

[192] E.L. Alpen, C.P. Butler, S.B. Martin, A.K. Davis, Physical Properties and Biological Effectivenss for Burn Production of Flame Sources, Technical Report USNRDL-TR-84 NM 006-015.02, 1955.

[193] W.L. Fons, H.D. Bruce, W.Y. Pong, A Steady-State Technique for Studying the Properties of Free-Burning Wood Fires, in: W.G. Berl (Ed.), Int. Symp. Use Model. Fire Res., 1959: pp. 219–234.

[194] P.H. Thomas, A Theoretical Model of the Rate of Spread of fire in a Continuous Bed of Fuel, Fire Research Note No. 459, 1961.

[195] P. Thomas, D.L. Simms, H.G.H. Wraight, Fire spread in wooden cribs, Fire Res Note No. 537. Boreham Wood, Herts, Engl. Dep. Sci. Ind. 120 Res. Fire Off. Comm. Jt. Fire Res. Organ. Fire Res. Stn. (1964) 38 p.

[196] P.H. Thomas, C.T. Webster, M.M. Raftery, Some experiments on buoyant diffusion flames, Fire Research Note No. 449, 1960.

[197] R.J. McCarter, A. Broido, Radiative and convective energy from wood crib fires, Pyrodynamics. 2 (1965) 65–85.

[198] Y. Perez-Ramirez, W.E. Mell, P.A. Santoni, J.B. Tramoni, F. Bosseur, Examination of WFDS in Modeling Spreading Fires in a Furniture Calorimeter, Fire Technol. 53 (2017) 1795–1832. doi:10.1007/s10694-017-0657-z.

[199] R. Kallada Janardhan, S. Hostikka, Predictive Computational Fluid Dynamics Simulation of Fire Spread on Wood Cribs, Fire Technol. 55 (2019) 2245–2268. doi:10.1007/s10694-019-00855-3.

[200] E.D. Reinhardt, First order fire effects model: FOFEM 4.0, user's guide, Intermountain Forest and Range Experiment Station, Forest Service, 1997.

[201] M.A. Finney, FARSITE, Fire Area Simulator--model development and evaluation, US Department of Agriculture, Forest Service, Rocky Mountain Research Station, 1998.

[202] P.L. Andrews, C.D. Bevins, R.C. Seli, BehavePlus fire modeling system, version 4.0: User's Guide, Gen. Tech. Rep. RMRS-GTR-106 Revised. Ogden, UT Dep. Agric. For. Serv. Rocky Mt. Res. Station. 132p. 106 (2005).

[203] M.A. Finney, J.D. Cohen, I.C. Grenfell, K.M. Yedinak, An examination of fire spread thresholds in discontinuous fuel beds A, Int. J. Wildl. Fire. 19 (2010) 163–170. doi:10.1071/WF07177.

[204] W.R. Anderson, E.A. Catchpole, B.W. Butler, Convective heat transfer in fire spread through fine fuel beds, Int. J. Wildl. Fire. 19 (2010) 284–298. doi:10.1071/WF09021.

[205] I. Emori, Y. Iguchi, K. Saito, I. Wichman, Simplified Scale Modeling Of Turbulent Flame Spread With Implication To Wildland Fires, Fire Saf. Sci. 2 (1989) 263–273. doi:10.3801/iafss.fss.2-263.

[206] B.W. Butler, W.R. Anderson, E.A. Catchpole, Influence of Slope on Fire Spread Rate, in: Fire Environ. Innov. Manag. Policy; Conf. Proceedings., 2007: pp. 75–82.

[207] X. Silvani, F. Morandini, J.L. Dupuy, Effects of slope on fire spread observed through video images and multiple-point thermal measurements, Exp. Therm. Fluid Sci. 41 (2012) 99–111. doi:10.1016/j.expthermflusci.2012.03.021.

[208] B. Butler, Experimental measurements of radiant heat fluxes from simulated wildfire flames, in: Proc. 12th Conf. Fire For. Meteorol., 1993: pp. 104–111.

[209] G. Parent, Z. Acem, S. Lechêne, P. Boulet, Measurement of infrared radiation emitted by the flame of a vegetation fire, Int. J. Therm. Sci. 49 (2010) 555–562. doi:10.1016/j.ijthermalsci.2009.08.006.

[210] G.F. Carrier, F.E. Fendell, M.F. Wolff, Wind-aided firespread across arrays of discrete fuel elements. I. Theory, Combust. Sci. Technol. 75 (1991) 31–51. doi:10.1080/00102209108924077.

[211] M.J. Gollner, Studies on Upward Flame Spread, University of California, San Diego, 2012.

[212] J.M. Prahl, J.S. Tien, Preliminary Investigations of Forced Convection on Flame Propagation along Paper and Matchstick Arrays, Combust. Sci. Technol. 7 (1973) 271–282. doi:10.1080/00102207308952367.

[213] C.C. Hwang, Y. Xie, Flame Propagation Along Matchstick Arrays On Inclined Base Boards, Combust. Sci. Technol. 42 (1984) 1–12. doi:10.1080/00102208408960366.

[214] H.W. Emmons, T. Shen, Fire spread in paper arrays, Symp. Combust. 13 (1971) 917–926. doi:10.1016/S0082-0784(71)80092-9.

[215] D.R. Weise, G.S. Biging, A qualitative comparison of fire spread models incorporating

wind and slope effects, For. Sci. 43 (1997) 170–180.

[216] M.A. Finney, J.D. Cohen, J.M. Forthofer, S.S. McAllister, M.J. Gollner, D.J. Gorham, K. Saito, N.K. Akafuah, B.A. Adam, J.D. English, Role of buoyant flame dynamics in wildfire spread, Proc. Natl. Acad. Sci. (2015). doi:10.1073/pnas.1504498112.

[217] V. Babrauskas, Heat Release Rates, in: SFPE Handb. Fire Prot. Eng., 2016: pp. 799–904. doi:10.1007/978-1-4939-2565-0.

[218] L.M. Krasner, Burning Characteristics of Wooden Pallets as a Test Fuel, Norwood, MA, Fact. Mutual Res. Corp. (1968).

[219] L.A. Mabli, Modeling Backing Fires in California Grassland Fuels, University of California, Berkeley, 2001.

[220] N.P. Cheney, J.S. Gould, W.R. Catchpole, The Influence Of Fuel, Weather And Fire Shape Variables On Fire-Spread In Grasslands, Int. J. Wildl. Fire. 3 (1993) 31–44. doi:10.1071/WF9930031.

[221] N.P. Cheney, J.S. Gould, Fire growth in grassland fuels, Int. J. Wildl. Fire. 5 (1995) 237–247. doi:10.1071/WF9950237.

[222] P. Bartoli, A. Simeoni, J.L. Torero, P.-A. Santoni, Experimental study on the combustion dynamics of forest floor fuel beds, in: VI Int. Conf. For. Fire Res., 2010.

[223] A. Simeoni, J.C. Thomas, P. Bartoli, P. Borowieck, P. Reszka, F. Colella, P.A. Santoni, J.L. Torero, Flammability studies for wildland and wildland-urban interface fires applied to pine needles and solid polymers, Fire Saf. J. 54 (2012) 203–217. doi:10.1016/j.firesaf.2012.08.005.

[224] F. Jervis, Application of fire calorimetry to understand factors affecting flammability of cellulosic material: Pine needles, tree leaves and chipboard, The University of Edinburgh, 2012.

[225] K.L. Clark, N. Skowronski, M. Gallagher, W. Heilman, J. Hom, Fuel consumption and particulate emissions during fires in the New Jersey Pinelands, Proc. 3rd Fire Behav. Fuels Conf. (2010) 1–19.

[226] F. Morandini, Y. Perez-Ramirez, V. Tihay, P.A. Santoni, T. Barboni, Radiant, convective and heat release characterization of vegetation fire, Int. J. Therm. Sci. 70 (2013) 83–91. doi:10.1016/j.ijthermalsci.2013.03.011.

[227] P.A. Santoni, F. Morandini, T. Barboni, Determination of fireline intensity by oxygen consumption calorimetry, J. Therm. Anal. Calorim. 104 (2011) 1005–1015. doi:10.1007/s10973-010-1256-0.

[228] V. Tihay, F. Morandini, P.A. Santoni, Y. Perez-Ramirez, T. Barboni, Combustion of forest litters under slope conditions: Burning rate, heat release rate, convective and radiant fractions for different loads, Combust. Flame. 161 (2015) 3237–3248. doi:10.1016/j.combustflame.2014.06.003.

[229] D.J. Frankman, Radiation and Convection Heat Transfer in Wildland Fire Environments, Brigham Young University, 2009.

[230] F. Morandini, X. Silvani, Experimental investigation of the physical mechanisms governing the spread of wildfires, Int. J. Wildl. Fire. 19 (2010) 570–582.

doi:doi:10.1071/WF08113.

[231] A.G. McArthur, Grassland fire danger meter Mk V, Canberra, Aust. (1977).

[232] J.B. Marsden-Smedley, W.R. Catchpole, Fire behaviour modelling in tasmanian buttongrass moorlands i. Fuel characteristics, Int. J. Wildl. Fire. 5 (1995) 203–214. doi:10.1071/WF9950203.

[233] J. Restaino, Fuel Loading, Encycl. Wildfires Wildland-Urban Interface Fires. (2019).

[234] K.J. Overholt, J. Cabrera, A. Kurzawski, M. Koopersmith, O.A. Ezekoye, Characterization of Fuel Properties and Fire Spread Rates for Little Bluestem Grass, Fire Technol. 50 (2014) 9–38. doi:10.1007/s10694-012-0266-9.

[235] X. Zhou, S. Mahalingam, D. Weise, Modeling of marginal burning state of fire spread in live chaparral shrub fuel bed, Combust. Flame. 143 (2005) 183–198. doi:10.1016/j.combustflame.2005.05.013.

[236] P.H. Thomas, The Rates of Spread of Head Fires in Gorse and Heather, Fire Research Note No. 796, 1970.

[237] E. Marino, J. Dupuy, F. Pimont, M. Guijarro, C. Hernando, R. Linn, Fuel bulk density and fuel moisture content effects on fire rate of spread: a comparison between FIRETEC model predictions and experimental results in shrub fuels, J. Fire Sci. 30 (2012) 277–299.

[238] K.A.M. Moinuddin, D. Sutherland, W. Mell, Simulation study of grass fire using a physics-based model: Striving towards numerical rigour and the effect of grass height on the rate of spread, Int. J. Wildl. Fire. 27 (2018) 800–814. doi:10.1071/WF17126.

[239] M.G. Cruz, A.L. Sullivan, J.S. Gould, The effect of fuel bed height in grass fire spread: Addressing the findings and recommendations of Moinuddin et al. (2018), Int. J. Wildl. Fire. (2020). doi:10.1071/WF19186.

[240] Grassfires - Rural - Country Fire Authority, (n.d.). https://www.cfa.vic.gov.au/plan-prepare/grassfires-rural (accessed 3 September 2020).

[241] N.S. Skowronski, M.R. Gallagher, T.A. Warner, Decomposing the Interactions between Fire Severity and Canopy Fuel Structure Using Multi-Temporal , Active , and Passive Remote Sensing Approaches, Fire. 3 (2020).

[242] R.T.T. Forman, R.E. Boerner, Fire Frequency and the Pine Barrens of New Jersey, Bull. Torrey Bot. Club. 108 (1981) 34–50.

[243] X. Silvani, F. Morandini, J.L. Dupuy, A. Susset, R. Vernet, O. Lambert, Measuring velocity field and heat transfer during natural fire spread over large inclinable bench, Exp. Therm. Fluid Sci. 92 (2018) 184–201. doi:10.1016/j.expthermflusci.2017.11.020.

[244] W.M. Pitts, I.E. Braun, R.D. Peacock, H.E. Mitler, E.L. Johnsson, P.A. Reneke, L.G. Blevins, Temperature Uncertainties for Bare-Bead and Aspirated Thermocouple Measurements in Fire Environments, Therm. Meas. Found. Fire Stand. ASTM STP 146. (2002).

[245] X. Silvani, F. Morandini, Fire spread experiments in the field: Temperature and heat fluxes measurements, Fire Saf. J. 44 (2009) 279–285. doi:10.1016/j.firesaf.2008.06.004.

[246] B.J. McCaffrey, G. Heskestad, A robust bidirectional low-velocity probe for flame and

fire application, Combust. Flame. 26 (1976) 125–127. doi:10.1016/0010-2180(76)90062-6.

[247] R. Gardon, An instrument for the direct measurement of intense thermal radiation, Rev. Sci. Instrum. 24 (1953) 366–370. doi:10.1063/1.1770712.

[248] C.T. Kidd, C.G. Nelson, How the Schmidt-Boelter gage really works, in: 41st Int. Instrum. Symp., 1995: pp. 347–368.

[249] International Standards Organisation, ISO 14934-3: Fire tests - Calibration and use of heat flux meters - Part 3: Secondary Calibration Method, (2012).

[250] ISO 14934, Fire tests - Calibration and use of heat flux meters - Part 4 : Guidance on the use of heat flux meters in fire tests, (2012).

[251] F. Morandini, T. Toulouse, X. Silvani, A. Pieri, L. Rossi, Image-Based Diagnostic System for the Measurement of Flame Properties and Radiation, Fire Technol. (2019) 2443–2463. doi:10.1007/s10694-019-00873-1.

[252] ISO, Uncertainty of measurement — Part 3: Guide to the expression of uncertainty in measurement (GUM:1995) Incertitude, Iso/Iec Guid. 98-32008(E). (2008). doi:10.1373/clinchem.2003.030528.

[253] D. Frankman, B.W. Webb, B.W. Butler, D. Jimenez, J.M. Forthofer, P. Sopko, K.S. Shannon, J.K. Hiers, R.D. Ottmar, Measurements of convective and radiative heating in wildland fires, Int. J. Wildl. Fire. 22 (2013) 157–167. doi:10.1071/WF11097.

[254] F. Morandini, X. Silvani, L. Rossi, P.A. Santoni, A. Simeoni, J.H. Balbi, J. Louis Rossi, T. Marcelli, Fire spread experiment across Mediterranean shrub: Influence of wind on flame front properties, Fire Saf. J. 41 (2006) 229–235. doi:10.1016/j.firesaf.2006.01.006.

[255] T. Barboni, F. Morandini, L. Rossi, T. Molinier, P.A. Santoni, Relationship between flame length and fireline intensity obtained by calorimetry at laboratory scale, Combust. Sci. Technol. 184 (2012) 186–204. doi:10.1080/00102202.2011.625373.

[256] M. El Houssami, A. Lamorlette, D. Morvan, R.M. Hadden, A. Simeoni, Framework for submodel improvement in wildfire modeling, Combust. Flame. 190 (2018) 12–24. doi:10.1016/j.combustflame.2017.09.038.

[257] J. Singh, D.R. Sprinkle, R.L. Puster, United States Patent: 4,761,744, 4,761,744, 1988.

[258] J.. Singh, D.R. Sprinkle, R.L. Puster, New Methods for Determining Heats of Combustion of Gaseous Hydrocarbons, NASA Technical Paper 2531, 1985.

[259] D.L. Sensenig, An Oxygen Consumption Technique for Determining the Contribution of Interior Wall Finishes to Room Fires, NBS Technical Note 1128, 1986.

[260] R.A. Bryant, M.F. Bundy, Improving the State-of-the-Art in Flow Measurements for Large-Scale Oxygen Consumption Calorimetry, Fire Technol. (2021). doi:10.1007/s10694-020-01066-x.

[261] S. Brohez, Uncertainty analysis of heat release rate measurement from oxygen consumption calorimetry, Fire Mater. 29 (2005) 383–394. doi:10.1002/fam.895.

[262] P. Enright, C. Fleischmann, Uncertainty of Heat Release Rate Calculation of the IS056604 Cone Standard Test Method, Fire Technol. 35 (1999) 153–169.

http://link.springer.com/article/10.1023/A:1015416005888.

[263] J. Axelsson, P. Andersson, A. Lönnermark, P. Van Hees, I. Wetterlund, Uncertainties in measuring heat and smoke release rates in the room/corner test and the SBI, SP Rapport; Vol. 2001:04, 2001.

[264] R.A. Bryant, G.W. Mulholland, A guide to characterizing heat release rate measurement uncertainty for full-scale fire tests, Fire Mater. 32 (2008) 121–139. doi:10.1002/fam.959.

[265] R.W. Yeager, Uncertainty Analysis of Energy Release Rate Measurement for Room Fires, J. Fire Sci. 4 (1986) 276–296. doi:10.1177/073490418600400404.

[266] W.M. Thornton, XV. The relation of oxygen to the heat of combustion of organic compounds, London, Edinburgh, Dublin Philos. Mag. J. Sci. 33 (1917) 196–203. doi:10.1080/14786440208635627.

[267] C. Huggett, Estimation of rate of heat release by means of oxygen consumption measurements, Fire Mater. 4 (1980) 61–65. doi:10.1002/fam.810040202.

[268] M. Janssens, Calorimetry, in: M. Hurley (Ed.), SFPE Handb. Fire Prot. Eng., 2016: pp. 905–951. doi:10.1007/978-1-4939-2565-0.

[269] W.J. Parker, An Investigation of the Fire Environment in the ASTM E84 Tunnel Test, NBS Technical Note 945, 1977.

[270] M.L. Janssens, Measuring rate of heat release by oxygen consumption, Fire Technol. 27 (1991) 234–249. doi:10.1007/BF01038449.

[271] M.C. Antoine, Nouvelle Relation Entre les Tensions et les Temperatures, C. r. Held Seanc. Acad. Sci. Paris. 107 (1888) 681–684.

[272] V. Babrauskas, S. Grayson, Heat Release in Fires, Elsevier Applied Science, New York, 1992.

[273] J.P. Hidalgo, Performance-Based Methodology for the Fire Safe Design of Insulation Materials in Energy Efficient Buildings, The University of Edinburgh, 2015.

[274] M.E. Alexander, Calculating and interpreting forest fire intensities, Can. J. Bot. 60 (1982) 349–357. doi:10.1139/b82-048.

[275] C.E. Van Wagner, Heat of combustion, heat yield, and fire behaviour, Canadian Forestry Service Information Report PS-X-35, 1972.

[276] K.L. Clark, N. Skowronski, M. Gallagher, The fire research program at the Silas Little Experimental Forest, New Lisbon, New Jersey, USDA For. Serv. Exp. For. Ranges Res. Long Term. (2014) 515–534. doi:10.1007/978-1-4614-1818-4_22.

[277] Silas Little Experimental Forest, n.d. https://www.nrs.fs.fed.us/ef/local-resources/downloads/nrs_inf_19_12-silaslittle-panels.pdf.

[278] L. Adams, Mary Beth; Loughry, Linda; Plaugher, Experimental Forests and Ranges of the USDA Forest Service. Gen. Tech. Rep. NE-321., (2004) 183.

[279] N.S. Skowronski, S. Haag, J. Trimble, K.L. Clark, M.R. Gallagher, R.G. Lathrop, Structure-level fuel load assessment in the wildland – urban interface : a fusion of airborne laser scanning and spectral remote-sensing methodologies, Int. J. Wildl. Fire.

25 (2015) 547–557.

[280] E. V. Mueller, N. Skowronski, K. Clark, M. Gallagher, R. Kremens, J.C. Thomas, M. El Houssami, A. Filkov, R.M. Hadden, W. Mell, A. Simeoni, Utilization of remote sensing techniques for the quantification of fire behavior in two pine stands, Fire Saf. J. (2017). doi:10.1016/j.firesaf.2017.03.076.

[281] N. Otsu, A Tlreshold Selection Method from Gray-Level Histograms, in: IEEE Trans. Syst. Man, Cybern., 1979: pp. 62–66. doi:10.1109/TSMC.1979.4310076.

[282] C. Moro, Détermination des caractéristiques physiques de particules de quelques espèces forestières méditerranéennes, (2006).

[283] P. Bartoli, A. Simeoni, H. Biteau, J.L. Torero, P.A. Santoni, Determination of the main parameters influencing forest fuel combustion dynamics, Fire Saf. J. 46 (2011) 27–33. doi:10.1016/j.firesaf.2010.05.002.

[284] J.L. Torero, A. Simeoni, Heat and Mass Transfer in Fires: Scaling Laws, Ignition of Solid Fuels and Application to Forest Fires, Open Thermodyn. J. 4 (2014) 145–155. doi:10.2174/1874396x01004010145.

[285] J.C. Thomas, R.M. Hadden, A. Simeoni, Experimental investigation of the impact of oxygen flux on the burning dynamics of forest fuel beds, Fire Saf. J. 91 (2017) 855–863. doi:10.1016/j.firesaf.2017.03.086.

[286] T.J. Duff, J.G. Cawson, T.D. Penman, Prescribed Burning, in: Encycl. Wildfires Wildland-Urban Interface Fires, 2018. doi:https://doi.org/10.1007/978-3-319-51727-8_120-1.

[287] G.J. Cary, M.D. Flannigan, R.E. Keane, R.A. Bradstock, I.D. Davies, J.M. Lenihan, C. Li, K.A. Logan, R.A. Parsons, Relative importance of fuel management, ignition management and weather for area burned: Evidence from five landscapefiresuccession models, Int. J. Wildl. Fire. 18 (2009) 147–156. doi:10.1071/WF07085.

[288] N.S. Skowronski, Multi-scale Analyses of Wildland Fire Combustion Processes in Open- canopied Forests using Coupled and Iteratively Informed Laboratory- , Field- , and Model-based Approaches, (2018). https://www.serdp-estcp.org/Program-Areas/Resource-Conservation-and-Resiliency/Air-Quality/Fire-Emissions/RC-2641.

[289] J.K. Agee, C.N. Skinner, Basic principles of forest fuel reduction treatments, For. Ecol. Manage. 211 (2005) 83–96. doi:10.1016/j.foreco.2005.01.034.

[290] K.P. Davis, Forest Fire: Control and Use McGraw-Hill Book Co, Inc.. New York. (1959).

[291] C.S. Wright, R.E. Vihnanek, R.D. Ottmar, P.C. Eagle, Digital Photo Series, Final Rep. to Jt. Fire Sci. Program. Boise, ID.[Accessed 6 Febr. 2019 Https//Www. Firescience. Gov/Projects/04-4-1-02/Project/04-4-1-02_final_report. Pdf]. (2007).

[292] P.H. Thomas, Rates of spread of some wind-driven fires, Forestry. 44 (1971) 155–175. doi:10.1093/forestry/44.2.155.

[293] B.M. Wotton, J.S. Gould, W.L. McCaw, N.P. Cheney, S.W. Taylor, Flame temperature and residence time of fires in dry eucalypt forest, Int. J. Wildl. Fire. 21 (2012) 270–281. doi:10.1071/WF10127.

[294] S.W. Taylor, B.M. Wotton, M.E. Alexander, G.N. Dalrymple, Variation in wind and crown fire behaviour in a northern jack pine - Black spruce forest, Can. J. For. Res. 34 (2004) 1561–1576. doi:10.1139/X04-116.

[295] N.D. Burrows, Flame residence times and rates of weight loss of eucalypt forest fuel particles, Int. J. Wildl. Fire. 10 (2001) 137–143. doi:10.1071/WF01005.

[296] A. Fuentes, J.L. Consalvi, Experimental study of the burning rate of small-scale forest fuel layers, Int. J. Therm. Sci. 74 (2014) 119–125. doi:10.1016/j.ijthermalsci.2013.06.002.

[297] C.G. Rossa, P.M. Fernandes, Fuel-related fire-behaviour relationships for mixed live and dead fuels burned in the laboratory, Can. J. For. Res. 47 (2017) 883–889. doi:10.1139/cjfr-2016-0457.

[298] A. Àgueda, E. Pastor, Y. Pérez, D.X. Viegas, E. Planas, Fire intensity reduction in straw fuel beds treated with a long-term retardant, Fire Saf. J. 46 (2011) 41–47. doi:10.1016/j.firesaf.2010.11.003.

[299] E. Mueller, W. Mell, N. Skowronski, K.L. Clark, M. Gallagher, R. Hadden, A. Simeoni, Field-Scale Testing of Detailed Physics-Based Fire Behavior Models, in: Proccedings 5th Int. Fire Behav. Fuels Conf. Int. Assoc. Wildl. Fire, 2016: pp. 62–67.

[300] S.L. Goodrick, D. Shea, J. Blake, Estimating fuel consumption for the upper coastal plain of South Carolina, South. J. Appl. For. 34 (2010) 5–12. doi:10.1093/sjaf/34.1.5.

[301] V. Babrauskas, Development of the cone calorimeter—A bench-scale heat release rate apparatus based on oxygen consumption, Fire Mater. 8 (1984) 81–95. doi:10.1002/fam.810080206.

[302] ASTM International, ASTM E648, Standard Test Method for Critical Radiant Flux of Floor-Covering Systems Using a Radiant Heat Energy Source, ASTM Int. (2015) 16. doi:10.1520/E0648-19AE01.flame.

[303] R.S.P. Hakes, H. Salehizadeh, M.J. Weston-Dawkes, M.J. Gollner, Thermal characterization of firebrand piles, Fire Saf. J. 104 (2018) 34–42. doi:10.1016/j.firesaf.2018.10.002.

[304] J.C. Thomas, E. V. Mueller, R.M. Hadden, Estimating net heat flux from surrogate firebrand accumulations using an inverse heat transfer approach, in: Adv. For. Fire Res. 2018 –, 2018: pp. 769–779.

[305] H. Salehizadeh, Critical Ignition Conditions of Structural Materials, University of Maryland, 2019.

[306] Z. Tao, B. Bathras, B. Kwon, B. Biallas, M.J. Gollner, R. Yang, Effect of firebrand size and geometry on heating from a smoldering pile under wind, Fire Saf. J. (2020) 103031. doi:10.1016/j.firesaf.2020.103031.

[307] S. McAllister, I. Grenfell, A. Hadlow, W.M. Jolly, M. Finney, J. Cohen, Piloted ignition of live forest fuels, Fire Saf. J. 51 (2012) 133–142. doi:10.1016/j.firesaf.2012.04.001.

[308] T. Laschütza, Numerical and experimental investigation of a Thin Skin Calorimeter (TSC), The University of Edinburgh, 2017.

[309] A. Warey, Influence of thermal contact on heat transfer from glowing firebrands, Case

Stud. Therm. Eng. 12 (2018) 301–311. doi:10.1016/j.csite.2018.04.018.

[310] E.E. Zukoski, Properties of fire plumes, in: G. Cox (Ed.), Combust. Fundam. Fire, Academic Press, 1995: pp. 101–220.

[311] P. Joulain, The behavior of pool fires: State of the art and new insights, Symp. Combust. 27 (1998) 2691–2706. doi:10.1016/S0082-0784(98)80125-2.

[312] C.G. Rossa, P.M. Fernandes, Empirical modeling of fire spread rate in no-wind and no-slope conditions, For. Sci. 64 (2018) 358–370. doi:10.1093/forsci/fxy002.

[313] C.G. Rossa, The effect of fuel moisture content on the spread rate of forest fires in the absence of wind or slope, Int. J. Wildl. Fire. (2017). doi:10.1071/WF16049.

[314] P.H. Thomas, D.L. Simms, H.G. Wraight, Fire Spread in Wooden Cribs Part II Heat Transfer Experiments in Still Air, Fire Saf. Sci. 599 (1965) 1.

[315] E. V. Konev, A.I. Sukhinin, The analysis of flame spread through forest fuel, Combust. Flame. 28 (1977) 217–223. doi:10.1016/0010-2180(77)90029-3.

[316] S.R. Ray, A.C. Fernandez-Pello, I. Glassman, A Study of the Heat Transfer Mechanisms in Horizontal Flame Propagation, J. Heat Transfer. 102 (1980) 357. doi:10.1115/1.3244288.

[317] G.C. Vaz, J.C.S. André, D.X. Viegas, Fire spread model for a linear front in a horizontal solid porous fuel bed in still air, Combust. Sci. Technol. 176 (2004) 135–182. doi:10.1080/00102200490255343.

[318] F. Morandini, A. Simeoni, P.A. Santoni, J.H. Balbi, A model for the spread of fire across a fuel bed incorporating the effects of wind and slope, Combust. Sci. Technol. 177 (2005) 1381–1418. doi:10.1080/00102200590950520.

[319] L. Jiang, C.H. Miller, M.J. Gollner, J.H. Sun, Sample width and thickness effects on horizontal flame spread over a thin PMMA surface, Proc. Combust. Inst. 36 (2017) 2987–2994. doi:10.1016/j.proci.2016.06.157.

[320] R. Bu, Y. Zhou, L. Shi, C. Fan, Experimental study on combustion and flame spread characteristics in horizontal arrays of discrete fuels, Combust. Flame. 225 (2021) 136–146.

[321] W.L. Fons, Forest Fire Modelling, Asme-Asce. (1963) 164–175. https://www.srs.fs.usda.gov/pubs/ja/1963/ja_1963_fons_001.pdf.

[322] Y.B. Zeldovich, On the theory of combustion of initially unmixed gases, Washington, 1951. http://www.archive.org/details/nasa_techdoc_19730007229.

[323] I.S. Wichman, Theory of opposed-flow flame spread, Prog. Energy Combust. Sci. 18 (1992) 553–593. doi:10.1016/0360-1285(92)90039-4.

[324] J.H. McGuire, The Calculation of Heat Transfer by Radiation, Fire Res. Notes. (1952).

[325] D.X. Viegas, C. Pinto, J. Raposo, Burning Rate, Encycl. Wildfires Wildland-Urban Interface Fires. (2018) 1–8. doi:10.1007/978-3-319-51727-8_50-1.

[326] K.N. Palmer, Smouldering combustion in dusts and fibrous materials, Combust. Flame. 1 (1957) 129–154. doi:10.1016/0010-2180(57)90041-X.

[327] H.E. Anderson, Fire spread and flame shape, Fire Technol. 4 (1968) 51–58.

doi:10.1007/BF02588606.

[328] A. Àgueda, E. Pastor, Y. Pérez, E. Planas, Experimental study of the emissivity of flames resulting from the combustion of forest fuels, Int. J. Therm. Sci. 49 (2010) 543–554. doi:10.1016/j.ijthermalsci.2009.09.006.

[329] J.N. De Ris, The Spread of a Diffusion Flame Over a Combustible Surface, Harvard University, 1968.

[330] F.A. Albini, Computer-based models of wildland fire behavior: A users' manual, (1976) 1–68.

[331] A.G. McArthur, The Tasmanian bushfires of 7th February 1967 and associated fire behaviour characteristics, 1969.

[332] R.C. Rothermel, How to predict the spread and intensity of forest and range fires., US Dep. Agric. For. Serv. Gen. Tech. Rep. (1983). doi:10.2737/INT-GTR-143.

[333] F.A. Heinsch, P.L. Andrews, BehavePlus fire modeling system, version 5.0: Design and Features, USDA For. Serv. - Gen. Tech. Rep. RMRS-GTR. (2010). doi:10.2737/RMRS-GTR-249.

[334] P.L. Andrews, C.H. Chase, BEHAVE: Fire Pehavior Prediction and Fuel Modeling System - BURN Subsystem Part 2, PMS 439-3, 1989. doi:10.2737/INT-GTR-260.

[335] P.L. Andrews, C.D. Bevins, BEHAVE Fire Modeling System: Redesign and Expansion, Fire Manag. Notes. 59 (1999) 16–19.

[336] D.R. Weise, E. Koo, X. Zhou, S. Mahalingam, F. Morandini, J.H. Balbi, Fire spread in chaparral - A comparison of laboratory data and model predictions in burning live fuels, Int. J. Wildl. Fire. (2016). doi:10.1071/WF15177.

[337] M. Athanasiou, G. Xanthopoulos, Fire behaviour of the large fires of 2007 in Greece, Proc. 6th Int. Conf. For. Fire Res. (2010) 15–18.

[338] R.E. Masters, D.M. Engle, Behave : Evaluated for Prescribed Fire Planning in Mountainous Oak : Shortleaf Pine Habitats, Wildl. Soc. Bull. 22 (1994) 184–191.

[339] K. Grabner, J. Dwyer, B. Cutter, Validation of Behave Fire Behavior Predictions in Oak Savannas Using Five Fuel Models, 11th Cent. Hardwood For. Conf. (1997).

[340] R.A. Norum, Predicting wildfire behavior in black spruce forests in Alaska, USDA Forest Service Research Note PNW-401, 1982.

[341] C. Hély, M. Flannigan, Y. Bergeron, D. McRae, Role of vegetation and weather on fire behavior in the Canadian mixedwood boreal forest using two fire behavior prediction systems, Can. J. For. Res. 31 (2001) 430–441. doi:10.1139/cjfr-31-3-430.

[342] J. Gould, Validation of the Rothermel fire spread model and related fuel parameters in grassland fuels, Proc. Conf. Bushfire Model. Fire Danger Rat. Syst. (1991) 51–64.

[343] P.M. Fernandes, H.S. Botelho, C. Loureiro, Models for the sustained ignition and behaviour of low-to-moderately intense fires in maritime pine stands, For. Fire Res. Wildl. Fire Saf. Proc. IV Int. Conf. For. Fire Res. 2002 Wildl. Fire Saf. Summit, Luso, Coimbra, Port. 18-23 Novemb. 2002. (2002) 98.

[344] R.J. Barney, N. V. Noste, R.A. Wilson, Rates of Spread of Wildfire in Alaskan Fuels,

USDA Forest Service Research Note PNW-311, 1978.

[345] M.E. Dell'Orfano, Fire Behavior and Fuel Modeling of Flammable Shrub Understories in Northeastern Pine-Oak Forests, Worcester Polytechnic Institute, 1996.

[346] B.W. Van Wilgen, D.C. Le Maitre, F.J. Kruger, Fire Behaviour in South African Fynbos ( Macchia ) Vegetation and Predictions from Rothermel ' s Fire Model, J. Appl. Ecol. 22 (1985) 207–216.

[347] T.J. Streeks, M.K. Owens, S.G. Whisenant, Examining fire behavior in mesquite-acacia shrublands, Int. J. Wildl. Fire. 14 (2005) 131–140. doi:10.1071/WF03053.

[348] M.G. Cruz, P.M. Fernandes, Development of fuel models for fire behaviour prediction in maritime pine (Pinus pinaster Ait.) stands, Int. J. Wildl. Fire. 17 (2008) 194–204. doi:10.1071/WF07009.

[349] R.S. Mcalpine, G. Xanthopoulos, Predicted vs Observed Fire Spread Rates in Ponderosa Pine Fuel Beds: A Test of American and Canadian Systems, Prof. 10th Conf. Fire For. Meteorol. (1989) 287–295.

[350] B.W. Van Wilgen, A.J. Wills, Fire behaviour prediction in savanna vegetation, S. Adr. J. Wildl. Res. 18 (1988) 41–46.

[351] J.W. Van Wagtendonk, S.J. Botti, Modeling Behavior of Prescribed Fires In Yosemite Fire behavior prediction, J. For. (1984) 479–484.

[352] J.K. Brown, Fuel and fire behavior in big sagebrush, Ogden, UT, USA US Dep. Agric. For. Serv. Intermt. Res. Stn. (1982) 14.

[353] W.L. McCaw, Predicting fire spread in Western Australian mallee-heath, University of New South Wales, 1997.

[354] J.K. Brown, Field Test of a Rate-of-Fire-Spread Model in Slash Fuels, USDA Forest Service Research Paper INT-116, 1972.

[355] G. Wells, The Rothermel Fire-Spread Model: Still running Like a champ, Fire Sci. Dig. (2008) 1–12. papers2://publication/uuid/DAC0A044-4352-4AA9-8C74-CEB762BD3EEC.

[356] P.L. Andrews, L.P. Queen, Fire modeling and information system technology, Int. J. Wildl. Fire. 10 (2001) 343–352. doi:10.1071/wf01033.

[357] R.D. Stratton, Guidance on spatial wildland fire analysis: models, tools, and techniques. USDA Forest Service, Rocky Mountain Research Station, Gen. Tech. Rep. RMRS-GTR-183, Ogden, UT. (2006) 15.

[358] P.L. Andrews, M.G. Cruz, R.C. Rothermel, Examination of the wind speed limit function in the Rothermel surface fire spread model, Int. J. Wildl. Fire. 22 (2013) 959–969. doi:10.1071/WF12122.

[359] A.L. Sullivan, A review of wildland fire spread modelling, 1990-present 3: Mathematical analogues and simulation models, (2007) 1–29. doi:10.1071/WF06144.

[360] P.L. Andrews, The rothermel surface fire spread model and associated developments: A comprehensive explanation, USDA For. Serv. - Gen. Tech. Rep. RMRS-GTR. 2018 (2018) 1–121.

[361] BehavePlus Fire Modelling System - Change Log, 2018. https://www.frames.gov/behaveplus/home.

[362] J.H. Scott, NEXUS: a system for assessing crown fire hazard, Fire Manag. Notes. (1999).

[363] M.A. Finney, An overview of FlamMap fire modeling capabilities, in: Andrews, Patricia L.; Butler, Bret W., Comps. 2006. Fuels Manag. to Meas. Success Conf. Proceedings. 28-30 March 2006; Portland, OR. Proc. RMRS-P-41. Fort Collins, CO US Dep. Agric. For. Serv. Rocky Mt. , 2006.

[364] S.A. Rebain, The Fire and Fuels Extension to the Forest Vegetation Simulator: Updated Model Documentation, United States Dep. Agric. / For. Serv. For. Manag. Serv. Center, Fort Collins, CO. (2015) 403.

[365] R. Wilson, Reformulation of Forest Fire Spread Equations in SI Units, USDA Forest Service Research Note - INT-292, 1980.

[366] W.H. Frandsen, Effective Heating of Fuel Ahead of Spreading Fire, USDA Forest Service Research Paper INT-140, 1973.

[367] R.C. Rothermel, Forest Fires and the Chemistry of Forest Fuels, 1976. doi:10.1016/b978-0-12-637750-7.50018-2.

[368] R.E. Burgan, R.C. Rothermel, BEHAVE: Fire Behavior Prediction and Fuel Modeling System - FUEL Subsystem, USDA Forest Service PMS 439-1, 1984.

[369] W.A. Hough, Caloric Value of Some Forest Fuels of the Southern United States, USDA Forest Service Research Note SE-120, 1969.

[370] F.J. Kilzer, A. Broido, Speculations on the Nature of Cellulose Pyrolysis, Pyrodynamics. 2 (1965) 151–163.

[371] A. Broido, Thermogravimetric and Differential Thermal Analysis of Potassium Bicarbonate Contaminated Cellulose, Pyrodynamics. 4 (1966) 243–251.

[372] F. Shafizadeh, Pyrolysis and Combustion of Cellulosic Materials, Adv. Carbohydr. Chem. 23 (1968) 419–474. doi:10.1016/S0096-5332(08)60173-3.

[373] A. Broido, M.A. Nelson, Ash Content : Its Effect on Combustion of Corn Plants, Science (80-. ). 146 (1964) 652–653.

[374] C.W. Philpot, The Pyrolytic Effect of Treating Cottonwood with Plant Ash, USDA Forest Service Research Note - INT-139, 1971.

[375] M.L. Ramadhan, S. Zarate, J. Carrascal, A.F. Osorio, J.P. Hidalgo, Effect of fuel bed size and moisture on the flammability of Eucalyptus saligna leaves in cone calorimeter testing, Fire Saf. J. (2020) 103016. doi:10.1016/j.firesaf.2020.103016.

[376] R.E. Burgan, Concepts and Interpreted Examples In Advanced Fuel Modeling, USDA Forest Service General Technical Report INT-238, 1987.

[377] K.L. Bocock, Changes in the Amounts of Dry Matter, Nitrogen, Carbon and Energy in Decomposing Woodland Leaf Litter in Relation to the Activities of the Soil Fauna, J. Ecol. 52 (1964) 273. doi:10.2307/2257595.

[378] J.D. Ovington, D. Heitkamp, The Accumulation of Energy in Forest Plantations in

Britain, J. Ecol. 48 (1960) 639–646.

[379] L.W. Richards, Effect of certain chemical attributes of vegetation on forest inflammability, J. Agric. Res. 60 (1940) 833–838.

[380] C.W. Philpot, Seasonal Changes in Heat Content and Ether Extractive Content of Chamise, USDA Forest Service Research Paper INT-61, 1969.

[381] H.L. Short, D.R. Dietz, E.E. Remmenga, Selected Nutrients in Mule Deer Browse Plants, Ecology. 47 (1966) 222–229.

[382] C.M. Countryman, Mass fires and fire behavior, U.S. For. Serv. Res. Pap. PSW. (1964) 53 p.

[383] T.W. Sylvester, R.W. Wein, Fuel characteristics of arctic plant species and simulated plant community flammability by Rothermel's model, Can. J. Bot. 59 (1981) 898–907. doi:10.1139/b81-125.

[384] L.C. Bliss, Caloric and Lipid Content in Alpine Tundra Plants, Ecology. 43 (1962) 753–757.

[385] P.L. Andrews, BehavePlus fire modeling system, version 4.0: Variables, USDA For. Serv. - Gen. Tech. Rep. RMRS-GTR. (2008) 1–110.

[386] G.M. Byram, F.M. Sauer, W.L. Fons, R.K. Arnold, Thermal Properties of Forest Fuels, USDA Forest Service Interim Technical Report AFSWP - 404, 1952.

[387] H.D. Tiemann, Effect of Moisture Upon the Strength and Stiffness of Wood, U.S. Department of Agriculture Forest Service - Bulletin 70, 1906.

[388] J.H. Scott, R.E. Burgan, Standard fire behavior fuel models: A comprehensive set for use with Rothermel's surface fire spread model, USDA For. Serv. - Gen. Tech. Rep. RMRS-GTR. (2005) 1–76. doi:10.2737/RMRS-GTR-153.

[389] D. Morvan, Numerical study of the effect of fuel moisture content (FMC) upon the propagation of a surface fire on a flat terrain, Fire Saf. J. 58 (2013) 121–131. doi:10.1016/j.firesaf.2013.01.010.

[390] X. Zhou, D. Weise, S. Mahalingam, Experimental measurements and numerical modeling of marginal burning in live chaparral fuel beds, Proc. Combust. Inst. 30 (2005) 2287–2294. doi:10.1016/j.proci.2004.08.022.

[391] W.C. Fischer, C.E. Hardy, Fire-Weather Observers' Handbook, Agriculture Handbook No. 494, 1976.

[392] F.A. Albini, R.G. Baughman, Estimating Windspeeds for Predicting Wildland Fire Behavior, 1979.

[393] B.D. Lawson, Fire spread in lodgepole pine stands, The University of Montana, 1972.

[394] N.D. Burrows, Fire behaviour in jarrah forest fuels : 2 . Field expenments, CALMScience. 3 (1999) 57–84.

[395] M.G. Cruz, M.E. Alexander, A.L. Sullivan, J.S. Gould, M. Kilinc, Assessing improvements in models used to operationally predict wildland fire rate of spread, Environ. Model. Softw. 105 (2018) 54–63. doi:10.1016/j.envsoft.2018.03.027.

[396] MATLAB - MathWorks - MATLAB & Simulink, (n.d.).

https://uk.mathworks.com/products/matlab.html (accessed 20 April 2021).

[397] P.L. Andrews, Current status and future needs of the BehavePlus Fire Modeling System, Int. J. Wildl. Fire. 23 (2014) 21–33. doi:10.1071/WF12167.

[398] M.J. Woolliscroft, M. Law, A Report on Forest Fire Fieldwork (New Forest, March 1965), Fire Research Note No. 647, 1967.

[399] R.A. Wilson, Observations of Extinction and Marginal Burning States in Free Burning Porous Fuel Beds, Combust. Sci. Technol. 44 (1985) 179–193. doi:10.1080/00102208508960302.

[400] D. V. Sandberg, C.L. Riccardi, M.D. Schaaf, Reformulation of Rothermel's wildland fire behaviour model for heterogeneous fuelbeds, Can. J. For. Res. 37 (2007) 2438–2455. doi:10.1139/X07-094.

[401] A.L. Sullivan, Wildland surface fire spread modelling, 1990–2007. 1: Physical and quasi-physical models, Int. J. Wildl. Fire. 18 (2009) 349–368. doi:10.1071/WF06144.

[402] H.M. Cekirge, Propagation of fire fronts in forests, Comput. Math. with Appl. 4 (1978) 325–332. doi:10.1016/0898-1221(78)90013-5.

[403] N. Fujii, J. Hasegawa, L. Pallop, Y. Sakawa, A nonstationary model of firespreading, Appl. Math. Model. 4 (1980) 176–180. doi:10.1016/0307-904X(80)90128-6.

[404] J.R. Gallacher, The Influence of Season , Heating Mode and Slope Angle on Wildland Fire Behavior, Brigham Young University, 2016.

[405] J.-L. Dupuy, M. Larini, Fire spread through a porous forest fuel bed: a radiative and convective model including fire-induced flow effects, Int. J. Wildl. Fire. 9 (1999) 155. doi:10.1071/WF00006.

[406] H.C. Hottel, A.F. Sarofim, Radiative transfer, McGraw-Hill, 1967.

[407] F.A. Albini, A physical model for firespread in Brush, Symp. Combust. 11 (1967) 553–560. doi:10.1016/S0082-0784(67)80180-2.

[408] H.C. Hottel, G.C. Williams, F.R. Steward, The modeling of firespread through a fuel bed, Symp. Combust. 10 (1965) 997–1007. doi:10.1016/S0082-0784(65)80242-9.

[409] B.M. Wotton, R.S. McAlpine, M.W. Hobbs, The effect of fire front width on surface fire behaviour, Int. J. Wildl. Fire. 9 (1999) 247–253. doi:10.1071/WF00021.

[410] F.A. Albini, A model for fire spread in wildland fuels by radiation, Combust. Sci. Technol. 42 (1985) 229–258.

[411] H.P. Telisin, Flame radiation as a mechanism of fire spread in forests, John Wiley New York, 1974.

[412] J.L. Borges, Dreamtigers, University of Texas Press, 1985.

[413] K.L. Clark, N. Skowronski, M. Gallagher, The fire research program at the Silas Little Experimental Forest, New Lisbon, New Jersey, USDA For. Serv. Exp. For. Ranges Res. Long Term. (2014) 515–534. doi:10.1007/978-1-4614-1818-4_22.

[414] L. Carroll, Sylvie and Bruno, Macmillan, 1889.

[415] W.L. Fons, D.R. Weise, T.R. Fons, U.S.F. Service, W. Fons, W. Leo, Wallace L. Fons,

For. Hist. Today. (2014) 57–59.

[416] R.B. Miller, Characteristics and availability of commercially important woods, Wood Handb. Wood as an Eng. Mater. Madison, WI USDA For. Serv. For. Prod. Lab. 1999. Gen. Tech. Rep. FPL; GTR-113 Pages 1.1-1.34. 113 (1999).

[417] G.M. Smith, Cryptogamic botany. Volume I, Algae and fungi., Cryptogam. Bot. Vol. I, Algae Fungi. (1938).

[418] J. Reardon, Ground Fire, in: S.L. Manzello (Ed.), Encycl. Wildfires Wildland-Urban Interface Fires, Springer International Publishing, Cham, 2019: pp. 1–6. doi:10.1007/978-3-319-51727-8_27-1.

[419] J.L. Rossi, F.J. Chatelon, T. Marcelli, Fire Intensity, in: S.L. Manzello (Ed.), Encycl. Wildfires Wildland-Urban Interface Fires, Springer International Publishing, Cham, 2018: pp. 1–6. doi:10.1007/978-3-319-51727-8_51-1.

## Appendix A – Rothermel Model: SI Unit Reformulation [From Wilson, 1980 [365]]

A full overview of the reformulation of Rothermel's original flame spread equations, into SI Units, was presented by Wilson [365]. A brief summary of the relevant changes to model equations and the value of experimental constants is provided here, along with a summary of the units for each model parameter in both the imperial and SI versions of these equations, as employed in this study.

- Reaction Intensity

$$\text{Original Version: } I_R = r' w_n h \eta_M \eta_s \text{ [BTU/ft}^2\text{.min]}$$

$$\text{SI Version: } I_R = \frac{1}{60} r' w_n h \eta_M \eta_s \text{ [kW/m}^2\text{]}$$

- Maximum Reaction Velocity

$$\text{Original Version: } r'_{max} = \sigma^{1.5}(495 + 0.0594\sigma^{1.5})^{-1} \text{ [min}^{-1}\text{]}$$

$$\text{SI Version: } r'_{max} = (0.0591 + 2.926\sigma^{-1.5})^{-1} \text{ [min}^{-1}\text{]}$$

- Optimum Packing Ratio

$$\text{Original Version: } \beta_{op} = 3.348\sigma^{-0.8189}$$
$$\text{SI Version: } \beta_{op} = 0.20395\sigma^{-0.8189}$$

- Constant 'A'

$$\text{Original Version (Albini Modification): } A = 133\sigma^{-0.7913}$$
$$\text{SI Version: } A = 8.9033\sigma^{-0.7913}$$

- Propagating Flux Ratio

$$\text{Original Version: } \xi = (192 + 0.2595\sigma)^{-1} \exp[(0.792 + 0.681\sigma^{0.5})(\beta + 0.1)]$$
$$\text{SI Version: } \xi = (192 + 7.9095\sigma)^{-1} \exp[(0.792 + 3.7597\sigma^{0.5})(\beta + 0.1)]$$

- Effective Heating Number

$$\text{Original Version: } \epsilon = \exp(-138/\sigma)$$
$$\text{SI Version: } \epsilon = \exp(-4.528/\sigma)$$

- Heat of Pre-ignition

$$\text{Original Version: } Q_{ig} = 250 + 1116M_f \text{ [BTU/lb]}$$
$$\text{SI Version: } Q_{ig} = 581 + 2594M_f \text{ [kJ/kg]}$$

| Parameter | Imperial Units | SI Units |
|---|---|---|
| $h$ | BTU/lb | kJ/kg |
| $I_R$ | BTU/ft$^2$.min | kW/m$^2$ |
| $r'$ | min$^{-1}$ | min$^{-1}$ |
| $r'_{max}$ | min$^{-1}$ | min$^{-1}$ |
| $R$ | ft./min | m/s |
| $w_n$ | lb/ft$^2$ | kg/m$^2$ |
| $w_o$ | lb/ft$^2$ | kg/m$^2$ |
| $\delta$ | ft. | m |
| $\sigma$ | ft$^{-1}$ | cm$^{-1}$ |
| $\rho_b$ | lb/ft$^3$ | kg/m$^3$ |
| $\rho_p$ | lb/ft$^3$ | kg/m$^3$ |

# Appendix B – Rothermel Model Matlab Script

```
% Script file: Rothermel_Models.m
%
% Purpose:
% To compare the predictions of Rothermels flame spread models with the
% experimental observations in this thesis.
%
% Record of revisions:
%     Date         Programmer                          Description of change
%     ====         ==========                          =====================
%   03/03/21    Z Campbell-Lochrie                        Original
%
%
%   Variable                    Description
%   ========                    ===========
%   ros                        Rate of Spread [m/s]
%   reac_int                   Reaction Intensity [BTU/ft^2 min]
%   prop_flux_rat              Propagating Flux Ratio
%   wind_coef                  Wind Coefficient
%   slope_coef                 Slope Coefficient
%   dry_bd                     Oven-Dry Bulk Density [lb / ft^3]
%   eff_heat                   Effective Heating Number
%   pre_ig_heat                Heat of Preignition [BTU / lb]
%   s_v_ratio                  Surface-to-Volume Ratio of Fuel Elements [ft^1]
%   fuel_depth                 Depth of Fuel Bed [ft]
%   wet_fl                     Wet Fuel Loading [lb / ft^2]
%   dry_fl                     Dry Fuel Loading [lb / ft^2]
%   net_fl                     Net Fuel Loading (lb / ft^2) (Using later Albini↙
formula)
%   fmc                        Fuel Mositure Content [%]
%   fmc_ratio                  Fuel Mositure Content Ratio
%   water_mass                 Mass of Moisture in Fuel [lb]
%   dry_mass                   Mass of Dry Fuel [lb]
%   opt_reac_vel               Optimum Reaction Velocity [min^-1]
%   heat_cont                  Fuel Particle Low Heat Content [BTU/lb]
%   moist_damp_coeff           Moisture Damping Coefficient
%   mineral_damp_coeff         Mineral Damping Coefficient
%   mineral_cont               Fuel Particle Total Mineral Content
%   eff_mineral_cont           Effective Mineral Content
%   moist_extinct              Moisture Content of Extinction
%   max_reac_vel               Maximum Reaction Velocity (min^-1)
%   pack_optimum               Optimum Packing Ratio
%   a_const
%   part_dens                  Particle Density (lb / ft^3)

%% Define Constants
wind_coeff = 0;                     % No WInd
slope_coeff = 0;                    % No Slope
ft_per_m = 3.28084;
pnd_sq_ft_per_kg_m_sq = 4.88243;
mineral_cont = 0.0555; %(Value from Andrews 2008)
heat_cont  = 8000; %(Value from Andrews 2008)
eff_mineral_cont = 0.010;   %(Value from Andrews 2008)
moist_extinct = 0.3;
```

```
verification_run = 0;

fuel_data=readtable('Fuel_Data.xlsx');

% Define Variables

    for ii = [1:11]
s_v_ratio(ii) = 1543;
part_dens(ii) = 44.0741;
    end
    for ii=[12:20]
s_v_ratio(ii) = 1493;
part_dens(ii) = 45.2603;
    end
    for ii = [1:20]
fuel_depth(ii) = fuel_data.Height(ii) * ft_per_m;
wet_fl(ii) = fuel_data.Wet_FL(ii);
fmc_ratio(ii) = fuel_data.FMC(ii);

% For verification case
if verification_run == 1
    part_dens(ii) = 32;
end


% Calculate Dry Fuel Loading
dry_fl(ii) = (wet_fl(ii) / (1 + fmc_ratio(ii))) / pnd_sq_ft_per_kg_m_sq;

%% Calculate Oven-Dry Bulk Density
dry_bd(ii) = dry_fl(ii) / fuel_depth(ii);

%% Calculate Packing Ratio
pack_ratio(ii) = dry_bd(ii) / part_dens(ii);

%% Calculate alpha sigma delta
alph_sig_delt(ii) = (1-pack_ratio(ii)) * s_v_ratio(ii) * fuel_depth(ii);

%% Calculate Effective Heating Number
eff_heat(ii) = exp(-138 / s_v_ratio(ii));


%% Calculate Net Fuel Loading (Using later Albini formula
net_fl(ii) = dry_fl(ii) * (1 - mineral_cont);
%% Calculate Heat of Preignition
pre_ig_heat(ii) = 250 + (1116 * fmc_ratio(ii));

%% Caclulate Propagating Flux Ratio
prop_flux_rat(ii) = (1 / (192 + 0.2595 * s_v_ratio(ii))) * exp((0.792 + (0.681↙
*s_v_ratio(ii)^0.5)) * (pack_ratio(ii) + 0.1));

%% Calculate Moisture Damping Coefficient
moist_damp_coeff(ii) = 1 - (2.59 * (fmc_ratio(ii)/moist_extinct)) + (5.11 *↙
((fmc_ratio(ii)/moist_extinct)^2)) - ((3.52 * (fmc_ratio(ii)/moist_extinct)^3));

%% Calculate Mineral Damping Coefficient
```

```
mineral_damp_coeff(ii) = 0.174 * (eff_mineral_cont^(-0.19)) ;

%% Calculate Maximum Reaction Velocity
max_reac_vel(ii) = (s_v_ratio(ii)^1.5) * (1/(495 + (0.0594*(s_v_ratio(ii)^1.5))));

%% Calculate Optimum Packing Ratio
pack_optimum(ii) = 3.348 * (s_v_ratio(ii)^(-0.8189));

%% Calculat value of constant A (Using Albini alternative)
a_const(ii) = 133 * (s_v_ratio(ii)^(-0.7913));

%% Calculate Optimum Reaction Velocity
opt_reac_vel(ii) = max_reac_vel(ii) * ((pack_ratio(ii)/pack_optimum(ii))^a_const(ii))↙
* (exp(a_const(ii)*(1-(pack_ratio(ii)/pack_optimum(ii)))));

%% Calculate Reaction Intensity
reac_int(ii) = opt_reac_vel(ii) * net_fl(ii) * heat_cont * moist_damp_coeff(ii) *↙
mineral_damp_coeff(ii);

%% Calculate Rate of Spread
ros(ii) = ((reac_int(ii) * prop_flux_rat(ii) * (1 + wind_coeff + slope_coeff) ) /↙
(dry_bd(ii) * eff_heat(ii) * pre_ig_heat(ii)));
    end

    if verification_run == 0
        save('roth_predicts.mat','reac_int','ros','prop_flux_rat')
    end
```